DEVELOPMENT OF AN EVALUATION TECHNIQUE IN NEAR ZERO SLOPE FURROWED BORDER SYSTEMS WITH COMMON WATER SUPPLY

A Thesis submitted by

Mohammed Tareq Khaleel AL SAFAAWE

B.Sc., M.Sc.

For the award of

Doctor of Philosophy

2020

Abstract

Near zero slope furrowed border irrigation systems with common water supply commonly known in Australia as bankless irrigation systems, were developed in Australia about three decades ago to reduce the labour requirements associated with siphon irrigation systems. Despite the recent trend to adopt these layouts, there is no methodology to estimate the irrigation performance of these systems. The presence of hydraulic interaction between the adjacent borders, and a considerable variation in diverging flows and water advance between furrows complicates the evaluation process. This study aims to identify and develop the appropriate measurement and analysis processes that can accommodate the special characteristics of these systems, and so allow evaluation of their irrigation performance.

A new naming convention for surface irrigation systems was developed reflecting the features of modern field designs. According to this scheme, the system under study is termed Furrowed Normal Slope BOrder with Reverse slope entry (FNSBO_Re).

A combination of conventional and nonconventional measurement techniques were trialled in two commercial cotton fields in New South Wales in Australia during two irrigation seasons (2016/2017 & 2017/2018). Flow rate measurements at the field scale were conducted using ultrasonic doppler meters. Pipe energy and weir equations were adopted in some cases due to site condition limitations. Measuring the flow rate at the furrow scale was performed using a range of techniques but the most reliable and efficient technique was using a hand-held acoustic doppler. IrriMATE^{TM} advance sensors provided a high level of accuracy but covered a small number of furrows. A GPS smartphone app captured a larger number of advance measurements, but data was of lower accuracy and required considerable time and effort to collect. A novel UAV technique provided an efficient approach to collect advance and recession at the border scale. Attempts were also made to measure furrow water depth using floats and fixed cameras but the most effective approach proved to be use of wooden stakes painted with water soluble dye. Cost, time, effort, performance, and site conditions were the main issues that influenced the choice and success of these various techniques.

The temporarily blocked calculation (TBC) technique was developed to evaluate the irrigation performance at the furrow scale for the real downstream condition (neither blocked nor free draining conditions) in the FNSBO_Re system. The TBC is a spreadsheet-based calculation based on the simulation results of the SISCO model. The TBC results for the furrow length after the sill showed high values of distribution uniformity, exceeding 96%. This high uniformity is due to a rapid water advance and low infiltration characteristics in this field. There was a considerable variation in the application efficiency (28% to 74%) and the requirement efficiency (19% to 65%) between furrows. These low efficiencies were attributed to high runoff losses caused by the large inflow rates and low infiltration characteristics. A complementary calculation process based on drain-back observations at the upstream part of the furrow was developed to evaluate that part of the furrow, which can then be combined with TBC results to find the irrigation performance for the entire length of the furrow.

A UAV technique was developed to evaluate the irrigation performance for the whole border scale. This approach involves obtaining the infiltration opportunity times from the UAV advance and recession data which is then combined with infiltration characteristics from intensive irrigation evaluation measurements. The results showed high distribution uniformity (96.6%) across the border. The results showed low values of the application efficiency (43.5% to 56.5%) and requirement efficiency (52.5% to 100%) in the FNSBO_Re system at the border scale.

Intensive measurements at the furrow scale showed a significant variation between furrows regarding the diverted flows, water advance, water depth, and cross-sectional areas. The greatest variation appeared between wheeled non-wheeled furrows. Statistical analysis using an independent-sample t-test indicated that machinery wheel traffic influences aspects of the irrigation such as peak water depth, cross-sectional area, and flow rate. Investigating the factors that influence the variability of the water advance showed the governing factors to this variability were the cross-sectional area and the flow rate with R^2 of 0.7038 and 0.6477, respectively. Whilst the furrow elevation, and peak water depth have insignificant impact on the water advance.

Importantly, this study outlines a recommended procedure for measurement and analysis of FNSBO_Re irrigation systems. A key part of this is the selection of positions for intensive field measurements. A simple approach based on understanding the water advance variability at the border scale through analysis of UAV advance data was developed to guide the selection of these intensive measurements. This evaluation procedure features use of the novel TBC and UAV techniques developed in this work.

Certification of Thesis

This Thesis is entirely the work of Mohammed Tareq Khaleel Al safaawe except where otherwise acknowledged. The work is original and has not previously been submitted for any other award, except where acknowledged.

Signature of Candidature_____ / / 2020

Mohammed Tareq Khaleel Al safaawe

Principal Supervisor: _____ / / 2020

Dr Malcolm GILLIES

Associate Supervisor: _____ / / 2020

Associate Professor Joseph Patrick FOLEY

Student and supervisors signatures of endorsement are held at the University.

Acknowledgment

I am grateful and indebted to many institutions and people who have contributed towards my PhD thesis. First, thanks to God, the Iraqi government, the University of Southern Queensland and the Research Training Program provided by Australian commonwealth government for giving me this opportunity.

I wish to sincerely thank my principal supervisor Dr Malcolm Gillies for his guidance, understanding, patience, expertise, feedback and most importantly, his positive encouragement to finish this thesis. It has been a great pleasure and honour to have him as my supervisor.

I also wish to express my sincere thanks and deepest appreciation to my associate supervisor, Dr Joseph Foley, for his valuable support and feedback. In addition to his academic assistance, I greatly value his determination to find a field site to conduct the experiments.

I am profoundly grateful to the Turkey Lagoon property owner Mr Hamish Clark for not only allowing and trusting me to undertake my experiments there, but also generously providing me with accommodation, facilities to recharge batteries for my instruments and drone and saving me hundreds of dollars! Mr Clark helped me personally on many occasions when I experienced difficulties.

I would like to extend my deepest gratitude to Mr Raymond Sinclair, Farm Manager at Turkey Lagoon, for numerous acts of kindness during the conduct of the field experiments. He kept me informed about irrigation scheduling and updates to the timing of these events, provided me with field management details, assisted in installing pipe rings in narrow, dark and wet environments, and responded positively to many spontaneous difficult situations.

I would like to express my sincere thanks to Open Access College, University of Southern Queensland and English Angles Program especially Dr Barbara Harems for her support and proofreading. I would like to extend my gratitude to Mr Bill Bryon for helping me in proofreading many chapters of the thesis.

Profuse thanks go equally to all people who work at the University of Southern Queensland who provided their time and expertise, especially Ms Emma Peters for her help with EndNote.

To my friends and colleagues who supported me along the study journey, I am very grateful for your support, time and effort.

Thanks for each smile and kind word I encountered during the study journey.

And above all to my wife, who so tolerantly and encouragingly endured the protracted labours associated with this PhD endeavour. Along with her, I want to acknowledge my children as the valuable treasures and endless sources of love and relief during the PhD endeavour.

Finally, I wish to dedicate this thesis to my late parents. To my father that he always believed in me and encouraged me to start the study journey away from my home country, and my mother who was always a constant source of inspiration in my life. I give the reward of anyone who obtains any benefit from this work to my parents' souls.

Contents

List of Figures

List of Tables

List of Symbols

α	Significance level, dimensionless
ϵ	Roughness of the pipe wall, mm
v	Kinematic viscosity, m^2/s
τ	Infiltration opportunity time, min.
σ_S	Surface storage shape factor, dimensionless
σ_{z1} and σ_{z2}	Subsurface shape factors, dimensionless
A_o	Flow area at the furrow inlet or entrance, m^2
A_1	Flow area of furrow at the sill, m^2
a	An empirical Kostiakov/ Modified Kostiakov infiltration parameter,
c	Geometry factor of the furrow shape
C_{db}	Discharge coeficient for broad-created weir, dimensionless
C_{ds}	Discharge coefficient for a sharp-created weir (dimensionless)
D	Pipe diameter, m
ED	Elevation Difference, m
E_{AD}	Advance error, dimensionless
f	Friction factor, dimensionless
f_o	Final infiltration rate, $m^3\ m^{-1}\ min^{-1}$
g	Gravitational constant, 9.81 $m\ s^{-2}$
ha	Hectare, 10000 m^2
h_f	Friction losses, m
h_m	Minor losses, m
hr	Hours
H_{total}	Total head losses, m
k	An empirical Kostiakov/ Modified Kostiakov infiltration parameter
k_m	Minor losses resistance coefficient in terms of the kinetic energy
K_{m1} and K_{m2}	Resistance coefficients at the pipe entrance and exit, respectively,
L	Advance distance for entire furrow length, m
$0.5L$	Mid-field advance distance, m
l	Pipe length, m
m	Metres
m	Geometry factor of the furrow shape

mm	Millimetres
min.	Minutes
n	Manning resistance coefficient, dimensionless
P	Height of the crest, m
p	An empirical parameter of water advance equation, dimensionless
Q_1	Inflow flow rate at the furrow sill, m^3/s
Q_o	Inflow flow rate at the furrow inlet or entrance, m^3/s
Q_{in} and Q_{out}	Furrow inflow and outflow rate, respectively, m^3/s
Re	Reynold number, dimensionless
RL	Furrow reduced level, m
r	Empirical parameter of water advance equation, dimensionless
s	Seconds
t	Time since commencement of the irrigation, min.
$t_{0.5L}$	Advance time at the mid-field, min.
t_L	Advance time for a distance L, min.
t_x	Advance time required to reach a distance x, min.
U	Length of the crest, m
V	Flow velocity, m/s
V_R	Runoff volume, m^3
V_S	Volume of water on soil surface, m^3
V_z	Infiltrated volume, m^3
W	Furrow spacing, m
W_B	Bottom width of the furrow, m
WL	Water level, m
$WL_{estimated}$	Estimated flat water level, m
x	Advance distance, m
x_c	Calculated advance distance, m
Y	Net water depth above the crest, m
y	Flow depth in the furrow, m
y_{new}	New depth of the flow, m
y_o	Flow depth at the furrow inlet or entrance, m
y_1	Flow area of furrow at the sill, m
Z	Cumulative infiltrated depth, mm

Z_p	Potential cumulative infiltrated depth, mm
Z_x	Cumulative infiltrated depth at a distance *x*, mm
Z_r	Infiltration rate, $m^3\ m^{-1}\ min^{-1}$

List of Abbreviations

ABS	Australian Bureau of Statistics
ADV	Acoustic Doppler Velocimetry
AE	Application Efficiency
ASAE	American Society of Agricultural Engineer
DU	Distribution Uniformity
FLBA	Furrowed Level Basin irrigation systems
FLBO	Furrowed Level BOrder irrigation systems
FNSBO	Furrowed Normal Slope BOrder irrigation systems
FNSBO_Le	Furrowed Normal Slope BOrder with Level slope entry irrigation
FNSBO_Re	Furrowed Normal Slope BOrder with Reverse slope entry irrigation
FRSBO	Furrowed Reverse Slope BOrder irrigation systems
GPS	Global Positioning System
IOT	Infiltration Opportunity Time
LBA	Level BAsin irrigation systems
LBO	Level BOrder irrigation systems
Non-WF	Non Wheeled Furrow
NSBO	Normal slope BOrder irrigation systems
NSBO_Le	Normal Slope BOrder with Level slope entry irrigation systems
NSBO_Re	Normal Slope BOrder with Reverse slope entry irrigation systems
NSF	Normal Slope Furrow irrigation systems
RE	Requirement Efficiency
RMSE	Root Mean Square Error
RSBO	Reverse Slope BOrder irrigation systems
SSA	Surface Storage Area on the furrow
SSE	Sum of all Squared Errors
SSV	Surface Storage Volume on the furrow
WF	Wheeled Furrow

CHAPTER ONE

Introduction

1.1. Introduction

This chapter will introduce irrigation terminology and cover the historical and technical development of irrigation systems. It also will cover the current situation of irrigation systems adopted in Australia including the factors, which have led to interest in alternative forms of surface irrigation.

This dissertation focusses on one of these new surface irrigation methods, a form of bankless furrow irrigation. This chapter introduces this design and discusses the reasons for adoption of this and similar alternate surface irrigation layouts. This chapter will also highlight the existing research gaps relating to both the lack of a technique to assess such systems and the lack of data available describing the behaviour and performance of these systems.

1.2. Background

The term, Irrigation refers to “the watering of land by artificial means to foster plant growth” (Merriam-Webster 2020).

Irrigation is one of the oldest agricultural practices that allowed humans to settle and build civilizations through providing a continuous source of food. The surplus in food production allowed a larger number of people to pursue non-farm activities that shaped the earliest form of urban society. Sumerians who settled in Mesopotamia (the fertile plains between Tigris and Euphrates Rivers of present-day Iraq) about 6000 years ago built the world’s first urban society (Postel 1999). Similarly, other ancient civilizations developed along rivers such as the Nile (in ancient Egypt), the Indus (in Pakistan and India), and the Yellow River (in north-central China) (Adrianov & Mantellini 2013). On the contrary, most ancient irrigation-based civilisations have failed because of water scarcity and degradation of soils due to reasons such as salinization and erosion (Postel 1999). In fact, these issues faced by ancient civilisations still speak to

challenges that we are experiencing today. Developing new efficient irrigation systems and improving irrigation management are key issues that should be considered by modern irrigation societies. Evaluating irrigation system performance is a critical step in any irrigation development or improvement.

1.3. Australian context

Australia is one of the world's major producers for many agricultural products such as grain, cotton, horticulture, and livestock. The agriculture sector is an important part of Australia's economy in terms of exports and employment.

In the year 2016-2017, Australia's total consumptive water use was 16,558 Gigalitres. The agriculture Industry consumed 10,305 Gigalitres which is about 62% of Australia's total water consumption (ABS 2019a). This consumption varies from year to year based on the availability of water. For instance, the amount of water used for irrigation increased by 9% in 2017 thus allowing the total irrigated area to increase by 2% compared to the previous year (ABS 2018). In 2017-2018, the production value of irrigated agricultural production accounted for $17.7 billion (ABS 2019b) of the total value of agriculture production of $59 billion (ABS 2019c). This significant portion of the agriculture production value (30%) has come from only 0.5% of the total agriculture land (Pink 2010).

Climate change and extreme weather events are a major challenge for the agriculture sector. In term of irrigation, paucity and variability in the amount and distribution of rainfall (or water) in many regions in Australia required more interest in irrigation systems to reduce the risk associated with agricultural production.

Although there is a trend to adopt high performance pressurised irrigation systems (such as drip and sprinkler), surface irrigation remains the most common system type in Australia. In the year 2003-2004, the majority of irrigated grains and cotton in Australia was grown with surface irrigation. For example, 96% and 95% of irrigated lands of rice and cotton, respectively, served by surface irrigation systems (ABS 2008). The total area irrigated in Australia by surface irrigation systems is influenced by water availability. For example, during the severe drought between 2006 and 2009 this area

reduced to 51% of the total irrigated area, but then raised to 59% between 2013 and 2014 (Koech et al. 2015).

The dominant soil across much of the irrigated land in Australia are heavy clay soils with low permeability which make them suitable for surface irrigation systems (McKenzie 1998). Generally, surface irrigation systems are suited to the irrigation of broad-acre crops and those requiring ponded conditions. Low initial capital cost, low energy requirements, low cost of water, and low labour expertise requirements are the general reasons behind these systems dominate in Australia and all over the world.

1.4. Development of alternative forms of surface irrigation such as bankless systems

Near zero slope furrowed border irrigation systems with common water supply were developed in the 1990s in southern New South Wales in Australia to reduce labour requirement that are associated with siphon systems. Common water supply is defined as a means to deliver water to set of furrows, part or entire irrigation unit (border or basin) from a single irrigation supply point. The original purpose of these systems was to improve the drainage conditions over traditional level border systems (WATERpak 2015). Some farmers have considered these layouts as a way to improve irrigation performance and ease of management (DEEDI 2011). Moreover, these systems provide the ability to grow a wide variety of crops including rice in rotation with cotton and grains (USDA 1974a). In terms of management flexibility, the capacity to maximise flow rates and minimise the irrigation times enables growers to complete the irrigation cycle in a relatively short time, (for instance, four days) (DEEDI 2011). Because of the reasons mentioned above, there is a recently trend to adopt these systems in many regions in Australia (Grabham et al. 2008).

Many growers in different regions in Australia have converted some of their conventional surface irrigation systems (such as siphons systems) to the near zero slope furrowed border irrigation system with common water supply, such as in Coleambally and Griffith in Southern NSW, Boggabilla and Bullamon Plains in Northern NSW and Southern QLD. Several standard layouts have been adopted in Australia including GL bays and roof top systems (DEEDI 2011).

1.5. Description of the system

Near zero slope furrowed border irrigation systems have the capacity to apply water from the common supplying channel and drain-back the surplus water to the same channel. Common water supply irrigation channels are constructed below the field level without banks on the field side. Therefore, they are also known as bankless channels. Water is applied from the channels to terraced borders that contain furrows. These terraced borders have declining levels along the field width to allow the watering of each border in turn. Naturally, a high level of hydraulic interaction is expected between furrows and among terraced borders of the field. This hydraulic interaction makes the evaluation of irrigation performance very complicated. Therefore, conventional evaluation procedures may not be appropriate to evaluate the irrigation performance of these forms of surface irrigation (Grabham 2012). Anticipated variability of flow rates between furrows is a distinctive characteristic of these irrigation systems and hence they require extensive measurements across many furrows at the border scale to obtain a good indication of irrigation performance. The anticipated variability of flow rates between borders requires the adoption of measurements at the field scale to account for any effect each terraced border might have on adjacent borders.

The key characteristics of the irrigation system layout of this study are shown in Figure 1.1, and are described in more detail in Section 2.11. The field is divided into a number of borders, the size of which reflects the number of furrows that can be irrigated simultaneously with the design inflow. The diversion of water to the furrowed borders is controlled by a series of outlet structures (e.g. check gates) installed across the bankless supply channel. Water is applied through the bankless channel to the first border, the one with the highest elevation. The check gate between the first and second border is initially closed, and it is opened once irrigation of the first border is complete, to allow surplus water to drain and to continue supplying water to the next border beyond this gate. This design features a vertical step (or separation) between these borders as shown in Figure 1.1 Section A-A. Depending on the magnitude of this separation, a hydraulic interaction between the adjacent borders will arise impacting the measurement and evaluation process, which requires the adoption of nonstandard methodologies. As shown in Figure 1.1 Section B-B, these layouts may include a

change in field slope along the border length. The potential scenario of varied slopes is another distinctive characteristic of these systems, which also requires nonstandard methodology. It is clear that the special characteristics of these irrigation systems require the development of a new methodology of measurement and analysis to evaluate their irrigation performance.

1.6. Hypotheses

The performance of near zero slope furrowed border irrigation systems with common water supply irrigation systems can be successfully evaluated to obtain reliable irrigation performance results to aid in industry investment decisions about these systems.

1.7. Research aim

This research aims to report reliable measured irrigation performance results to industry by developing new measurement techniques for near zero slope furrowed border irrigation systems with a common water supply.

1.8. Objectives

The objectives of this research are as follows:

1. Understand the possible range of furrowed border irrigation system designs and any performance results from the literature;
2. Develop a new terminology to define surface irrigation systems.
3. Establish appropriate performance measurement techniques for common supply irrigation systems at the individual furrow, and whole border scale, for experimentation;

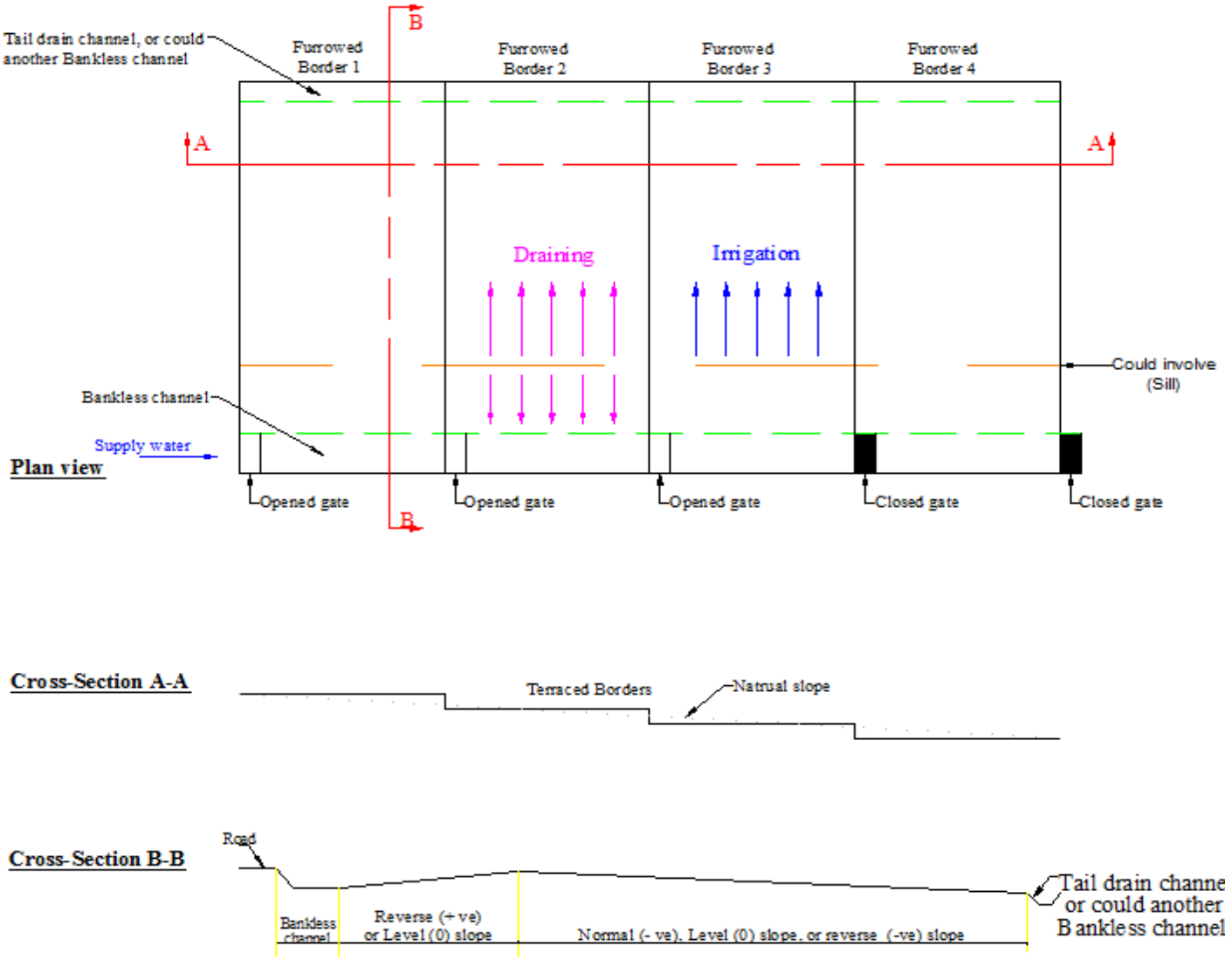

Figure 1.1 Characteristics of the irrigation system involved in this study.

4. Develop a viable practical performance measurement technique that has proven effective over a number of widely varying trial circumstances for industry;
5. Obtain quality measured performance results for furrowed border systems with near zero slope with common water supplies at the border and field scale.

1.9. Outcome and significance

The expected outcomes of this study, represented by determining a new technique and tools to collect reliable measurements for near zero slope furrowed border irrigation systems with common water supply, are to achieve robust assessment of the irrigation performance of these systems. This study will provide the essential data, which is used to calibrate and validate computer simulation models, through evaluation measurements for a number of irrigation events. Having reliable quality measurements will reinforce understanding of the key design and management factors that should contribute to improving the irrigation performance of these surface systems. This understanding helps irrigation designers and growers to select an appropriate design and management practice. On the basis of the good quality, reliable irrigation performance results, the Australian surface irrigation industry can make good decisions on the capital investment in these expensive irrigation systems. Depending on the irrigation performance results, industry advisors may need to communicate the impact of poor irrigation results and irrigation efficiency measures to the large number of growers who have invested in these systems. Growers need to consider the importance of irrigation performance against the importance of the large labour and possible energy savings, machinery operation efficiency gains, and clear improvement in plant establishment rates on hard-setting red soils through the irrigated Australian cotton and grain industries.

The expected outcomes of this study are:

1. A new technique and tools to collect reliable measurements which will be used to achieve robust assessment of the irrigation performance

2. Provision of the essential data which is used to calibrate and validate computer simulation models.
3. An improved understanding of the key design and management factors that contribute to the irrigation performance in furrowed borders systems that use a common water supply.

1.10. Structure of this thesis

This thesis consists of 12 chapters as follows:

Chapter 1 provides background, and the justification to conduct this study according to the Australian context, and then introduces the objectives of this study.

Chapter 2 provides a general review which includes the aspects that influence the irrigation performance of the studied system, defines the important irrigation performance indices, summarises available performance results, and importantly, develops a new terminology of the surface irrigation systems that considers the possible unconventional features of these modern developed systems.

Chapter 3 provides a review of the surveying, and main field irrigation measurement aspects and techniques for irrigation evaluation, and their capacity to accommodate the special hydraulic characteristics of the current irrigation system. It also provides a brief description of the soil infiltration concept and the most relevant factors that impact the infiltration rate in the studied system. This chapter then introduces the common direct and indirect techniques to estimate the infiltration characteristics.

Chapter 4 covers the field work for the first irrigation season conducted in the summer of 2016-2017. It includes the description of the field study sites, the general irrigation process, flow rate instrument calibrations, field preparation and instrument installation, and surveying and field hydraulic measurements. The field measurements include both conventional and unconventional techniques to capture aspects such as field geometry, field elevations, flow rates, and water advance.

Chapter 5 summarises the field measurements results for the first irrigation season. These results show the field slope and special layout features of the first field site, and the noticeable variation in the flow rate, water advance, and cross-sectional areas between furrows of the FNSBO_Re irrigation system. It also shows the distinctive behaviour of the water advance.

Chapter 6 covers the field work for the second irrigation season conducted in the summer of 2017-2018. This includes a description of the irrigation process and hydraulic measurements such as flow rate measurements at furrow and field scales, water advance measurements at the furrow and border scales and water depth for the furrows. The collected measurements also include soil water deficit estimation based on the remote sensing tool, IrriSAT.

Chapter 7 provides the field measurements results for the second irrigation season. These results show the field slope and special layout features of the second field site, and the noticeable variation in the flow rate, water advance, and cross-sectional areas between furrows of the FNSBO_Re irrigation system. The data collected in the second season are more comprehensive and provides a far better understanding of the distinctive behaviour of the water advance in these systems.

Chapter 8 examines the capability of a sample of common surface irrigation models to estimate the infiltration characteristics on a single furrow basis for set of adjacent furrows. It then describes the development of a novel technique, temporarily blocked calculation (TBC) to simulate the irrigation process at the real downstream condition of the furrow through medication of existing modelling tools. This chapter also includes the development of a complementary technique to describe the irrigation process for the part of the field upstream of the sill which is then combined with the results of the TBC technique to provide the irrigation performance for the entire furrow.

Chapter 9 describes the development of a new technique to determine the infiltration opportunity time from the advance and recession measurements for the whole border scale using UAV. When combined with the estimated infiltration characteristics from Chapter 8, these opportunity times can be used to estimate the distribution uniformity for the whole border.

Chapter 10 discusses the factors that influence the variability of the water advance in the FNSBO_Re irrigation system through statistical analysis.

Chapter 11 discusses the key findings of this study regarding the evaluation measurements and analysis techniques. This chapter the outlines a recommended evaluation technique to measure and evaluate FNSBO_Re irrigation systems.

Chapter 12 presents the conclusions, limitations, and recommendation for future work.

CHAPTER TWO

Literature Review: Surface Irrigation

2.1. Introduction

This chapter covers the general concept of surface irrigation and aims to develop a new terminology for surface irrigation systems. It also defines the important indices of irrigation performance and provides a review for many aspects of reported performance results (modelled and actual field). Discussion follows on the factors that impact irrigation performance, focusing on aspects that are associated with irrigation systems studied in this research.

2.2. Basics (or Important terms) of surface irrigation

When, where, and how much to irrigate are the main questions relating to improving and developing the performance of surface irrigation systems. Making the right decision regarding these questions needs a good understanding of the factors which affect irrigation performance.

The main concept of surface irrigation methods is gravity delivering water to plants across the soil surface. Once the delivery of water is completed, other forces other than gravity work to redistribute the water inside the soil profile (Jensen 1980). The process of surface irrigation begins by diverting water directly to a field from a supply channel via siphon pipes, gated pipe, ditch gates, or other supply channel opening. Naturally, some water infiltrates into the soil and the remainder continues its flow path along the soil surface until it reaches the downstream end of the field. Water may then exit the field if the downstream end is open to surface runoff, or alternatively infiltrate into the soil if the downstream end is closed by a barrier of some kind: e.g. levee or dike. The rate of infiltration (unit depth/ unit time) into the soil decreases with time. Diverting water is terminated (cut-off) once the desired amount of water has been supplied. After supply water has been cut-off, water continues flowing for a while with a decrease in depth until it all infiltrates (becomes zero) at the upstream end of the field, and

infiltrates successively passing to the downstream end of the field. Movement of the wetting front is called a water advance, while movement of the drying front is called a recession (James 1988). Technically, there are specific definitions of the phases or terms that describe the surface irrigation process. Figure 2.1 shows the important definitions of the surface irrigation process (Jensen 1980). The advance phase is the period of irrigation time required for surface flow of a wetting front to reach the downstream end of a field. The storage phase commences immediately after the advance phase ends, and finishes as the supply water is cut-off. The depletion phase commences after the storage phase ends, and ends when the flow depth at the upstream end of the field becomes zero. The recession phase is the period of irrigation time which commences when water depth at the upstream end becomes zero and water recedes towards the downstream end until it disappears (Jensen 1980). However, in reverse slope systems, water receding and disappearing from a field during the recession phase will occur in the opposite direction.

The duration of standing water above each position in the field represents an opportunity time for water infiltration, which can be estimated by calculating the difference between recession time and advance time at each position in the field as shown in Figure 2.1. Ideal behaviour of these phases would provide evenness of infiltration opportunity time across the entire field. These phases are governed by soil hydraulic properties, land form and topography (Jensen 1980).

2.3. Performance measures

2.3.1. Introduction

There are many common indicators or terms developed by irrigators to describe the irrigation system performance: irrigation efficiency, application efficiency, water requirement efficiency, distribution uniformity (Burt et al. 1999; Jensen 1980; Kruse 1978). These indicators help in the objective comparison of irrigation performance among different systems. The three essential correlative terms which describe irrigation performance status sufficiently are: application efficiency, distribution uniformity, and water requirement efficiency (Sanchez et al. 2008). Relying solely on

efficiency and disregarding adequacy and uniformity concepts, for instance, limits the understanding of irrigation performance (Kruse 1978).

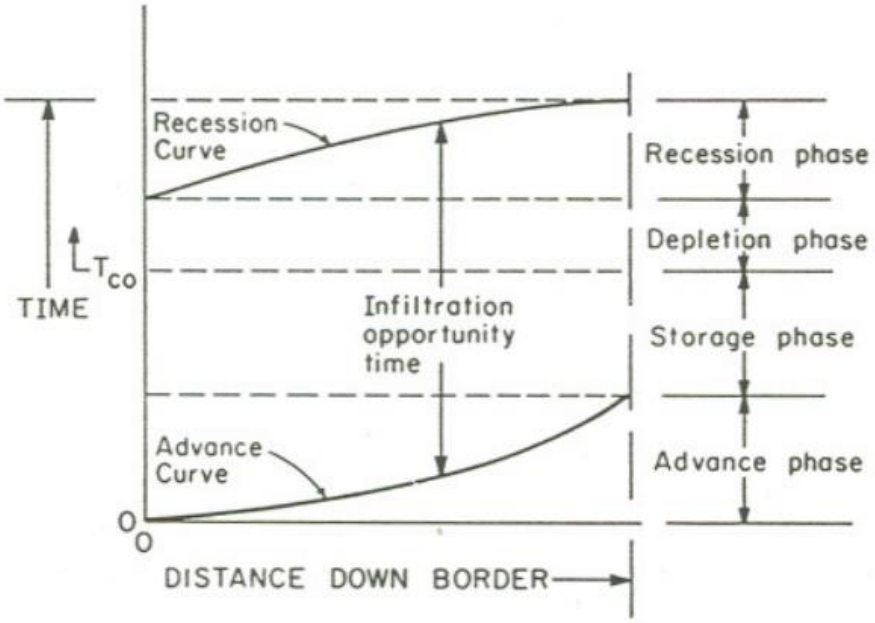

Figure 2.1 shows the important terms of the surface irrigation process, taken from (Jensen 1980).

Israelsen and Hansen (1962) considers that the irrigation efficiencies concept helps to specify positions where it is possible to improve by redesigning field topography, and/or implementing other appropriate operation and management techniques.

2.3.2. Application efficiency

Application efficiency (AE) is defined as the ratio of the average depth of irrigated water stored in the root zone to the average depth of water applied to the field, commonly expressed as a percentage (%)(Jensen 1980).

$$AE\ \% = \frac{\text{Average depth of irrigated water stored in the root zone}}{\text{Average depth of waterapplied to the field}} \times 100\% \quad 2.1$$

Efficient applications in surface irrigation systems are difficult to achieve, because on the one hand, the quick flow of water over the soil results in an inadequate depth of infiltration, while on the other hand, the slow flow of water over the soil results in excessively deep percolation losses below the effective root zone (Israelsen & Hansen 1962).

2.3.3. Uniformity

Uniformity is about the evenness of the water application in the field and describes how the applied water distributes evenly across the field.

Distribution uniformity (DU) 'is the ratio of the average of the lowest quarter values of irrigation depths infiltrated to the average depth of irrigation water infiltrated (Kruse 1978, p. 38), often expressed as a percentage (%).

$$DU\ \% = \frac{\text{Average low quarter depth of water infiltrated}}{\text{Average depth of water infiltrated}} \times 100\% \qquad 2.2$$

A low percentage value for distribution uniformity indicates that a big amount of deep percolation losses have occurred when the irrigation applied to the lower part of the field is only just adequate (Kruse 1978).

2.3.4. Requirement Efficiency

Requirement efficiency (RE) is defined as the ratio of the amount of water stored in the root zone during irrigation to the amount of water required to replenish the root zone to reach either field capacity or an alternative specific water content (USDA 2012), expressed as a percentage (%).

$$RE\ \% = \frac{\text{amount of water applied to the root zone}}{\text{amount of water required in the root zone}} \times 100\% \qquad 2.3$$

A low value for RE indicates that a large percentage of the land that is under irrigated (USDA 2012).

The ability of these indicators to accurately describe surface irrigation performance depends on the level of accuracy which can be achieved when measuring the volume balance components. Unfortunately, it is very hard to provide highly accurate measurements of volume balance components (Burt et al. 1997; Clemmens 2000a).

2.3.5. Other important performance aspects

Labour requirement per unit irrigated area is an important indicator of the ease of irrigation event management. Surface irrigation systems generally have a higher labour requirements compared to other forms of irrigation. Surface irrigation systems which do not require individual siphon pipes to be primed and stopped, will have greatly reduced labour input. Reducing labour costs is one of the key drivers behind the adoption of bankless systems.

In one case study near Thallon in Queensland, Australia, the grower stated that one labour unit could irrigate the whole farm once converted to bankless irrigation whilst siphon irrigation over this same area would require five labour units, in addition to a tractor driver preparing rotobucks (GVIA 2019). From the financial aspect, in a comparison study at a commercial field-scale between four irrigation systems (sprinkler lateral move, sub-surface drip, furrow siphon, and bankless) conducted at the Keytah Irrigation System Comparison Trial at Moree in NSW, Australia over four irrigation seasons (from 2009-2010 to 2014-2015), it was found that annual labour cost was AUD $11.2/ha for the bankless system compared with AUD $134.4/ha for a siphon system. Although the bankless system had significantly lower labour requirements, the siphon system had lower operating energy costs. The combined total annual cost per hectare of operational (labour and energy) and field maintenance was lower in the bankless system (AUD $196) compared with the siphon system (AUD $291) (GVIA 2016).

Construction and maintenance constitute another important factor for selection of the appropriate irrigation system. Anecdotal reports suggest that these systems incur earth moving costs of approximately $2500 USD/ha, when existing surface irrigation

systems need to be modified. Regarding the efficiency of cropping machinery movement, anecdotal reports suggest that the economical movement of tractors and harvesters through these systems represents a considerable cost reduction. In a case study near Boggabilla, New South Wales, in Australia, the grower stated that the tractor efficiency increased from 100 ha/day to 130 ha/day (GVIA 2019).

In regards to germination, growers report an ability of modern Australian bankless systems with furrows and beds to germinate crops on hard setting red soils. This is possible due to the high water level that can be obtained in these systems. The water surface can be raised to the level of the top of the beds where small seeds are planted at shallow depths.

2.4. Forms of surface irrigation

2.4.1. Introduction

Until the early 1900s, surface systems were the dominant form of irrigation (Jensen 1980). The primary form of surface irrigation is called wild flooding (or uncontrolled flooding) and is considered the oldest irrigation method, having been utilised in Asia, southern Europe and Egypt for millennia. In this form of surface irrigation, water flows from a water source and spreads out across a field (or water is allowed to spill across the river banks and spread to adjoining lands) without constructed earthen banks (levees) to guide or control water application. This method requires application of a large flow rate to avoid percolation losses (Israelsen & Hansen 1962). It is characterized by quite low water distribution uniformity (Jensen 1980). However, shortages in water resources impose the necessary adoption of newer forms of surface irrigation to provide higher levels of control for the accurate spread of water across the field. Burt (1995) states that these new forms of surface irrigation initially resembled wild flooding, but had higher performance levels in regard to saving water, energy and labour.

Burt et al. (1999) categorized two main forms of surface irrigation: “ponded” and “moving water”. According to Grabham (2012), surface irrigation methods can be broadly classified into two groups: sloped and levelled systems.

In this review, surface irrigation systems will be divided into three main groups:

1. Normal slope systems (or negative slope downwards from the supply, or elevation is decreasing with distance from supply),
2. Level systems (or zero field slope), and
3. Reverse slope systems (or positive slope, elevation is increasing with distance from supply).

The term "normal slope" (NS) refers to a field grade where the soil surface falls gradually from the higher water supply point in the field to the bottom end with a lower elevation where the field outlet is positioned. Hydraulically, in the normal slope system, water moves from the high point in the field to the lower end where the gradient is the driving force behind moving the water. The term "level system" (L) does not mean that the field has perfect (mathematically) zero slope. In level systems the differences in elevation are insignificant. Therefore to initiate water movement across the field, a high applied flow rate per unit width is provided, in order to build up a head of water to act as the driving force (Walker & Skogerboe 1987). Reverse slope (RS) systems have a field elevation which rises from a lower supply end to the higher end farthest from the supply position.

Some surface irrigation systems involve a combination of two longitudinal slopes in the field. Usually this combination could exist in surface irrigation systems that are served by a common irrigation supply system.

The terms "Level entry" (Le) or "Reverse entry" (Re) refer to the slope status of the entry part of the field when this part is relatively short compared to the entire length of the field.

In this document, there is an intent to distinguish between the two terms "basin" and "border", where the "basin" (BA) or "Level BAsin" term refers to a system which is level (zero/near zero slope), does not demonstrate any drainage or runoff capability, and could be flat or furrowed. The term "border" (BO) describes a system that could have any given slope (zero, +ve or -ve), does have drain-back and/or tail runoff capability, and could be flat or furrowed, which is consistent with (Walker &

Skogerboe 1987). A Normal Slope Furrow (NSF) irrigation system is an important layout that uses an individual furrow water supply system (gated pipes outlet or siphons) instead of common water supply system (e.g. large gate or below ground bankless channel) normally utilized by the various basin and border layouts.

There are two types of basin layouts (BA) and six main types of border (BO) layouts as shown in Table 2.1 which summarises the acronyms, physical characteristics and hydraulic concepts of these different surface irrigation systems.

Naturally, layouts of these surface irrigation systems could be constructed to be level, or have a gradual slope with a regular or irregular shape, or alternatively follow natural contours with a small amount of land levelling work.

2.4.2. Normal slope systems

Normal slope irrigation systems involve negative slope in the direction of irrigation, using gravity acting as a driving force to deliver water down the furrows or borders (Jensen 1980).

Border check and furrow systems are the most common normally sloped surface irrigation systems (Jensen 1980). Normal slope furrows (NSF), normal slope borders (NSBO), and furrowed normal slope borders (FNSBO) are the three normal sloped layouts, which are constructed by dividing the field into furrows (with plants grown in rows on linear hills), border strips, or furrowed border strips, respectively (Burt et al. 1999; Israelsen & Hansen 1962). Normally, the ends of the furrows and borders are not blocked by dikes, thereby providing free drainage conditions (Burt 1995; USDA 1974b). Figure 2.2 shows a normal slope furrow (NSF) irrigation systems using two methods of applying water: gated pipe and siphons tubes.

Table 2.1 Acronyms of surface irrigation systems used in this thesis and their main features.

Acronym	Name of irrigation system	Slope	Flat or furrowed	Supplying system	Drainage condition
LBA	Level Basin	Near zero	Flat	Common [4]	None
FLBA	Furrowed Level BAsin	Near zero	Furrowed	Common	None
NSBO	Normal slope BOrder	Negative [1]	Flat	Common	Separate tail water sys.
FNSBO	Furrowed Normal Slope BOrder	Negative	Furrowed	Common	Separate tail water sys.
NSBO_Le or NSBO_Re	Normal Slope BOrder with Level or Reverse slope entry	Negative	Flat	Common	Separate tail water sys.
FNSBO_Le or FNSBO_Re	Furrowed Normal Slope BOrder with Level or Reverse slope entry	Negative	Furrowed	Common	Separate tail water sys.
LBO	Level Border	Near zero	Flat	Common	Separate tail water sys. / In supply sys.
FLBO	Furrowed Level BOrder	Near zero	Furrowed	Common	Separate tail water sys. / In supply sys.
RSBO	Reverse Slope BOrder	Positive [2]	Flat	Common	In supply sys.
FRSBO	Furrowed Reverse Slope BOrder	Positive	Furrowed	Common	In supply sys.
NSF	Normal Slope Furrow	Negative	Furrowed	Individual [3]	Separate tail water sys.

[1] Negative slope: elevation decreases with distance from supply end;
[2] Positive slope: elevation increases with distance from supply end;
[3] Individual: when water is applied to each furrow and there is limited interaction between furrows (such as with siphons);
[4] Common: where water is applied to a border, basin or group of furrows and there is a high level of interaction between flows within that unit of the field (such as bankless channel).

Figure 2.2 Normal slope furrow (NSF) irrigation systems, the left side photo showing application water using gated pipe, while the right side photo showing application water using siphon tubes.

The irrigation process in normal slope systems begins by diverting water from the main supply ditch to the upper end of the field, so that it then flows toward the lower end (Jensen 1980). Diverting water in NSFs is typically conducted by using siphons, gated pipes, fluming with outlets, or a small pipe through a bank (small PTB) (Burt et al. 1999; James 1988). In NSBO, slide gates, ditch gates, alfalfa valves and large diameter siphons are typically used, whereas FNSBO can be supplied by below ground bankless channels, large PTBs, gated culverts or gated structures from the main supply channel (USDA 2012). One common way to improve uniformity of flow between furrows is to use a positive slopped area at the upper end of the field for roughly 50 metres. These systems commonly have a level section or "sill" after the positive sloped section but the majority of the field is still normal negative slope. In these cases, it is suggested to add the "Le" (level entry) or "Re" (reverse entry) to the end of the irrigation system acronym to refer to this relatively small part of the field length. For example, FNSBO_Re is the acronym for "Furrowed Normal Slope BOrder with Reverse slope Entry". The irrigation process in systems which include different slopes at the upper end of the field (Levelled or Reverse slope) and are served by below ground bankless channels, resemble reverse slope systems (see Section 2.4.4).

The main reason for the positive slope at the furrow entrance is to improve the uniformity of flows. Theoretically, the existence of the positive or reverse slope and sill provide better stability for the furrow cross sections and water elevations compared with what can be achieved at the furrow entrances. This design allows approximately

the same head of water across all furrows, which acts to reduce the differences in the flow rates between furrows.

The flow into each furrow is governed by the furrow shape and by the water depth at the hydraulic control point, that occurs at the upstream of the sill. The water is applied to the bankless channel at one point or one end of the border which means that the water surface will vary between furrows depending on the cross fall of the channel and the distance from the water source. The use of a positive slope at the start of the field creates a region with greater depth and so this water surface becomes more uniform between furrows. The elevation and channel shape are difficult to maintain at the start of the furrow particularly considering machinery operations. The positive slope moves the control point into the field to the sill where furrow shape and elevation are more likely to be uniform between furrows.

The nature of NSBO and FNSBO systems and their supply structures impose lower labour requirements compared with NSF (USDA 2012). However, furrowed systems are more adaptable to terrain and soil texture variations across the field (Jensen 1980), are better suited to row crops that suffer under pond conditions, and suit soils which could be subject to crusting (Walker & Skogerboe 1987). However, they limit the movement of machinery laterally across furrows.

The most common length of furrows range from 90 to 180 metres (Jensen 1980) but in the Australian cotton industry typical lengths are between 400 and 1000 metres. Typical slopes range from 0.05% to 0.3% (Burt 1995). This method is widely adapted to medium and moderately fine textured soils (Jensen 1980). Typical lengths of borders range between about 90 to 360 metres, and the typical widths range between about 5 to 30 metres, while in Australia typical widths are between 40 to 50 metres (Burt 1995). Typical slope gradients are less than 0.5% (Burt 1995; USDA 1974b). The most suitable soils are those with infiltration rates considered as moderately low (Jensen 1980). This method can be adapted to orchards and vineyards and most row crops except those requiring prolonged inundation, like rice.

2.4.3. Level systems

The main concept with level systems (or zero slope systems) is the ponding of water on levelled land that is surrounded by earthen embankments or dikes to ensure infiltration of all of the applied water without any runoff (Burt et al. 1999; Erie & Dedrick 1979; Walker & Skogerboe 1987). With an absence of gradient along and across the field, application of high flow rate per unit width is required (from one or more sides) to build up a head of water that acts as a driving force to move water across the entire field. This ensures near to equal infiltration opportunity time over the entire field, and a high uniformity in the distributed water (Burt 1995).

The merits of these systems are ease of management, efficient machinery operation and labour saving benefits (Erie & Dedrick 1979). However, irrigation performance of these systems is more sensitive to variation in the terrain and soil texture (Grabham 2012).

Theoretically, in levelled systems, the land surface is intended to be zero slope. However, the practical ability to achieve this accuracy of grading is challenging when using even the best laser land levelling equipment and instruments. Practically, these level control instruments provide inadequate accuracy where the difference in topography is insignificant. There are four possible layouts in the levelled systems: Level BOrders system (LBO), Furrowed Level BOrders system (FLBO), Level BAsins system (LBA), and Furrowed Level BOrders system (FLBO), as shown in Table 2.1. Figure 2.3 shows a Level Border (LBO) irrigation system using multiple siphon tubes for applying water. Figure 2.4 shows level irrigation systems (the left photo is LBA and the right photo is FLBA).

LBO and FLBO have the same layouts as NSBO and FNSBO respectively, with the difference being an absence of field slope (Walker & Skogerboe 1987). Typical irrigation structures in LBO and FLBO resemble those used in NSBO and FNSBO respectively (James 1988). In addition to bankless channels, gates can be used to control the diversion of water flow into the field (Grabham 2012). When a supply channel bed is constructed below the benched LBO and benched FLBO, it serves as a surface drainage channel as well as supply channel (North 2008). Therefore Clemmens (2000a) called this form of layout a drain back level basin system. These systems are

adapted to most crop types and soils with low to moderate permeability (USDA 1974b).

Figure 2.3 Level Border (LBO) using multiple siphones tubes for applying water is an example of level irrigation systems (Bos et al. 2009).

Figure 2.4 Level irrigation systems, the left side photo is Level Basin (LBA), while the right side photo is Furrowed Level Basin (FLBA) (Bos et al. 2009).

The layouts of LBASs and FLBASs consist of a group of basins, which are usually rectangular in shape, and are served by a supply channel constructed between two rows of basins. Both systems have a very similar resemblance, with the exception of existing furrows in FLBASs (Walker & Skogerboe 1987). Water is delivered by the supply

channel, then diverted to each basin individually utilising outlet structures (Booher 1974). Typical irrigation (outlet) structures used to divert water into the basins include gates (lift gates and slide gates), underground gated pipes, and large siphons. (Burt 1995; Erie & Dedrick 1979). Both systems are suitable for field and row crops and are applicable to soils of low to medium water infiltration rates (Burt 1995; Erie & Dedrick 1979). Basin areas range from one square metre up to 10 or 15 hectares (Burt et al. 1999; James 1988).

2.4.4. Reverse sloped systems

Reverse sloped systems are defined as those with a distinct existence of longitudinal positive slope with water supplied to the field from the bottom end of the slope. The original purpose of this design was to improve the drainage conditions over traditional level border systems. Other farmers have considered these layouts as a way to improve irrigation performance and ease of management. These systems were developed in the 1990s in southern New South Wales in Australia to reduce labour and energy requirements associated with siphon systems (USDA 1974a). Despite improving machinery operation efficiencies (Grabham 2012), reverse slopes and hydraulic interactions (between furrows or borders) has complicated the evaluation of these systems (Grabham 2012).

The Reverse Slope BOrders (RSBO) system, and Furrowed Reverse Slope BOrder (FRSBO) systems are the only possible reverse sloped layouts. Both have similar layouts, the difference being that furrows exist in FRSBO.

RSBOs system is a variance of the standard LBORs system with a slight positive slope (1:8000 to 1:10000) upwards away from the supply (Grabham et al. 2009). This slope assists in the drainage of any surplus irrigation water, after completion of the water advance, back to the supply/drainage channel which is constructed below the level of these borders (Grabham 2012). The field layout of this system consists of a series of terraced borders served and connected by a bankless channel. Terraced borders are arranged in a series, having stepped declining levels down the length of the bankless channel to allow the watering of each border in turn (USDA 1974a). In the bankless channel, there are a series of outlet structures or gates which are responsible for controlling water flow up into the border. The gate on the downstream side of the

border is closed during irrigation advance, then opened on completion of the irrigation, to allow drainage of surplus water and the continuous supply of water to the adjacent lower border. This hydraulic interaction between adjacent borders is considered as another distinctive characteristic of RSBO or FRSBO, in addition to the positive slope (Grabham 2012). Typical widths of these borders are from 130 to 160 m and in some instances, up to 250 m. The use of these systems requires high supply flow rates to ensure uniform distribution of applied water (North 2008).

Furrows in the FRSBO system run away from the bankless supply channels at angles anywhere between 50º and 100º, and are commonly perpendicular. The irrigation process in FRSBO is similar to RSBO in that water diverts directly from the common water supply channel (such as a bankless channel) into all furrows. This is the converse to what occurs in NSF systems where water is diverted to each furrow through siphons or individual PTBs (Gillies 2008). In this process of irrigation, all furrows supposedly receive the same individual flow rate from the common supply channel. Grabham (2012) refers to the FRSBO system as a bankless channel irrigation system to distinguish it from a siphon irrigation system, where the bankless channel is below the level of the field. Figure 2.5 shows a furrowed reverse slope irrigation system (FRSBO) irrigation systems using bankless channel to divert water to the field, and two means of interconnection between adjoining borders (left side photo with culvert, while the right side photo contains check gates).

Figure 2.5 Furrowed reverse slope irrigation systems (FRSBO), the left side photo showing an interconnecting (wingwall) culvert between the adjoining borders, while the right side photo showing an interconnecting check gate between the adjoining borders.

2.4.5. Selection of the system used in this study

As mentioned in Chapter One, this study will focus on the specific characteristics of a surface irrigation layout generally described as a near zero-slope furrowed border irrigation systems with a common water supply. According to the classification of surface irrigation systems proposed in this thesis (Table 2.1), the current study will focus on an example of a FNSBO_Re irrigation system (Section 2.4.2).

2.5. Reported performance results

2.5.1. Introduction

Few attempts have been made in Australia to improve the irrigation performance of level and reverse slope surface irrigation systems (Hood & Carrigan 2006). As well, there is no definitive procedure for the design and management of these systems (Khanna et al. 2003). Only a few studies have taken into account the impact of the distinctive characteristics of these systems and the interaction at the field (between borders) and furrow (within border) scale. Khanna et al. (2003) studied the hydraulic interaction at the borders in RSBO, where a focus was on the drain-back from the borders to the supply channel and from one border to another, in combination with the continuing inflow through the supply channel. Grabham (2012) studied the effect of positive slope and the hydraulic interaction between borders in a FRSBO. Grabham et al. (2009) claims that the performance of the FRSBO system at the furrow scale does not represent the performance at the border scale, and the performance at the border scale does not represent the performance at the field scale.

For border scale evaluations (within borders) in the FRSBO system, Grabham (2012) states that the variations of discharge into, and the advance along individual furrows leads to a decline in irrigation uniformity. These variations occur due to the presence of elevation variations between each furrow. For field scale evaluations (between borders), the variations between borders occurred in the applied depth due to the hydraulic interaction between borders, where ponded surface water moved from border to border through interconnecting structures.

2.5.2. Modelled irrigation performance (simulated results)

Simulation models of overland flows in surface irrigation systems are useful in evaluating irrigation performance for actual irrigation events and to investigate the performance of hypothetical changes to design and management. However, availability and accuracy of field measurements of surface irrigation parameters such as infiltration and roughness coefficients are the main restrictions in applying these models (Khanna & Malano 2006; Strelkoff et al. 1999).

Many computer models have been used to simulate the irrigation process of surface systems such as B2D (Playán et al. 1994), AIM (Austin & Prendergast 1997), SIRMOD (Walker 2003), WinSRFR (Bautista et al. 2006), COBASIM (Khanna et al. 2003), SISCO (Gillies & Smith 2015) and B2B (Grabham 2012). These models have been used to study several parameters that impact irrigation performance, such as slope, border dimensions, aspect ratio (the ratio of width to length of field/bay), local micro topography, inflow rates, irrigation deficits, cut-off time, vertical separation between borders, and the numbers of check bank outlets.

There are many studies that have reported simulation results for AE, RE, and DU of irrigation systems that use individual supply (NSF) such as (Smith et al. 2005), (Bakker et al. 2006), (Gillies & Smith 2015), and (Alejo 2020). For instance, Smith et al. (2005) and Bakker et al. (2006) state that the AE in an NSF system can be raised by about 20 to 30% through simple practices suggested by the simulation model SIRMOD such as adjusting time to cut-off, or altering the flow rate.

Pereira et al. (2007), Playán Jubillar and Martínez-Cob (1999), Playan and Faci (1996), De Sousa et al. (1995), Liu et al. (2020) and Fadul et al. (2020), reported a range of irrigation performance results for many forms of level systems using different simulation models. Some of these studies focused on the impact of improving land levelling and increasing inflow rates on irrigation performance and labour requirements for these systems.

In contrast, there are insufficient studies and data that report and discuss the irrigation performance of FNSBO_Re irrigation system. In one recent example however, Grabham (2012) developed the B2B model to simulate the following special

characteristics of the FRSBO system: positive field slope and hydraulic interaction between borders. Simulation results showed that to overcome the influence of these characteristics on the performance of FRSBO, it is recommended that the width of the first and last border be reduced to overcome the influence of the hydraulic interaction between borders where an increase is created in the inflow rates entering the second and following borders.

In order to achieve reliable results from the simulation models, it is important to collect sufficient and accurate field measurements which suit the unique characteristics of these systems.

2.5.3. Actual field results (farms and research stations)

This subsection will report field results for the following important irrigation performance measures: AE, DU, and RE. Moreover, it will report other important measures in the Australian context, such as labour input and capital costs.

Many studies have been conducted to report the irrigation performance of normal slope systems ((Merriam and Keller 1978), (Raine & Walker 1998), (El-Dine & Hosny 2000), (Eldeiry et al. 2005), (Gillies et al. 2010), (Gillies & Smith 2015), (Sayari et al. 2019), and (Chavez & Fuentes 2019)). These studies have reported differing ranges of AE, DU, and RE. For instance, Gillies and Smith (2015) reported field results of AE and RE in the NSBO system of 78 and 97% respectively. El-Dine and Hosny (2000) reported field results on two farms using the NSFs system with AE of 82.8 and 59%, respectively, and DU of 83 and 77% respectively. Sayari et al. (2019) reported average field results of AE in NSF system of 49.07%.

There are many studies which have reported the irrigation performance of level systems. For instance, Pereira et al. (2007) reported a range of DU for several irrigation events in a LBO system of between 53 to 98%. In a FLBA system, Payne (1997), cited in Clemmens (2000b), reported AE in two basins of 92% and 95%.

In contrast, only a few studies have been conducted to report and discuss the irrigation performance of furrowed border systems which adopt common irrigation supply systems, such as RSBO and FRSBO. Grabham et al. (2009) states that the seasonal AE

in the FRSBO system at the field scale was 93%. In this case study, it was found that irrigation processes were quicker in the FRSBOs (bankless channel) compared to the NSF (siphons). A quicker irrigation process supposes some savings in the applied water amount, and in evaporation losses as well (CottonInfo 2014), both of which improve AE.

Level systems are characterised by lower labour requirements compared to sloping systems (Clemmens 2000b). Clemmens (2000a) claims that the labour requirement in systems that include drain-back characteristics are lower than the LBASs system, where the latter required six labour units for 1000 hectares while one labour unit is sufficient for systems with drain-back behaviour (USDA 2012). In the FRSBOs system, labour requirements were reduced significantly to the point where one labour unit could manage a farm of 4000 hectares, whereas 10 to 12 labour units would be necessary for the same area in NSF according to the farm manager.

In conclusion, many studies have covered common conventional irrigation systems, while few studies have focused on near zero slope furrowed border irrigation systems with a common water supply, such as FNSBO_Re and FRSBO. Therefore, further intensive field work and analysis is required in order to understand these systems. The initial evaluations in these systems showed great potential for improvement.

2.6. Factors influencing irrigation performance in surface irrigation systems

There are many variables that influence the irrigation performance of surface irrigation systems. Some of these variables represent the natural characteristics of the field where a change within a cropping season cannot be made, such as soil infiltration characteristics and soil roughness. Other variables such as field slope and field length can be selected in the design stage but remain fixed (excessive cost and effort would be required to change it) during their operating life. The final types of variable that are more manageable, with changes being possible at more localised irrigation events, are the flow rate, cut-off time, or desired depth of applied water (Smith 2014).

Manipulating these variables at the design or management stage for any surface irrigation system aims to deliver adequate amounts of water to the field evenly, whilst

minimising potential water losses such as deep percolation or runoff. Theoretically, all potential manipulation attempts will govern stream behaviour. Appropriate manipulation of these variables must occur with an understanding of the phases that describe the surface irrigation process (Section 2.1).

2.6.1. Factors that represent the natural characteristics of the field

Soil infiltration and soil roughness are key parameters to determine the performance of surface irrigation (Xu et al. 2019).

2.6.1.1. Soil Infiltration

Infiltration is the process of the entry of water into the soil profile through the soil surface. It reflects the soil's capacity to absorb applied water without runoff occurring. (Jensen 1980).

Soil infiltration is one of the most significant factors affecting surface irrigation performance, as the infiltration rate of the soil and the infiltration opportunity time determine the depth of water infiltrated at a given position in the field, and the evenness of the distribution of these depths over the entire field (Gillies 2008).

Soil infiltration characteristics represent the most important factor in designing and managing surface irrigation systems, because infiltration rates impact directly on the required inflow rates and inflow cut-off time (NRCS 1997). Important factors influencing infiltration rates of the field site used in this study will be covered in Section 3.5.2.

2.6.1.2. Soil roughness

Soil surface roughness influences the speed of the advance and the recession. Theoretically, with lower roughness values (expressed by Manning's value, *n*) a higher advance rate can be expected which leads to reduced variation in infiltration

opportunity time and consequently improves the uniformity of distribution of water and efficiency of irrigation (North 2008).

A number of studies have been completed where soil surface roughness has been manipulated within seasons to alter outcomes.

2.6.2. Design variables

There are several design variables which influence irrigation performance: cross-section of the furrow; length and width of the border; longitudinal slope of the furrow; and layout conditions relating to flow conditions upstream and downstream in the field. This section will focus on the variables that define the unique features of the irrigation system in this study (FNSBO_Re).

2.6.2.1. Field Slope and variability in the soil surface elevation

The longitudinal slope of a field is an important variable that impacts the performance of surface irrigation systems. It obviously impacts the rate of advance and recession of water from the field. Naturally, the advance rate of the water front decreases with increasing positive slope and the advance phase duration decreases with steeper negative slope. COBASIM modelled results by Khanna et al. (2003) showed that a 20% reduction in the advance time resulted in a greater uniformity and reduced deep percolation losses. Faster advance rates coupled with steeper negative slopes, result in a more even application of infiltrated depth over the entire border. González et al. (2011) found in their theoretical study, that a 20% saving in water can be achieved by selecting an optimum slope. They also found that having a very gradual slope (1:2500) compared with a levelled field reduced irrigation time by 18%.

For irrigation systems that adopt a common water supply, the presence of a positive slope for part or the entire length of the field is a design feature which improves the uniformity of flow into individual furrows and promotes optimal drainage during the

recession phase (Clemmens 2000a; Grabham et al. 2009). However, the anticipated variation in flow between furrows is still a big challenge without the existence of a controlling feature with a positive slope. Promoting rapid drainage conditions could raise the AE by approximately 8 to 20%, whereas about 25 to 45% of the surface storage water in furrows can be drained back in RSBO or FRSBO (Dedrick & Clemmens 1988). Martin and Eusuff (2000) also found that adopting the drain back system promotes water saving (about 33% of applied water drained back), which in turn increases AE.

Generally, Patin et al. (2012) found that in bare soil the infiltration increases when the slope decreases. However, the role that the gradient plays on infiltration is governed by other additional factors such as soil texture, flow rate, and micro-topography (Morbidelli et al. 2018).

Proper grading of the field improves the irrigation performance (Clyma & Clemmens 2000), where small amounts of spatial variability in the soil surface elevation can have a considerable influence on the post-irrigation distribution pattern of infiltration (Strelkoff & Clemmens 2007). Laser land levelling equipment offers a standard deviation (SD) in soil surface elevation of about 10 mm from the average slope (Strelkoff & Clemmens 2007). Fangmeier et al. (1999) stated that in the LBA system, when SD of soil surface elevation exceeds 20 mm, uniformity and efficiencies decline rapidly. Hunsaker (1991) found that distribution uniformity can exceed 85% in the LBA system when 85% of the basin elevation is within ±15 mm of the average.

Delivering water evenly to furrows in the surface irrigation systems that adopt common supply systems depends on the water surface elevation in the channel (bankless channel) which is in turn governed by how much levelling work (using laser-levelled equipment) has been conducted (Strelkoff & Clemmens 2007).

Designing the appropriate slope for border irrigation depends on the type and depth of the soil profile (Feyen & Zerihun 1999). Border directions can be oriented to follow the natural slopes to reduce earth moving costs and effort (Clemmens 2000b).

Waterlogging is expected in surface irrigation systems with slopes flatter than 1:2000. On the other hand, higher soil erosion can be expected with increasing slope (North 2008).

2.6.2.2. Border dimensions

Selecting inappropriate lengths for furrows and borders may result in excessive water loss as deep percolation or runoff (Jensen 1980). Kaur et al. (2019) considered that optimising border dimensions is a practical way to raise water use efficiency.

Optimal border dimensions (both length and width) depend on supply flow rate, soil infiltration characteristics, and roughness, and crop sensitivity to waterlogging during prolonged ponding of water on the soil surface (length of infiltration opportunity time) (North 2008).

Fadul et al. (2020) found that the vertical division of the border area could lead to significant improvement in AE (from about 50% to over 70%), RE (from 68% to 100%), and DU (from 34% to 87%). Khanna et al. (2003) found that the aspect ratio (the ratio of width to length of the basin or border) impacts significantly on irrigation performance, when a range of aspect ratios (0.3 to 1.0) was studied by maintaining a constant length of the basin (200 m) while the basin widths varied between 60 and 200 metres. The AE and DU decreased when the aspect ratio increased from 0.3 to 0.5. This agrees with the fact that increasing the aspect ratio results in greater deep percolation losses as the advance duration increases. The AE and DU show a greater sensitivity in the low range of aspect ratios, but remain mostly unchanged for the higher range of the aspect ratio. The behaviour of the RE was opposite to that shown in the AE and DU. However, basins with aspect ratio higher than 0.4 were completely irrigated (RE ~ 100%) due to an increasing advance duration that coupled with higher aspect ratios, translates into a larger amount of applied water. By increasing the basin width, the advance duration increases, which in turn augments deep percolation losses. The advance duration increased significantly when the aspect ratio increases from 0.3 to 1.0, for the same inflow rate per unit width.

In terraced borders with common supply systems (FRSBO), to reduce the variability between borders, some designers recommend reducing the width of the first and last

borders by about 60 and 40%, respectively, compared with the intermediate borders ((Grabham 2010) according to (Grabham 2012)). The reason for reducing the width of the first and last borders was to obtain approximately even flow rates per unit width, for each border. The first border only receives flow from the supply channel but the intermediate borders will receive additional inflow rates due to the drain-back portion of the surface storage in the upstream border and thus can be wider that the first. The reason behind reducing the border width of the lowest border is to drain water from the penultimate border without incurring excess runoff away from the entire field (Grabham 2012).

2.6.2.3. Vertical step between borders

The inclusion of a vertical step between borders is one of the special features of the particular case used in this study. The magnitude of this feature depends on both the natural field topography, and the border width (Grabham 2012; Khanna et al. 2003).

This step height measurement should be equal to or exceed the furrow depth to ensure that complete drainage from the upstream border occurs before the next downstream border completes its advance phase (Grabham 2012). Attending to this design condition could avoid waterlogging that results from prolonged ponding at the upstream border (Grabham 2012; Khanna et al. 2003). The optimal value of this vertical step will be achieved when the hydraulic interaction between adjoining borders is minimal (Grabham 2012).

According to North (2008), growers in Murrumbidgee Valley found that 0.075 m for the vertical step is insufficient, and suggested 0.15 m be adopted as a minimum value. While Clemmens (2000b) suggested approximately 0.3 m in order to obtain proper drainage from the upstream border into the adjoining downstream border. Khanna et al. (2003) found that the irrigation performance is not affected significantly by slightly increasing the vertical step. He stated that an increase in the vertical step reduces the advance time to some degree, and the advance time remains slightly unchanged at greater values of the vertical step (> 0.07 m). Generally, increasing the vertical step leads to an increase in the hydraulic gradient which in turn increases the advance rate.

2.6.3. Operational or management variables

2.6.3.1. Flow rate and cut-off time

Flow rate and cut-off time are very important factor that impacts the design and performance of surface irrigation systems. Many studies have linked achieving high irrigation performance to selecting an appropriate combination of flow rates and cut-off time ((Salahou et al. 2018; Sayari et al. 2019; Smith & Uddin 2020; Smith et al. 2018; Tadele et al. 2019)).

Generally, surface irrigation systems with level or nearly level surfaces require relatively large flow rates per unit irrigation width (NRCS 1997). Smith and Uddin (2020) mentioned that the AE increases of about 20% when adopt higher flow rates than those traditionally recommended. However, substantially reduced irrigation durations (cut-off time) is required to achieve this improvement. Also, they mentioned that selection and management of these shorter cut-off times need high precision. Khanna et al. (2003) found that an increase in flow rate per unit width led to improved AE and DU to some degree, but remained slightly unchanged at higher flow rates when runoff was not recycled. This approach can decrease deep percolation losses which in turn raises the AE. Adopting higher flow rates reduces the time required for water to advance to the end of the field which consequently improves the chances of distributing water uniformly along the field, by reducing the variance between infiltration opportunity times down the field.

The high flow rates associated with a level basin can help to achieve high AE in excess of 85% (Martin & Eusuff 2000). However, high flow rates could also lead to substantial erosion of soil at the supply point, upstream of the earthen in-field distribution channel (Martin & Eusuff 2000). Xu et al. (2019) concluded that adopting optimal combinations of inflow rate and cut-off time, taking into account temporal variation in soil infiltration and soil roughness, could maintain a high value of AE.

2.7. Conclusions

A wide range of surface irrigation systems and water supply combinations exist, but the focus of this study is on systems incorporating the following characteristics:

- The water supply into individual furrows is common;
- The border will include drainage capacity;
- The border will be furrowed;
- A combination of all three slopes (negative, positive and levelled) may be exhibited along the furrow length; and
- Irrigation will involve hydraulic interaction between borders

The FNSBO_Re irrigation system, (as per the developed terminology), has been selected for this study because there has been little to no research conducted on the performance of this type of popular system here in Australia.

Factors influencing the irrigation performance of the FNSBO_Re have been discussed in this chapter. These factors had been classified to the three main categories including: natural characteristics of the field, design and management.

It is clear from the literature reviewed (Chapter Two), that there is limited field data available for these types of surface irrigation systems. It is also clear from this literature review that it is possible to improve the irrigation performance of these systems.

CHAPTER THREE

Literature Review: Measurements of Surface Irrigation Systems

3.1. Introduction

The selected system (FNSBO_Re) is anticipated to have a number of special characteristics including variation in diverting water to the furrows, the presence of reverse slope and hydraulic interaction between adjoining borders. These characteristics represent significant challenges in conducting irrigation evaluation measurements. Selecting appropriate techniques to measure any unconventional conditions associated with these irrigation systems was one of the primary objectives of this study. The following sections will discuss the suitability and the ability to apply both conventional and unconventional techniques to the current study system. A selection of these techniques are evaluated through field trials on FNSBO_Re systems in later chapters.

3.2. Flow rates

A variety of hydraulic devices can be utilized to measure the amount of water inflow and outflow in surface irrigation systems. Some of these devices are appropriate to use in conventional field layouts of surface systems such as weirs, flumes and orifices (Walker & Skogerboe 1987). Other devices, such as propeller meters and ultrasonic doppler meters, may be more appropriate for more unique situations, such as water flowing in FNSBO_Re surface irrigation layouts.

Weirs are notches of regular forms (such as rectangular and trapezoidal) through which water flows (French 1999). Flumes are channels with regular cross sections (rectangular and trapezoidal) supported above ground, and usually made from different materials such as metal, concrete, and wood (Chaudhry 2007). Orifices are walls placed perpendicular to stream flow, with holes at their centres (Wall 1996). These devices rely on the fact that discharge can be predicted from water depth measured at

a specified location. The issue is that they typically rely on free flowing conditions which may not exist irrigation layouts such as those considered in this study. Furthermore, these devices may obstruct the flow and change the behaviour of these systems. Moreover, the unwanted collection of soil, gravel and plant remains above weirs or orifices prevents accurate measurements from being taken (Israelsen & Hansen 1962).

A more suitable approach is to use devices which measure flow velocity directly without altering the dimensions of the channel. A propeller meter is one such device that adopts a mechanical approach to estimate flow velocity. It estimates velocity of the stream flow by establishing a relationship between the rotation rate of the propeller and velocity of the water stream. Another important approach for estimating flow velocity is the potential use of ultrasonic sensors. Sending and receiving ultrasound waves in the water stream will determine the flow velocity by knowing the transmitting speed of these waves (RISC 2009).

In this study, flow rate measurements will be applied at two scales: furrow and field scale.

3.2.1. Flow rates at furrow scale

Measuring flow rates for furrows is considered one of the greatest challenges in surface systems with common supply systems such as bankless channels. In these systems, the water distribution will vary between furrows according to the geometry and water elevation of each furrow adjacent to the supply channel. This anticipated variation can either be dealt with by measuring individual flow into a large number of furrows or by capturing the total flow applied to the entire border. Cost and installation flexibility of conventional devices are deemed to be the main limitations, because many flumes would be required to conduct flow rate measurements in an adequate number of furrows at each border during the irrigation event. Moreover, the field measurements could include irrigation events for two fields on the same day. For instance, the cost of one Parshall flume (maximum 20 l/s) is greater than AUD $2500. Installing this kind of device requires considerable time and effort. In addition, conventional devices such as flumes might not suit flow conditions in furrows with reverse or near zero slopes, as mentioned in Section 3.2.

A smart phone application is available which can infer flow rates in open channels such as rivers and furrows using the device camera. Calculation of the flow rate is performed by analysing a short video clip of the stream. The analysis does require prior knowledge of the channel geometry. Once this is established, the video clip is used to capture the water level and water surface velocity (Beat et al. 2014; Peña-Haro et al. 2015) from which the flow rate can be calculated.

The SonTek FlowTracker2 is a hand-held acoustic doppler velocimeter (ADV). The principle of its functionality is based on measuring the flow velocity by sending a short sound pulse through the water, then receiving and processing the sound wave which is reflected by particulate matter suspended in the water such as sediment or air bubbles (SonTek 2016). Grabham (2012) states that the SonTek FlowTracker offered less flow resistance and a greater suitability compared to other similar ADV when used in shallow flows such as furrows in a reverse slope irrigation system. His study included measuring the flow velocities for many selected furrows during multiple irrigation events. The success of the ADV in Grabham's field trials meant that this apparatus was chosen to capture individual furrow flows in this study. All velocity measurement techniques require measurement of the cross sectional area of flow in order to calculate corresponding flow rates. Application at the furrow scale involves measurement of the furrow cross section at a location, which is representative of the majority of the field length.

3.2.2. Flow rates at field scale

The purpose behind collecting flow rate measurements at the field scale is to calculate the average applied depth of water for each border, thus to enable evaluation of the whole field performance.

Bankless systems such as the FNSBO_Re layout involve the use of irrigation structures or gates, which serve three main functions, generally arranged in the following order: (1) supplying (on-off) water from the main channel to the field; (2) controlling and diverting water between borders at the head and tail of these borders; and (3) controlling and removing tailwater. These structues come in a range of designs including canal turnout structures controlled by a knife gate or slide gate; concrete pipes between borders; check gates (or inter-bay structure) between borders; and drain

boxes. Each of these stuctures have different geometries and unique challenges for positioning and operation of the flow rate measurement device.

The general concept of measuring flow rates in these structures is based on measuring the average flow velocity and the effective cross-sectional area of the flow stream. Flow velocity could be measured using sophisticated techniques involving electromagnetic or ultrasonic equipment. Alternatively, more simple techniques such as using propeller velocity meters or float instrumentation could be undertaken.

A number of past studies have used Starflow^{TM} instruments to conduct flow rate measurements in surface irrigation systems (Edraki et al. 2003; Gillies 2008; Gillies et al. 2008; Grabham 2012). A Starflow is an ultrasonic Doppler instrument installed at the bottom of pipes or relatively small channels to measure water velocity, depth and temperature. The measurements can be recorded by an intelligent data logger (Unidata 2013) within the device or transmitted to an external logger.

An alternative approach which could be used to determine flow rates is to calculate the flow based on a measured head loss or water depth as water flows through the control structure. This may include use of a weir, flume, or friction and minor losses in a pipe culvert.

3.3. Water advance and recession

Water advance measurements are vital pieces of data to evaluate the real quantity of consumptive water in surface irrigation systems. Advance measurements refer to the collection of the time taken for the water front to reach specified distances along the length of an irrigated furrow or border. Completion times refer to the time taken for this advancing front to reach the downstream end of the field. In the evaluation process, advance times are required for the inverse solution of the soil infiltration function as discussed later in this thesis. In many situations, farm managers depend solely on their personal and professional experience to determine water advancement times or completion times in the field, they often decide time cut-offs based on their intuition and sight observations alone. However, for evaluation purposes, a robust approach should be adopted for obtaining these data. Advance sensors are electronic contact sensors which detect the instant that water reaches that location in the field. One

example device which is commonly used in the evaluation of furrow irrigation systems in Australia is the IrriMATE ™ advance sensor (Gillies & Smith 2015; Koech et al. 2010). Each IrriMATE ™ advance sensor consists of eight pairs of terminal contacts placed at specific distances to take into account the common intervals between furrows. These sensors are designed to capture the water advance front for up to eight adjoining furrows. The terminal contacts of the advance sensor are installed at the base of each furrow to log the arrival time of the water front for every furrow.

An alternative approach is to deploy depth probes to measure both arrival of the water advance and water depth throughout the duration of the irrigation .Rojas-Ponce et al. (2011), Grabham (2012), and Morris et al. (2015) used Mindata capacitive water depth probes to record both advance and recession measurements in furrows.

Advance sensors might give reliable data for a select number of furrows or positions but deployment over large numbers of furrows is cost prohibitive. Satellite navigation techniques such as Differential Global Positioning System (dGPS) or real-time kinematic (RTK) surveying equipment have both been utilized to measure water front advance for multiple furrows. A portable navigation device is used to record the movement of a person walking across the field tracing the path of the water advance (Grabham 2012). This navigation approach could be implemented using a smart phone running a GPS app such as Motion X-GPS, which will record the path and times of the persons movement.

Alternatively, water advance can be observed using a camera capturing either visual or thermal-infrared imagery set up in a balloon, tower or a small unmanned aerial vehicle (UAV) (Long et al. 2016).

3.4. Water depth

Water depth (at the furrow scale) is another important measurement. Infield depths can be used to determine surface storage volume required for the volume balance analysis.

These measurements can be collected using either simple methodology, such as using a hand-held ruler, or using more sophisticated techniques such as utilising water depth sensors (Mindata™ water depth probes, Unidata™ water depth probes). Water depth

sensors can also be useful in collecting water advance measurements (Grabham 2012) or flow rate measurements, for instance by installing them on a flume, (Koech et al. 2010).

The prohibitive cost of using large numbers of depth sensors limits their usefulness in irrigation systems characterised with variability of distribution flows between furrows such as FRSBO and FNSBO_Re. However, these sophisticated sensors can provide dynamic data during irrigation events.

Saxon and Dye (1995) developed a simple and relatively inexpensive gauge ($50-$75 in 1995) which can be used to measure peak water level once during each irrigation event (Figure 3.1). This device works based on the buoyancy force which lifts a float when the water is rising. The float slides along a stainless-steel rod which is driven into the soil. A rubber washer glued beneath the float serves as a break to prevent the float from sliding down when the water level falls, which produces an accurate measurement.

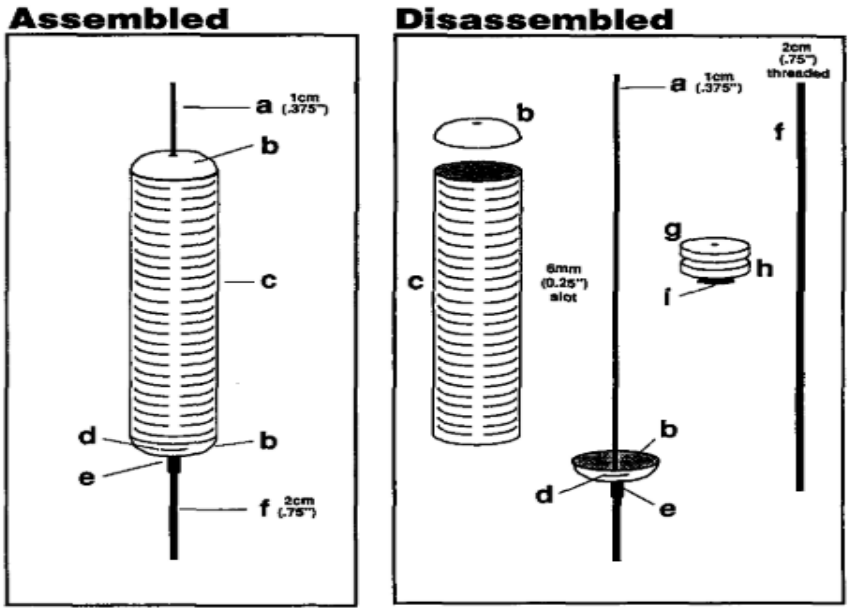

Figure 3.1 components of a simple water-level gauge: a) 1 cm diameter stainless rod; b) 10 cm PVC slip cap; c) 10 cm slotted well screen; d) 1 cm diameter welded steel washers; e) galvanized 2 cm diameter pipe coupling; f) 2 cm steel pipe with threaded upper end; g) Styrofoam floats; h) aluminium needle; rubber washer. Figure adapted from (Saxon & Dye 1995).

3.5. Infiltration

3.5.1. Introduction

Infiltration is a particularly significant parameter in the design and management of surface irrigation. Unfortunately, it is also one of the hardest parameters to measure accurately in the field (Nasseri et al. 2008; Walker & Skogerboe 1987).

The infiltration process could be described as one dimensional soil water movement (vertical) as it occurs in level basins, or two-dimensionsional if occurring in the furrow (Jensen 1980).

The term 'Intake rate' refers to the infiltration from the furrow into the soil, so it depends on both furrow dimensions and soil properties. The term 'infiltration rate' applies to a level surface ponded with water (Israelsen & Hansen 1962).

Infiltration rate is commonly described as an empirical function of opportunity time. Empirical equations such as Kostiakov and Kostiakov-Lewis (Modified Kostiakov) are widely used in surface irrigation (Holzapfel et al. 2004). Clemmens (1983) found that a Modified Kostiakov model provided reliable estimations for both cumulative depth of infiltration and infiltration rate.

The original Kostiakov equations of cumulated infiltrated depth (Equation 3.1) and infiltration rate (Equation 3.2) are:

$$Z = k\,\tau^{a} \qquad 3.1$$

$$Z_r = ak\,\tau^{a-1} \qquad 3.2$$

Where: Z is cumulative infiltrated depth (mm);

Z_r is infiltration rate (mm/min);

τ is infiltration opportunity time (min);

k is an empirical parameter ($mm^3\ min^a\ mm^{-1}$) representing the value of Z at time of one minute;

a is an empirical parameter (unit less)

There are theoretical limitations in the Kostiakov equation associated with long infiltration time where the infiltration rate value approaches zero. This could suit surface irrigation systems which involve (undergo) short ponding times (infiltration opportunity times do not exceed 3 to 4 hours). To overcome this limitation, it was suggested to add the value of final infiltration rate (f_o) to the Equation 3.2 to obtain the Modified Kostiakov equation of infiltration rate (Walker et al. 2006). The Modified Kostiakov equations of cumulated infiltrated depth (Equation 3.3 and infiltration rate (Equation 3.4) are:

$$Z = k\,\tau^a + f_o\tau \qquad 3.3$$

$$Z_r = ak\,\tau^{a-1} + f_o \qquad 3.4$$

3.5.2. Factors influencing infiltration

There are several factors which impact on the infiltration rate such as: depth of water; furrow dimensions; soil texture; soil structure; soil compaction; initial water content; surface sealing and crusting (Benami & Ofen 1983; Israelsen & Hansen 1962). In addition, the infiltration rate varies both spatially and temporally across the field, which made the evaluation of the surface irrigation performance a major challenge.

The following sections will discuss the most relevant factors to the fields studied in this PhD.

3.5.2.1. Soil compaction

Compaction is one of most important factors in this study that has an influence on the irrigation evaluation. Some furrows become compacted due to machinery wheel tracks, which leads to a variation in the infiltration characteristics between furrows, and because of the common supply system in FNSBO_Re systems could change the amount of water flowing into that furrow. The severity of compaction might change throughout the season depending on machinery and cultivation operations.

The relative size and weight of agricultural machinery has significantly increased in the last few decades, which may have increased the compacted depth and its severity within the soil profile in agricultural lands (Sivarajan et al. 2018; Van Dijck & Van Asch 2002). It is reported the wheel tracks contribute significantly to runoff because those furrows display low infiltration capacity (Van Dijck & Van Asch 2002; Voorhees et al. 1979). Van Dijck and Van Asch (2002) studied the effect of soil compaction over two layers of the soil profile (topsoil and subsoil) on the infiltration and run off. They found that lower values of saturated infiltration rates occur in the subsoil compared to the topsoil, as a result of soil compaction.

Allen and Musick (1997) stated that the variation in the infiltration rate between wheeled and non-wheeled furrows decreased from between 40 to 50% when using heavy tractors (approximately 8.2 tons). Furthermore the infiltration rate declined by an additional 23% when using tractors weighing 8.2 tons compared with tractors weighing 4.1 tons.

Grabham (2012) found that the average inflow rate in the wheeled trafficked furrows (WF) was 37% higher than the non-trafficked wheeled furrows (non-WF), and the average elevation of the furrow bottom of the WFs was 17 mm lower than the non-WF.

On the other hand, Khalid and Smith (1978) found that furrow compaction as an intended practice to improve irrigation performance in sandy soils can reduce the infiltration rate by 40%, whilst tillage practices could increase cumulative infiltration by up to 61% (Lipiec et al. 2006).

3.5.2.2. Furrow size and shape

When machinery occurs, the properties of the furrow and the soil contained within the furrow may change. The size of the wheeled tracked furrows is often greater than the non-wheeled furrows, and the profile of the furrow shape changes accordingly.

Furrow size and shape influences the amount of infiltrated water because it determines the area of contact (wetted perimeter) between water and the soil (Trout 1992). Holzapfel et al. (2004) found that the accumulated infiltrated water in a wide furrow was 30% larger than in a narrow furrow. Izadi and Wallender (1985) found that about a third of the variability of infiltration can be attributed to variances in the wetted perimeter. These studies have shown there is a noticeable correlation between infiltration and the wetted perimeter. It should be noted however that soil cracks can dominate the infiltration process and reduce the effect of the wetted perimeter (Izadi & Wallender 1985).

3.5.2.3. Infiltration opportunity time

Nasseri et al. (2008) studied the impact of several variables on cumulative infiltration using blocked furrow infiltrometers on sandy loam soil. They found that the cumulative infiltration was highly sensitive to the opportunity time compared with other variables such as flow depth, initial soil water content, flow area, and wetted perimeter. (Nasseri et al. 2004) claim that 63.52% of the variation in cumulative infiltration correlates to infiltration opportunity time when the other variables are assumed constant.

3.5.2.4. Soil texture

The proportion of gravel, sand, silt, and clay sized particles which comprise the mineral fraction of the soil, determines soil texture. Particle sizes (measured by effective particle diameter in mm) range from gravel (>2.0), to sand (2.0 to 0.05), silt (0.05 to 0.002) and the much smaller clay particles (<0.002) (Jensen 1980).

Infiltration rates in coarse-textured (or light) soils such as sand or loam are greater than in fine-textured (or heavy) soils such as clay, because the coarse soils have larger macro pore space than fine soils (Israelsen & Hansen 1962). Ben-Hur et al. (1985)

studied the effect of soil texture on the infiltration rate in crusted soil using a rain simulator. They found that soils with approximately 20% clay had the lowest infiltration rate. Much of the soils in Australian cropping regions have in excess of 50% clay content. Cracking clay soil (black earths and grey and brown clays) dominating most cotton growing areas in Australia (McKenzie 1998). Higher clay content soils are more likely to exhibit cracking when dry which leads to high initial infiltration rates in the first few minutes after wetting followed by low continuing infiltration rates.

3.5.3. Infiltration measurements

Several approaches can be adopted to estimate infiltration characteristics in surface irrigation systems based on the suitability and capacity to evaluate the system, and the time and effort which can be invested in the evaluation (Walker & Skogerboe 1987).

In the past, cylinder infiltrometers, ponding and inflow-outflow field measurements were the most commonly adopted techniques to estimate infiltration (Walker & Skogerboe 1987). A typical cylinder infiltrometer consists of a metal cylinder opened from both sides (diameter not less 25 cm, height 40 cm) driven into the soil to approximately 150 cm. The cylinder is then filled with water to a reference level usually equal to the desired depth of irrigation. Infiltration measurements are conducted by taking water depths at appropriate time intervals. The ponding method has the same concept as the cylinder infiltrometer method. However, ponds or earth dikes are constructed on the ground surface rather than driving a metal cylinder being into the soil (James 1988).

Cylinder infiltrometers and ponding methods are more suited to level basins rather than furrows because they do not take into account the geometric conditions (wetted perimeter) of a furrow. In a furrow, a considerable proportion of infiltration occurs at the furrow sides rather than at the base of the furrow (Walker & Skogerboe 1987). The infiltration process could be described as one dimensional (vertical) in level basins, as opposed to two-dimensional in furrows (Jensen 1980).

The blocked furrow method was developed to overcome this drawback in both cylinder infiltrometer and ponding methods. The blocked furrow method requires selecting

three adjoining furrows for the measurement. The infiltration measurements are conducted on a section of the middle (intermediate) furrow isolated by two ends plates driven into the soil to a depth 150 cm. Usually the measured part of the furrow ranges from 30 to 120 cm in length. That specific part of the furrow is then filled with water to about the same depth as would be expected in the irrigation event. Infiltration measurements are then conducted by measuring the volume of water required to maintain that precise depth of water (Walker & Skogerboe 1987). The smaller the section measured in the blocked furrow method, the less representative the results would be of real conditions in the furrow such as initial water content, slope, flow area or wetted perimeter.

Estimating the infiltration based on methods which use stagnant conditions such as cylinder infiltrometers, ponding and blocked furrows, fails to present realistic flowing conditions (Walker & Skogerboe 1987).

The inflow-outflow method can overcome the limitations of small scale measurements and stagnant conditions. As the name suggests this method involves the measurement of inflow and outflow conducted during the irrigation at two ends of a specified length of furrow. Flumes or weirs can be used to collect the flow rate measurements. The distance between the two flow rate devices ranges from 30 to 100 m. The infiltration rate is determined when the water depth in the furrow reaches an approximately constant value, by calculating the differences between inflow and outflow rates (James 1988). The main concern related to this method is the overestimation of the infiltration rate at the downstream part of the measured furrow, due to backwater occurring at the downstream flume (Walker & Skogerboe 1987). It is important to remember that the inflow-outflow method represents the total infiltration for the entire measured length but not necessarily the infiltration distribution along that length. Therefore, combining advance measurements with the inflow-outflow method will provide better representation for infiltration parameters (Walker & Skogerboe 1987).

Advance and recession measurements are used to determine the infiltration opportunity time over the whole field (or furrow), which can be used in estimation performance indicators such as application efficiency and distribution uniformity (Walker & Skogerboe 1987). Walker and Skogerboe (1987) concluded that estimating

the infiltration parameters based on the volume balance method will yield parameters which are the most representative of the whole furrow.

3.5.4. Infiltration estimation from irrigation measurements

Selecting the most appropriate technique to estimate the soil infiltration parameters in the irrigation study is a considerable challenge.

Adopting an indirect or inverse approach to estimate the infiltration parameters from other irrigation field measurements is a more reliable approach for evaluation at the field scale than compared with infiltrometer measurements (Gillies 2008). The inverse approach involves fitting the adopted hydraulic model to field measurements by solving for the unknown infiltration parameters. The estimation of soil infiltration parameters at the field scale is normally reliant on flow rates and water advance measurements (Benami & Ofen 1983).

Most inverse approaches are based on the volume balance model, due to its simplicity and the possibility of a direct solution. The following subheadings will introduce selected inverse solution techniques

3.5.4.1. Volume balance

The volume balance principle can be used to describe the irrigation process in surface irrigation systems. During the irrigation process, part of the water diverted into the furrow infiltrates into the soil, while the rest either keeps flowing to the end of the furrow to leave the furrow as runoff, or if the furrow's downstream end is blocked will gradually infiltrate. The volume balance principle based on the conservation of mass can be applied to this system. The volume balance states that at any time during the irrigation process, the entire volume of diverted water into the furrow is equal to the infiltrated volume into soil, plus the temporarily stored volume at the soil surface, plus runoff (if present) (Strelkoff & Clemmens 2007), as described in the Equations 3.5 or 3.6.

The infiltration parameters can be determined based on the inverse approach of volume balance (ASAE 2008; Gillies 2008; James 1988; Walker & Skogerboe 1987). The

basic form of the volume balance equations is given below. The volume balance during the advance phase is comprised of the inflow (Q_0t), the infiltrated volume (V_I) and surface storage volume (V_S).

$$Q_o t = V_Z + V_S \quad 3.5$$

Where

Q_o is constant flow rate m^3/s

t is the time since commencement of the irrigation, seconds.

V_Z is infiltrated volume, m^3.

V_S is volume of water on soil surface, m^3.

Equation 3.5 states that the applied water volume equals the sum of infiltrated volume and surface storage volume. The volume of applied water is determined by the product multiplication of constant flow rate (Q) by elapsed irrigation time.

Runoff volume (V_R) can be added to the right hand side of Equation 3.5 (Strelkoff & Clemmens 2007) to give an equation which is valid for the entire length of the event:

$$Q_o t = V_Z + V_S + V_R \quad 3.6$$

The average infiltrated volume can be estimated from Equation 3.6 if the surface storage volume and runoff volume are known using the inverse solution for that equation.

The infiltrated depth at any given infiltration opportunity time (IOT) can be determined by the chosen infiltration equation such as the Modified Kostiakov Equation 3.3,

The opportunity time at a given position *x* along the furrow can be determined using the advance time to that distance, t_x. Substituting this opportunity time into Equation 3.3 gives an expression to define the cumulative infiltrated depth at a certain distance during the advance phase:

$$Z_x = k\,(t - t_x)^a + f_o(t - t_x) \qquad 3.7$$

Where

Z_x is cumulative infiltrated depth at a distance *x*.

t_x is the advance time, i.e. time required to reach a distance *x*.

t is the time since commencement of the irrigation, min.

The advance trajectory can be represented mathematically using a simple power function (ASAE 2008).

$$x = p\,t_x^r \qquad 3.8$$

Where: *x* is the advance distance;

t_x is the time of advance;

p, *r* are empirical parameters.

The volume of infiltrated water at any distance during the advance phase can be obtained by substituting in Equation 3.8 into Equation 3.7 and integrating over the advance distance:

$$V_z = \sigma_{z1} k \tau^a x + \sigma_{z2} f_o \tau x \qquad 3.9$$

Where: σ_{z1} and σ_{z2} are the subsurface shape factors defined as ((Walker & Skogerboe 1987)):

$$\sigma_{z1} = \frac{a + r\,(1 - a) + 1}{(1 + a)(1 + r)} \quad 3.10$$

$$\sigma_{z2} = \frac{1}{1 + r} \quad 3.11$$

The volume of water above the soil surface (V_S) is determined by integrating the flow area over the advance distance:

$$V_S = \sigma_S A_o x \quad 3.12$$

Where σ_S is the surface storage shape factor (usually chosen as a constant between 0.74 – 0.8, for furrows (Elliott & Walker 1982; Mailhol & Gonzalez 1993; Scaloppi et al. 1995).

A_o is cross sectional flow area at the furrow inlet.

Substituting Equations 3.9 and 3.12 into Equation 3.6 yields:

$$Q_o t = \sigma_S A_o x + \sigma_{z1} k \tau^a x + \sigma_{z2} f_o \tau x + V_R \quad 3.13$$

The infiltration parameters (k and a) can be solved in Equation 3.13 using the inverse solution where the other field measurements are collected.

The final infiltration rate (f_o) for can be estimated separately as described in the inflow-outflow method in Section 3.5.3, where the value f_o can be estimated when the outflow rate reaches a constant value using the following equation (ASAE 2008):

$$f_o = \frac{(Q_{in} - Q_{out})}{WL} \quad 3.14$$

Where: Q_{in}, Q_{out} are furrow inflow and outflow rate, respectively;

W, L are furrow spacing and furrow length, respectively.

However, when the outflow rate measurements are unavailable or not applicable (as is the case when the outflow does not reach a constant value (Gillies 2008)), the value of

f_o may be assumed to be zero thereby reducing the infiltration equation to the primary form of Kostiakov's infiltration Equation 3.1

3.5.4.2. Two-Point method

The Two-Point method (Elliott & Walker 1982) is an example of the inverse solution for the volume balance. It is one of the most common techniques used to estimate the average infiltration parameters. Only a few measurements are required and mathematical simplicity leads to this method being widely adopted (Bautista et al. 2009). As the name suggests, the method depends on two measurement points of water front advance, one approximately half way and the other at the end of the measured furrow. The Two-Point method formulation will be covered in detail in Section 8.2.1.1. Elliott and Walker (1982) who developed this method, claimed that it is superior to the traditional methods in estimating infiltration parameters. Holzapfel et al. (2004) found that the Two-Point method offered more accurate values of the Kostiakov infiltration parameters for a wide furrow (furrow top width 60 cm) compared with other methods including the furrow infiltrometer method, advance method, and One-point method. However, Bautista et al. (2009) and Moravejalahkami (2020) considered that the estimated parameters using the Two-Point method can be unreliable for any times in excess of the advance phase.

3.5.4.3. Computer models to estimate infiltration parameters using the volume balance

There are many computer models which have been developed to estimate infiltration parameters based on the volume balance approach. These models typically require field measurements such as water advance, flow rate, flow area and field slope. The INFILT model (McClymont & Smith 1996) and IPARM model (Gillies & Smith 2005) are two examples of such models. Both of these models use a volume balance approach in estimating the infiltration parameters.

IPARM (Infiltration Parameters from Advance and Runoff Model) can utilise two possible sets of data to estimate the infiltration parameters: both advance and runoff data, or only advance data. The estimation can be made more accurate by including both advance and runoff measurements during the storage phase of irrigation, rather

than relying solely on advance measurements. In one case, this reduced the error of estimation of the total infiltrated volume from 22% to 1% (Gillies & Smith 2005). Including the runoff data provides greater ability to represent the infiltration parameters for a time extending beyond the completion of the advance phase (Gillies & Smith 2005). IPARM's capacity to use variable inflow rather than a constant value of inflow rate has been shown to reduce the variability in the fitted infiltration function. Gillies (2008) found that accounting for the variable inflow rate reduced the variation coefficient (CV) of cumulative infiltrated depths by 18.6% and 11.5% at opportunity times of 100 and 500 minutes, respectively.

Surface irrigation simulation models such as SISCO, WinSRFR, and SIRMOD also offer the functionality to estimate infiltration parameters as a basic feature that allows them to evaluate irrigation performance and optimise operational variables. Section 3.6 will cover these models.

3.6. Simulation Models to evaluate performance

The main purposes of computerised hydraulic models are to identify the infiltration characteristics and hydraulic characteristics of a field, evaluate irrigation performance, and optimise the design and management of a field (Gillies 2008). There are four main categories of hydraulic model relevant to surface irrigation which can be ordered from the highest accuracy and complexity as follows: full hydrodynamic model, zero-inertia, kinematic wave and volume balance models (Walker & Skogerboe 1987).

Over the last few decades, there has been considerable advances in the theoretical knowledge regarding soil water physics and irrigation science, and advances in measurement technologies (such as instruments for surveying, flow rate, water advance, and soil water content.) to achieve reliable design and evaluation of the performance of irrigation systems. However, conducting evaluation of irrigation systems requires considerable resources, effort and time. The advent of the personal computer enabled users to employ hydraulic models that simulate the irrigation process. Computerized hydraulic models provide an exceptional opportunity to conduct unlimited trails to adjust many of the design and management parameters for optimal status, then evaluate these design and management parameters rather than conducting these trials in the field. They also provide an opportunity to evaluate the

irrigation performance of an existing irrigation system. This evaluation is only possible after calibration of the infiltration through an inverse approach based on conducting applicable measurements such as inflow rates, runoff and water advance and recession measurements, rather than conducting difficult and expensive direct measurements such as measuring the distribution of applied water and the deep percolation at the soil profile (Gillies 2008). The reliability of the models to evaluate the irrigation performance depends on the quality of these measurements, and again, the accuracy of the hydraulic model.

The majority of available hydraulic models are developed to accommodate the common features of surface irrigation systems. Usually, each model is developed to treat a specific range of hydraulic characteristics for certain field layouts. However, some of the hydraulic characteristics of recently developed irrigation layouts have not yet been accommodated, such as the hydraulic interaction between borders and flow entering furrows from the bottom of the field which are associated with FRSBO and FNSBO_Re irrigation systems.

3.6.1. Volume balance

The volume balance model has been the basis of many surface irrigation designs and evaluation procedures. However, it involves broad assumptions in order to avoid the complexity of the mathematical solutions of the hydrodynamic approach which result from the infiltration and advancing water on a dry bed. The volume balance disregards the dynamic nature of the flow over the surface of the porous soil media, meaning that it is unable to accommodate the temporal and spatial changes in depth and velocity of that flow. It also supposes that the average area of flow is constant and that the infiltration function is dependent only on the infiltration opportunity time and independent on flow depth. Moreover The volume balance produces an average infiltration function for the whole length of furrow (Walker & Skogerboe 1987). The Volume balance approach was designed for normal and constant slope and therefore does not suit reverse or variable slopes.

Many studies have been undertaken which improve the reliability of the volume balance techniques to estimate infiltration parameters. For instance, instead of uniform assumption for depth of flow, Bautista et al. (2012) proposed a power function of flow

depth as a function of distance along the stream in order to improve the estimation of the surface storage volume. Valiantzas (1997) suggested that the constant surface storage shape factor could be replaced by a factor which was dependent on time.

3.6.2. SISCO

Surface Irrigation Simulation Calibration and Optimisation (SISCO) is a hydraulic simulation model based on the full hydrodynamic equations (Figure 3.2) (Gillies & Smith 2015). The full hydrodynamic model, which includes the momentum and continuity equations, provides the highest reliability to represent the surface water flow. The SISCO model has the ability to simulate surface flows in either a single furrow, border or basin with temporal variability in inflow rates and spatial variability in longitudinal slope, furrow cross-sections, soil roughness and infiltration characteristics. It also provides an ability to simulate multiple furrows but that does not take into account any hydraulic interaction between the adjoining furrows.

The SISCO model has the capacity to calibrate the infiltration and roughness parameters from field measurements, which include either constant or variable inflow rates, field slopes, and furrow cross-sections utilising the full hydrodynamic model. The calibration process can accept either one or a combination of the following inputs: water advance; runoff; recession times; or water depth.

SISCO can also accommodate either blocked or free draining conditions at the downstream end of the field.

The main limitation with SISCO in relation to this research is that both the calibration and simulation functionality in the SISCO model is limited to a single furrow, border, or basin without including any hydraulic interaction between these adjoining units.

Once calibrated, the SISCO model can simulate the irrigation process then display it dynamically with animation and generate performance results for a either a single furrow, or multiple furrows.

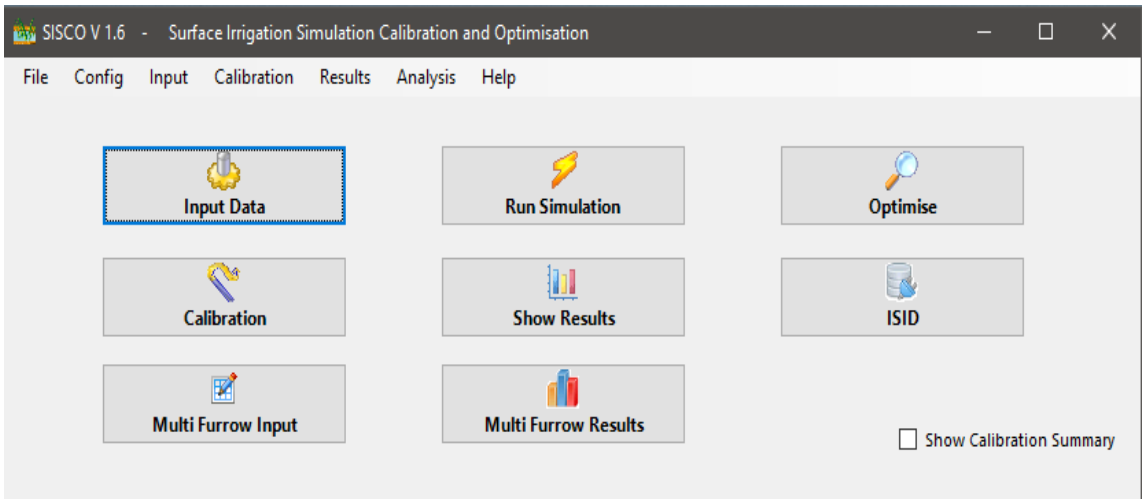

Figure 3.2 Main screen of SISCO.

3.6.3. WinSRFR

WinSRFR model (version 4.1.3) is an analysis, design, operational, and simulation model based on zero-inertia or kinematic-wave models. The zero-inertia and kinematic wave approaches employ a simplified form of the momentum equation to simulate the process of irrigation of surface systems. WinSFRF was developed by the United States Department of Agriculture (USDA). This software consists of three programs: BASIN; BORDER; and SRFR (Bautista et al. 2006). The WinSRFR model has the capacity to estimate the infiltration parameters from field measurements based on the volume balance model during the water advance phase (Elliot-Walker Two-Point method) or post-irrigation (Merriam-Keller volume balance analysis).

The estimation of infiltration parameters is implemented via the “Event Analysis” (Figure 3.3). Like SISCO, the evaluation function in the WinSRFR model allows estimating infiltration parameters for both constant or variable inflow rates, and field slopes under blocked or free draining conditions at the downstream end of the field for a single furrow, border or basin. Like SISCO, the WinSRFR model cannot accommodate the hydraulic interaction among adjoining furrows, borders or basins that are normally associated with the FRSBOs and FNSBO_Re irrigation systems. It is worth noting that the SISCO model is based on the more accurate full hydrodynamic model to estimate the infiltration parameters, whereas the WinSRFR model is based on the volume balance model.

In addition to the "Event Analysis" function, the WinSRFR model also incorporates the following functions (which are known as WinSRFR Worlds): Simulation; Physical Design; and Operational Analysis, as shown in Figure 3.3.

The "Simulation" function is utilised to predict the surface flow and infiltration and generate the irrigation performance results. The "Physical Design" function allows to optimise field dimensions for known soil infiltration and roughness characteristics. The "Operational Analysis" function allows to optimise inflow rates and cut-off times for a given combination of field characteristics.

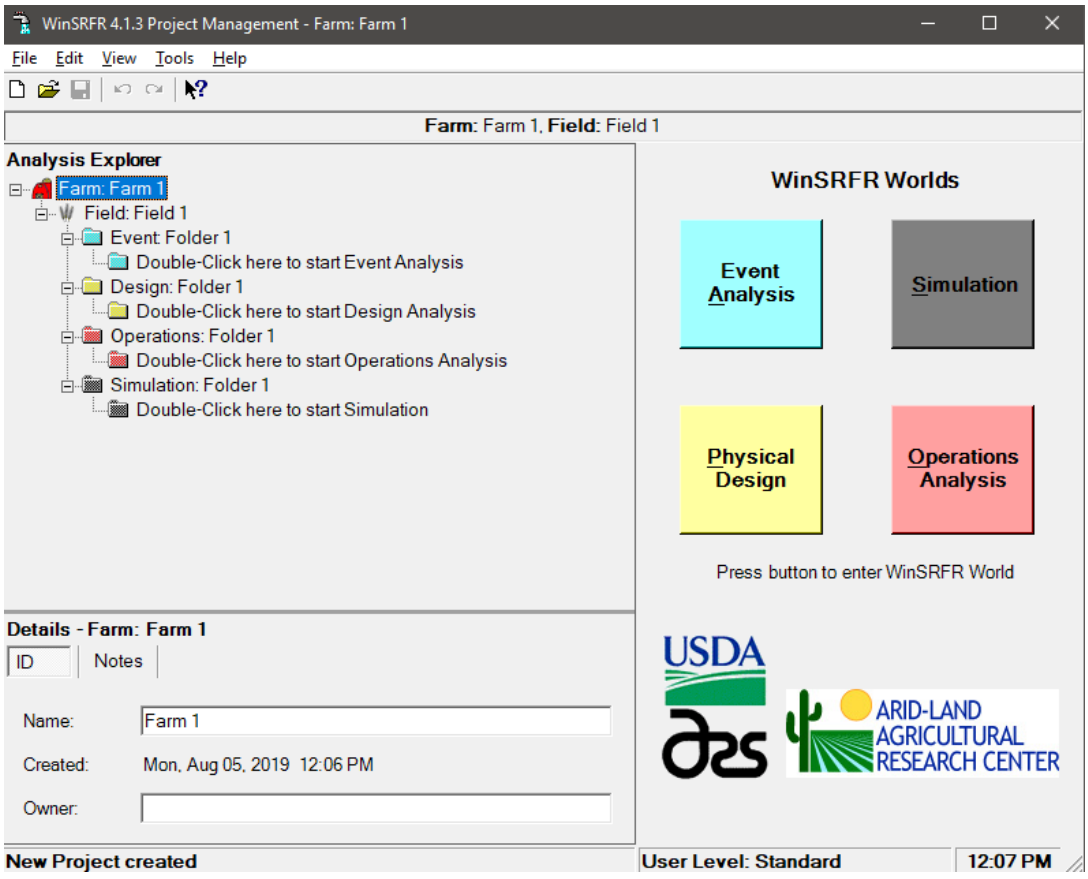

Figure 3.3 The main screen of the WinSRFR model.

3.6.4. SIRMOD

SIRMOD is a surface irrigation simulation, evaluation and design model (Walker 2003). The SIRMOD III software (Figure 3.4) provides the ability to model the surface irrigation process in one dimension utilising either a kinematic-wave model, zero-

inertia model, or full hydrodynamic model. The SIRMOD model has two options to estimate the infiltration parameters. The first option is the standard Two-Point method from advance measurements and the second is a multilevel calibration utilising the full hydrodynamic model and requiring a combination of advance, runoff and recession measurements. SIRMOD III can accommodate variable inflow rate, and up to three constant values of field slope, and blocked or free draining conditions at the downstream end of the field. It does not have the capacity to define reverse slope. It also does not accommodate the draining-back condition at the upstream end of the field.

Figure 3.4 The main screen of SIRMOD III.

3.6.5. Clemmens' approach

Clemmens (2007a) and Clemmens (2007b) developed a simple procedure which can be used in the design of modern irrigation systems such as FLBAS, and which can be easily implemented via spreadsheet programs. The calculation procedure was developed based on a one-dimensional volume balance approach. Empirical approximations are used where needed, for instance to describe infiltration and

roughness. Water advance and recession curves are determined based on the volume balance, assuming that the recession occurs simultaneously across the length of the field. This procedure assumes a constant inflow rate is applied into the furrows of the FLBAS irrigation system.

The calculations include computing the advance, recession, application times and the resulting distribution of infiltrated water for a specific set of conditions. A trial and error process is implemented to compute solutions. The spreadsheet can then determine appropriate field dimensions and management variables.

3.6.6. B2B

The B2B model (Grabham 2012) is based on the volume balance procedure developed by (Clemmens 2007b). In the B2B model, the Clemmens' procedure was modified to accommodate the hydraulic characteristics associated with the FRSBO system. The B2B model is coded via Microsoft Visual Basic instead of adopting an arduous trial and error system (using spreadsheet-based calculations), as adopted by (Clemmens 2007a) (Figure 3.5).

The B2B model was developed to simulate the hydraulics of a FRSBO irrigation system to describe the irrigation event of each individual border in the context of the whole field. Therefore, it has the capacity to simulate the hydraulic interaction between adjoining borders (up to nine borders) and simulate the irrigation process within borders, but does not accommodate the variability in diverting water to different furrows within each border. Darcy-Weisbach's equation was used to describe flows between borders, where a pipe was the interconnecting structure between them. B2B was developed to accommodate the specific hydraulic conditions associated with the fields measured by Grabham (2012) and therefore it may not accommodate the field layout measured in this PhD. As the model name suggests, B2B simulates the border to border hydraulic interaction (or bay to bay as in Grabham's (2012) terminology) to obtain the appropriate size of the interconnecting structure, vertical separation between borders and other important design features of this system. B2B does not estimate the infiltration characteristics but instead requires use of one of the other available methods.

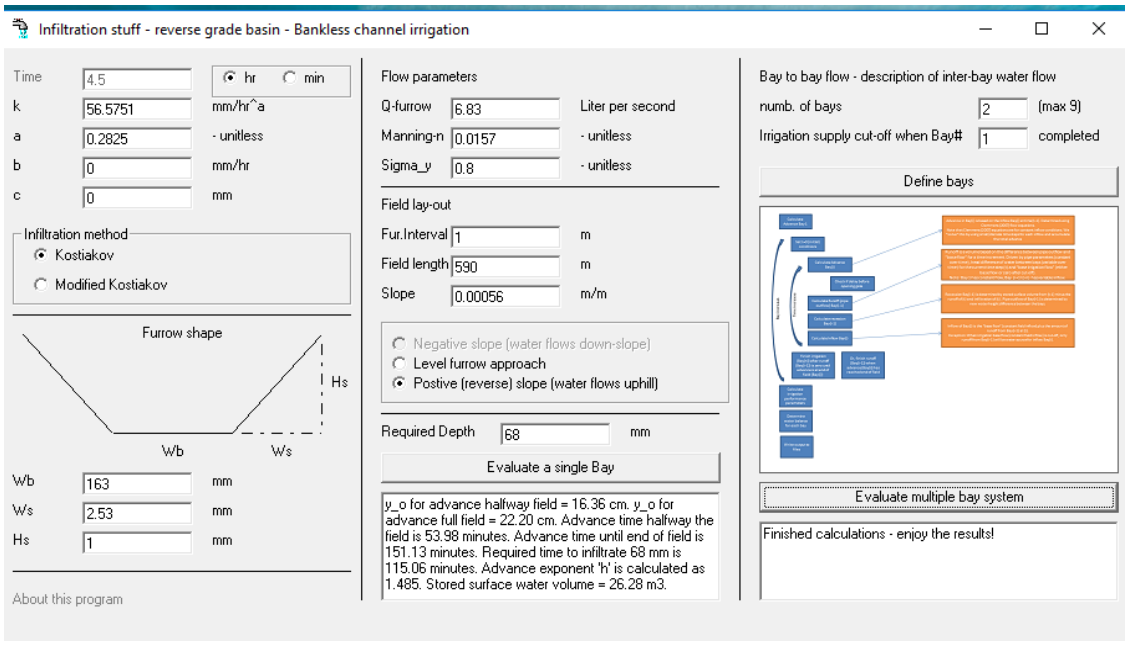

Figure 3.5 The main screen of the B2B model.

As a result, B2B is a design model with the capacity to provide the performance behaviour for combinations of design and management variables. While this model provides the capability to examine the impact of special characteristics associated with FRSBO systems (reverse slope and vertical separation between borders on the irrigation performance of the system), it also has the capacity to examine normal variables such as border dimensions (number of furrows), field supply inflow rate, irrigation deficits, and irrigation duration.

On the other hand, the B2B model disregards flow entering furrows from the bottom end of the field, which will have an impact on the predicted performance (Grabham 2012). In addition, this model assumes that all water drains back to the top end of the field, and that no runoff from the bottom end of the field occurs. Finally, this model does not accommodate the normal (or negative) slope of the field which means that it will not satisfactory model the FNSBO_Re systems which are the focus of this PhD.

Table 3.1 shows a summary of hydraulic models and their main features and their capacity to model the irrigation process of the current irrigation system.

Table 3.1 Hydraulic models and their main features and capacity to model the irrigation process of the current irrigation system.

Features	**Model Name**						
	Two-Point	**IPARM**	**SISCO**	**WinSRFR**	**SIRMOD**	**Clemmens**	**B2B**
Governing equation for estimating infiltration)	Volume balance	Volume balance	Full hydrodynamic	Volume balance	Volume balance/ full hydrodynamic[1]	Volume balance	Volume balance
Governing equation for simulation	n/a	n/a	Full hydrodynamic	Zero-inertia, and Kinematic Wave	Full hydrodynamic, Zero-inertia or Kinematic Wave	Volume balance	Volume balance
Model functions	Estimating infiltration	Estimating infiltration	Estimating infiltration, Evaluation and Design	Estimating infiltration, Evaluation and Design	Estimating infiltration, Evaluation and Design	Design	Design
Field or furrow longitudinal slope	Constant	Variable / Constant	Variable / Constant	Variable / Constant	Variable / Constant	Constant	Constant (level or
Interaction between borders	No	No	No	No	No	No	Yes
Difference in Flows among furrows	No	No	Yes	No	No	No	No
Backwards flow off top of field (drain-back)	No	No	Yes	Yes	No	No	Yes
Flow entering furrows from bottom of field	No	No	No	No	No	No	No

[1] SIRMOD III includes a multilevel calibration which uses the full hydrodynamic model

3.6.7. Conclusion:

Examples of hydraulic models were reviewed in the previous sections (Sections 3.6.2 to 3.6.6). Table 3.1 shows a summary of hydraulic models and their main features and their capacity to model the irrigation process of the current irrigation system. It is clear that none of the hydraulic models reviewed are ideal for the near zero slope furrowed border irrigation system with a common water supply (FNSBO_Re). There are limitations in each model which are unable to accommodate certain specific hydraulic characteristics associated with these systems.

None of the available models accommodate the variability in diverting flows between adjoining furrows. All available models were designed to model the irrigation process in a single furrow, border, or basin individually with the exception of B2B and SISCO. SISCO does model multiple furrows simultaneously within a single border with differing infiltration characteristics and flows. However, the user must specify these flows as SISCO lacks the ability to predict behaviour of furrows with a common interconnected supply. The B2B model provides the capacity to accommodate the hydraulic interaction between adjoining borders, but for design purposes only. The B2B model assumes that all furrows within each border have identical inflows and infiltration characteristics.

The B2B model was developed to suit specific hydraulic conditions associated with Grabham's study. A relatively small pipe (0.58 and 0.755 m) was the interconnecting structure between the borders, compared with the large check gate (7 to 10 m width) in the current study. Hydraulically, the water flow characteristics in the bankless channel of Grabham's field are dominated by this small pipe, which causes a larger head loss compared with an insignificant head loss associated with the larger interconnecting structure in the current study. Also, the B2B model assumes that there is no runoff from the bottom end of the field, which is not the situation in the current field studied.

Theoretically, it is possible to derive the hydraulic parameters of B2B in terms of equivalent pipe diameter, pipe length and pipe friction factor to replicate the characteristics of the large structures in the current study. However, the assumption of

draining back all the water to the top end of the field within B2B does not fit the layout or flow conditions in the current study, thus the B2B model cannot be adopted.

Therefore, none of the available models considered have the capacity to evaluate a set of adjoining furrows within a border with a common water supply or the interactions between adjacent borders for the FNSBO_Re layout.

3.7. Surveying

The movement and distribution of applied water in a surface irrigation system is governed by gravity and therefore gaining an understanding of field slopes and elevations is desired. This data is of particular importance for FNSBO_Re systems because of the reverse of field slope partway down the field and the common water supply. Conducting a field elevation survey provides a useful data set to aid in evaluating the irrigation performance of surface systems. Surveying measurements are required to measure field dimensions, longitudinal slope, furrow cross sections, geometry of entry from head channel into furrows and water levels. These measurements can be collected in a number of ways but a total station provides the means to collect accurate measurements in a short period of time. A total station is an electronic/optical instrument which is commonly used in surveying which measures distances and angles using laser reflectors. Staff, bubble, and tripod are necessary accessories of this surveying instrument, as well as measuring tape and a ruler.

3.8. Analysis Techniques

3.8.1. Introduction

The special circumstances associated with near zero slope furrowed border irrigation systems with a common water supply (FNSBO_Re) require the adoption of unique methodologies for analysis. Developing a new methodology will be part of this study, which is particularly focussed on the anticipated variation in flows between furrows and the hydraulic interaction between borders.

The analysis will focus on the following unique characteristics of the FNSBO_Re such as:

- Impact of inter-furrow variability in infiltration characteristics
- Non uniformity of furrow flow rates caused by infiltration characteristics differences (because of compaction and changes in furrow size and shape).
- Impact of elevation variation at both the furrow and border scale.
- The initial part of the field with reverse grade and drainback which is not accommodated by existing approaches

3.8.2. Inverse Solution for Infiltration

Estimating the infiltration parameters using measured field data through the inverse approach provides a more representative prediction of the infiltration compared with direct physical measurement (which is expensive and difficult to perform) or other approaches such as using a cylinder infiltrometer, ponding method and inflow-outflow measurements that were discussed in Section 3.5.3.

From the literature review a list of components required by most inverse solution methods and performance evaluation approaches is as follows:

- Field geometry and slope
- Furrow cross sections
- Inflow discharge for individual furrows basis or entire border basis,
- Outflow water discharge,
- Advance measurements
- Recession measurements,
- Water depths or surface storage volumes at various times during an irrigation event, and
- Soil moisture status (deficit/depletion) prior to and post irrigation events,

The technique described in later chapters will utilise a subset of these important measurements.

3.8.3. Techniques to develop performance measures based on opportunity time at border scale

Advance sensors, which are commonly used in the evaluation of furrow irrigation systems in the Australia typically only measure between 4 and 8 adjacent furrows. It is anticipated that the variability in the water advance between furrows within the same border in the FNSBO_Re systems is higher than for traditional furrows. Therefore it was concluded that traditional advance sensors are not considered appropriate for this study as they only represent a small part of the border.

An overall border irrigation performance may be developed based on opportunity time analysis from a combination of advance sensors and aerial images. The opportunity time at each position in the field defines the depth applied at that point. A camera installed in a small remote-controlled Unmanned Aerial Vehicle (UAV) or a helium balloon, could be used to snap a series of photos/images during irrigation events to monitor both advance and recession phases. This device could fly above the field at a predefined height and on a programmable flight path, to enable it to cover the whole field. A simple technique could then be developed to extract opportunity time data from the collected measurements.

3.8.4. Evaluation of performance

Irrigation performance indicators (AE, DU and RE) as discussed in Section 2.6 will be calculated from the measured data. This process may require development of novel techniques depending on the characteristics of the systems and data collected.

3.8.5. Statistical analysis

Statistical analysis can help in determining the most important factors that cause variability in the water advance and inflow rates between furrows in the FNSBO_Re irrigation system.

3.9. Conclusion

There are a number of hydraulic characteristics particular to the near zero slope furrowed border irrigation systems with a common water supply (FNSBO_Re) which require special consideration. The unique field layout poses significant issues to both the measurement and evaluation of these systems. These characteristics include: the presence a reverse slope for parts of or the entire length of the field; the common water supply resulting in variability in diverting flows between adjoining furrows; and the hydraulic interaction in the interconnecting hydraulic structures between adjoining borders. Existing evaluation techniques could be applied but it is likely that new methods must be adopted in order to adequately assess these systems.

For example, utilising conventional devices such as weirs to measure the furrow flow rate are not appropriate for the hydraulic conditions associated with flows on reverse or near-zero slopes. Therefore, adopting new techniques to measure flow velocity based on electromagnetic or ultrasonic technologies might be more appropriate. However, variability in flows between furrows means that intensive measurements are required in order to accurately represent the entire field. Also, traditional advance sensors are inadequate to accommodate the anticipated variance in the water advance in the system studied. Therefore, developing new techniques such as utilisation of a UAV could provide adequate broad scale measurements to overcome the variability associated with this kind of surface irrigation system.

The inverse approach to estimate the infiltration parameters based on the measurements obtained during the irrigation event, is be the most reliable approach because of its capacity to represent the infiltration characteristics of the whole furrow, as opposed to the use of direct physical measurements, which are both expensive and difficult to perform. Also, the widespread availability of many computerised hydraulic simulation models, which adopt the inverse solution approach to solve infiltration parameters using measured field data, make the inverse approach a more attractive option. Having said that, it should be noted that none of these simulation models can accommodate all the special aspects associated with the system studied (3.6.7). Hence some modification is required in terms of data collection and analysis approach in order to apply the inverse method for FNSBO_Re systems.

CHAPTER FOUR

Methodology - Season 1

4.1. Introduction

The discussion in Chapters 2 and 3 has identified several special characteristics associated with near zero slope furrowed border irrigation systems with a common water supply (FNSBO_Re) which pose challenges for measurement and modelling. As a result, existing techniques for evaluation of surface irrigation systems are unable to accommodate FNSBO_Re systems. Finding and developing appropriate tools and concepts to understand the hydraulic behaviour of these systems is one of the main goals of this study. This chapter describes the activity during the first year of field trials towards the development of an appropriate methodology to assess the irrigation performance of these systems.

4.2. Field site

Field measurements were conducted on a commercial farm in Boggabilla in New South Wales. Specifically, the study was carried out on two fields, each planted with cotton in the summer of 2017, belonging to property called Turkey Lagoon (Latitude and Longitude are -28.684662, 150.378044, respectively) (Figure 4.1). The APSOIL database (Dalgliesh et al. 2012; Holzworth et al. 2014) was used to provide a general idea of the soil characteristics such as soil texture and bulk density at the closest possible location to the study fields. APSoil is a database of soil water characteristics that covers many cropping regions of Australia.

There was no evidence at the site of the existence of any impervious layer that may influence crop growth or infiltration rates. Therefore, no measurements of bulk density or hydraulic permeability were performed to quantify these effects.The water table was likely to be at a significant depth from the root zone such that it would not have any impact on plant growth or infiltration processes.

4.3. Surveying field and furrow geometry

4.3.1. Field survey

A robotic total station (Leica TCRA1203) was used to collect accurate level measurements in Field 3. These measurements were taken to find the changes in longitudinal slope down the field and the geometry of the bankless channel. These measurements will be used to interpret the hydraulic behaviour in Field 3. Level measurements were undertaken on 13 adjoining furrows at the second furrowed border at variable intervals along the field length. They were also carried out along the bankless channel across the width of the border.

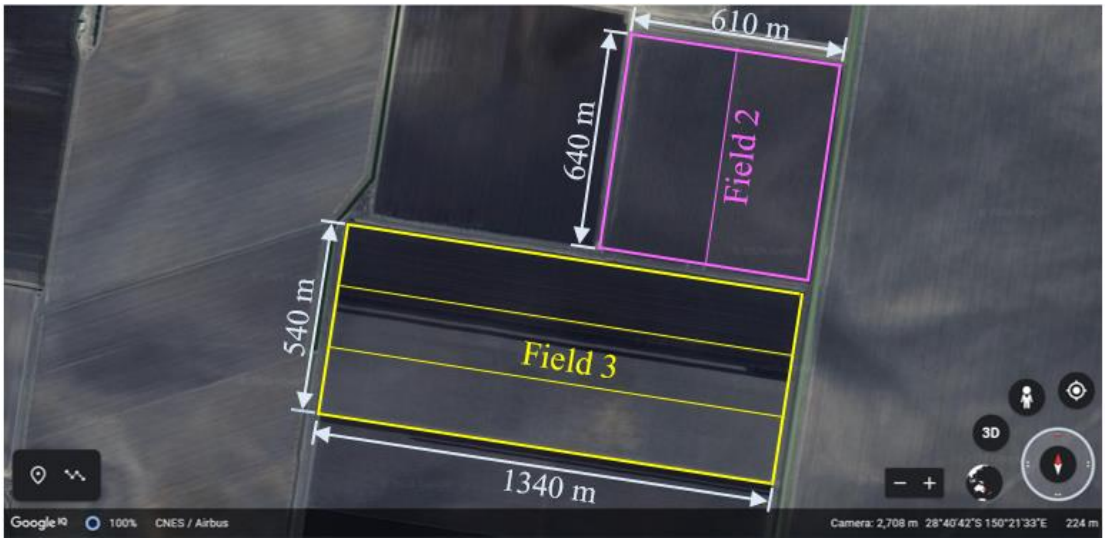

Figure 4.1 Satellite map of Field 2 and 3 sites in 2017/2018.

4.3.2. Furrow geometry

Simple field measurements, using a ruler, had been conducted on 12 adjoining furrows at the 2nd furrowed border (starting from the 3rd furrow to the 14th furrow) to record furrow cross sections in Field 3. These measurements were conducted at different interval distances measured from the entrance of the furrows (5, 90, 300, 900 m). The idea behind selecting 12 adjoining furrows was to cover the repeated pattern of adjoining furrows due to utilizing machines running on controlled traffic with a spacing of either 6 or 12 m throughout the cultivation, planting, fertilizing, and

harvesting process. These measurements include the top width, middle width, bottom width, and the maximum depth of the furrows, as shown in Figure 4.2. These measurements display a rudimentary level of accuracy; specifying the start and end points using two rulers and looking at the furrow cross section closely. These measurements give a general conception of the flowing cross-sectional areas of the furrows and impact of the machines' movement on furrow size and soil compaction.

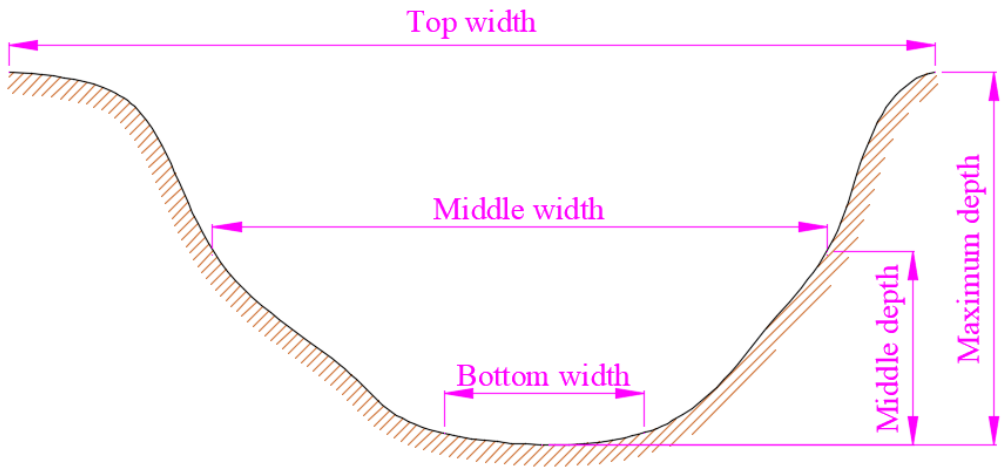

Figure 4.2 Furrow cross section dimensions.

4.4. Field 2

Field 2 displays laser-graded surfaces with approximately zero slope. The first 50 m from the top end of this field was designed to have slight positive (averaged of + 0.223% (or 1:450), from the second season surveying) slope and then negative slope (~ - 0.0597% (or 1:1750), from the second season surveying) for the remainder of the field, according to the farm manager. Also, no slope was evident across the border. A vertical separation exists between the borders of about 150 mm (according to the farm manager). Figure 4.3 shows the schematic arrangement of Field 2. The dimensions of Field 2 are 640 m in length and 612 m in width. Field 2 consists of two furrowed borders connected with a bankless channel. The first furrowed border has 312 furrows while the second border has 300 furrows. The cotton was planted in beds (Figure 4.4) with a furrow spacing of one metre (from bed to bed or furrow to furrow). This represents a common crop spacing used in the Australian cotton industry. Field 2 has

one check gate at the top end of the field set between the two adjoining borders, and another check gate at the bottom end of the field set between the two adjoining borders (Figure 4.3). The check gate at the top end of field 2 consists of four multi linked Padman Stops box culverts (Figure 4.5). The dimensions of the top field check gate are 7.08 m wide by 0.645 m high, while the check gate at the bottom end of Field 2 consists of three multi linked Padman box culverts. The total dimensions of the bottom field check gate are 5.31 m wide by 0.645 m high. To close the check gate, there is a reel and metal cable to control the opening angle, where at the vertical position (90º) the gate is completely shut, while at the horizontal position (0º) the gate is completely open. To obtain partial opening, the gate could be inclined at an angle less than vertical.

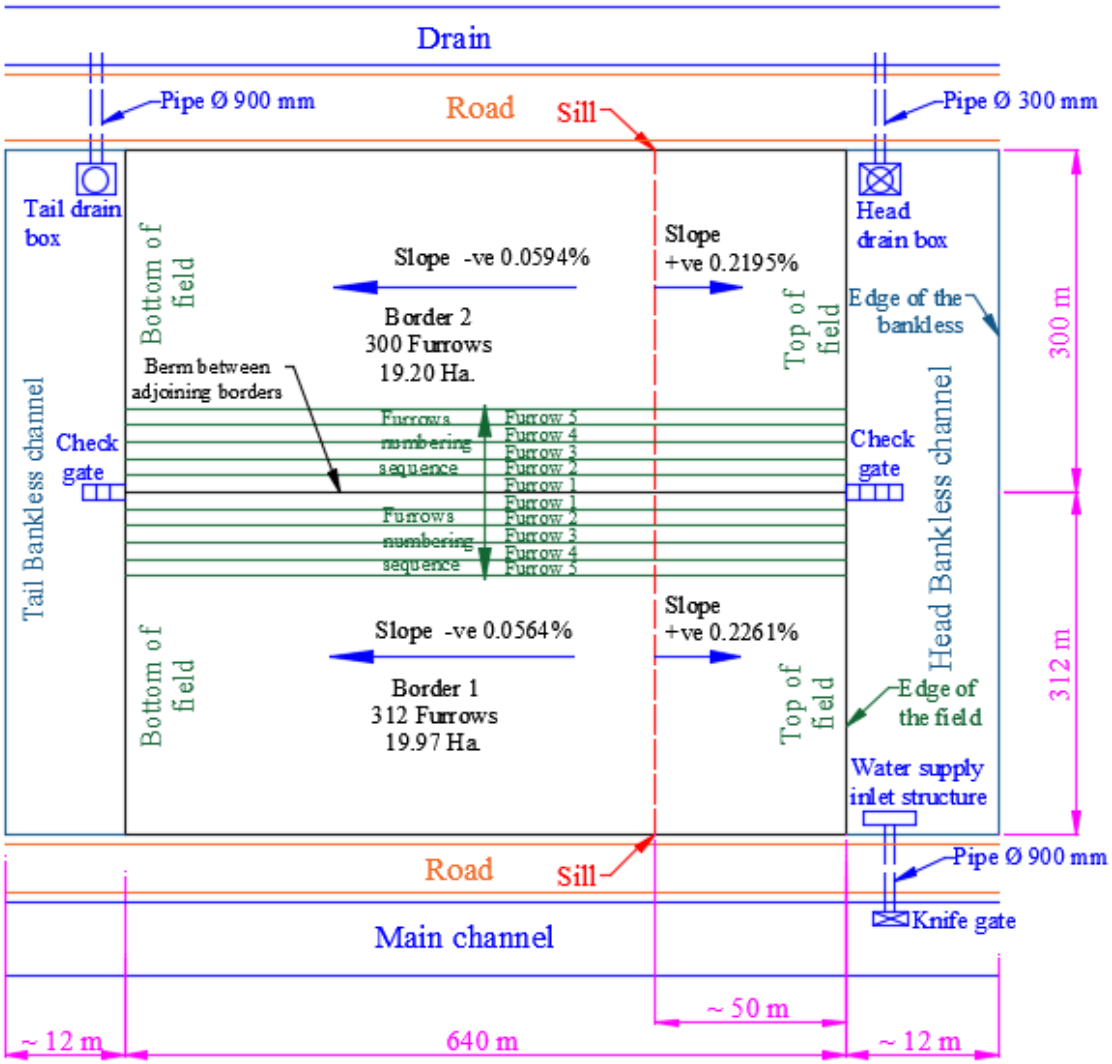

Figure 4.3 Schematic representation of Field 2.

Figure 4.4 Furrows and beds in Field 2

Figure 4.5 Check gate at the top of Field 2 (Padman Stops type - multi linked Padman box culverts).

Water is diverted into Field 2 from the main supply channel through a pipe (with a diameter of 900 mm) extending underground reaching the upper end of the top field (upstream of the bankless channel at the first border) through an inlet structure appearing at the soil surface (Figure 4.6 and Figure 4.7). This inlet structure works to dissipate the energy of the flowing water and thereby reduces soil erosion and plant damage. The flow of water to the field is controlled by a knife gate installed at the side of the main supply channel (Figure 4.8). The knife gate includes a walkway and a handle wheel to control the discharge of water.

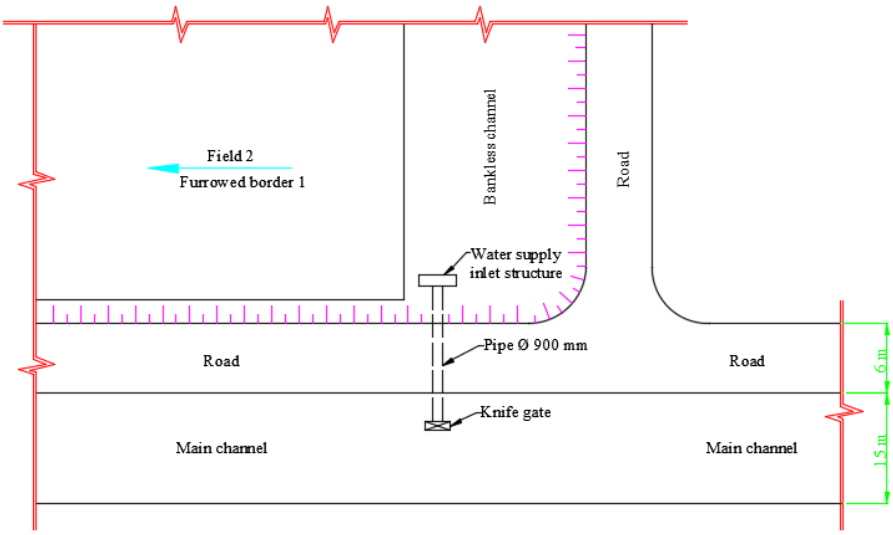

Figure 4.6 Schematic representation of inlet supply structure of Field 2 with knife gate in the main supply channel, buried pipe into water supply inlet structure.

Figure 4.7 Inlet structure at Field 2, and knife gate at the top of Field 2 (includes walk way and hand wheel mounted in the main channel) that feed from the main channel to the water supply inlet. Photo taken in the Season 2, 2018. The main channel was empty.

Figure 4.8 Knife gate at the top of Field 2 (includes walk way and hand wheel mounted in the main channel) that feed from the main channel to the water supply inlet, during the irrigation event.

4.5. Field 3

Field 3 has laser-graded surfaces with approximately zero slope. The first 50 m from the top end of this field was prepared to have slightly positive slopes (of around +0.354% (or 1:280), and then had negative slopes around -0.060% (or 1:1660) for the reminder of the length of the fields. As with Field 2, no slope is evident across the border. A vertical separation exists between the borders of about 150 mm (CottonInfo 2014). Figure 4.9 shows the schematic arrangement of Field 3. The dimensions of Field 3 are 1340 m in length and 540 m in width. Field 3 consists of three furrowed borders connected and served with a bankless channel. Each furrowed border has 180 furrows. Furrow spacings are one metre (the spacing from bed to bed, or from furrow to furrow). The cotton crop is planted in beds (Figure 4.4). Field 3 has two check gates at the top end of the field (set between the adjoining borders: first and second borders, and second and third borders, respectively), while the other two check gates are positioned at the bottom end of the field (also set between the adjoining borders: first and second borders, and second and third borders, respectively), (Figure 4.10). The check gates in Field 3 consist of concrete structures with five openings with grooves.

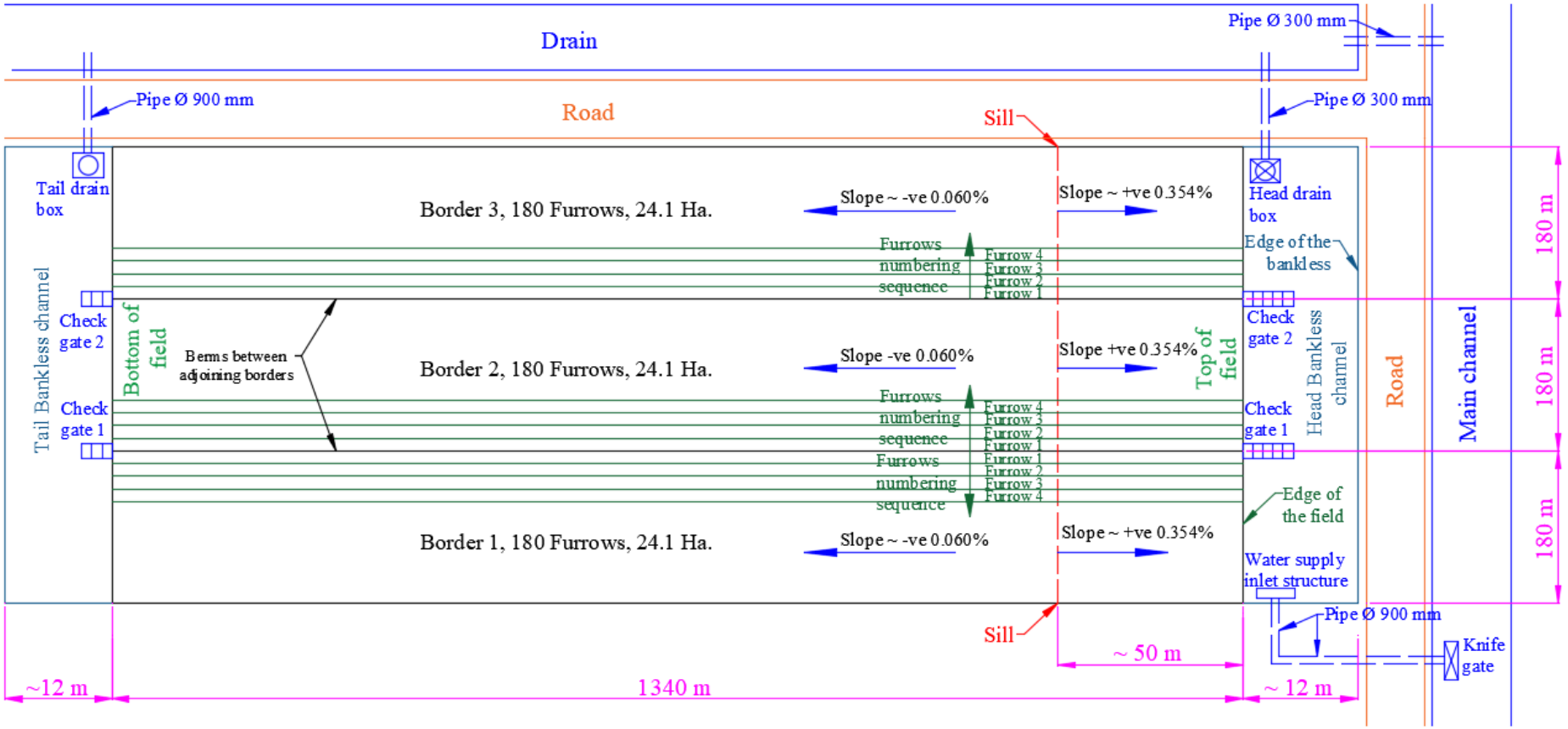

Figure 4.9 Schematic representation of Field 3.

Figure 4.10 Check gate at the top of Field 3

These grooves are used to slide steel boards placed at four rows on the vertical plane to shut the whole gate. To open the check gate, it is necessary to pull out all the boards to obtain full opening or some of the boards to obtain partial opening. The dimensions of the top field Check-gates (1 and 2) are 10 × 0.9 m (width × height, respectively). The check gate at the bottom end of Field 3 consists of three openings with dimensions 5.98 × 0.55 m (width × height, respectively), and 6.01 × 0.683 m (width × height, respectively) for Check-gates 1 and 2, respectively (Figure 4.11). Check-gate 1 is set between the first and second adjoining borders, while Check-gate 2 is set between the second and third adjoining borders.

Water is diverted into the Field 3 from the main supply channel through a pipe (with a diameter 900 mm) extending underground reaching the upper end of the top field (upstream of the bankless channel at the first border) through an inlet structure appearing at the soil surface (Figure 4.12 and Figure 4.13). This inlet structure works to dissipate the energy of the flowing water and thereby reduces soil erosion and plant damage. Water is diverting to the field and the flow controlled by a knife gate installed at the side of the main supply channel. The knife gate includes a walk way and a handle wheel to control the discharge of water in a similar manner as described for Field 2 (Figure 4.7 and Figure 4.8).

Figure 4.11 Check gate at the bottom of Field 3

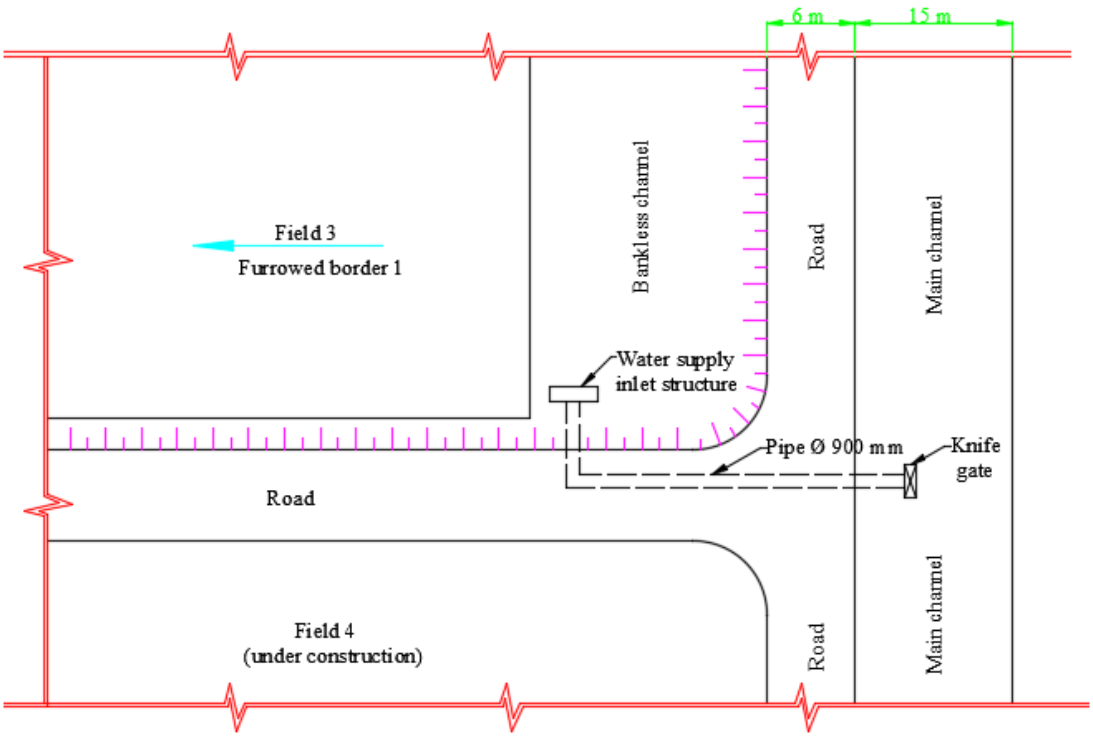

Figure 4.12 Schematic representation of inlet supplying structure of Field 3

Figure 4.13 Inlet structure at Field 3

Both Fields 2 and 3 have a gated drain box at the far end of the upstream bankless channel running along the top of the field (Figure 4.14). Water is drained from the gated drain box through a pipe, with a diameter of 300 mm, extending underground. Figure 4.15 shows this pipe (300 mm in diameter) that extends underground from the gated drain box to the drain. Gated drain boxes at the top of the fields are identical for both Fields 2 and 3. These drain boxes are only typically opened to remove the water from head channel after the end of the irrigation event.

Additionally, both fields have drain boxes at the downstream end of the bottom of the fields (Figure 4.16). Water is drained from the tail drain from the drain box through a pipe (with a diameter of 900 mm) extending underground. Figure 4.17 shows this pipe (900 mm in diameter) that extends underground from the drain box to the drain. Drain boxes at the bottom of the fields are similar in design for both Fields 2 and 3.

Figure 4.14 Gated drain box at the downstream end of the top of Field 3.

Figure 4.15 Pipe that extends underground from the gated drain box, which is located at the downstream end of the top of Field 2.

Figure 4.16 Tail drain box at the downstream end of the bottom of Field 3.

Figure 4.17 Pipe that extends underground from the tail drain box, which is located at the downstream end of the bottom of Field 2.

4.6. Irrigation management

This farm is typical of many commercial fields in the northern Murray–Darling Basin in Australia with dedicated on-farm water storage and delivery. Here the water is stored on farm in large earthen bank storages and can be delivered to the field whenever water is required. If water is available in the storage, the main restriction to water supply is competition from other fields on the farm. The flow required to irrigate a field might be close to the capacity of the storage outlet and delivery channels and only allow one field to be irrigated at a time. The other potential restrictions include labour availability and requirement to account for any in-field machinery operations which require dry fields.

Generally, the irrigation practice commences by diverting water from the main supply channel to the field through a pipe with a diameter of 900 mm extending underground. Diverting water is regulated by a knife gate (Figure 4.7 or Figure 4.8) set to the side of the main supply channel. The diverting pipe ends at a concrete inlet which appears at the field surface and functions as a structure to dissipate the massive energy of flowing water (Figure 4.13).

The irrigation event commences by irrigating the first border of the field while keeping Check-gate 1 (located between the first and the second borders) shut. Water flows from the inlet structure at the upstream end of the top field into the bankless channel, and once this channel fills, water starts entering the furrows and flowing towards the bottom end of the first border. When the water front advances to the bottom end of the first border, Check-gate 1 is opened to commence irrigation at the next border. At this time water now flows into the bankless head channel of the second border and ceases to flow into the furrows in the first border providing there is a sufficient elevation step between the borders.

The opening of the check gates between borders is typically performed in an incremental way in an effort to reduce the risk of erosion. For example, in Field 3 two rows of metal boards were removed from the check gate at the top of the field when the water front advanced to the bottom end of the border, to obtain partial opening of the check gate. The second step in the process was to proceed quickly to the bottom end of the field and fully open the check gate (by pulling out all the metal boards).

Finally, by quickly going to the top of the field and removing the remaining boards, the check gate was completely opened. At this moment, the irrigation of the next border was commenced. Similarly, this practice was conducted in Field 2 with the only difference being the partial opening of the check gate by inclining the two middle gates about 30^{o} from the vertical.

The head drain box at the downstream end of the top of the field was closed throughout the irrigation event, then subsequently opened to drain surplus water after complete irrigation of the field. Similarly, the tail box at the downstream end of the bottom of the field was closed throughout the irrigation event, then subsequently opened to drain surplus water after complete irrigation of the field.

As a special adopted irrigation practice in both Fields 2 and 3, water diversion started at a low discharge rate for about 10 to20 minutes to reduce the potential damage to soil and plants in the first border, due to the power of the water flow. Subsequently, water was diverted at full discharge capacity during the remainder of the irrigation event. The volume of discharge was controlled by the number of turns of the hand wheel mounted on the knife gate. The low discharge was obtained by turning the hand wheel 20 turns, whilst 75 turns were required for full discharge capacity (full opening).

In addition, another special irrigation practice was adopted in both Fields 2 and 3, so that during irrigation on the first border of the field, some streams of water were allowed to intentionally cross across the check gate to the next border (Figure 4.18 and Figure 4.19). This was induced either by partially opening the two middle multi linked Padman Stops box culverts of Field 2 check gate, or through natural leakage between boards in the check gate in Field 3. The purpose of this practice in both fields was to protect each downstream border and stop erosion of soil and damage to plants that occurs when check gates are opened fully in one movement.

During the early part of the cotton growing season (November-December 2016) when cotton is in the juvenile and early stages of growth, the decision to divert water from the first border to the adjacent one is conducted by visually monitoring the advance of the water front in the furrow bottoms between the crop rows in the field. When the water reaches the end of the border for all furrows, the check gate is opened to allow irrigation water into the next border. Then, at later stages in the season, visual

monitoring of the water advance front becomes impractical because the furrow bottom is covered due to crop row closure from the height and density of the cotton plant canopy. Later in the season, when it is impossible to see the furrow bottomsdecisions to complete irrigation and divert water into the next border are made based on the irrigation durationsrecorded earlier in the season.

The times required to complete the irrigation events in Fields 2 and 3 were different because of differing field area considerations. The area of Field 2 is 39.17 ha while for Field 3 it is 72.3 ha. Accordingly, the time required to irrigate Field 2 was approximately 6 hours, (approximately 3 hours for each border), whereas 16 hours was required for Field 3, (approximately 5.5 hours each for three borders).

Table 4.1 shows the important irrigation management information for Fields 2 and 3 in Season 1 including irrigation intervals, and planting and harvesting dates.

Figure 4.18 An irrigation event in Field 2. It also shows the intentionally reduced stream flow crossing the check gate from the two middle gates only.

Figure 4.19 An irrigation event in Field 3. This shows the intentional water leakage through the check gate between the metal boards.

Table 4.1 Irrigation intervals, and planting and harvesting dates for Fields 2 and 3 in Season 1.

Irrigation event no.	Event date of Fields 2 and 3	Irrigation intervals, days	Season information
	24-10-2016		Planting of Field 2 and 3
0	28-10-2016		
1	16-01-2017	59	
2	4-02-2017	19	
3	11-02-2017	7	
4	18-02-2017	7	
5	28-02-2017	10	
6	11-03-2017	11	
	18-04-2017		Picking of Field 3
	22-05-2017		Picking of Field 2

4.7. Hydraulic measurements

Calibration experiments were conducted on Starflows instruments in a small flume at the hydrology laboratory at USQ Toowoomba.

4.7.1. Starflow calibration

Starflow^{TM} instruments are used to measure water velocities and water depths in streams, irrigation or drainage channels and large pipes. Configurations and calibrations of Starflow instruments are necessary steps to prepare these instruments before going into the field. Starflow configuration can be set up and implemented in the office to suit expected field conditions such as channel shape and dimensions. Each Starflow can also be configured to alter parameters which influence the accuracy and duration of measurements. Initially, it is necessary to install the Starflow support software (Starlog Version 4) to manage the Starflow loggers. Starlog V4 software features a Windows interface. The following specific configuration parameters were used in preparing the schemes of the Starflow of the calibration experiments and field experiments:

- Scan rate, which is the frequency of Starflow measurement cycle (units = seconds);

- Log interval, which is the frequency of Starflow recordings (units = scans);

- Starflow flow calculation inputs, which includes cross section type, channel dimensions, flow range, and display units.

After configuring a specific scheme, the next step is to programme the Starflow logger with the saved scheme from the PC. Once completed, the Starflow logger becomes ready to take measurements. A downloading command will copy the data stored in the Starflow logger into a CSV (comma separated value) file on the PC. These CSV files can be opened in Microsoft Excel for analysis.

The Starflow calibration process is conducted by carrying out measurements of each Starflow device under controlled conditions (rectangular open channel, Figure 4.20).

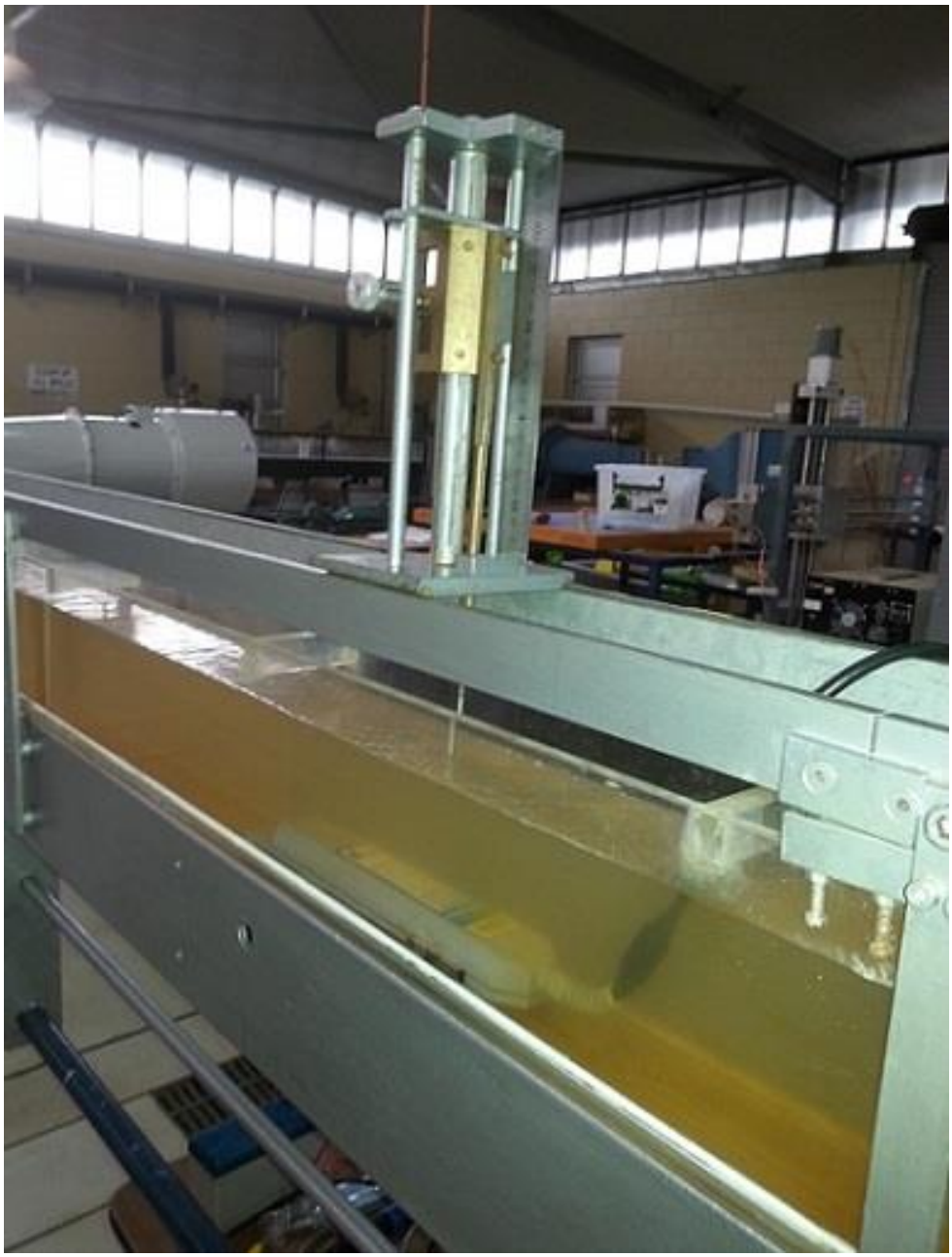

Figure 4.20 Starflow calibration in the small flume

These conditions enable measurements of water depth and flow rate to be captured simply and reliably through independent means. With these pairs of measurements, an analysis for both reference and instrument data helps in evaluating and rectifying instrument measurements whilst reinforcing the reliability of data produced later by these instruments in the field. Calibration measurements included conducting 24 runs for 16 Starflows mounted in a small flume in the hydrology laboratory. Measurements

of water depth, velocity and flow rate. Were logged by each Starflow. Simultaneously, corresponding measurements for both water depth and flow rate were conducted manually using a travelling depth gauge (or travelling pointer gauge), and a volumetric bucket and stopwatch technique for flow out of the downstream end of the flume. Two Starflows were mounted on the flume (484 cm length) for each experiment. The Starflows were mounted so that their sensors were located at precisely 374 and 184 cm away from the upstream end of the flume, respectively. Depth gauges were mounted about 25 cm upstream of the Starflows sensors, to ensure steady flow conditions at this suggested distance. Figure 4.21 represents calibration experiments diagrammatically.

The calibration process commences as soon as the pump is turned on. A control valve on the upstream end is used to control flow rates. When the water surface profile reaches steady state, volume – time and water depth readings can be taken. Flow rate measurements start by moving the lever arm (located on the side of the balancing tank) downwards to shut the vent valve. This confines the water which accumulates inside the balancing tank. The balancing tank hangs at one end of the balancing arm, and weights (masses) hang at the other end. After a while, the weight of accumulated water in the balancing tank equalises the weight of the fixed mass mounted at the other end of the balancing arm. At this moment the stop watch is started. The desired mass is added to the balance overbalancing the lever arm. After a short period of time the balancing tank will fill with sufficient water to balance the added mass and the time on the stop watch is recorded. Given the time elapsed and a volume of water equivalent to the added mass, flow rates can be calculated. During the flow rate measurement, water depth is carried out using the travelling depth gauge. Water depths readings are determined by subtracting the flume bed level from the water depth that measured by depth gauge. Table A-1 in Appendix A contains the calibration equations of the Starflows in the small flume.

After completing the calibration experiments using the Starflow instrument in the laboratory, the resulting calibration factors can be programmed into each device and the instruments were ready to be installed in the field. Flow rate measurements were conducted in the field at two scales: between borders (field scale) and within borders (furrow scale).

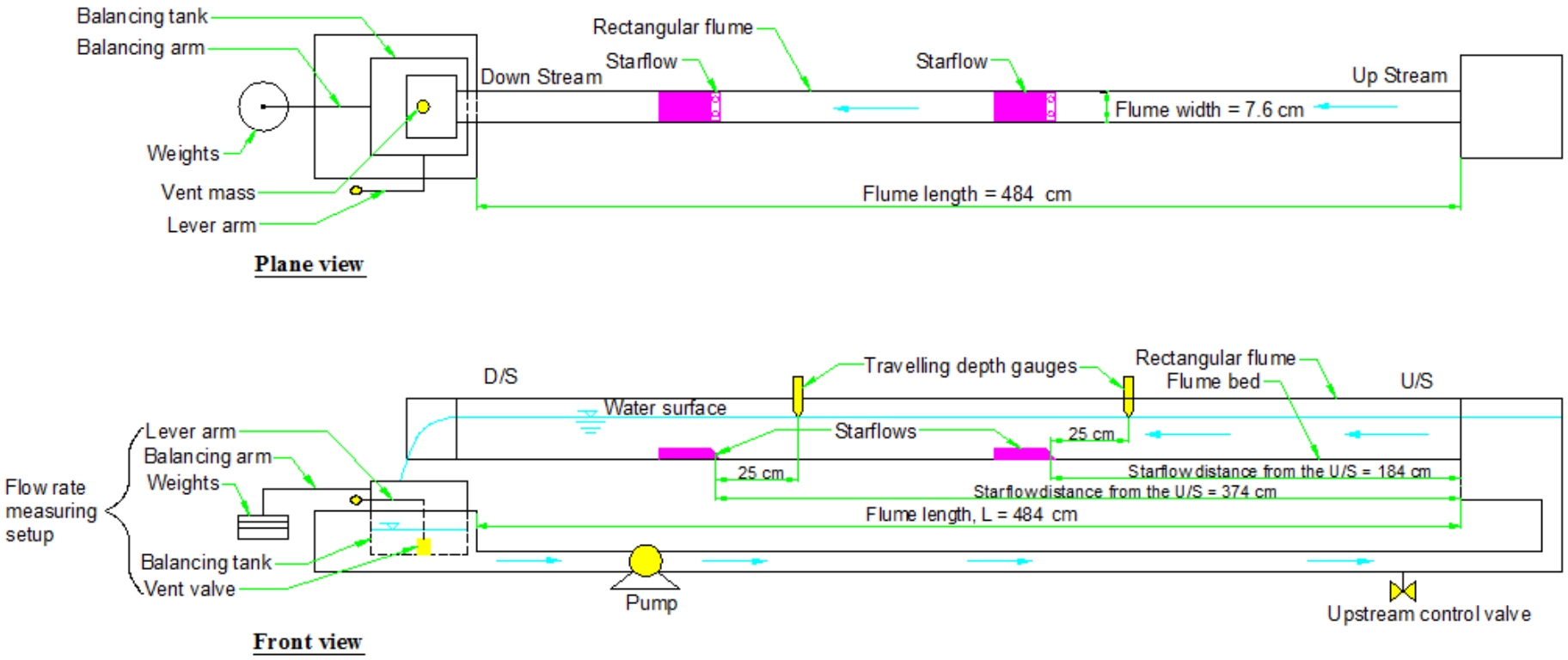

Figure 4.21 Starflow calibration experiments in a small flume

4.7.2. Flow rate measurements at field scale

At the field scale, the Starflow^{TM} Ultrasonic Doppler meters were utilized to measure water velocities and water depths at the check gates, which were located between the borders (Figure 4.22 a and b). The Starflows were installed prior to the event and logged data throughout the duration of each irrigation on a 5 minute time interval.

Figure 4.22 Starflow; a) Starflow mounted directly on the concrete at check gate 1, b) Starflow mounted on a bracket above the concrete to avoid being covered by deposition of eroded silt and mud at gate 2.

Two attempts were made in season 1, 2017 to install Starflow devices inside the supply pipe of the water inlet structure, but each failed. Instead, a piece of flat steel which included a bracket on which to mount the Starflow, was used to place the Starflow inside the suppling pipe of the water inlet structure (Figure 4.23). The first attempt used approximately 9.8 kg flat steel with the dimensions 100×25×500 mm. The second

attempt used a heavier piece of flat steel (about 38.3 kg) with the dimensions 130×25×1500 mm. A metal chain was hung with a small piece of steel welded at the back end of the flat steel to orient or drag it in the water. Using the chain to move this heavy piece of steel was appropriate in the submerged conditions.

The reason behind using this technique to install the Starflow inside the pipe of the inlet structure was due to the difficulty of working in the submerged conditions. The field work actually commenced during the season. It was anticipated (wrongly) that the heaviness of the flat steel would be enough to resist the stream power, because of its weight. However, ultimately heavy stream flow either lifted or pushed these flat pieces of steel from their placements inside the pipe.

Figure 4.23 a) An attempt to mount the Starflow in the pipe of the outlet structure using a heavy piece of flat steel. B) Small piece of metal. C) Large piece of flat steel.

In addition, the SonTek FlowTracker2 (handled-acoustic doppler velocimeter) was utilized to take velocity measurements at the check gates at arbitrary times during the irrigation events (Figure 4.24). The measurement steps started by specifying the appropriate location which involved a controlled cross section with minimum measurements requirements, and appropriate flow conditions. The measurements were conducted on the downstream side of the check gate (Figure 4.24). The flow area was

divided into an appropriate numbers of stations. The intervals between stations were irregular, ranging between 0.5-1 m. Selecting the interval distance depended on the width of the check gate. Also, there was a need to consider avoiding the impact of eddies which may occur behind the check gate pylons. A graduated tag line (measuring tape or graduated rope) was hung tightly across the flow cross sectional area in order to check the position of the SonTek sensor in relation to the gate. Alternatively, interval values could be written on the check gate structure as a tag line. The tag line should be perpendicular to the flow direction.

Figure 4.24 Measuring the flow rate at check gate in Field 3 (photo inset SonTek FlowTracker 2 taken from SonTek a Xylem brand website.

After entering information such as site number, site name, operator and optional comment, the SonTek FlowTracker2 will suggest the establishment of an 'automated beam check'. To complete this check successfully, the SonTek FlowTracker2 probe (Figure 4.25) should be placed in the stream away from any obstacles, and should be oriented as shown in Figure 4.26. The wading rod which holds the probe must be vertical during the measuring process. "Passed check" indicates that the flow conditions are appropriate to proceed and the data collection stage is then ready to start.

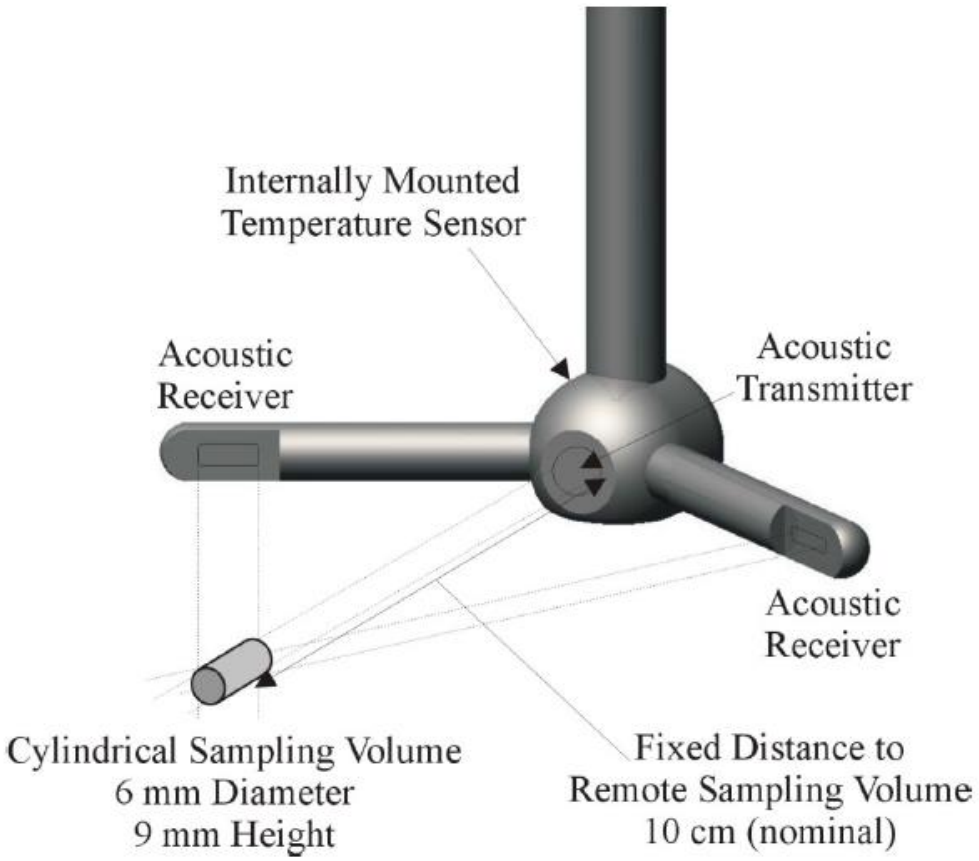

Figure 4.25 SonTek FlowTracker2 Probe and Sampling Volume

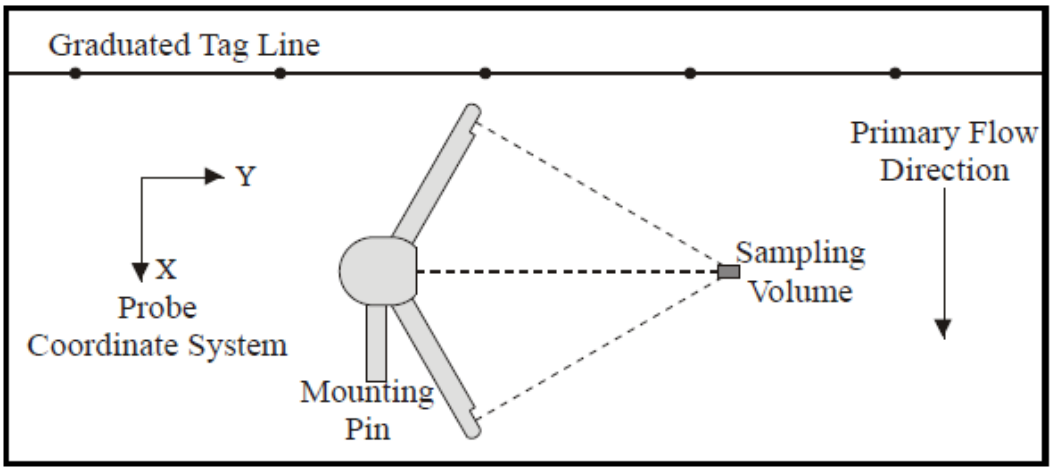

Figure 4.26 SonTek FlowTracker2 Coordinate System.

The water depth at each station of the flow area is measured manually by a staff gauge board or ordinary ruler. The water depth and its corresponding station location is entered into the SonTeck handheld for each measurement, then the velocity measurement at that station is performed. The total discharge is computed based on the water depths, station locations and water velocity combinations. The mean section formula was used to compute the discharge at the check gate. The actual measurements were conducted at a fractional depth of the water depth. In fact, the measurements were conducted according to the SonTek FlowTracker2 manual. The number of required measurement locations depended on the water depth at each station. Measuring the mean velocity at each station was conducted at one location of 0.6 (60%) of water depth when the water depth was less than 0.5 metres. Whilst, measuring the mean velocity at each station was conducted at two locations of 0.2 and 0.8 of water depth when the water depth was more than 0.5 metres. Measuring the depth of each fractional value (0.6, 0.2 and 0.8) depended on the selected reference. Where, it could be measured from the water surface or bottom based on the selected setting. In the current measurements, the bottom was selected as a reference to compute the fractional value (0.6, 0.2 and 0.8). As a personal practice, the measurements were repeated twice before accepting them, to reinforce their reliability of the measurements.

SonTek FlowTracker2 desktop software and the handheld version (1.4 (30-11-2016)) can be communicated via a micro USB cable or Bluetooth in order to upgrade the handheld software or downloading the data.

4.7.3. Flow rate measurements at furrow scale

At the furrow scale, SonTek FlowTracker2 was utilized to measure water velocities and calculate flow rates in the furrows (Figure 4.27). The measurements were conducted for about 6 to 12 selected adjoining furrows at 20 m downstream from the furrows' entrance. The selected adjoining furrows were chosen from near the middle of the borders. Measurements were conducted in the middle of the flow cross sectional area of each furrow.

As explained in Section 4.7.2, the water depth in the furrow and the station location were measured manually using a ruler and then entered into the handheld. Because of local undulations in the furrows, water depth was measured at multiple locations close

to the SonTek measurement location and their average entered. It is believed that the accuracy of measuring the water depth in the furrow was not been significantly affected by erosion or sedimentation, as the erosion was minimal apart from the areas immediately at the upstream and downstream ends of the field. Lower sedimentation is anticipated to impact measurements when conducted during the irrigation event under flowing condition.

Once, the probe was precisely positioned (at the right measured depth with a right orientation in the stream), an automated beam check was conducted in the stream. If the check passed, measurements could commence. The measurements were repeated twice or more at each location to reinforce their reliability. A mid-section formula was used to compute the discharge of the furrow. Measurements were only conducted for four irrigation events.

Figure 4.27 Flow rate measurement in the furrow via SonTek FlowTracker2.

4.7.4. Water advance measurements

Water advance measurements were collected via two different techniques in this season. Firstly, measurements were collected using IrriMATE ™ advance sensors on a small number of adjacent furrows. Secondly, a GPS technique was trialed in order to capture water advance over a larger number of furrows, by chasing the water advance manually (by walking).

4.7.4.1. Water advance measurements using IrriMATE

Water advance measurements were conducted using IrriMATE ™ advance sensors installed in the furrows (Figure **4.28**). One or two sets of sensors were installed at predetermined intervals (see below) along the lengths of the furrows to record the arrival time of the water front advance at each interval. Every set had eight terminal ends to log the arrival time of the water front at eight adjoining furrows. These 8 or 16 adjoining furrows were located in the second border of Field 3, starting from the fourth furrow of this border. The determined intervals of these sensors were 90, 300, 600, 900 and 1200 m for most irrigation events.

Figure 4.28 **IrriMATE advance sensor, Photo taken in Season 2, 2018.**

4.7.4.2. Water advance measurements using a smartphone GPS

Difficulties in using the IrriMATE ^{TM} advance sensors and the limited field coverage of these sensors encouraged the investigation of an alternative for measurement of advance over a large spatial area. Grabham (2012) used a technique whereby he walked through the field during the irrigation with a RTK GPS receiver chasing the water advance. Hence, a similar but more cost effective option using a smartphone GPS was trialled in Season 1. The MotionX-GPS smartphone app allows the user to record a track with GPS coordinates. It was proposed that the data from this software could be analysed to create advance data. Walking with the water advance front in different furrows with a MotionX-GPS app installed on a smart phone was tried in one event in each field in Season 2. Measuring water advance in a larger number of adjoining furrows was at two arbitrary time intervals. It was intended to record the advance measurement one early in the advance phase and another later in the advance. Google Earth browser was then used to open the files created by the MotionX-GPS app (Figure 4.29). Then advance distances were extracted for each furrow using the "Measure distance and area" tool in the Google Earth browser. The water advance measurement was recorded at each significant direction (Figure 4.29) and represents a furrow position extracted by measuring two distances. The first distance is the water advance, while the second distance represents the furrow number in the border, at one metre spacing. As explained above, the measurements do not include all furrows covered on the walking paths.

4.8. Conclusion

Many measurements were conducted in this season and covered the essential aspects of evaluation measurements. Though the previous studies had identified several of the field measurement challenges associated with the special layout and hydraulic characteristics of near zero slope furrowed border irrigation systems with a common water supply, conventional techniques were adopted to conduct the measurements in the FNSBO_Re irrigation in this season. It was suggested that developing appropriate techniques to measure and analyse the FNSBO_Re systems can be started by examining the irrigation process of these systems using conventional techniques. In

fact, the field measurements and observations, and anecdotal information from the grower had provided a good idea about the hydraulic behaviour of the FNSBO_Re system. These sources of information revealed to a large degree the variability in the measurements (flow rate, cross-sectional area, and water advance) and the special behaviour in the irrigation process in this system.

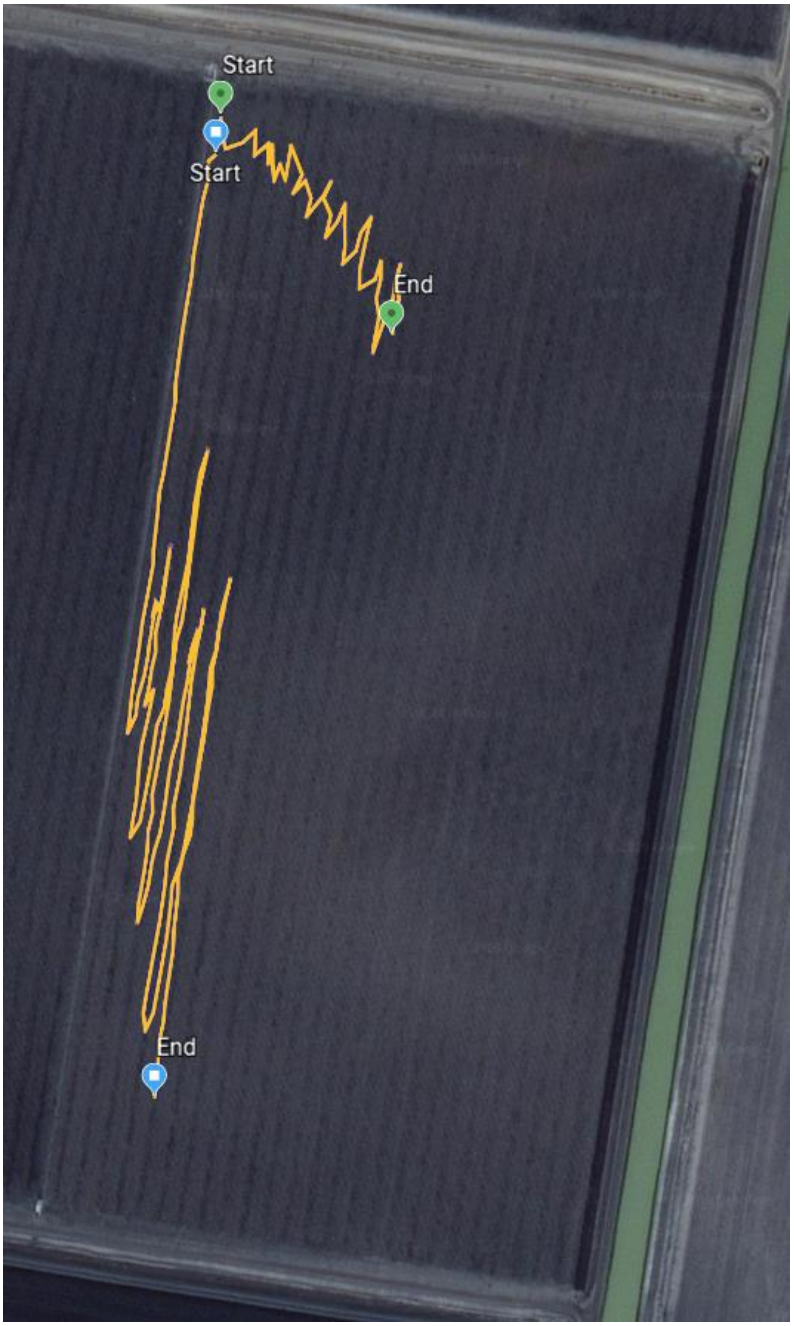

Figure 4.29 Water advance measurements using MotionX-GPS at two time intervals on Border 1 of Field 2 in irrigation event 4-02-2017. It shows two files with extension "KML" have been created by MotionX-GPS app and opened using Google Earth.

It was concluded that for these systems, it will always be important to measure the actual flow rate in the same furrow where the advance rate is measured as these measurements are significantly different between furrows. For example, adopting the average flow rate or the advance measures of the next furrow are not acceptable. On the other hand, there were limitations in conducting some measurements. For example, the submerged condition in the inlet structure prevented mounting the Starflows instruments in main supply pipe. Therefore, it is important to install some instruments during the period before the season commences.

CHAPTER FIVE

Results from Season 1

5.1. Introduction

This chapter presents the data collected during Season 1, the 2016-2017 summer cotton season. This data was collected utilising the methodology documented in Chapter four. The results are split into four areas; field geometry and levels, furrow geometry, flow rates, and water advance.

5.2. Soil characteristics

Based on the APSOIL database ((APSIM 2019; Dalgliesh et al. 2012; Holzworth et al. 2014)), soil type, soil texture and average soil bulk density in the top 120 cm of soil profile, and other related information were provided from the two closest possible locations to study fields 2 and 3 as shown in Table 5.1.

Table 5.1 Soil characteristics information of the study fields (2 and 3) based on APSOIL database.

APSoil number:	1287	1288
Australian Soil Classification Order:	Vertosol	Vertosol
Australian Soil Classification Sub-	Black	Black
Sand (%)	45.6	27.4
Silt (%)	11.7	25.4
Clay (%)	42.7	47.2
Soil type, texture	Sandy Clay	Clay
Average bulk density (g/cc)	1.5042	1.3243
APSoil site location	~27 km west of the field site	~27 km west of the field site
Site:	Goondiwindi	Goondiwindi
Nearest town:	Goondiwindi	Goondiwindi
State:	New South Wales	New South Wales
Country:	Australia	Australia
Latitude	-28.64885	-28.70119
Longitude	150.09651	150.09399
Year of sampling:	2014	2014

5.3. Field surveying

A level survey was conducted on Field 3 using a robotic total station (Leica TCRA1203). These measurements were used to determine the longitudinal slopes or elevations down the field and to determine the vertical separation between the adjoining borders of Field 3.

The first part of the surveying measurements was carried out on 13 adjoining furrows, starting from the 3rd furrow of Border 2 in Field 3, at variable intervals along the length of the field (Figure 5.1). The measurements down the furrows (field) indicated a positive slope of approximately 0.354% for approximately the first 50 m from the top of Field 3, followed by a slight negative slope (-0.060%) along the rest of the length of the field, as shown in. The second aim of the surveying operation was to determine the elevations for some cross sectional profiles of the head and tail bankless channels, at different distances along their length. Figure 5.2 shows cross-sectional profiles of the head bankless channel for Field 3. Figure 5.3 shows cross-sectional profiles of the tail bankless channel for Field 3.

The vertical separation between adjoining borders at the head of the bankless channel was estimated at approximately 0.075 m based on the surveying data (Figure 5.2), compared with approximately 0.12 m at the tail bankless channel (Figure 5.3).

5.4. Furrow geometry

Figure 5.4 shows the calculated furrow cross-sectional area for 12 adjoining furrows at different intervals (5, 90, 300, 900 m) in Border 2, starting from Furrow 4 through to Furrow 15 in Field 3. As shown in Figure 5.4, Furrows 6 and 8 had the highest cross-sectional areas, which is to be expected because they are the wheeled tracked furrows (WF). Cross-sectional areas demonstrate noticeably more stability from 90 m into the field to the end of the field, compared to narrower furrow cross-sections towards the upper end of the field.

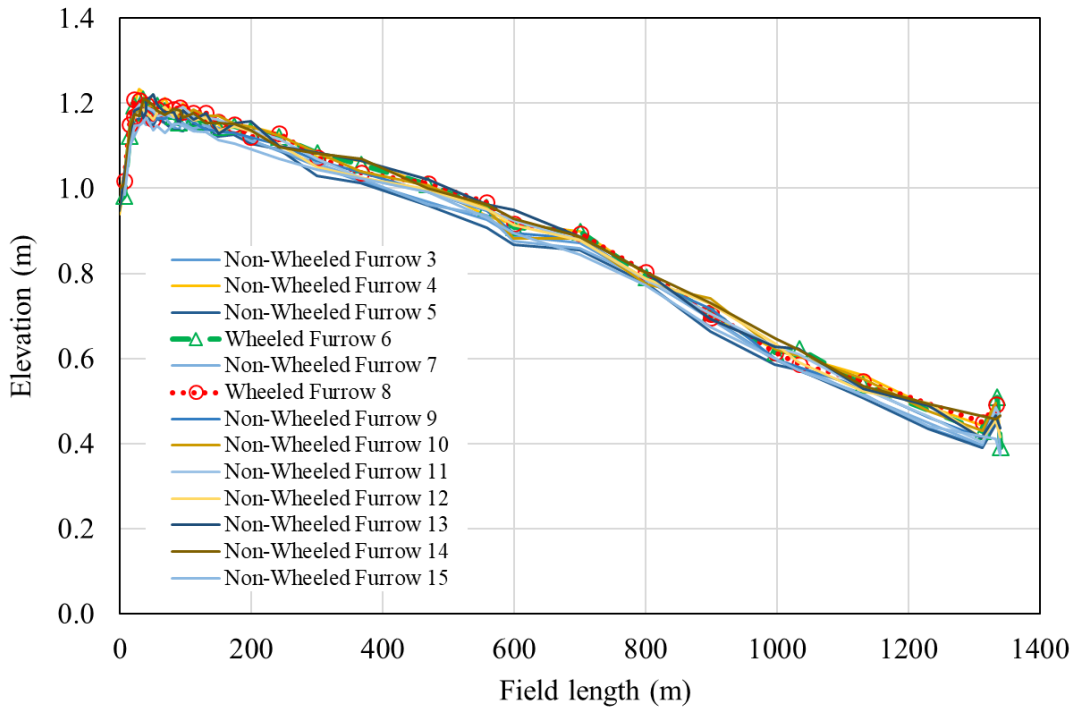

Figure 5.1 Furrow elevations for 13 adjoining furrows, starting from the third furrow, in the 2nd border of Field 3.

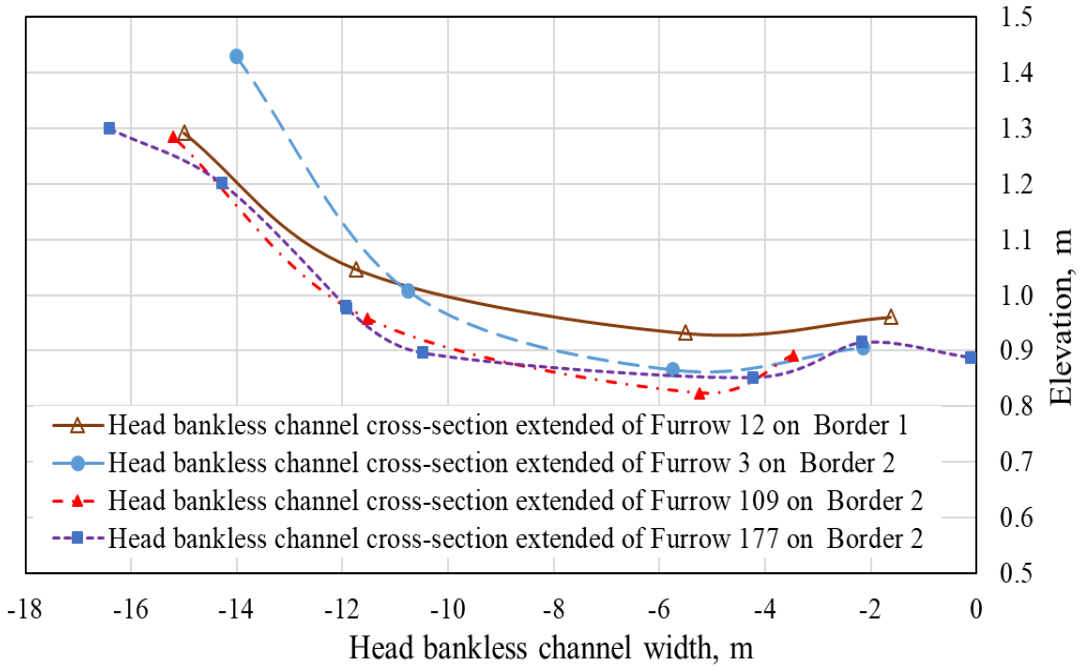

Figure 5.2 Cross-sectional profiles of the head bankless channel for Field 3.

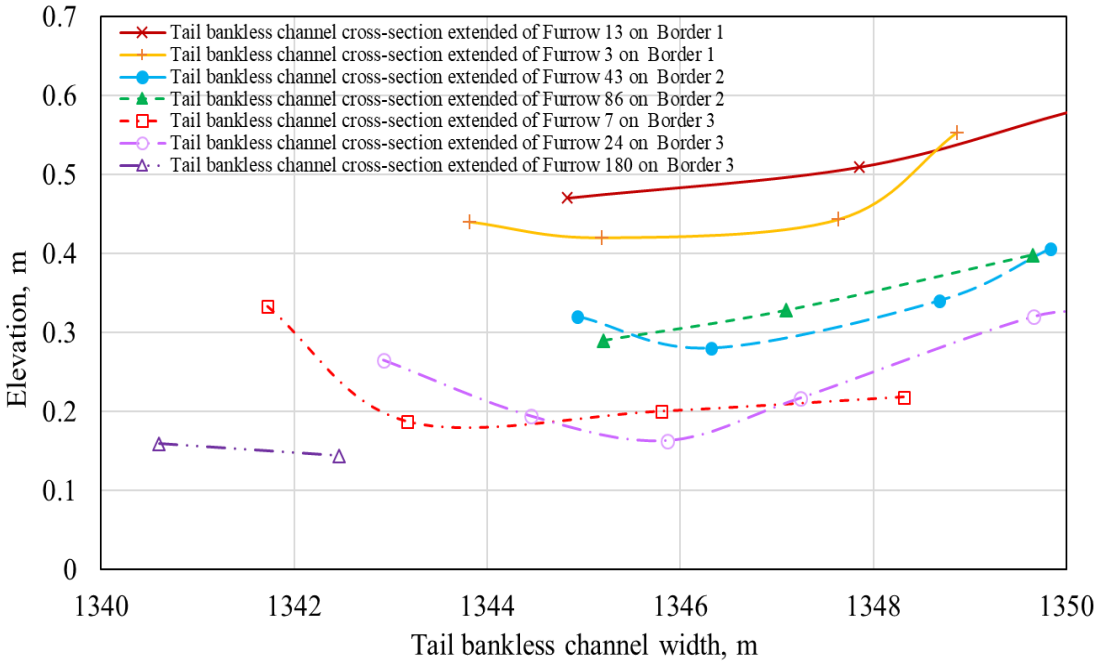

Figure 5.3 Cross-sectional profiles of the tail bankless channel for Field 3.

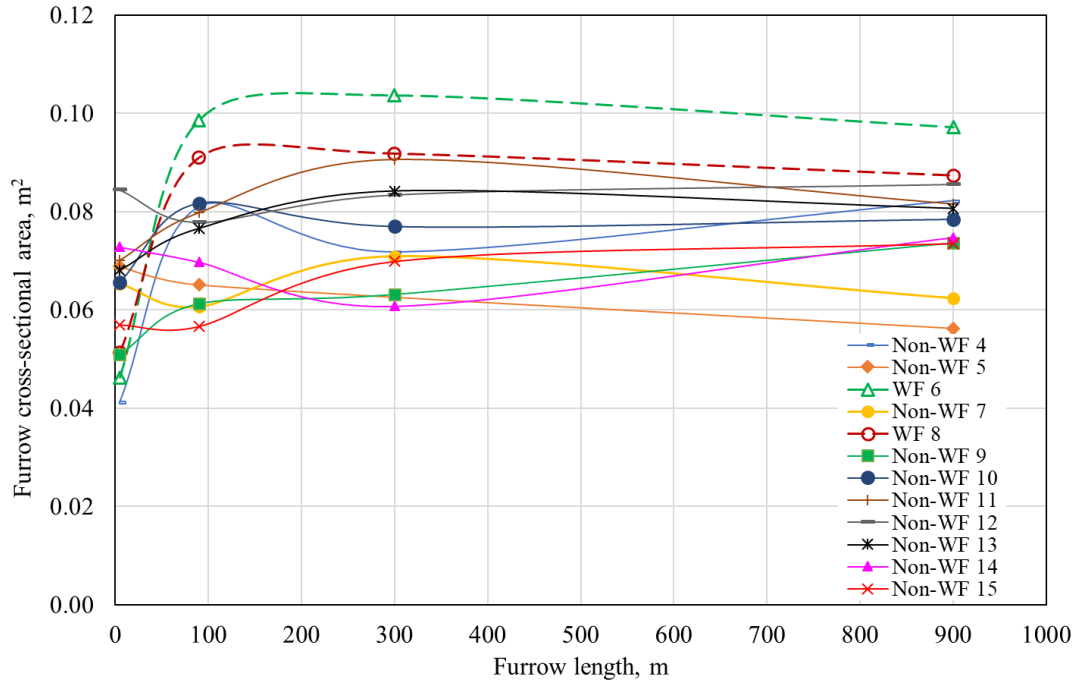

Figure 5.4 Furrows' cross sectional area for 12 adjoining furrows (4th to 15th) in Border 2 along Field 3.

5.5. Flow rate measurements

As explained in the previous chapter, hydraulic measurements were conducted on two scales: between borders (field scale) and within borders (furrow scale).

5.5.1. Flow rate measurement calibration at the check gates

In order to check the reliability and ability of the Starflows to measure the flow rates at the check gates, it was suggested that a few measurements should be taken at these check gates using the Flow Tracker2. Figure 5.5 shows the water velocities, water depths and discharges (flow rates) at Check gate 1 (between Borders 1 and 2) located at the top of Field 3. These measurements were conducted using SonTek FlowTracker2 between 6:39 AM and 6:47 AM on 11-2-2017. This figure shows generally uniform distribution of the values of water velocities, water depths, and discharges along the cross section of the check gate. Therefore, the possibility of adopting Starflow instruments to conduct the flow rate measurements is realistic. However, by comparing flow rates measured by FlowTracker2 with the Starflow flow rates at the same check gates, it is noticed that there are overestimations in the Starflows' flow rates. Table 5.2 shows the flow rate values measured at the downstream side of the check gates of Field 2 and 3 by SonTek FlowTracker2 and Starflow. The comparison between these values were conducted at the same corresponding times of the measurements.

The average overestimations in flow rates were approximately 19% and 10% for Fields 2 and 3 respectively. Starflow flow rates overestimation could be explained by analysing velocities and depths distribution across the check gates and also the blocking factor.

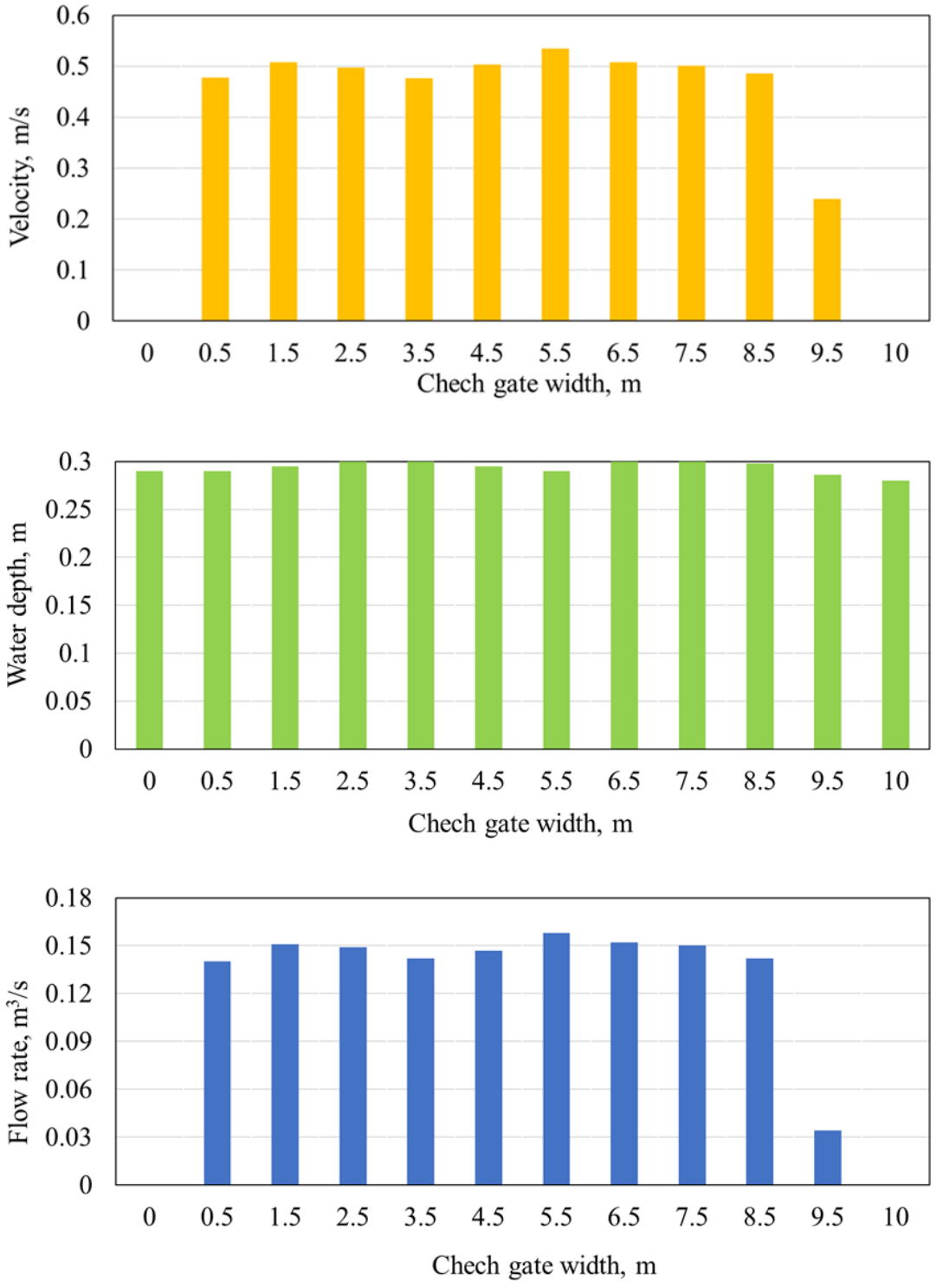

Figure 5.5 Water velocities, water depths and discharges at Check gate 1 located at the top of Field 3. Measurements conducting by SonTek FlowTracker2 between 6:39 AM and 6:47 AM on 11-2-2017.

Table 5.2 Comparison between the flow rate measurements conducted at the check gates of the Field 2 (Figure 4.3) and Field 3 (Figure 4.9) via SonTek FlowTracker2 and Starflows at corresponding times of conducting measurements.

SonTek FlowTracker2 data					**Starflow data**					Flow rates Overestimation, %
Field no.	Measurements location	Date	actual time of measurements	Flow rate, m^3/s	Starflow SN	Flow rates, m^3/s			Average flow rates, m^3/s	
2	Top Check-gate	11/02/2017	9:41 to 9:51 AM	1.558	1652	1.792	1.913	1.933	1.879	17%
2	Top Check-gate	11/02/2017	10:19 to 10:28 AM	1.5316	1652	1.798	1.702	1.666	1.722	11%
2	Top Check-gate	18/02/2017	11:02 to 11:11 AM	1.334	1652	1.872	1.869	1.926	1.889	29%
2	Top Check-gate	18/02/2017	11:13 to 11:22 AM	1.587	1652	2.061	1.785	1.904	1.917	17%
									Average	**19%**
3	Top Check-gate 2	4/02/2017	6:59 to 7:07 AM	1.479	1642	1.671	1.569	1.650	1.630	9%
3	Top Check-gate 1	11/02/2017	6:39 to 6:47 AM	1.395	20088	1.499	1.580	1.464	1.514	8%
3	Top Check-gate 1	11/03/2017	12:54 to 1:04 PM	1.600	20088	1.616	1.970	1.799	1.795	11%
3	Top Check-gate 1	11/03/2017	2:31 to 2:39 PM	1.526	20088	1.820	1.856	1.709	1.795	15%
3	Top Check-gate 1	11/03/2017	2:42 to 2:46 PM	1.491	20088	1.709	1.869	1.760	1.779	16%
3	Top Check-gate 1	11/03/2017	5:20 to 5:27 PM	1.601	20088	1.754	1.724	1.634	1.704	6%
3	Top Check-gate 1	11/03/2017	5:35 to 5:42 PM	1.532	20320	1.651	1.546	1.730	1.642	7%
3	Top Check-gate 1	11/03/2017	6:08 to 6:16 PM	1.482	20320	1.700	1.621	1.599	1.640	10%
									Average	**10%**

If we consider the first hypothesis above, it was noticed from the SonTek FlowTracker2 measurements that the distribution of both water depths and velocities across the check gates was not perfectly uniform (Figure 5.5), where, there was drop in the water depths and velocities values near to the edges of the check gate. However, in order to calculate flow rates via Starflow it was assumed that water depths and velocities would be uniform across the check gate section, but this was not the case. Starflow measurements are based on sending and receiving sonic pulses from the eyes (transmitter and receiver) of the transducer. These eyes are located at the front of the Starflow instruments, so they cover a narrow strip of the water stream to determine its flow velocity. The position of this covered strip depends on the Starflow mounting location and its orientation angle. For this study, wherever possible, Starflows were mounted at approximately the middle of the check gate width. Additionally, the pressure transducer measures water depths only at the mounted location of the Starflow. Therefore, Starflows are probably logging higher water velocities and depths values compared with the average velocities and depths values.

Now, to address the second possible reason for the overestimation of the Starflow measurements, let us consider the blocking factor resulting from the obstacle of flow by the check gate pylons. Starflows were mounted at the middle of the sub-gates of the check gates, hence, Starflow readings exhibited higher possible values of the flow velocities. In other words, the Starflow measurements did not take into account the impact of the blocking factor caused by the check gates pylons.

The overestimation correction factor for Fields 2 and 3 was determined to be 19% and 10% respectively, because each field had different types of check gates. Where, as discussed about the impact of the blocking factor on the Starflows' measurements overestimation, flow behaviour is dependent upon the check gate geometry at each field.

In fact, the difference in the measurement position for each instrument could lead to differences in flow rate measurements. The Starflows were mounted at approximately 1.8 metres downstream of the check gate in the middle of the check gate, while SonTek FlowTracker2 was positioned at approximately 0.2 metres downstream of the check gate, at regular intervals along the check gates. Naturally, the flow area is diverged downstream of the check gate as the water depths and velocities change. Therefore,

the instantaneous measured depths and velocities measured via the SonTek FlowTracker2 are more reliable than the corresponding values logged via Starflows. In general, the reliability of the SonTek FlowTracker2 data should be higher because it represents the latest technology for measuring water velocities in open streams, although, the measurement error associated with the SonTek FlowTracker2 depends on user experience.

5.5.2. Flow rate measurements at field scale

Flow rate measurements using Starflow instruments were conducted at the check gates between the borders of Fields 2 and 3. Flow rates were calculated based on the calibrated logged data (water depth and velocity), see Section 4.7.1. Flow rate measurements of at the check gates were adjusted based on SonTek FlowTracker2 measurements (see Sections 5.5.1). Flow rate measurements at the supply pipe and drain boxes were not conducted.

Figure 5.6 shows water flow rate downstream of the check gates between borders in Field 3, for an irrigation event conducted on 4-02-2017. Applying a volume balance at the border scale was only possible for the middle border (Border 2) of Field 3. The net volume of water held in Border 2 was estimated by conducting an algebraic addition of flow rates in and out of Border 2. The algebraic addition was conducted by assuming positive magnitudes for water flow rate entering Check gate 1 at the top of Field 3, located between Borders 1 and 2) and Check gate 1 (at the bottom of Field 3 located between Borders 1 and 2). The algebraic addition also assumed negative magnitudes for water volumes entered across Check gate 2 (at the top of Field 3 located between Borders 2 and 3) and Check gate 2 (at the bottom of Field 3 located between Borders 2 and 3). The values of the net volume of water (in cubic metres) held in Border 2 for the irrigation events of the 4-02-2017, 11-02-2017, 18-02-2017, 28-02-2017, and 11-03-2017 were 12509, 11400, 10322, 7586, and 5890, respectively. The net depths of water held in Border 2 were calculated by dividing these volumes by the border area (24.1 ha). The values of the net water depths (mm) held in Border 2 were: 52, 47, 43, 31 and 24, respectively. The estimated depths of water held in Border 2 of Field 3 were low especially for the last two events (31 and 24 mm). In fact, there is no specific reason to doubt the flow rate measurements for these last two irrigation events, but the

soil water deficits were higher than these values during relatively long intervals between irrigation (ten days) and the border could be under irrigated. Regarding the first three values of the net water depths, it can also be seen that they are small but still possible, especially given the irrigation interval of approximately seven days. A possible way to fix this problem is to have independent measurements which can be linked to water flow rate measurements such as soil moisture. This kind of measurement can be used as a reference to decide whether the net depth held in the soil profile is logical.

The flow rate measurements for Field 2 were insufficient to calculate the net water volumes or depths held in the field.

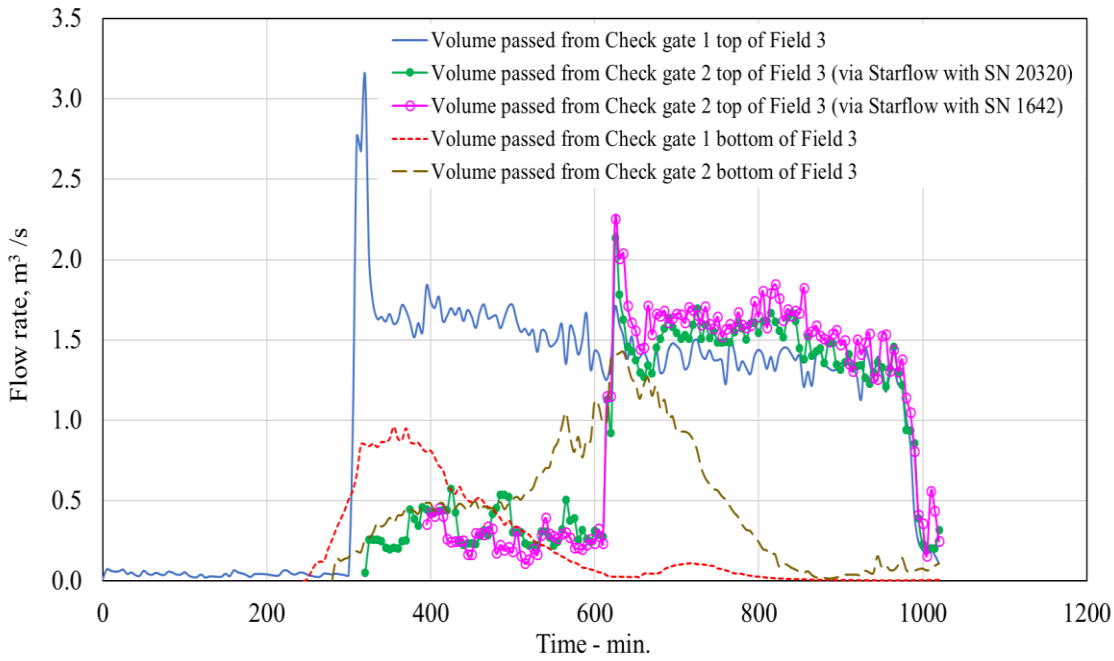

Figure 5.6 **Volumes of water passed downstream of the check gates of Field 3 for the irrigation event conducted on 4-02-2017.**

5.5.3. Flow rate measurements at furrow scale

A few flow rate measurements for adjacent furrows in Border 2 of Field 2 and Border 1 and 3 of Field 3 were collected using the SonTek FlowTracker2. Figure 5.7 shows the flow rate entering seven adjoining furrows (approximately Furrows 151 to 157) near the middle of Border 2 in Field 2 for the irrigation event conducted on 11-2-2017. As is clear, there is a large variation (four and half times) in flow rates among the

measured furrows, ranging between 0.002 and 0.009 m3/s. Generally, this large variation could be traced back to the impact of the WFs, where simple observations show that WFs have the highest water advance rates and flow rates. However, it is uncertain whether the furrows measured included WFs. Naturally, the larger cross sectional areas of the WFs leads to delivery of a significantly higher amount of flow compared with non-WFs. Figure 5.8 shows the flow rate entering for seven almost adjoining furrows (approximately numbers 90, 92, 94, 95, 96, 97 and 98) selected towards the middle of Border 3 of Field 3, for an irrigation event operated on 18-02-2017. Also, this figure shows a variation in flow rate values ranging between 0.009 to 0.015 m^3/s for Furrows 94 and Furrow 97, respectively. Again, it is uncertain whether these furrows included WFs.

The flow rate measurements at the furrow scale were relatively few compared to other important measurements of water advance, furrow cross-sectional area, and surveyed elevation. Therefore, it was impossible to use these measurements to conduct the irrigation evaluation using well-known methods such as the Two-Point method. However, flow rate measurements for furrows located towards the middle of the field provided a good indication of average flow rate for all furrows in the field and showed the large variation in diverted water in FNSBO_Re irrigation systems.

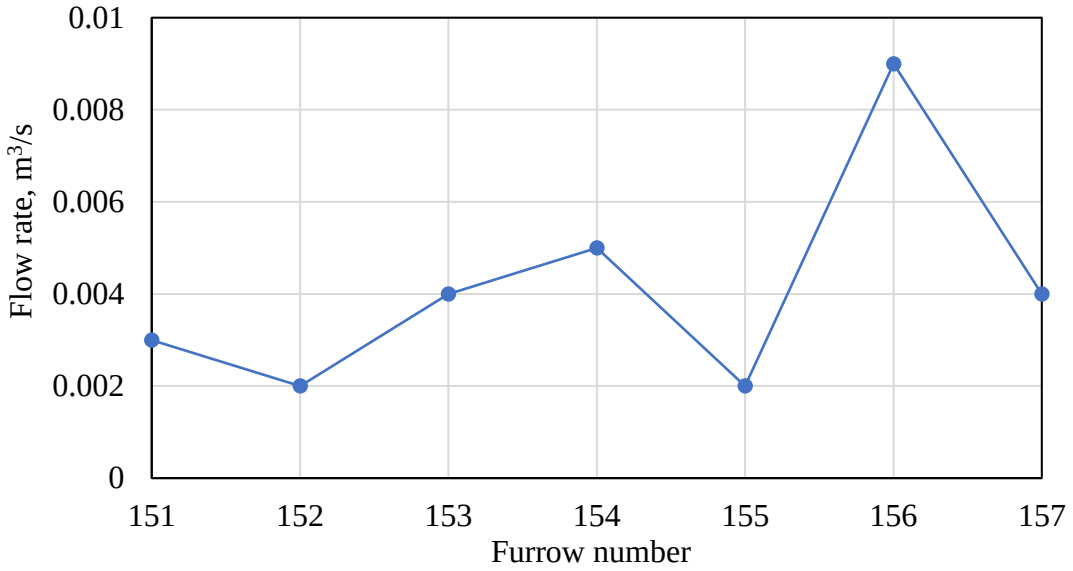

Figure 5.7 Flow rates values for seven of adjacent furrows selected near the middle of Border 2 of Field 2 for the irrigation event conducted on 11-02-2017.

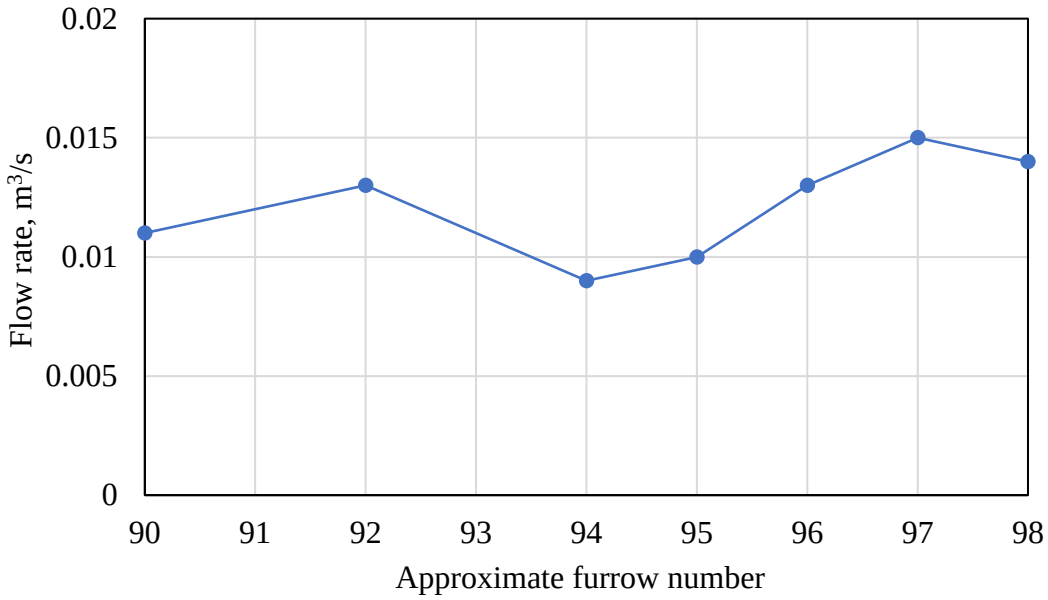

Figure 5.8 Flow rates values for seven furrows near the middle of Border 2 of Field 3 for the irrigation event conducted on 18-2-2017.

5.6. Water advance measurements

Water advance measurements were conducted in this season using two different techniques. Firstly, intensive measurements were collected using IrriMATE ™ advance sensors on a small number of adjacent furrows. Secondly, the MotionX-GPS smartphone app was trialled in order to capture water advance over a larger number of furrows by collecting water advance measurements manually.

5.6.1. Water advance using IrriMATE

Water advance Measurements were conducted using IrriMATE ™ advance sensors on the three irrigation events of irrigation Season 1, 2017. The measurements took place over 8 or 16 adjacent furrows in Border 2 of Field 3. The measured furrow numbers commenced from the fourth furrow towards the middle check bank between adjoining Borders 1 and 2. The location of furrows as shown in Figure 4.9. There were some missing advance measurements for certain furrows, possibly caused by either damaged wire terminal ends due to rodents, or alternatively, bad data where the logged arrival time was immediately after setting the advance sensor, perhaps due to the existence of some moisture in the soil or other technical reasons.

Figure 5.9 shows the water advance for seven adjoining furrows in Border 2 of Field 3 during the irrigation event on 11-02-2017. The advance measurement of Furrow 9 is missing. The position intervals of these sensors were 90, 300, 600, and 1320 m. Due to the intentional leakage at the bottom check gate between Border 1 and 2, negative values of advance times were recorded by the advance sensors that were placed at the farthest interval distance (1320 m), when (backwards flowing) water reached these sensors before commencing flow into Border 2 when the top check gate between Border 1 and 2 was opened)(see Section 4.6). This figure shows the difficulty of evaluating of FNSBO_Re irrigation systems using standard approaches because it has a rapid advance phase with large quantities of tail water coming from the adjoining border.

Installing advance sensors at the downstream end of the border (e.g.1200 or 1250 m) provides a good understanding of the impact of the backwards advance, leading to a better understanding of the advance phase for the whole border in FNSBO_Re systems. However, the lack of advance sensors reduces the ability to have more advance measurements for more intervals. Also, because the current methodologies of irrigation evaluation are based on normal advance measurements (forward advance data), it was decided to adopt different advance intervals at the distances of 90, 300, 600, and 900 m, as shown in Figure 5.10. Figure 5.10 shows the water advance for fifteen adjoining furrows in Border 2 of Field 3 during the irrigation event on 28-02-2017. The advance measurement of Furrow 14 is missing. Figure 5.11 shows the water advance for sixteen adjoining furrows in Border 2 of Field 3 during the irrigation event on 11-03-2017. The intervals of these sensors were 90, 300, 600, 900, and 1200 m. This figure shows the distinctive behaviour of the water advance backwards from the bottom end of the field, back up into the field again. This occurred when the water advance had been completed (reached the bottom end of the field) in some furrows (probably WFs) which then began to flow backwards up into the field through adjoining furrows (non-WF). The tail water obtained from the leakage at the check gate between adjoining borders, augments the backward advance. This complex behavior led to the evolution of the FNSBO_Re irrigation system as mentioned above. Figure 5.9, Figure 5.10, and Figure 5.11 show that the advance rates in the WFs were relatively high compared with non-WFs.

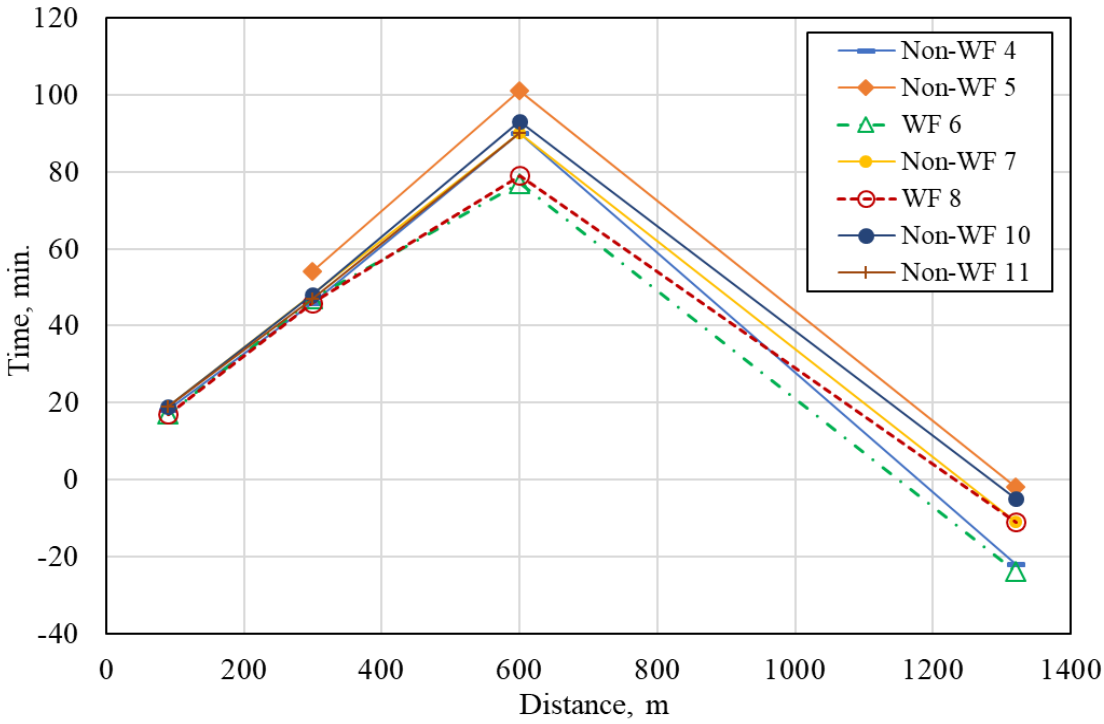

Figure 5.9 Water advance of seven adjoining furrows on Border 2 of Field 3 during the irrigation event on 11-02-2017.

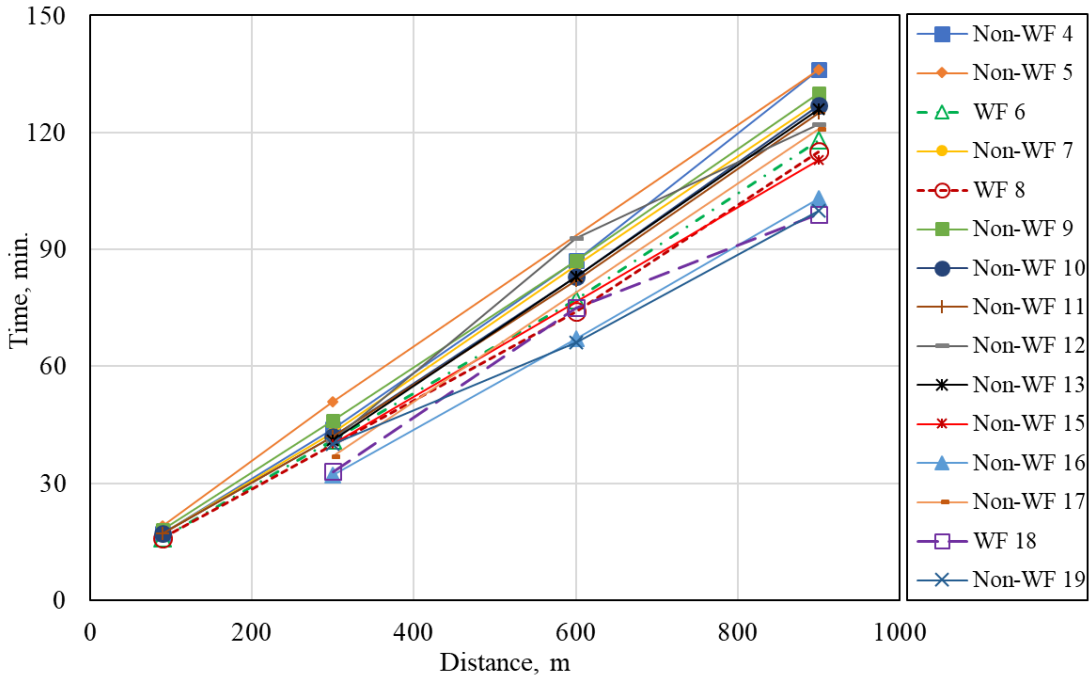

Figure 5.10 Water advance of fifteen adjoining furrows on Border 2 of Field 3 during the irrigation event on 28-02-2017.

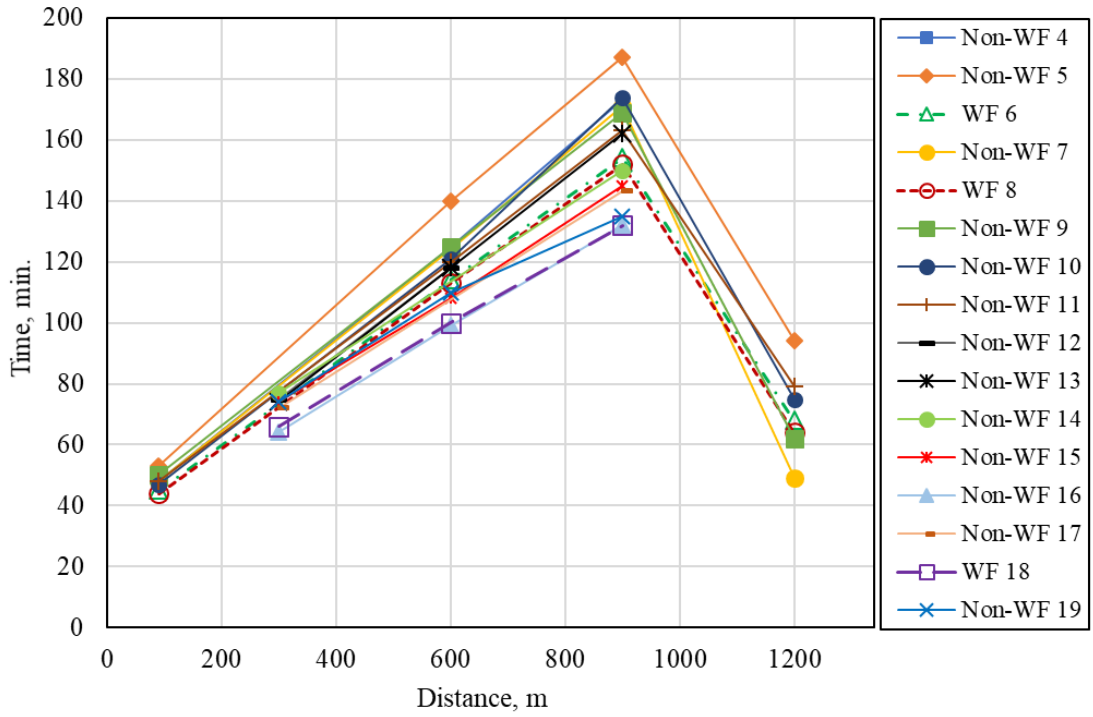

Figure 5.11 Water advance of sixteen adjoining furrows on Border 2 of Field 3 during the irrigation event on 11-03-2017.

5.6.2. Water advance using MotionX GPS app

Water advance measurements using the MotionX GPS app were trialled in one irrigation event on each of Field 2 and 3 on 4-02-2017. The measurements in each field covered two sets of adjoining furrows at two arbitrary interval times. Figure 5.12 shows the advance measurements captured by MotionX-GPS in Border 1 of Field 2 at two time intervals for the irrigation event conducted on the 4-02-2017. The first set of furrow measurements commenced at 6:33 AM and finished at 6:54 AM. The second set of furrow measurements commenced at 8:07 AM and finished at 8:49 AM. As shown above, the required time to conduct the first set of measurement was 21 minutes, while it took 42 minutes for the second set of measurements. The irrigation inflow commenced at 6:00 AM, while the water entered furrows at 6:15 AM. The advance time for the first and the second set of the advance data were about 29 and 133 minutes, respectively. The advance time was calculated by subtracting the time water entered furrows (6:15 AM) from the average ofthe MotionX GPS advance measurement.

As shown in Figure 5.12, there was a variability in water advance data, especially for the second set of advance measurements. The significant variability in the water advance in the second set of water advance measurements can be understood in the total walked distance of 2194 metres to cover 53 adjoining furrows compared to 564 metres to cover 121 adjoining furrows for the first set of advance measurements. Considerable effort was required to conduct these measurements for approximately 53 and 121 adjoining furrows for the first and second sets of the measurements, respectively, with the total distance walked in the first and the second set of the advance measurements taking about 21 and 42 minutes, respectively. In fact, conducting these measurements is considered impractical because it requires considerable time and effort which can impact on the collection of other important measurements such as flow rate in furrows using the SonTek FlowTracker2 instrument. Another drawback of this technique was the inaccuracy in these measurements regarding the furrow number. A simple GPS that does not include a base station correction has an expected accuracy level was in the order of 5 metres. This was tested and compared with surveying and the differences was between 2 to 5 metres over 1000 metres.

The advance measurements presented did not properly account for the real time of the water advance for each single point between the first (Start point) and the last (End point), as per Figure 4.29. Technically, the adjustment can be based on the average walking speed which were 1.6 and 3.1 km/hr for the first set and the second set of the advance measurements, respectively. The real time at each point can be estimated based on the average walking speed, and the distance between the points, by dividing the distance by the average speed, to yield the time to the previous position. Adjusting the first set of the advance measurements presented in Figure 5.12 could be easier than the second set because the latter includes more variation in the advance measurements which required relatively uneven adjustment times compared with the first set.

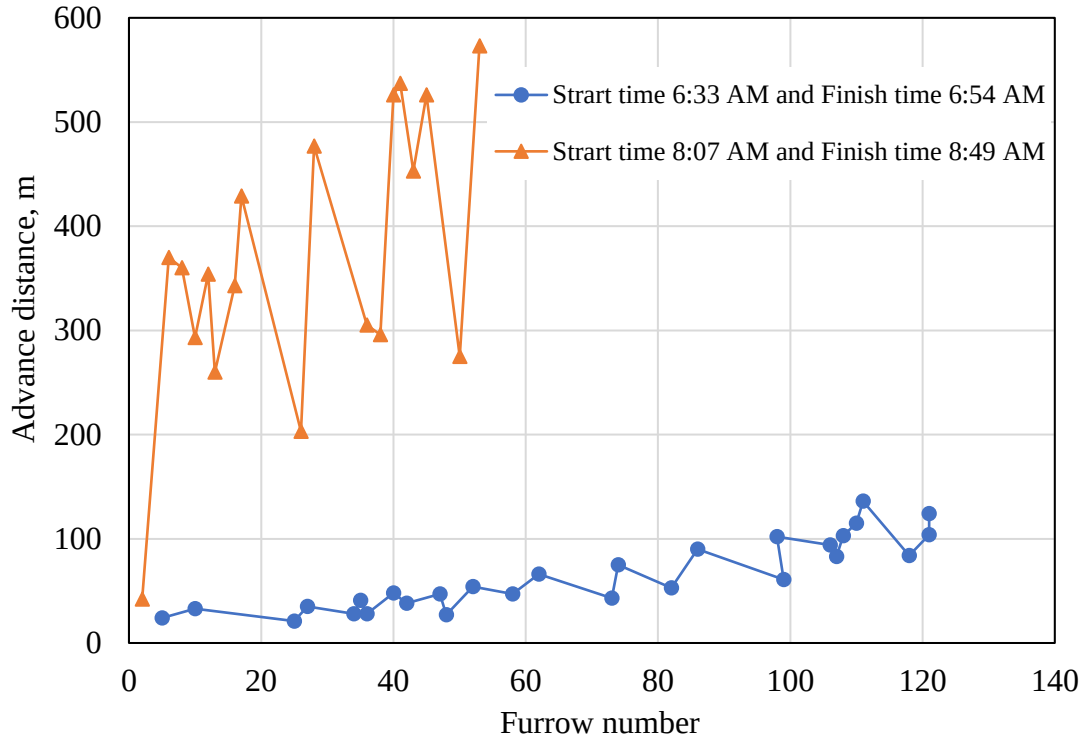

Figure 5.12 Water advance measurements using MotionX GPS for a set of adjoining furrows on Border 1 of Field 2 during the irrigation event on the 4-02-2017.

5.7. Conclusion

The measurements were conducted in Fields 2 and 3 were insufficient to conduct an irrigation evaluation using the well know Two-Point Method because flow rates and advance measurements were captured for different furrows.

Surveying measurements indentified the longitudinal slopes of Field 3 and the location of the sill. The vertical step between adjoining Borders 1 and 2 of Field 3 were estimated.

Furrow cross-sectional area values fluctuated significantly at the furrow entrances whilst maintaining more stable for the remaining length of the furrows.

Commencing field measurements during the irrigation season in both fields made it difficult to conduct specific important measurements such as flow rate measurements at the main supply pipe. This led to an inability to estimate the net volume of water

applied to each border based on the volume balance calculation at the field scale. Mounting the Starflows in the supply pipe was highly risky because the main channel was full of water. There were some trials on which to mount the Starflows, but that proved unsuccessful.

The uniformities of distribution of both water depths and velocities across the check gate suggested that it was appropriate to use one or two Starflows to measure the flow rates. The SonTek FlowTracker2 measurements showed an overestimation trend for the Starflow measurements. Therefore, the Starflow flow rate measurements were modified based on the SonTek FlowTracker2 measurements. Conducting an independent sort of measurement, such as soil moisture content which can be linked to flow rate measurements, and the net water depth held in the soil profile, provides a greater reliability in the measurements and an understanding of the real performance of the irrigation system.

Furrow flow rate measurements showed a large variation in flow rates between furrows, which suggest an inherent difficulty in evaluating this irrigation system, where the whole field could require more measurements for this system compared with the conventional normal slope irrigation systems.

Advance measurements showed a distinctive behavior of water advance from both ends of the border (forward (normal) and backward advance) which made evaluation of the FNSBO_Re irrigation system difficult. Being restricted to a limited number of advance sensors restricted the ability to understand this distinctive behaviour of the water advance where the later focus was on the forward advance. Rapid advances and variations in advance rates between borders were the other significant issues which made the evaluation of this system difficult. Availability of advance sensors for only half of the season led to a shortfall in this data.

The MotionX-GPS smartphone app was used to walk with the water advance in the furrows as an alternative technique that might be applied over a larger scale compared with the IrriMATE advance sensors. However, walking to collect advance measurements was not practical because the height and density of cotton plants made it difficult to collect this data. Moreover, when in the field it was difficult to see the water advance front unless standing in the furrow, because of the density of the crop.

Also, the noticeable variance in the water advance between WFs and non-WFs meant that walking with the advancing front required walking long distances in a zig zag pattern to cover a number of furrows. Combined with the fact that several other important and consuming time tasks also occurred during the irrigation meant that collection of this data during other events was abandoned.

Conducting assessment of the irrigation events for both fields on the same day impacted the collection of sufficient measurements, exacerbated by a lack of both materials and human resources. Usually, the irrigation event in Field 2 was conducted between about 5:30 AM and 12:00 PM, while for Field 3 between 3:30 PM and 7:30 AM of the following day. Therefore, irrigation of two borders (2 and 3) of Field 3 was conducted in darkness which restricted certain measurements such as flow rates in furrows.

Though it was impossible to conduct the irrigation evaluation using the methods explained in the literature (such as the Two-Point Method), this study can be considered a training exercise using many instruments, and proved an adequate understanding of the nature of the irrigation system which requires a special methodology to conduct measurements and analysis. The field work undertaken during this season provided a good understanding of the irrigation process for the current system (FNSBO_Re), which has only been be obtained in a few previous studies.

CHAPTER SIX

Methodology – Season 2

6.1. Introduction

As outlined in Chapter 5, there were an array of data collection techniques used in Season 1, 2017 which were sub-optimal in regard to the ability to estimate the irrigation performance. Therefore, it was necessary to continue to formally develop new measurement techniques in this research, such as the measurement of water depth within the furrows, capturing water advance over a greater scale, and ensuring that flow and advance measurements were conducted in the same furrows. This chapter describes the methodologies developed and used during the field trials in Season 2.

6.2. Field site

The Season 2 field trials took place at the same commercial farm near Boggabilla in New South Wales. The field measurements were conducted on Field 2, which was also measured in Season 1. Field 3, described in the previous chapters, was left unplanted for this season, and thus no irrigations took place. The soils characteristics in Fields 2 and 3 are the same as described in Section 5.2, Table 5.1.

6.3. Surveying field and furrow geometry

6.3.1. Field survey

A robotic total station (Leica TCRA1203) was used to collect position and elevation measurements. These measurements were collected in Field 2 to find the longitudinal slope down the field and the bankless channel. These measurements would be used to interpret the hydraulic behaviour in Field 2. Surveying measurements were carried out on 13 and 24 adjoining furrows in Borders 1 and 2, respectively, at variable intervals along the field length. The measurements were also carried out for several cross sections of the head and tail bankless channels along each end of the field.

6.3.2. Furrow geometry

A simple profile meter was manufactured and used to conduct furrow cross sectional measurements (Figure 6.1). The profile meter consisted of a frame (tempered wood) with the dimensions 90×12×1600 mm. 15 holes (9 mm diameter) were drilled along the profile meter frame with an interval distance of 70mm between holes. The holes were arranged in such a way that there was a zero labeled hole positioned half way along the profile meter frame, then 7 holes positioned on the right side of the zero labeled hole and another 7 holes positioned on the left side. Fifteen graduated sticks (dowel wood) with a circular cross section (8 mm diameter, 700 mm length) were slid inside the holes to measure the depths across the width of the furrow. These dowel sticks were graduated with a centimeter scale taking into account the thickness of the tempered wood. The profile meter was designed to measure the furrow depth every 70 mm interval over 980 mm of furrow width. The profile meter was designed to measure the top width of furrows to investigate whether they would reach to 1600 mm. However, the highest recorded furrow top width was 1010 mm.

The furrow cross sectional area measurements included 12 adjoining furrows in Border 1, from Furrow 1 to Furrow 12 adjacent to the middle bank between borders, and Furrow 13 to Furrow 24 near the middle bank between adjoining borders in Border 2 of Field 2. Location of the measured furrows is shown in Figure 4.3.

Only three sets of furrow cross-sectional measurements were conducted throughout Season 2. The first set of measurements was conducted on 29-12-2017 in Border 2 of Field 2 at about 51 to 52 m from the furrow entrances. The second and the third sets of measurements were conducted on 10-01-2018 and 18-01-2018, respectively on Border 1 of Field 2, about 53 to 54 m from the furrow entrances. As previously mentioned in Section 4.3.2, the idea behind selecting 12 adjoining furrows was to capture measurements of the repeated pattern of adjoining furrows, because the field machinery being used have a width 6 or 12 m when cultivating, planting, fertilizing, and harvesting. The measurements began by measuring the furrow top width from the centre of the furrow where the middle (zero labeled) graduated dowel was positioned. After ensuring that the profile meter frame was level between both beds either side of

the furrow, the graduated dowels were passed through the holes to touch the soil gently. Then the coordinates of the furrow cross section were manually recorded.

These measurements gave a general concept of the cross-sectional areas of flow in the furrows, and the impact of machinery movement and soil compaction on the furrow shape.

Figure 6.1 Profile meter with graduated dowels, used to measure the furrow cross sectional area.

6.4. Site description

The field measurements were conducted in Field 2 which has the characteristics of a near zero slope furrowed border irrigation systems with common water supply. Field 2 was previously described in Section 4.4.

6.5. Irrigation management

Generally, the irrigation process in Field 2 was the same as that adopted in the Season 1 and in most irrigation events of Season 2 (Section 4.6). However, there were some unusual irrigation processes that happened in two irrigation events.

Firstly, on the 30-12-2017, the water supply to the field from the main pipe was temporarily stopped for 76 minutes. It is believed that the reason was to increase the water level in the main channel through additional pumping of water from the dam. A declining water level in the main channel impacts the ability to supply the required flow rate for Field 2. The second unusual practice was also in the event of the 30-12-2017, when one of the sub-sections of the top and bottom check gates was opened for approximately one hour before all check gates were completely opened. Thirdly, on the 26-01-2017, the tail drain box at the end of the bankless channel at the bottom of the field was left closed for about three hours after the water supply was stopped. This was to provide better uniformity through the backward advance and ponding at the bottom end of the field. This practice also attempts to reduce the possible erosion that occurs when opening the tail drain box immediately after stopping the water supply.

Table 6.1 reports the important irrigation management information for Fields 2 in Season 2, which are irrigation intervals, and planting and harvesting dates.

Table 6.1 Irrigation intervals, and planting and harvesting dates of Fields 2 in Season 2.

Irrigation event no.	Event date	Irrigation intervals, days	Growing information
0	30-10-2017	-	Planting
1	15-12-2017	55	
2	30-12-2017	15	
3	1-11-2018	12	
4	19-01-2018	8	
5	26-01-2018	7	
6	2-10-2018	15	
7	17-02-2018	7	
	10-05-2018		Picking

6.6. Hydraulic measurements

6.6.1. Flow rate measurements at field scale

At the field scale, calibrated Starflow^{TM} Ultrasonic Doppler meters were used to measure water velocities and water depths at the inlet water structure and the check

gates of Field 2. Flow rates were calculated based on the logged data (water depth and velocity), as detailed in Section 4.7.1. Flow rate measurements at the check gates were adjusted using comparative SonTek FlowTracker2 measurements (see Sections 5.5.1).

A pipe ring was used to mount two of the Starflows in the main supply pipe of the inlet structure in Field 2 (Figure 6.2). Starflows were offset from the bottom of the pipe to avoid silt deposition blocking the transducers, which would have led to poor data. It was decided that two Starflows would be installed in the pipe to reinforce the reliability of the measurements and reduce the risk of data loss in the case of any damage or fault. Whenever two Starflows were positioned at one measurement position the average flow rate was used. Starflow installation was carried out during the maintenance period of the main supply channel before Season 2 when the channel was empty. As shown in Figure 6.2 (a), there was a requirement to pump out the remaining water in the supply pipe before completing the pipe ring installation. There are a number of parameters required to define a Starflow logging scheme to measure flow in pipes. The pipe diameter, sensor invert offset, and dead sector are illustrated in Figure 6.3. The pipe diameter was 900 mm, and the offsets were 287 and 256 mm for the Starflows with the serial numbers 1619 and 1912, respectively. The dead sector value was entered as zero, leading to the assumption that the high stream velocity would remove all the deposited silt in the pipe. The supply pipe extended 15.6 m underground from the main channel to the inlet structure. The pipe ring was mounted 8 m from the upstream end of pipe at the main channel side, a distance of more than 9 pipe diameters. This distance would minimise the impact of turbulent flow conditions (Unidata 2013).

Two Starflows were mounted at each check gate at the top and bottom of Field 2 (Figure 6.4 and Figure 6.5). All the Starflows mounted on a bracket have the same height (offset) of 66 mm. It should also be taken in account that it is important to avoid the impact of eddies caused by the pylons when mounting the Starflows. At the top check gate of Field 2, the Starflow was positioned at the mid distance between the pylons of the second and third sub-gate, as shown in Figure 6.4. The distance between these Starflows and the top check gate was 1800 mm. The position of the Starflows at the check gate at the bottom of Field 2 were at the middle of the second sub-gate, as

shown in Figure 6.5. The distance between these Starflows was 170 mm, and the distance between these Starflows and the bottom check gate was 1800 mm.

Figure 6.2 a) the inlet structure appearing at the soil surface, showing the supplying pipe 900 mm in diameter. B) Pipe ring used to mount two of Starflow in a main supplying pipe has 900 mm in diameter.

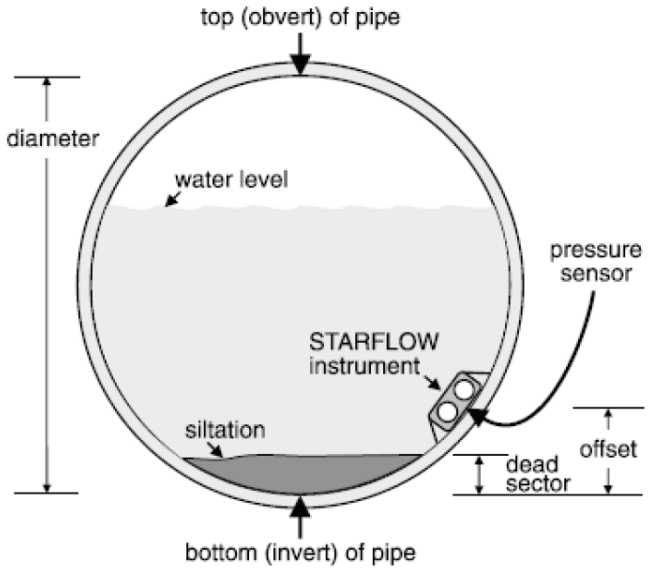

Figure 6.3 The required parameters to define a scheme of the Starflow for the flowing in the pipes. The figure taken from the Starflow Manual (2007).

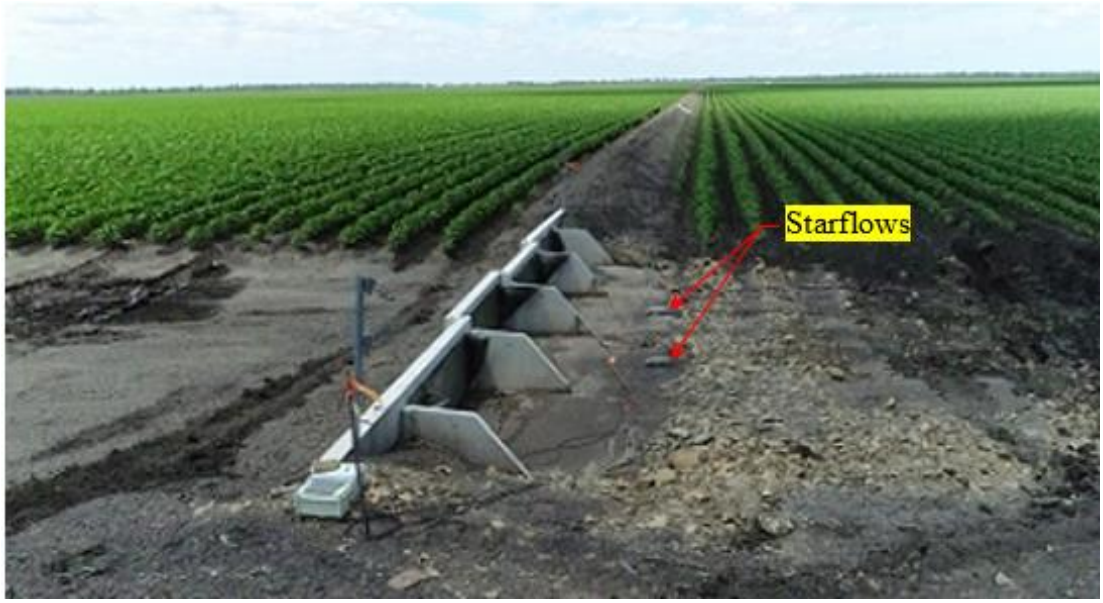

Figure 6.4 Two Starflows mounted on brackets (to avoid mud deposits), downstream of the check gate at the top of Field 2.

Figure 6.5 Two Starflows mounted on bracket (to avoid mud deposits), downstream of the check gate at the bottom of Field 2.

At the head-end drain box at the top of Field 2, a Starflow was mounted inside the concrete structure on a bracket because of the deposited silt (Figure 6.6). This Starflow was only used to log the water depths during the irrigation events so that flows could be inferred through use of appropriate hydraulic theory. Flow rates from the outlet pipe to the drain ditch were estimated based on total head losses (H_{total}) due to friction (h_f) and minor losses (h_m), as shown in Equation 6.1 (Chadwick & Morfett 2013).

$$H_{total} = h_f + h_m \qquad 6.1$$

The Darcy-Weisbach Equation 6.2 was used to estimate the friction losses in the pipe (Chadwick & Morfett 2013).

$$h_f = f \frac{l}{D} \frac{V^2}{2g} \qquad 6.2$$

where:

f is friction factor, dimensionless

l is the pipe length, m

Figure 6.6 Starflow mounted on a bracket inside the concrete structure of the head drain box top of Field 2.

D is the pipe diameter, m

V is flow velocity, m/s

g is gravitational constant, m/s^2

The friction factor (*f*) was calculated using the Barr Equation 6.3 (Chadwick & Morfett 2013).

$$\frac{1}{\sqrt{f}} = -2\ log\left(\frac{\epsilon}{3.7\ D} + \frac{5.1286}{Re^{0.89}}\right) \quad 6.3$$

where:

ϵ is the roughness of the pipe wall, (assumes ϵ = 0.03 mm for wrought iron (PIA 2013))

Re is Reynold number (dimensionless) calculated using the equation below.

$$Re = \frac{VD}{\nu} \quad 6.4$$

where:

ν is kinematic viscosity, m^2/s. (ν = 0.000001133 for water at 20 ºC)

The minor losses are expressed in terms of the kinetic energy and a resistance coefficient (k_m) which reflect the impact of the sudden changes in the direction or magnitude of the water velocity at the pipe exit and entrance as shown in Equation 6.5 (Chadwick & Morfett 2013).

$$h_m = K_m \frac{V^2}{2g} \quad 6.5$$

where:

$$K_m = K_{m1} + K_{m2} \quad 6.6$$

where:

K_{m1} and K_{m2} are the resistance coefficients at the pipe entrance and exit, respectively (assumed 0.5 and 1.0, respectively (PIA 2013), and so combined, K_m is 1.5).

Substituting Equations 6.2 and 6.5 into 6.1 yields:

$$H_{total} = f \frac{L}{D} \frac{V^2}{2g} + K_m \frac{V^2}{2g} \quad 6.7$$

The elevation difference (*ED*) between the inlet and outlet pipe was measured using a dumpy level instrument. The total head losses (H_{total}) between the inlet and outlet pipe can be calculated from the combination of the measured elevation difference (*ED*) and the water depths logged via Starflow at the pipe inlet. Pipe length and diameter were measured by a measuring tape. The pipe roughness coefficient (ϵ), the resistance coefficient (K_m), and the water kinematic viscosity (v) are explained above. Table 6.2 shows the values of the variables required to conduct the flow rate calculation for the gated drain box at the top of Field 2. The calculation commences by assuming a value for the flow rate (Q) then calculating the water velocity based on the following equation:

$$V = \frac{Q}{\left(\frac{\pi D^2}{4}\right)} \quad 6.8$$

Reynolds number is then determined using Equation 6.4, then friction factor (f) using Equation 6.3 followed by velocity using Equation 6.7. This process is repeated until the value of velocity does not change significantly. Table A-6 in Appendix A shows the calculation of the flow rates that from the head drain box for the irrigation event conducted on the 10-02-2018.

Table 6.2 Required information to calculate the flow rate in the drain box at the top of Field 2 based on the total head losses.

Item	Value	Note
Pipe length (l), m	10	Measured by tape
Pipe diameter (D), m	0.3	Measured by tape
Elevation difference between the inlet and outlet pipe (ED), m	0.2821	Measured by dumpy level instrument
Total head losses (H_{total}) equals to (ED + water depth logged via Starflow)		
Roughness of the pipe wall, (ϵ), mm	0.03	(PIA 2013)
Minor losses resistance coefficients at the pipe entrance and exit, K_{m1} and K_{m2} respectively (dimensionless)	1.0 and 0.5, respectively	(PIA 2013)
Combined minor losses resistance coefficient ($K_{m1} = K_{m1} + K_{m2}$)	1.5	
Kinematic viscosity (v), m^2/s.	0.000001133	for water at 20 ºC

At the tail drain box at the bottom of Field 2, a Starflow was mounted next to the concrete structure on a bracket because of the deposited silt (Figure 6.7). This Starflow was only used to log the water depths during the irrigation event. It was decided that a weir equation could be used to estimate the flow rate drained from this tail drain box. The characteristic of the top crest of the tail drain box structure can not be considered explicitly as a broad or sharp-crested weir. The breadth of the top crest of the tail drain box structure was 85 mm and does not have a sharp cross section. Both equations of the broad crested weir (Brater et al. 1996) and sharp-crested weir (Kindsvater & Carter 1959) were investigated for estimating the flow rates drained from the tail box. The difference in the estimated flow rate was 8.8% between the two weir types.

Flow rates for the tail drain box were estimated using the equation of broad-crested weir 6.9 (Brater et al. 1996) as following:

$$Q = C_{db} U Y^{1.5} \qquad 6.9$$

where:

C_{db} is discharge coeficient for broad-created weir, dimensionless (C_{db} = 1.83 (Brater et al. 1996)).

U is the length of the crest (perimeter of the crest measured by tape), in metres.

Y is the net water depth above the crest, in metres, measured by the Starflow. This net water depth is found by subracting the difference between the Starflow depth transducer head and the crest top edge from each Starflow depth value.

Alternatively, flow rates for the tail drain box were estimated using the sharp-crested weir Equation 6.10 (Kindsvater & Carter 1959).

$$Q = C_{ds} \frac{2}{3} \sqrt{2g} U Y^{1.5} \qquad 6.10$$

C_{ds}, the discharge coefficient for a sharp-created weir (dimensionless), can be calculated using the following equation (Kindsvater & Carter 1959):

$$C_{ds} = 0.602 + 0.075 \frac{Y}{P} \qquad 6.11$$

where, *P* is the height of the crest in metres.

Table A-7 in Appendix A shows the calculation of the flow rates through this tail drain box structure for the irrigation event conducted on the 10-02-2018, using sharp-crested weir equations. It was decided to adopt the results of the sharp-crested weir to estimate the net water volume held in Border 2 of Field 2 as it is believed that is the closer to the real situation for the flow over the tail drain box.

Unfortunately, this Starflow did not function well for all irrigation events. In most cases the Starflow failed to log data for the whole period of the irrigation event.

Figure 6.7 Starflow mounted on a bracket next to the concrete structure of the tail drain box at the bottom of Field 2.

6.6.2. Flow rate measurements at furrow scale

6.6.2.1. SonTek FlowTracker2

At the furrow scale, the SonTek FlowTracker2 was used to measure water velocities in individual furrows. The flow depths required to determine cross sectional area and discharge were measured manually using a ruler. Because of local undulations in the furrows, water depth was measured at multiple locations in the same furrow, but close to the SonTek measurement location, and the average value was adopted.

Unlike Season 1, the area of flow was calculated based on the measurements of cross-sectional area measured by the profile-meter. Each flow area at the corresponding flow depth was estimated from the relationship between furrow cross-sectional areas and depths. This relationship was calculated based on the extracted pairs of areas and depths from the furrow profile meter measurements, using AutoCAD. The flow rates were calculated separately in a spreadsheet program using the water velocities (measured by SonTek FlowTracker2) and corresponding flow area (as explained above).

The measurements were conducted for 12 adjoining furrows in both Borders 1 and 2 of Field 2. These furrows coincide with the same furrows that were used for the shape cross section measurements, i.e. 12 furrows starting from No. 13 in Border 1 and 12 furrows starting from number 1 in Border 2. The location of the selected furrows sets are shown in Figure 4.4.

The measurements conducted in Field 2 were for all irrigation events in this season (7 events) in Border 2, and for the last five irrigation events for Border 1. For four events, the measurements were conducted twice for each border at two different times, while inflow into that border was still occurring. The methodology for these measurements was explained in Section 4.7.2.

6.6.2.2. Starflow

In parallel to the SonTek FlowTracker2 measurements, Starflow instruments were also used to measure flow rates in individual furrows at both borders of Field 2 in the irrigation event conducted on the 10-02-2018 (see Figure 6.8). Installation of such devices in small furrows was difficult because of the small size of the water stream in comparison to the dimensions of the instrument.

At the fourth and sixth furrows of Border 1 and Border 2, four calibrated Starflow instruments were mounted in the middle of the furrow at approximately 60 metres downstream from the furrow entrance, to log water depths and velocities during the whole irrigation event. Flow rates were calculated based on the logged data (water depth and velocity), and the cross-sectional area measurements from the profile-meter, as explained in Section 6.6.2.1. The idea behind the selection of these specific furrows was to represent both wheeled and non-wheeled furrows (WFs and non-WFs), where the fourth furrow in both borders represented the non-WFs, while the sixth furrow in both borders represented the WFs. Because of the short length of the Starflow cable (wire), it was decided to install the Starflows in the fourth and sixth furrows in Border 1 rather than the normal measured ones (Furrow 13 to 24). This meant that the battery power supply could be placed on the check bank between the two borders thus avoiding damage to the batteries by water. Unfortunately, two of these measurements failed (Furrow 4 in Border 1, and in Furrow 6 in Border 2) inconsistent data was logged due to plant residue covering the transducers of the instrument.

All devices used in the furrow flow measurements were mounted on a piece of wood board with a thickness of 12 mm to avoid disrupting the water depth sensor with soil particles. The thickness of the wooden board has been taken into account in all depth calculations.

Figure 6.8 Flow measurements at the furrow scale using Starflow instruments mounted in the Furrows 4 and6 in Borders 1 and 2 of Field 2.

6.6.2.3. Flow rate measurements using fixed camera technique

The difficulty and intensive manual effort in measuring furrow depth and flow during Season 1 suggested that action cameras positioned at the correct location might be able to capture the flow velocity in the set of adjoining furrows (Figure 6.9). The suggested methodology was to mount an action camera on a wooden stake and faced towards two stakes inserted in the middle of the measured furrow, to record water velocities for many time intervals during the irrigation event (Figure 6.10). Water velocity measurements in the furrows were conducted by recording a video with an action camera to measure the water velocity between two stakes with a 1 m distance between them, at a specific time at a specific furrow. The velocity was detected by identifying the movement of floating debris or bubbles in the irrigation water. Water depth measurements in the furrows were measured manually with a ruler at the time of video recording. The area of flow was calculated based on the cross-sectional area measured with the profile meter, as explained in Section 6.6.2.

The video recording was manually inspected for floating trash or bubble movements. The millisecond timing feature was displayed to precisely capture the duration that

floating trash or bubbles took to pass between two stakes set at a predetermined distance.

In this trial, three action cameras were tested. Two of these cameras were EKEN H9R 4K brand and the third one was Inca 4K brand. These cameras were provided with a waterproof housing. Regarding the EKEN H9R action camera the photo and video commands can be triggered using a remote control and have a control range of about 10 m. Both cameras can be triggered by one remote control. Its operation is simple: the remote control has two buttons, the first one for photo and the second for video. The main advantage of this technique was the ability to control these action cameras from one place by one remote control. The suppliers (in Europe, Japan, and USA) of this brand on state the ability to trigger 12 action cameras via one remote control. For the Inca 4K action camera the remote control was deployed through a mobile app. Testing indicated that this camera could be remotely triggered over a range exceeding 20 m. Apart from the remote triggering most other specifications are close to the EKEN H9R action camera. The main drawback of these cameras was their sensitivity to high temperature. These cameras became hot once installed in the field, and attempts to cool them so that they could continue working was impractical because of the necessity to conduct other important evaluation measurements, such as flying the UAV and measuring furrow flow rates.

Figure 6.9 **Three action cameras mounted on wooden stakes to record water velocities in three furrows at many time intervals during the irrigation event.**

Figure 6.10 Image from a video recorded by an action camera to measure the water velocity between two stakes spaced 1 m apart.

6.6.2.4. Flow rate measurements using UAV and food colouring technique

Attempts were made to measure flow rates in furrows using UAV and food colouring as an alternative measurement technique. The planned methodology was to estimate the flow rate in four adjacent furrows (Furrows numbers 18, 19, 20, and 21 located in Border 1 of Field 2) based on measuring the food colour velocity along a certain distance in the furrow using the UAV (Figure 6.11). The measured water velocity represents the surface velocity of the flow which is detected with the UAV camera. The water depth in each furrow was measured manually using a ruler immediately after completing the velocity measures in the middle of the trial distance (20 metres from the furrow entrance). The area of flow was calculated based on the measurements of the cross-sectional area measured with the profile meter, as explained in Section 6.6.2. The measurement was conducted by hovering the UAV above the start point at the furrow entrance and, immediately applying the dye at the beginning of the furrow (Figure 6.12). Then the UAV was guided to chase the dye front edge at the determined distance. Wood stakes were mounted at 10 metres intervals commencing from the furrow entrance to 40 metres down the field. A coloured ribbon was put in these stakes

to recognize them easily. A few colours were tested before conducting this measurement to determine which colour was more visible in the water stream. Blue colour is suggested as it is the most visible colour.

While the use of the UAV provides the ability to measure food colouring movement compared to walking in muddy furrows, the quick dispersion of the blue food dye and the obstruction by the plant canopy made it very difficult to detect the dye any further than a few metres from the furrow entrance.

Figure 6.11 Selected furrows to conduct the flow rate measurements using UAV and food colouring technique. Wood stakes mounted at 10 metres intervals.

Figure 6.12 Estimating the flow rate in the furrows using UAV and food colouring technique.

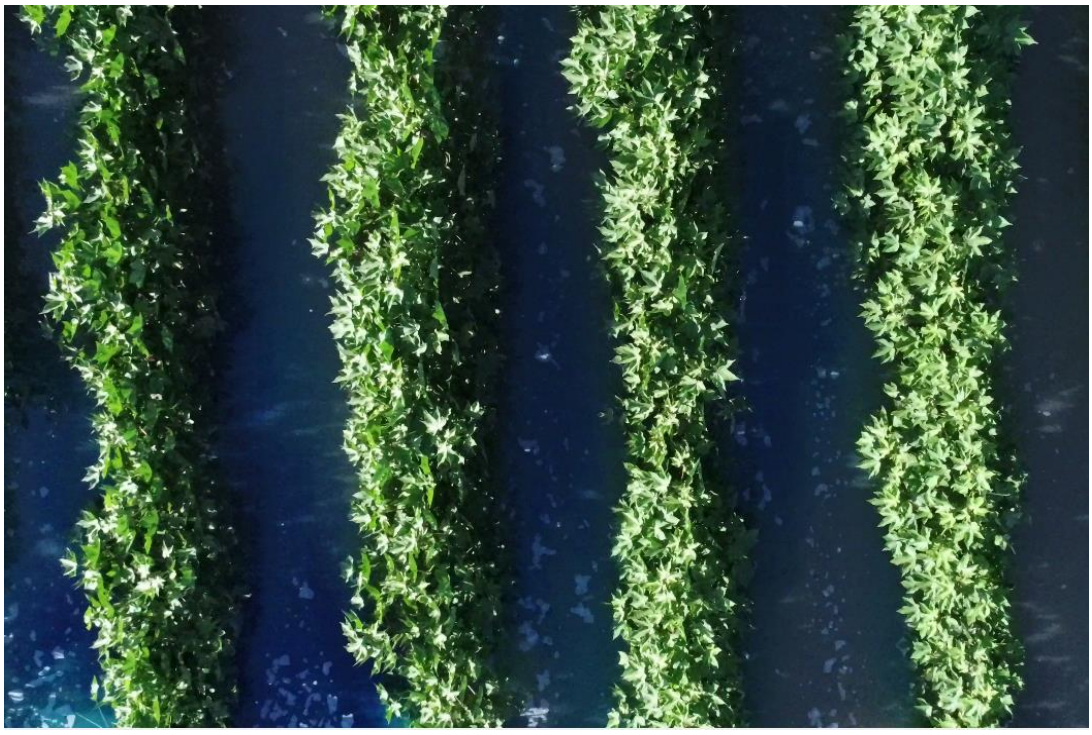

Figure 6.13 Detecting the food colouring front edge in the furrows using UAV.

6.6.3. Water advance measurements

Water advance measurements were conducted in Season 2 using the same technique as was adopted in the previous season (IrriMATE advance sensors), and, additionally using a new technique with an unmanned aerial vehicle (UAV).

6.6.3.1. IrriMATE advance sensors

Water advance measurements were conducted using IrriMATE advance sensors in two events in Season 2 in Border 1 of Field 2 (Figure 4.28). The measurements were conducted during the events on the 10-02-2018 and 17-02-2018. As explained in Section 4.7.4, two sets of advance sensors were installed at certain distance intervals along the lengths of the furrows, to record the arrival time of the water front advance. Each sensor has eight terminal ends to log the arrival time of the water front at eight adjoining furrows. Therefore, advance was measured in sixteen adjoining furrows. The adjoining instrumented furrows in Border 1 commenced from Furrow 13 to Furrow 28, with Furrow 13 being the closest to the check bank between the two borders (see Figure 4.3). The determined intervals of these sensors for the event on 10-02-2018 were 166.5, 312.8, 438.5, and 542.8 metres, whilst for the event on the 17-02-2018 these were 166.5, 312.8, 438.5, 520, and 600 metres.

6.6.3.2. Unmanned aerial vehicle (UAV).

In Season 2 an unmanned aerial vehicle (UAV) or drone technique was trialed in order to collect the water advance and recession measurements. The water advance front can be recognised based on the reflection of the sunlight on the water surface, as captured by the drone's camera. Variations in the soil colour due to the wet soil conditions did also help in recognising the water advance front.

A Phantom 4 Advanced drone from DJI was selected to conduct these measurements because of its high specifications and the comparison with the cost in the Australian market. The Phantom 4 Advanced drone includes a camera with 20 Mega Pixels, and 84°Angle of view (FOV). The maximum flight time is about 30 minutes, and the maximum speed is 72 km/hr. The maximum control range of the remote controller is about 7 km, with a live view on the screen.

The Litchi App, which is compatible with Phantom 4 Advanced, was installed in the tablet to set up the flying missions of the drone. The Litchi application supports the Waypoint flight mode, where predetermined flight missions can be created and uploaded to the UAV.

Waypoint flight mode enables the user to create a specific path on a Google map, where GPS waypoints can be entered to specify the path track. This technology enables the drone to fly on its own, according to predetermined points on the map, while adhering to specified speeds and altitudes, and to perform actions such as recording videos or taking photos at specific points during the flying mission.

Litchi provides the flexibility to create and edit flight missions through its website (https://flylitchi.com/hub), which are then automatically synchronised to the tablet when it is connected to the internet. Figure 6.14 shows the Litchi hub website with one of the waypoint flight missions in Border 1 of Field 2. As shown in Figure 6.14, the flight paths are labelled with numbers that refer to the sequence of the flight, as well as the length and altitude of each path. It also includes other information such as the user account name, file name, total length of the flight mission, and the expected time to accomplish it. Flight missions were conducted in both borders of Field 2, from the second irrigation event to the last in this season. Generally, flight missions were designed to record water advance and recession measurements in furrows across the field at approximately constant interval along the field length. For Field 2 it was decided that the paths would be spaced at 100 m intervals, starting from near the top edge of the field. The last flight path across the field was at 148 metres from the bottom end of the field (Figure 6.14). In some flight missions, the flight paths were longitudinal paths as shown in Figure 6.15.

Setting up flight missions in the Litchi app included adjusting several inputs depending on the particular factors: drone specifications (camera capacity and battery life); field size; growing stage; and sunlight beam angle. The main flight missions inputs that were adjusted in the Litch app were flight altitude, length and speed of flight.

Part of the objective in this season was to identify the optimal altitude and travel speed in order to successfully capture water advance and recession, while furrows were

partially covered by the cotton crop. Flight missions were conducted at several altitudes: 25, 15, 8, and 5 m. Flight mission speeds tested were 25 and 15 km/hr.

Figure 6.14 Litchi hub website with one of the flight mission with cross paths in Border 1 of Field 2.

Figure 6.15 Litchi hub website with one of the flight mission with longitudinal paths in Border 2 of Field 2.

Higher flight altitudes and speeds were adopted in the earlier stages of the growing cotton, where the canopy was less likely to obscure the water in the furrow, while at the later stages of the season, a lower flight altitude and speed was more appropriate.

From the middle of the season onwards, the influence of the canopy was unavoidable. The starting time of the irrigation event and the sunlight angle were significant at these advanced stages of growing. When the canopy was tall, the reflection of the sunlight on the water surface could not be easily recognized using the visible camera, as easily as when the sunlight was at an angle.

Flying longitudinal paths along the length of the furrow (Figure 6.15) at low altitude was an alternative, which reduced the impact of the canopy and improved the ability to detect the advance, and most particularly the recession. Tests of this approach succeeded, but it was observed that these longitudinal paths did not cover much of the field, focussing only on a small number of furrows, and also unable to determine the location of the advance or recession measurements accurately.

On the other hand, the flight mission with the longitudinal paths covered small number of furrows and was unable to determine the location of the water front edge accurately.

Camera specifications of the drone determined the maximum flight altitude with acceptable quality of recorded videos and photos. The aim was to complete the maximum number of flight paths and missions possible with the permitted flight time and number of batteries, given the field dimensions. Wind conditions, the number of flight path changes (drone manoeuvres), and the flight speed all increased the power draw, and influenced the maximum flight time. The number of high cost drone batteries, and accessibility to charge them in the field determined how many flights could be achieved during one irrigation event.

Selection of a start time for the flight mission during the irrigation event, depended on the overall advance time in each border. Where possible, the first flight was attempted when the water advance reached between one third to one half of the field length of each border. Sometimes, more than one flight was conducted in each border. Regarding the recession phase, more than one flight mission in each border can be

allocated to record the recession data at prolong intervals to make sure completing the recession phase at least from the majority of the border.

As discussed earlier, it was easier to identify water advance in the early growth stages, and hence the altitude of the UAV was increased to capture a path on each pass across the field. It can be concluded that the water advance measurements conducted by the drone at the earlier growth stages of cotton were better than the measurements at the mid to late stages of the growing period.

Forward and backward water advance front distances, and recession data were extracted from the videos recorded by the UAV camera. The process to extract advance and recession data from the UAV images was as follows:

1. Use VLC media player to generate a series of screen shots for each mission
2. Number each furrow in the screenshots
3. Identify any visible forward or backward water front advance in the images
4. Measure the distances of the identified advance and recession on the image either using a ruler on a printout, or using the VLC measure tool
5. Convert these distances to real distances using the known path of the flight and the scale ratio of the image
6. Compile all water advance / recession measurements in Excel.

Although the actual flight paths are located at distances of 100, 200, 300, 400 and 500 metres from the furrow entrances at the top end of the border, in many instances the water advance may not be detected in the photos, because it is located just outside the visible regions from the flight path videos. For example, water may be detected at 100 metres, but no water is present at 200 metres. In this case it is uncertain if the water has just passed 100 metres or is closer to 200 metres. In these situations, the intermediate positions (150, 250, 350, 450, and 570 metres) located halfway between flight paths are adopted. The adopted distance of 570 metres is located at the midpoint distance between the actual distance (500 metres) and full length of Field 2, which is 640 metres. Similarly, these intermediate positions are adopted for the recession measurements.

The advance time or recession time in each flight mission is calculated by subtracting the time that water first enters the furrows at the top of the border, from the flight mission commencing time. If there is more than one flight mission is conducted to capture the recession phase, it is suggested that the average time between the first and the second flight mission is adopted as the recession time for the second mission. The average of the second and the third flight mission time is adopted as the recession time for the third recession flight mission, and so on. The time of the first recession flight mission is not adjusted. This is because of the uncertainty in identifying the receding edge and associating a recession time with the given flight mission time.

6.6.4. Water depth measurements

Water depth measurements were collected in Season 2 as it was thought that this information could improve the understanding of water distribution among furrows during the irrigation event. The high cost of water depth probes required adoption of other inexpensive means to measure the water depth in the furrows. Three techniques were used to conduct these measurements: a fixed camera, a float, and a painted wood stake with food colouring.

6.6.4.1. Water depth measurements using fixed camera technique

Following the same approach for the fixed camera for measuring water velocity in the furrow (Section 6.6.2.3), water depth measurements in two furrows were conducted by taking many photos of the graduated stake in the middle of the furrow during the irrigation event (Figure 6.16).

Figure 6.16 Photo taken by an action camera to measure the water depth at specific time in one furrow.

6.6.4.2. Peak water depth measurements using a float technique

A simplification of a peak water depth gauge developed by (Saxon & Dye 1995) was also tried in the furrow in this study (Section 3.4). The device developed (gauge) consists of three parts: a stainless-steel rod, a float and a rubber washer (Figure 6.17). This gauge works based on a buoyancy force which lifts up a float when the water is rising. The float slides along a stainless-steel rod 1200 mm long with a diameter of 9 mm. A rubber washer glued beneath the float serves as a brake to prevent the float from sliding down when the water level falls (upper right corner of Figure 6.17) to produce an accurate measurement. The stainless-steel rod is inserted into the soil to 300 mm depth in the middle of the furrow using a hammer and spirit level to ensure that it is vertical. The float is made from a buoyant plastic foam cylinders 70 mm in diameter cut into 90 mm lengths. The rubber washer is made from used tyre tubes. A mark was put on the float to indicate the position that the measurement of peak water depth should commence from. The position of the mark was determined based on a calibration process conducted with a bucket of water, gradually filled to simulate water rising in the furrow. The float is positioned about 50 mm above the ground (at the

lower end of the stainless-steel rod) before calibration or measurement in the field is started.

Three gauges were manufactured and each one was labelled with a number and a letter indicating the furrow and border number. One gauge was inserted at each measured adjoining furrow, at about 55 m from the furrow entrance in order to be close to the sill where the normal downstream slope commences. In Border 1 measurements were completed in furrows numbered 13, 14 and 15 near to the middle check bank.

Figure 6.17 Peak water depth gauge inserted in the middle of the furrow, and a picture insert of the foam float with the rubber washer on top.

6.6.4.3. Peak water depth using painted wood stakes with food colouring technique

Wooden stakes painted with food colouring were used to conduct peak water depth measurements in the furrows, as also shown in Figure 6.18. The food colour painted on the stake (17×17×1200 mm) dissolves easily in water, so the peak water depth that had been reached in the furrow (during the irrigation event) can be identified by recognising the washed part of the painted stake. Wooden stakes were prepared by painting them with a low sheen white interior paint, to protect the wood and to allow

the food colouring to be recognised easily. Then, the stakes were marked with a whiteboard marker with a simple line 200 mm from the sharp bottom end of the stakes. This mark indicated the part that should be inserted into the soil. The stakes were painted with food colouring to slightly more length than expected to be covered with water. The part of the stake from the mark to the sharp end did not need to be painted with food colouring, as it would be underneath the soil surface. Each stake was inserted into the middle of the furrow using a hammer and a spirit level to ensure that it was vertical. Each stake was labelled with a number and a letter indicating the furrow and border number.

Peak water depths in the furrows were measured for several irrigation events at Field 2. These measurements encompassed either one or both borders. The set of measured furrows at each border consisted of 36, 24, or 12 adjoining furrows. One painted stake was inserted in each measured adjoining furrow, at about 52 m from the furrow entrance in order to be close to the sill where the normal downstream slope commences. The furrows measured in Border 1 were near the middle check bank between the adjoining borders, from furrows 13 to 36 or 48. The measured furrows in Border 2 started from the furrow number 1 near the middle check bank between the adjoining borders, to furrow number 12 or 24.

At the end of the irrigation event, the painted stakes were collected to measure and record the peak water depths in the furrows. The stakes were then cleaned of any mud and painted again for the next event.

It was noticed that the washed part of the paint from the stake had a different level on each of the four sides of the stake (Figure 6.19). The surface of the stake that faced upstream (front surface) mostly indicated a higher magnitude of peak water depth. The opposite surface of the stake that faced downstream mostly indicated a lower magnitude of peak water depth. The other two lateral surfaces of the stake that were parallel to the stream direction marked the inclined surface of the painted stakes reaching the higher and lower washed painted marks at the front and rear faces of the stake, respectively. The value adopted for the peak water depth was the average of these four different values from every side of the stake. However, in the case of existing noticeable differences among these values, the downstream value on the stake was adopted. Generally, there were no significant difference among these four values.

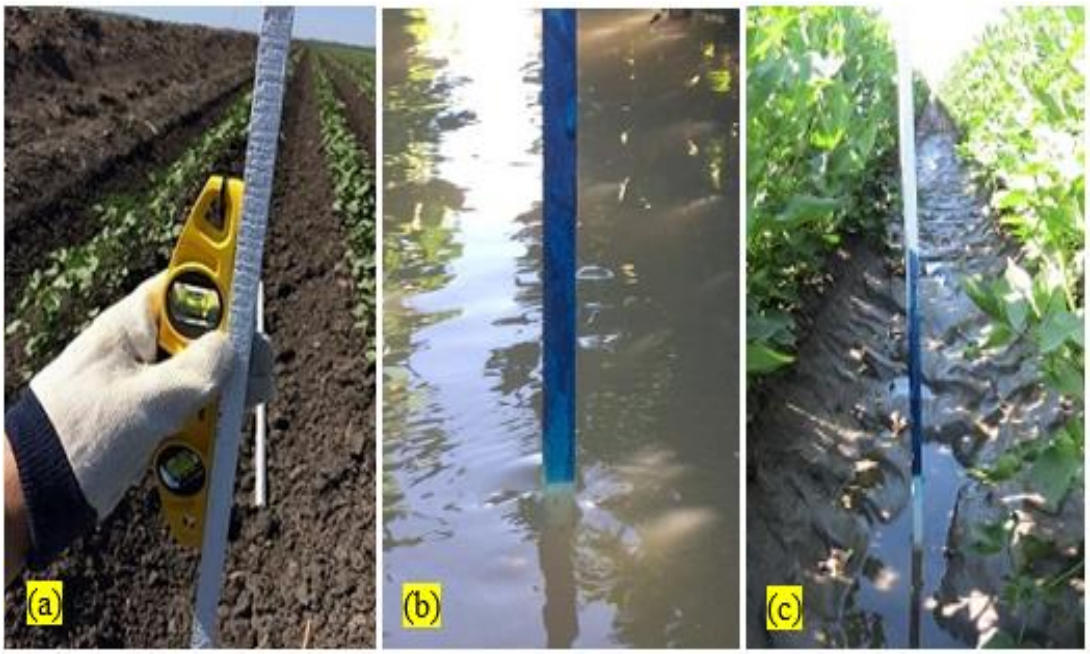

Figure 6.18 Peak water measurement via food-colouring painted stake in the furrows, showing a) insertion of the painted stake into soil using a hammer and a spirit level, b) a painted stake during an irrigation event, c) a painted stake after an irrigation event.

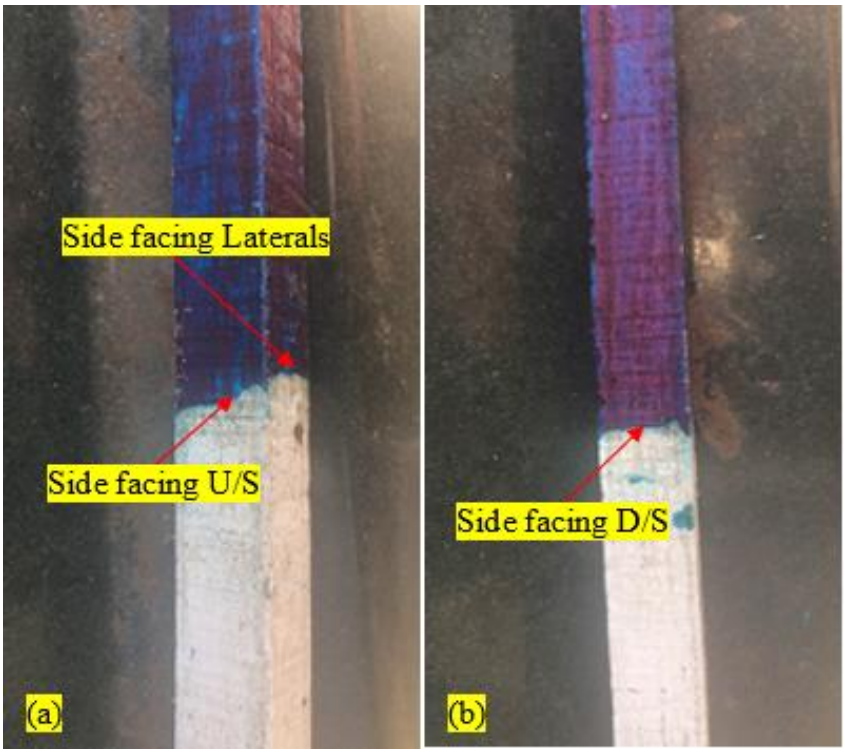

Figure 6.19 Different levels of the washed part of the paint from the stake, for a) the front surface side of the stake facing upstream and one of side surface parallel to the flow direction, and b) the downstream side of the stake.

6.7. Soil water deficit estimation

Knowing the soil water deficit (SWD) value prior to each irrigation event is important for estimating the application efficiencies (AE and RE). This field study used a simple water balance tool, IrriSAT (https://irrisat-cloud.appspot.com/) to estimate the SWD prior to each irrigation event throughout the whole season. Appendix C explains the steps for estimating the SWD using IrriSAT.

6.8. Conclusion

The shortcomings identified in methodologies trialled in Season 1 were overcome in Season 2 trials. As a result, the data collected during this season was of far greater quality and permitted the evaluation of soil infiltration rates, simulation of irrigation events, and determination of efficiency and uniformity, as described in later chapters.

Flow rate measurements were collected at all major field structures including the inlet (main pipe), intermediate (check gates) and outlet (drain boxes) structures. Direct and indirect approaches were adopted to estimate the flow rates at these important points. Regarding the head drain box, it was not possible to mount the Starflow instrument inside the small pipe (300 mm in diameter) of the head drain box to a sufficient upstream distance (9 pipe diameters) to minimise the impact of flow turbulent. Also, it was not possible to measure velocities in the tail drain box as the pipes were fully submerged with water even before the season commenced. Mounting the Starflow next to the tail drain box or in the pool of water immediately upstream of the drainage pipe was as an alternative way to conduct this measurement. The flow rates were then inferred from the measured water depths using the pipe energy loss equations for the drainage from the head channel and the weir equation at the drainage structure in the tail channel. Some of the Starflow measurements were lost due to technical and environmental reasons, but this was mostly overcome by installing two Starflow instruments in important positions such as the main pipe supply.

Flow rate measurements at the furrow scale were conducted using four techniques. Firstly, the SonTek FlowTracker2 was used to measure water velocities in individual adjoining furrows, as adopted in the previous season. However, calculating the flow area was improved by adopting profile-meter measurements as explained in Section

6.6.2.1. Secondly, Starflow instruments were used to measure flow rates in two individual furrows during a whole irrigation event. These measurements provide data to determine the flow characteristics during the whole irrigation event. The third technique trialled to collect additional flow rate measurements are based on recorded video. Flow rate estimation will be based on recorded video of water velocity, and flow area, determined from manual measurements of flow depths on a ruler and the cross-sectional area measurements from the profile-meter. Three action cameras were used to record water velocities in three adjoining furrows. However, high temperature in the field caused these cameras to stop. A UAV and food colouring technique was the last trialled technique to estimate the flow rates in four adjoining furrows. This technique involved measuring the water velocity dyed by food colouring across a certain distance along the furrow. It was difficult to detect the front edge of the dye (food colouring) in the furrows using the UAV as it disappeared quickly (Figure 6.13). Plant canopy made detecting the dye edge very difficult especially after few metres from the furrow entrance.

A novel technique to determine advance measurements from UAV flight missions was proposed and tested. This technique allows a single person to rapidly collect field scale advance data and should provide a far better understanding of the variability that characterises the FNSBO_Re system. There were some factors limiting sufficient and good advance and recession data. Battery life, flight duration, shortage of time for other evaluation measurements (such as furrow flow rate), and camera resolution are the main factors impact data collection. Sunlight angle and plant canopy density are the main factors that impact the ability to extract reliable data. It was concluded that the best advance and recession measurements that can be conducted using the UAV technique can be achieved in the earlier growth stages of the crop where crop canopy impacts less.

Water depth measurements in the furrow were conducted using three different techniques. Firstly, a fixed camera was used to capture the water depth in the furrow at several times during the irrigation event. The sensitivity of the action cameras to heat restricted this technique. Secondly, a float gauge technique was trialled to measure three furrows in one irrigation event. Finally, a wooden stake and painted food colouring was the last technique used to measure the peak water depth in the furrow.

Relatively speaking, the low cost of the wooden stake painted with food colouring technique compared with the fixed camera and the float techniques, encourage its adoption at a larger number of furrows between 24 and 36 furrows.

The soil moisture in the field was based on a simple water balance approach using the IrriSAT tool. However, soil moisture measurements from the field would raise the reliability of the estimation of the calculated irrigation performance indices.

CHAPTER SEVEN

Results from Season 2

7.1. Introduction

This chapter presents the data collected during Season 2, the 2017-2018 summer cotton season. This data was collected utilising the methodology documented in Chapter Six, which represents a set of techniques developed following the experiences of Season 1. The results are split into five areas; field geometry and levels, furrow geometry, flow rates, water advance, water recession and water depth.

7.2. Field surveying

Field surveys were conducted over Field 2 using the Total Station instrument. These measurements were used to determine the longitudinal slopes down the field and the vertical separation between the adjoining borders within Field 2

The first part of the survey was carried out on a set of adjoining furrows in each border to determine the longitudinal slopes down Field 2. The level measurements were collected by placing the staff at the middle of the bottom of each furrow at variable intervals along the field length. In Border 1, the measurements involved the adjoining furrows numbered 12 to 24, while in Border 2 it involved the adjoining furrows numbered 1 to 24 (Figure 7.1 and Figure 7.2, respectively). The measurements down the furrows showed that the upper 35 to 50 m at the top end of Field 2 have a positive slope of about 0.2261% and 0.2195% for Border 1 and 2, respectively. A slight by negative slope of -0.0564% and -0.0594% exist for Border 1 and 2, respectively, along the remaining length of the field, as shown in Figure 7.1 and Figure 7.2. These measurements also showed that the WFs located in Border 1 have approximately the same elevation compared with the non-WFs, while the WFs tend to have a slightly lower elevation in Border 2.

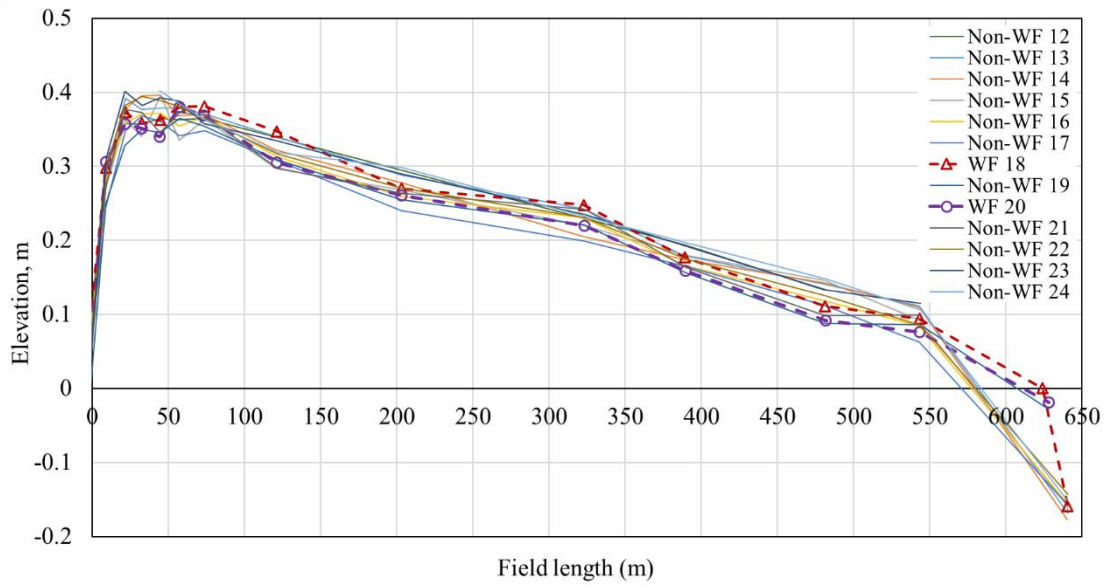

Figure 7.1 Furrow elevations for 13 adjoining furrows, starting from Furrow 12 to 24 located in Border 1 of Field 2.

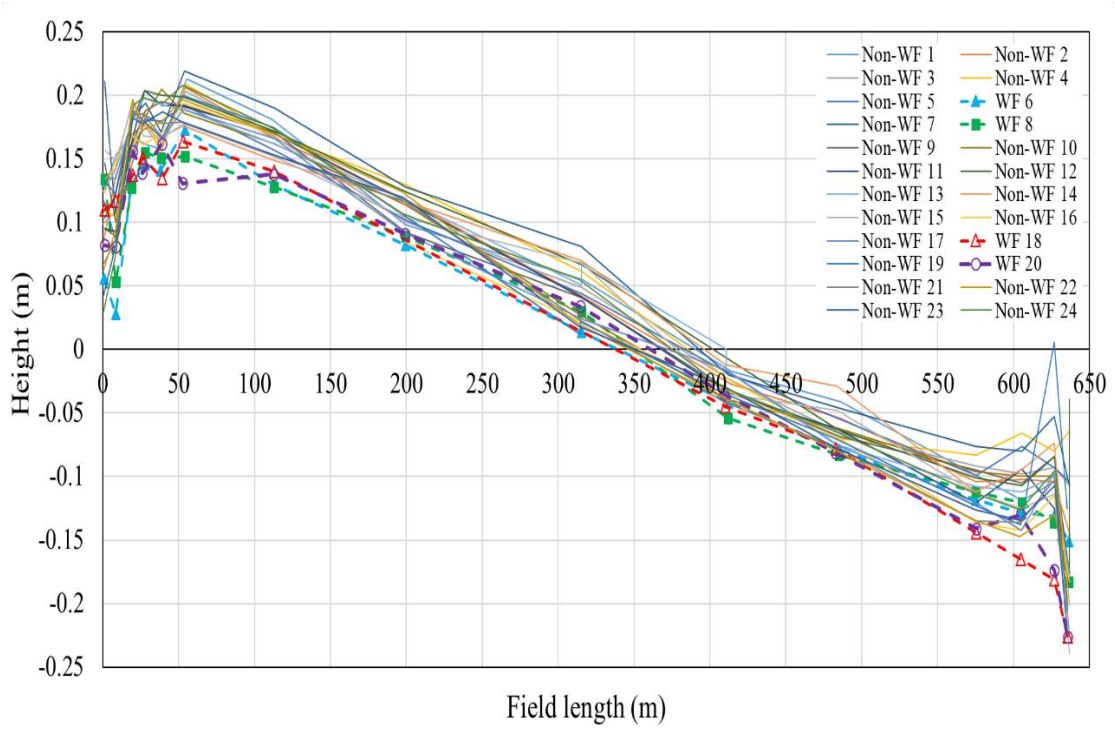

Figure 7.2 Furrow elevations for 24 adjoining furrows, starting from Furrow 1 to 24 located in Border 2 of Field 2.

The second part of the surveying was to determine some of the cross-sectional profiles of the bankless channels at the head and tail of Field 2 (Figure 7.3 and Figure 7.4, respectively). Vertical separation between adjoining borders was estimated based on the surveying data. The vertical separation between the adjoining borders at the head bankless channel is about 0.12 metres (Figure 7.3), while at the tail bankless channel it is about 0.20 metres (Figure 7.4). Changes in shape or elevation along the length of the bankless channels may influence the uniformity of water applied to the top of the field, or drained from the bottom of the field. The two transects taken within the head bankless channel for each border do not suggest any significant change in shape or elevation across the width of the border. It is suggested that additional transects of the channel would be required in order to properly verify this conclusion. In the tail bankless channel (Figure 7.4) the channel elevation rises at the far end of the channel away from the check gate between Borders 1 and 2, but the shape is similar between Furrows 175 and 250 indicating that the reverse advance should be relatively uniform for this border with the exception of the furrows closest to the supply end of the field.

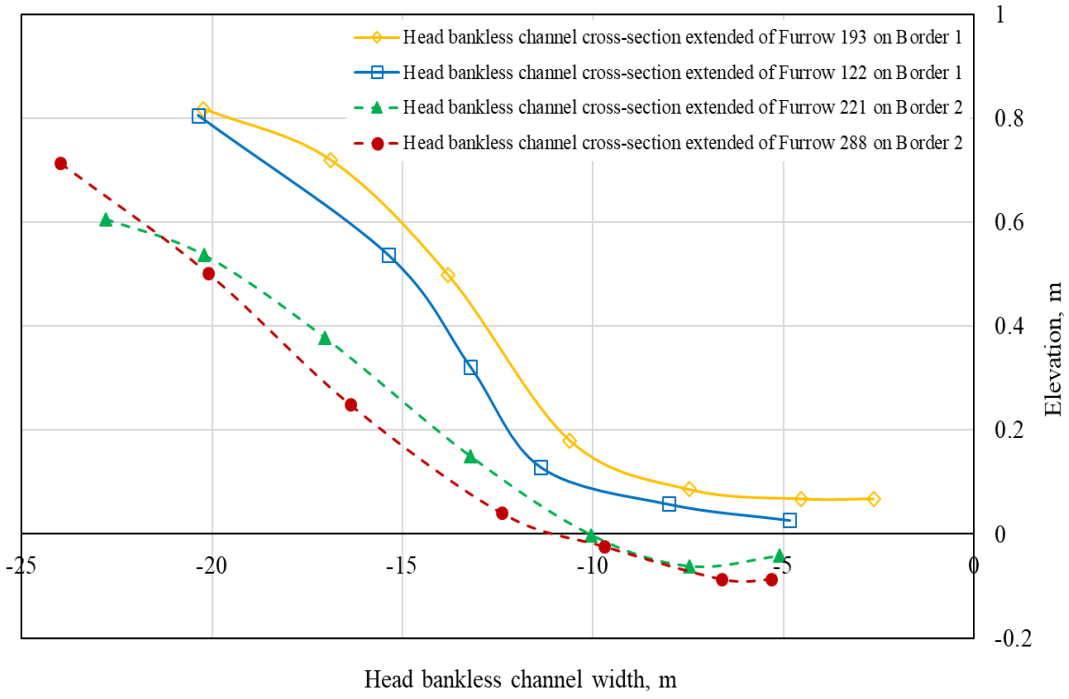

Figure 7.3 Different cross sectional profiles of the head bankless channel across the width of Field 2.

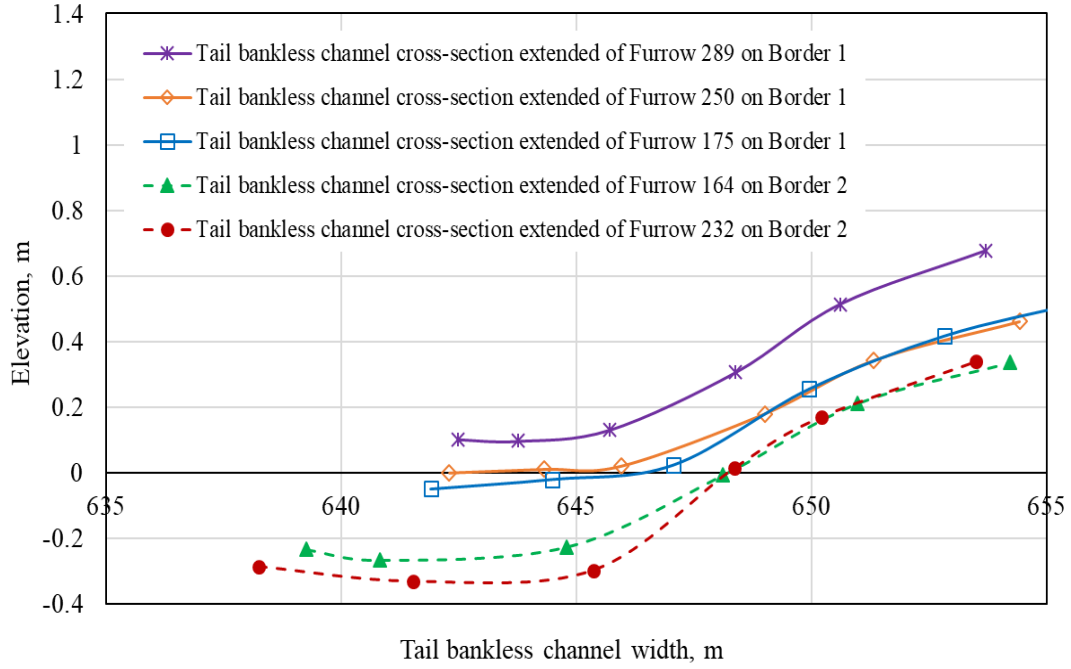

Figure 7.4 Different cross sectional profiles of the tail bankless channel across the width of Field 2.

7.3. Furrow geometry

Figure 7.5 shows cross-sectional area measurements on 12 adjoining furrows at about 53 to 54 m from the entrance for furrows numbered 13 to 24 located in Border 1 of Field 2. These measurements were conducted using the profile meter on 10-1-2018 and 18-1-2018, a day before the irrigation events. As is shown in Figure 7.5, the WFs number 18 and 20 had the highest cross-sectional areas. Figure 7.6 shows the furrow perimeter for the same 12 adjoining furrows at 53 to 54 m from the furrow entrance. Similarly, the WFs number 18 and 20 had the highest perimeter values.

On 29-12-2017, the cross-sectional area and perimeter measurements were conducted on 12 adjoining furrows at 51 to 52 m from the entrance of furrows numbered 1 to 12 in Border 2 of Field 2. The measurements of furrow shape were conducted by taking a photo of the profile meter once it was placed in each furrow. Because of the high temperature during conducting the measurements some of the photos (of four furrows, 3,4,5 and 10) were lost. Later, the profile meter measurements were taken manually to rectify this problem. The cross-sectional area and perimeter values for this event

exhibit the same trend where the highest area and perimeter values occurred in the WFs (6 and 8).

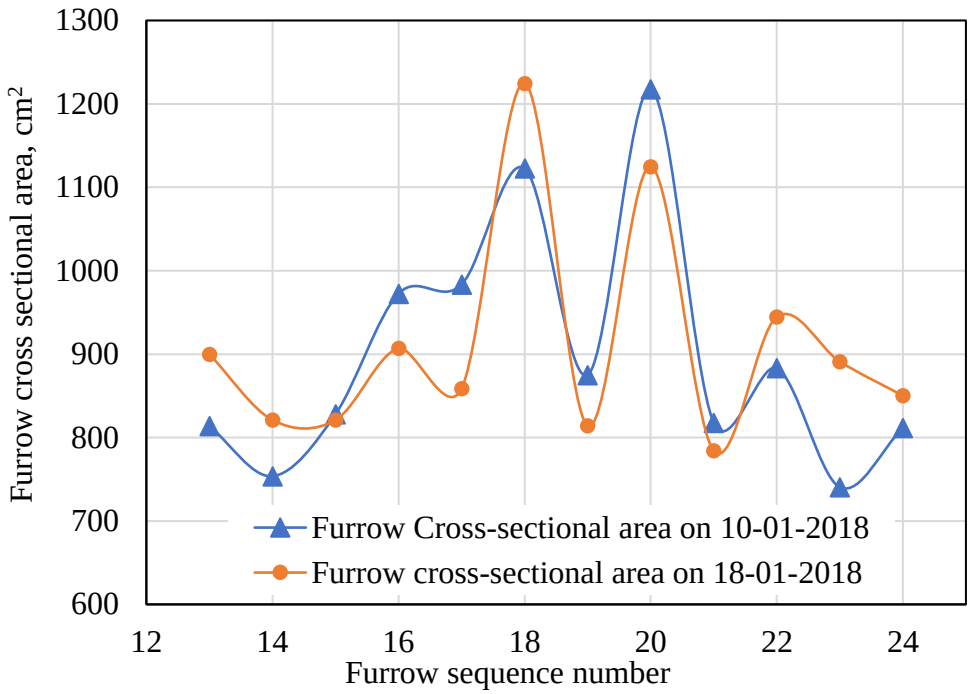

Figure 7.5 Furrow cross-sectional areas at 53 to 54 m from the entrance for the 12 adjoining furrows in Border 1 of Field 2.

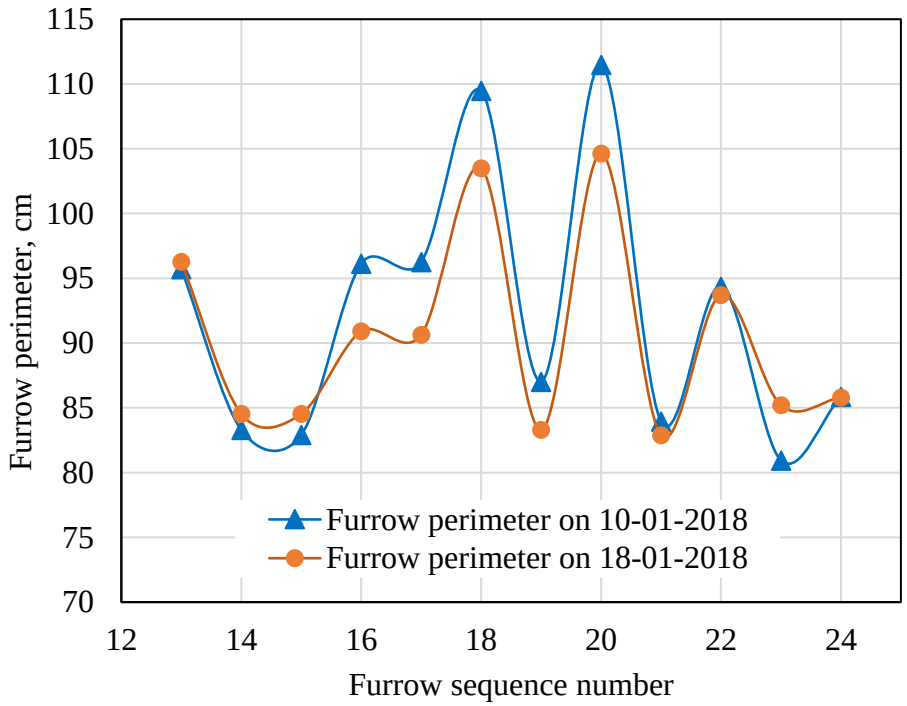

Figure 7.6 Furrows perimeters at 53 to 54 m from the entrance for the 12 adjoining furrows in Border 1 of Field 2.

7.4. Flow rate measurements

As explained in the last chapter, flow rate measurements were conducted at two scales: between borders (field scale), and within borders (individual furrow flows for a set of furrows).

7.4.1. Flow rate measurements between borders (field scale) at Field 2 in Season 2.

In Season 2 in Field 2, flow rate measurements at the main inlet pipe and at the check gates between borders were conducted using Starflow instruments logging water velocities and depths. The flow rate measurements at the head and tail drain boxes of Field 2 were estimated based on total losses in the pipe and the sharp-crested weir formula respectively, with the water depth measured by the Starflow instruments. Flow rates were calculated based on the calibrated logged data (water depth and velocity), see Section 4.7.1. Flow rate measurements of at the check gates were adjusted by SonTek FlowTracker2 instrument (see Sections 5.5.1).

Figure 7.7 shows the flow rates or the discharges from the main supply pipe, and the check gates at the top and bottom of Field 2, for the irrigation event conducted on 11-01-2018. The net water volume held in Border 1 of Field 2 was estimated by conducting algebraic addition of these instantaneous flows from the flow duration.

Generally, regarding the Border 1, the algebraic addition assumes positive magnitude for the water volumes that enter from the main supplying pipe and negative magnitude for the water volumes that entering cross the check gates at the top and the bottom of the Field 2. Similarly for Border 2, the algebraic addition assumes positive magnitude for the water volumes entering into that border through the check gates at the top and bottom of the Field 2, and assumes negative magnitude for the water volumes that leave this border through the drain boxes at the top and the bottom of the Field 2.

Table 7.1 shows the calculation of the net volume of water (m^3) and water depth (mm) held in Border 1 and 2 of Field 2 for the all irrigation events of Season 2. The net depths of water held in Border 1 and 2 were calculated by dividing the volumes of

water which held on Border 1 and 2, respectively, by their respective border areas (19.97 ha and 19.2 ha, respectively).

There was noticeable overestimation in the Starflow flow rate measurements at the check gates compared with the instantaneous flow rate measurements using the SonTek FlowTracker2. However, the instantaneous flow rate measurements using SonTek FlowTracker2 showed the possibility of adopting the Starflow instrument to conduct the flow rate measurements at the check gates. The reliability and ability of Starflow to measure the flow rates at the check gates was explained in Sections 5.5.1 and 5.5.2.

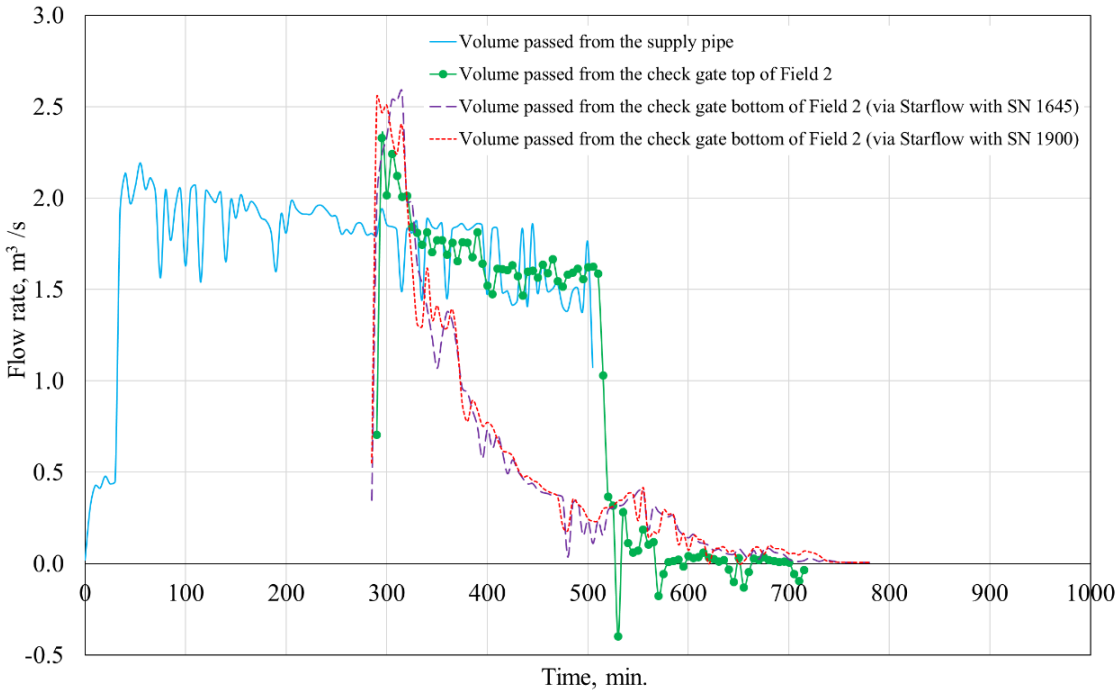

Figure 7.7 flow rates from the main supply pipe, and downstream the check gates in Field 2 for the irrigation event conducted on 11-01-2018.

Table 7.1 the calculation of the net volume of water (m^3) and water depths (mm) held in Border 1 and 2 of Field 2 for the all irrigation events of Season 2.

Event date	Volume from supply pipe (m^3)	Average volume through check gate top of Field 2 (m^3)	Average volume through check gate bottom of Field 2 (m^3)	Volume through head drain box (m^3)	Volume through tail drain box (m^3)	Net water volume in Border 1 (m^3)	Net water volume in Border 2 (m^3)	Net water depth in Border 1 (mm)	Net water depth in Border 2 (mm)
Starflow(s)	S.N 1619	S.N. 1652 and 1904	S.N. 1645 and 1900	S.N. 20320	S.N. 1410				
15/12/2017	54552	30159	9775	No data	No data	14618	n/a	73.2	n/a
30/12/2017	52524	26661	11970	2629	No data	13893	n/a	69.6	n/a
11/01/2018	52023	23433	15284	3183	No data	13306	n/a	66.6	n/a
19/01/2018	46751	21233	13595	4183	No data	11923	n/a	59.7	n/a
26/01/2018	51437	20043	16982	4214	No data	14411	n/a	72.2	n/a
10/02/2018	53187	22813	15004	5081	17148	15369	15588	77.0	81.2
17/02/2018	45702	17023	16550	3519	No data	12129	n/a	60.7	n/a

7.4.2. Flow rate measurements at furrow scale

7.4.2.1. SonTek FlowTracker2

Flow rate measurements using the SonTek FlowTracker2 were completed in twelve adjoining furrows in each border of Field 2. The measurements conducted in Field 2 encompassed all seven irrigation events in Season 2 in Border 2, while only including the last five irrigation events in Border 1. The measurements were collected at two different times during one event in Border 1, and for three events in Border 2. All other events were measured once. Flow rates were calculated using point velocities and cross-sections of furrows, as explained in Section 6.6.2.1.

Figure 7.8 shows the flow rates values for twelve adjoining furrows located in Border 1 of Field 2 from Furrow 13 to 24 (see Figure 4.3). The flow rate measurements were collected at two different times (I and II) during the event on 11-01-2018 while the other events were measured once. Figure 7.9 shows the flow rates for twelve adjoining furrows located in Border 2 of Field 2 from the 1st furrow adjacent to the check bank between the adjoining borders (Figure 4.3). The measurements were collected at two different times (I and II) during the events on 15-12-2017, 30-12-2017, and 26-01-2018, while the other events were measured once.

It is clear in Figure 7.8 and Figure 7.9 that there are considerable variations in the flow rates among the furrows, with values ranging from 0.0024 to 0.018 m^3/s in the first border, and from 0.0014 to 0.0308 m^3/s in the second border. Fundamentally, these variations appear to be caused by the impact of the WFs. The WFs in Figure 7.8 are Furrows 18 and 20 while for Figure 7.9 they are Furrows 6 and 8. WFs had the higher flow rates compared with the non-WFs. The average flow rate values in the WFs were approximately 60% higher than the non-WFs in Border 1, and were 280% higher in Border 2. Naturally, the larger cross-sectional areas of the WFs leads to deliver a significantly higher amount of flow rates compared with non-WFs. It takes about an hour to complete the flow rate measurements for the twelve adjoining furrows utilizing the SonTek FlowTracker2. This relatively long time leads to the risk that flow conditions in the furrows might change during the measurement process. As shown in Figure 7.8 and Figure 7.9, for the events involving two runs of measurements, it can be noticed that the flow rates had changed over time. However, the spatial trends

between furrows remained the same between tests in a single event and persisted across multiple irrigation events.

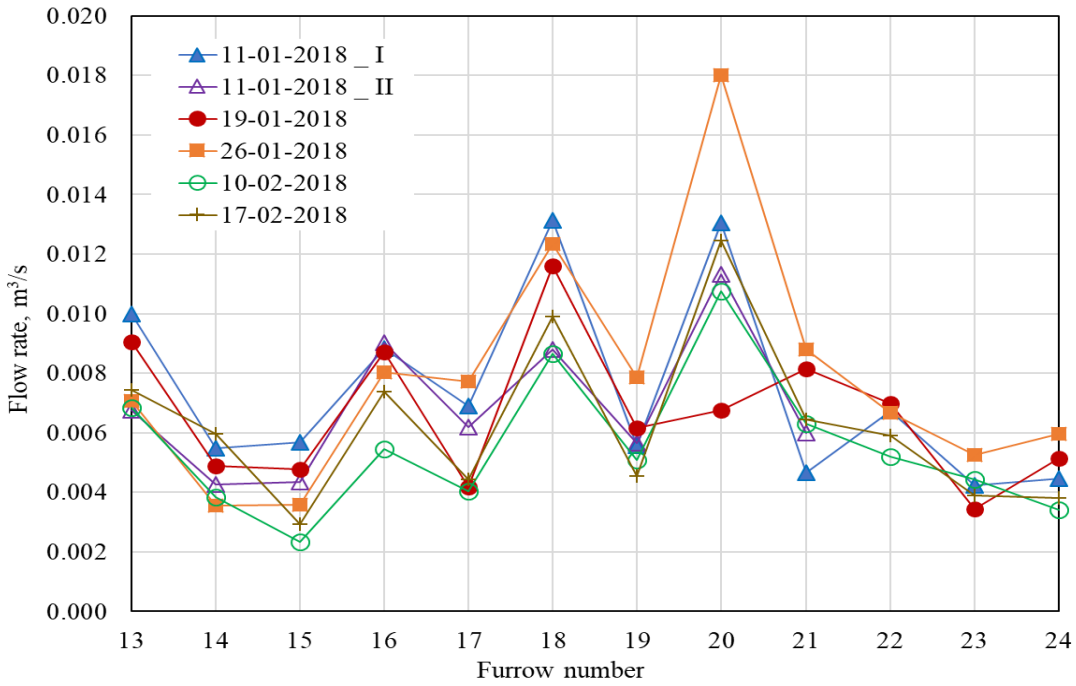

Figure 7.8 Furrow flow rates for 12 adjoining furrows in Border 1of Field 2 at one or two different times during each irrigation event. Note the higher flow rates in WFs 18 and 20.

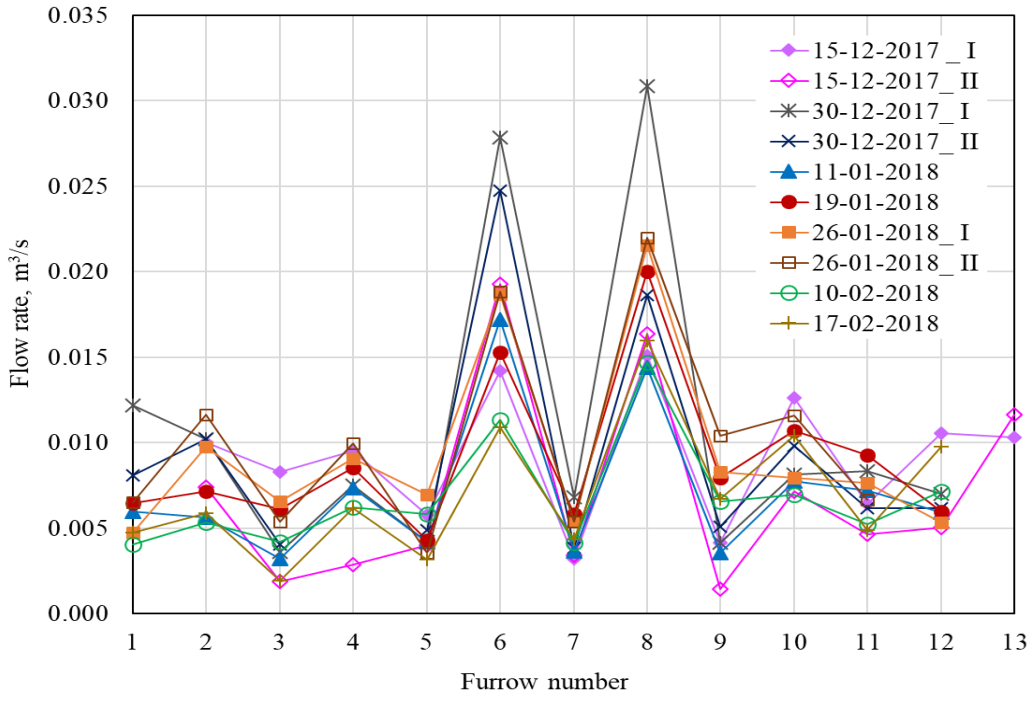

Figure 7.9 Furrow flow rates values for 12 adjoining furrows in Border 2 of the Field 2 at one or two different times during each irrigation event. Note the higher flow rates in WFs 6 and 8.

The difference in flowrates between adjacent furrows is significant, particularly for the WFs in comparison to the non-WFs. This large difference is a concern for evaluation of these systems. Generally, it can concluded that there is little change in the flow rates over time for most measured furrows. The furrow flow rate measurements in other irrigation events show similar trends.

Comparison of flow rates between the measured furrows in adjacent borders in Field 2 highlighted that those in Border 2 were higher than Border 1. Across all furrow flow rates measured in both borders it is found that the average flowrates in WFs and Non-WFs in Border 2 were higher than Border 1 by 38% and 11.7%, respectively. This can be explained by the augmented water volume drained-back from Border 1 to Border 2.

Generally, this variance in the received volumes between adjacent borders can be minimised by reducing the irrigation duration for Border 2 and considering the application of a precise amount of water. Actually, because the unit-width flow rate across Border 2 is increased due to the drain-back water from Border 1, the irrigation duration can be reduced in Border 2. In practice across Field 2, the irrigation duration in Border 2 over most irrigation events was lower than Border 1 by about 7% as shown in Table 7.2.

Table 7.2 Irrigation duration in Borders 1 and 2 in Field 2 during Season 2.

Event number	Irrigation event date	Irrigation Duration in Border 1, min.	Irrigation Duration in Border 2, min.	Percentage Change
1	30-10-2017	290	270	-7%
2	15-12-2017	275	235	-15%
3	30-12-2017	260	220	-15%
4	11-01-2018	195	210	+7%
5	19-01-2018	240	220	-8%
6	26-01-2018	230	250	+8%
7	10-02-2018	235	195	-17%

In terms of field design approaches, this variance could be minimised by reducing the size of Border 1. Reducing the size of Border 1 sufficiently (compared with Border 2), leads to similar unit-width flow rates across both borders, which can enhance the irrigation uniformity across the field and across borders (Grabham, 2012). Grabham (2012) mentions that when the last border is designed to be sufficiently narrow, the surface water from the penultimate border (Border 1 in the current study) can irrigate the last border alone (Border 2 in the current study), which leads to no runoff losses and improved irrigation application efficiency. However, this approach was not considered in the design of Field 2, as Border 1 consists of 312 furrows while Border 2 consists of 300 furrows.

The location of the 12 individually measured furrows in adjoining borders was at the downstream end of Border 1, while, the individually measured furrows were located at the upstream end of Border 2. These different locations still included differences in the elevation of furrow entrances and differences in the longitudinal slopes and elevations of the bankless channel. These differences did not diminish the comparison of flow rates between borders.

7.4.2.2. Starflow

In addition to the FlowTracker2, furrow flow measurements were also collected by Starflow instruments. Figure 7.10 shows the furrow flow rate measurements logged by the SonTek-IQ and Starflow instruments mounted in Furrows 6 and 4, respectively, located in Borders 1 and 2, respectively, of Field 2. These instruments were mounted at approximately 60 m from the furrows entrance to the furrow and the cross-sectional areas were measured using the profile meter. Both devices successfully measured the flow rate despite the challenging conditions of low velocities and small cross sectional areas within the furrow. As shown in Figure 7.10, the flow rate values of the WF (6) were unsteady during the irrigation event while for the non-WF (4) were relatively steady.

Generally, it can assumed that the flow rate measurements should be somewhat stable during each irrigation event. Hence, measuring instantaneous flow rates (e.g. using SonTek FlowTracker2) could be sufficient for evaluation purposes. At the other extreme, logging the flow rate measurements over the duration of whole irrigation

event within only two furrows cannot provide a reliable understanding of the flow behaviour of FNSBO_Re irrigation systems because of the large variation in flows between furrows. Continuously logged flow rates are valuable because they can indicate whether flows experience steady or unsteady conditions through the event.

7.4.2.3. Fixed camera

Furrow flow rate measurements were conducted using a fixed camera, at about 55 metres from the furrow entrance. Figure 7.11 shows the furrow flow rate measurements on two furrows (one is WF, and another is non-WFs) located in Border 1 of Field 2 for irrigation event conducted on 30-12-2017. As shown in Figure 7.11, the flow rate in the WF is larger than the non-WFs. Camera sensitivity to heat limited the usefulness this technique. In addition, the high cost of the camera would also limit large scale measurement using this technique.

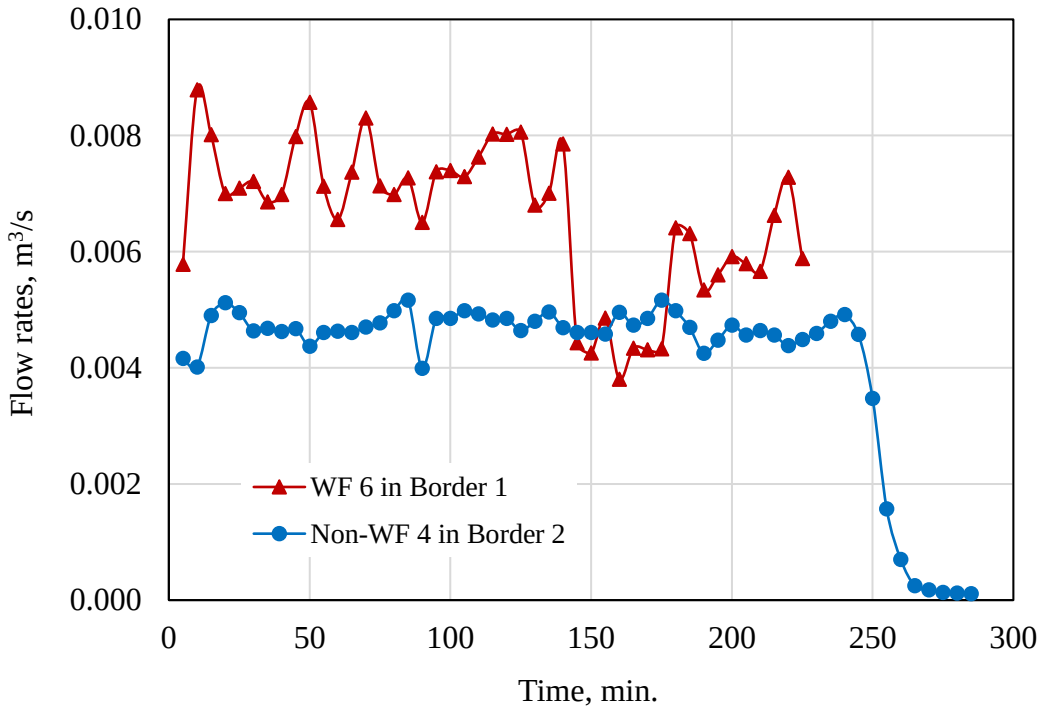

Figure 7.10 Furrows flow rate measurements logged by Starflow instrument mounted in Furrows 6 and 4, respectively, located in Borders 1 and 2, respectively, of Field 2.

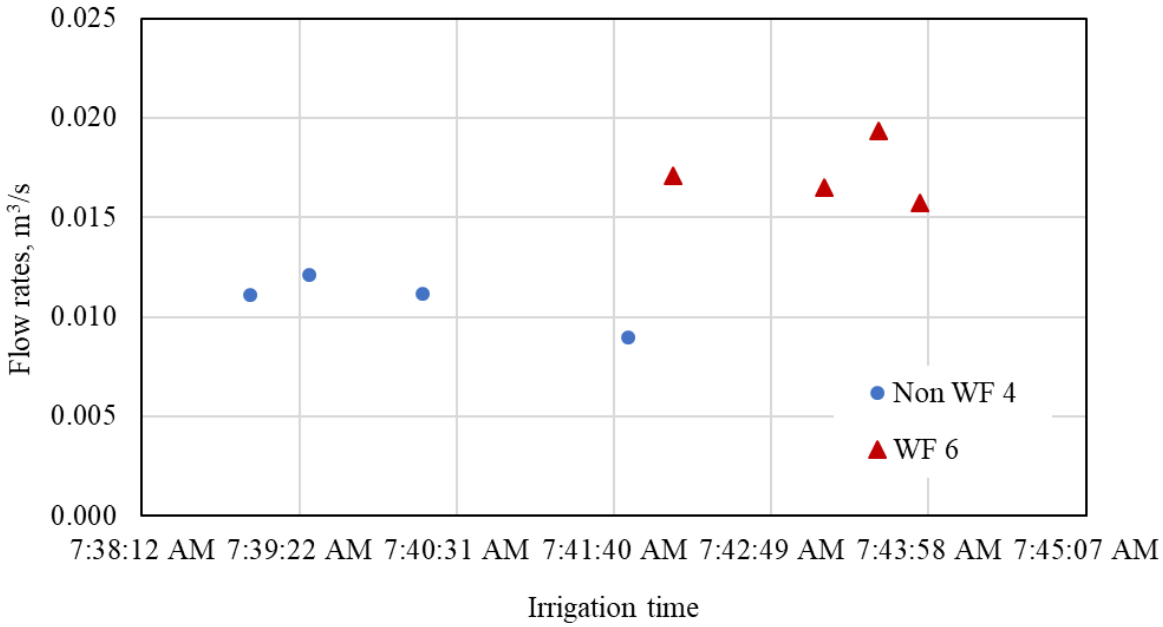

Figure 7.11 Furrow flow rates from fixed camera in Border 1 of Field 2 for irrigation event conducted on 30-12-2017.

7.4.2.4. UAV and food colouring

UAV and food colouring technique was trialled to detect the water velocity in the furrow but the food dye quickly dissipated restricting the performance of this technique. This technique did not involve measurements.

7.5. Water advance in the furrows

Water advance measurements were collected via two different techniques in Season 2. Firstly, intensive measurements were collected using IrriMATE ™ advance sensors on a small number of adjacent furrows. Secondly a new technique was trialled in order to capture water advance over the entire irrigated border using a UAV.

7.5.1. Water advance measurements using IrriMATE sensors

Figure 7.12 shows the water advance in sixteen adjoining furrows in Border 1 of Field 2, during the irrigation event conducted on 10-02-2018. Two sets of IrriMATE™ advance sensors were installed, spanning Furrows 13 to 28 and at positions of 166.5, 312.8, 438.46 and 542.8 metres down the length of Border 1. Figure 7.13 shows the water advance within the same 16 adjoining furrows during the irrigation event

conducted on 17-02-2018, but sensors were installed at slightly different distances down the field length (166.5, 312.8, 438.46, 520, and 600 metres). Figure 7.12 and Figure 7.13 show rapid water advance in all measured furrows, where water has reached the last advance distance in approximately 2.5 hours. It can be observed that the shortest time of water advance is associated with the WFs (18 and 20). In other words, the fastest advance of the water front occurred in the WFs compared with non-WFs. This variation in advance rates decreases the reliability of the evaluation process using conventional methods which typically utilise a single or small number of furrows. This significant variation in the advance rates will require field evaluation measurements at a wider scale than is usually adopted.

A slight downward curvature can be observed in the later part of water advance curves of the irrigation events shown in Figure 7.12 and Figure 7.13. Practically this can be explained by the fact that water advance has reached the bottom end of the field in some furrows (probably WFs) and is then flowing backwards up the field in the other furrows. This behaviour was also observed during the first season in Field 3. It is clear that this behaviour is a distinctive hydraulic characteristic associated with the FNSBO_Re irrigation system. This behaviour shows the difficulty of evaluating FNSBO_Re irrigation systems using standard approaches, as explained in Section 5.6.1.

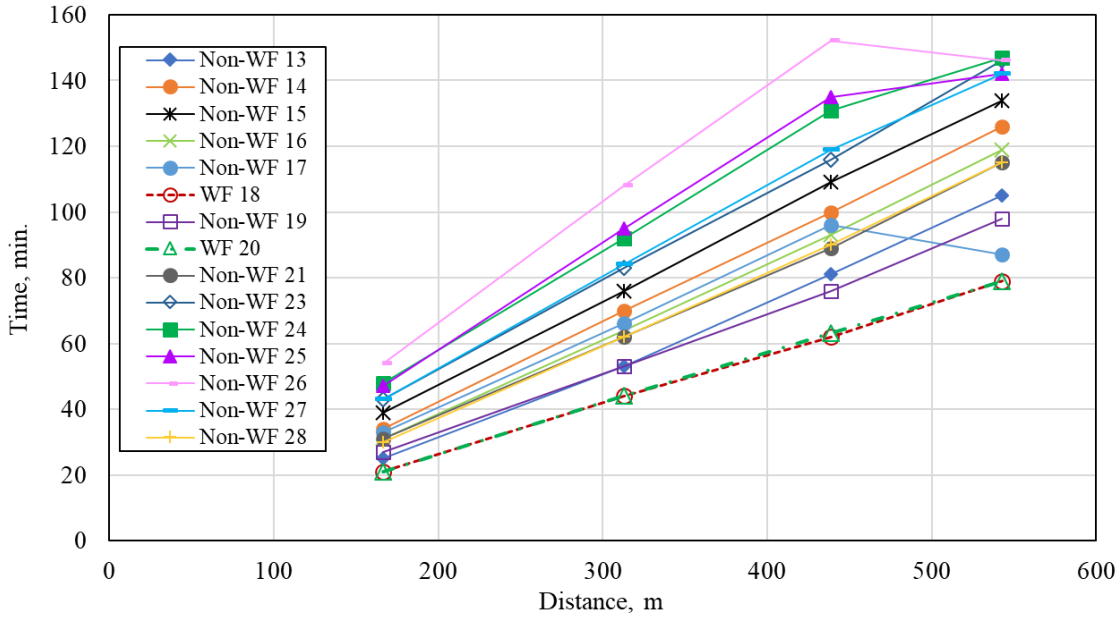

Figure 7.12 Water advance in sixteen adjoining furrows in Border 1 of Field 2 during the irrigation event conducted on 10-2-2018.

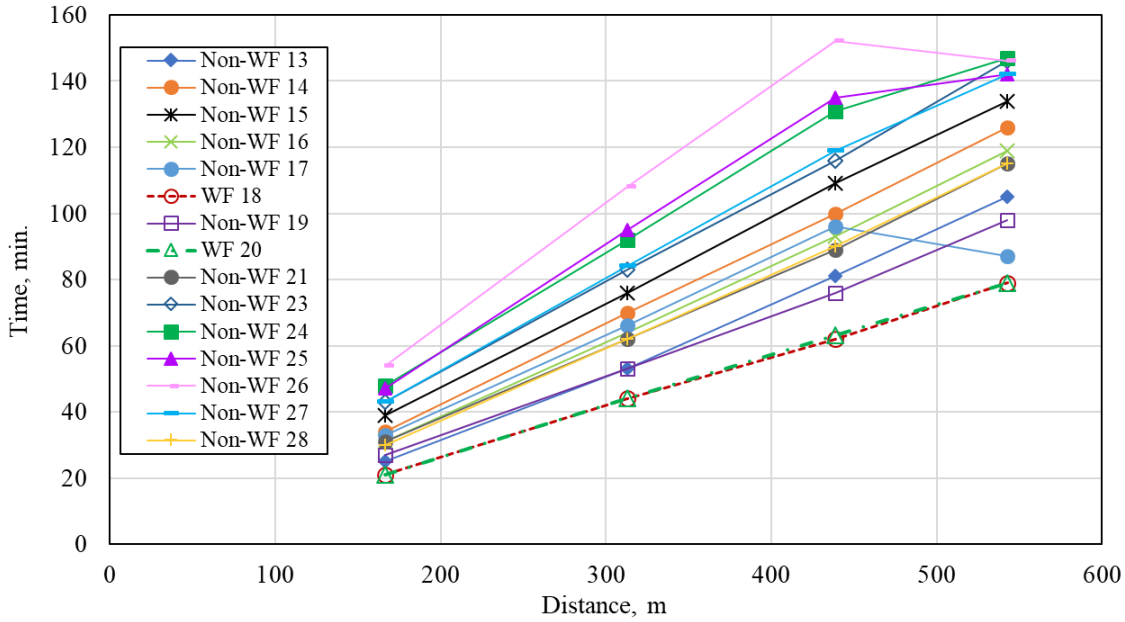

Figure 7.13 Water advance in 16 adjoining furrows in Border 1 of Field 2 during the irrigation event conducted on 17-2-2018.

7.5.2. Water advance measurements using UAV

The UAV (Phantom 4 Advanced drone from DJI) technique as described in Section 6.6.3.2 was used to collect water advance measurements in Season 2 at Field 2. Many flight missions were conducted throughout the season, capturing all irrigation events. Images from a number of these flights could not be used due to lighting conditions and those flights have not been used in the irrigation evaluation process.

One or more flight missions for each border of Field 2 were conducted during each irrigation event to cover the advance and recession phase. Figure 7.14 represents the water forward advance front from the top end of Border 2 and the water backward advance from the bottom end of Border 2 of Field 2, for the irrigation event conducted on 11-01-2018. The measurements obtained from the first UAV flight mission commenced on 10:55 AM at an altitude 25 m. The flight paths were the same as presented in Figure 6.14, but for Border 2. The check gate at the top of Field 2 opened at 9:42 AM. The resulting advance time was 73 minutes, calculated by subtracting the check gate opening time from the commencing time of the flight mission. For Border 1, the advance time is calculated by subtracting the time of commencing supplying

water to the field (water commence entering furrows in Border 1) from the commencing time of the flight mission. Figure 7.14 shows a large variation in the water advance between furrows in general and between non-WFs and WFs. It can recognise that the fastest advance of water fronts occurred at the WFs compared with non-WFS.

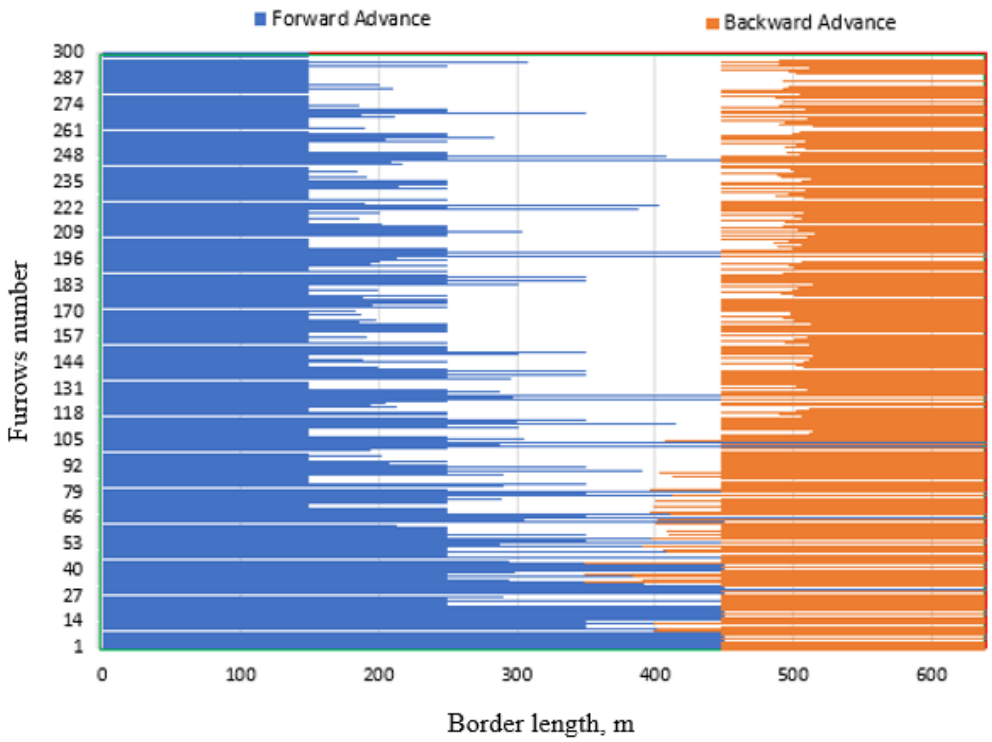

Figure 7.14 Forward and backward water advance in Border 2 of Field 2 of the irrigation event conducted on 11-01-2018, for the first flight mission that commenced at 10:55 AM at an altitude of 25 metres. The check gate at the top of Field 2 opened at 9:42 AM, and the advance time was 73 minutes.

There is a large variation between the furrows located at both sides of the border where the furrows with low numbers (close to the check bank or the check gate supply) have greater advance distances compared to furrows further (located in middle and the other side of the border further from the water supply). On the other hand, Figure 7.14 shows the distinctive behaviour for water advance from the bottom end of the border (backward advance) characteristic of the FNSBO_Re irrigation system. Large variability in the water advance between furrows and the distinctive behaviour of the advance (backward advance) in the furrows makes the irrigation evaluation of the FNSBO_Re system difficult. Determining suitable field evaluation measurement

techniques, and adopting appropriate methodologies for analysis are challenging. Advance measurements collected by the UAV (e.g. Figure 7.14) and by IrriMATE™ advance sensors (e.g. Figure 7.12 and Figure 7.13) show the same trends, showing that this behaviour was not a result of the approach used to collect the data.

7.5.3. Ability of UAV to measure advance rates

According to the methodology adopted to extract the water advance measures from UAV videos images water advance detection in furrows depends on flight altitude, plant canopy, and sunlight angle during the flight mission. Higher altitudes increase the possibility of detecting the water advance front in more furrows. However, the permissible magnitude of the flight altitude depends on the UAV's camera resolution. The maximum altitude is where the images still provide enough detail to distinguish the wetting front. In this study, the flight missions typically commenced when the water advance front reached about the half the length of the furrows. The flight missions occurred after about one hour of supplying water to the field in Border 1 of Field 2, and approximately after one hour of opening the check gate regarding the Border 2 of Field 2.

Based on a few trials at the early stage of the season the camera on the Phantom 4 Advanced UAV, the most appropriate flight altitude magnitude was 25 m. At this altitude the image cover about 20 furrows (spaced 1m apart) over a furrow length of 22.6 m with adequate resolution to recognize wet and dry parts of the furrows (Figure 7.15). However, at the later stage of plant growth, this high flight altitude could not provide an adequate resolution to detect the advance front due to the plant canopy, shadows from inappropriate sunlight angles (Figure 7.16). Some trials were conducted at every growth stage to determine appropriate altitudes for image capture. Figure 7.17 shows the water advance front for a flight mission at 8 m altitude for one of the late irrigation events in the season (26-01-2018). This figure showed the good ability to detect the advance front using low flight altitudes (8 metres).

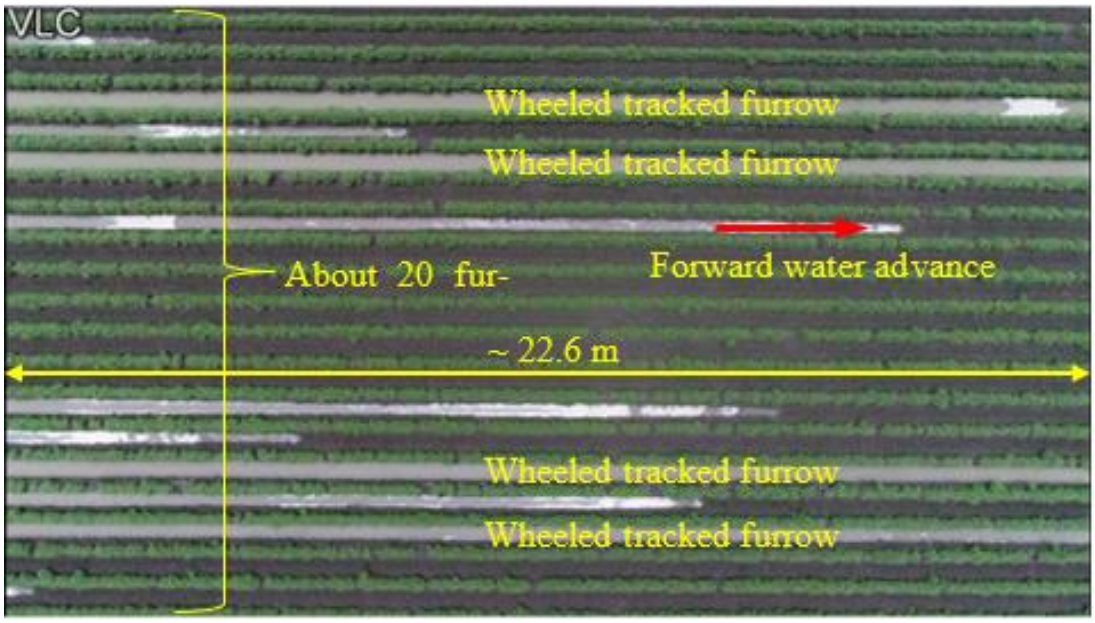

Figure 7.15 Forward water advance extracted from a video clip recorded during a flight mission with 25 metre altitude in Border 2 of Field 2, for one of the early season irrigation events (30-12-2018).

Figure 7.16 Undetected water advance front edges due to the impact of plant canopy and sunlight angle. This photo was extracted from a video clip recorded during a flight mission with 15 metres altitude in Border 1 of Field 2 for irrigation on the 19-01-2018. The flight mission commenced at 8:20 AM.

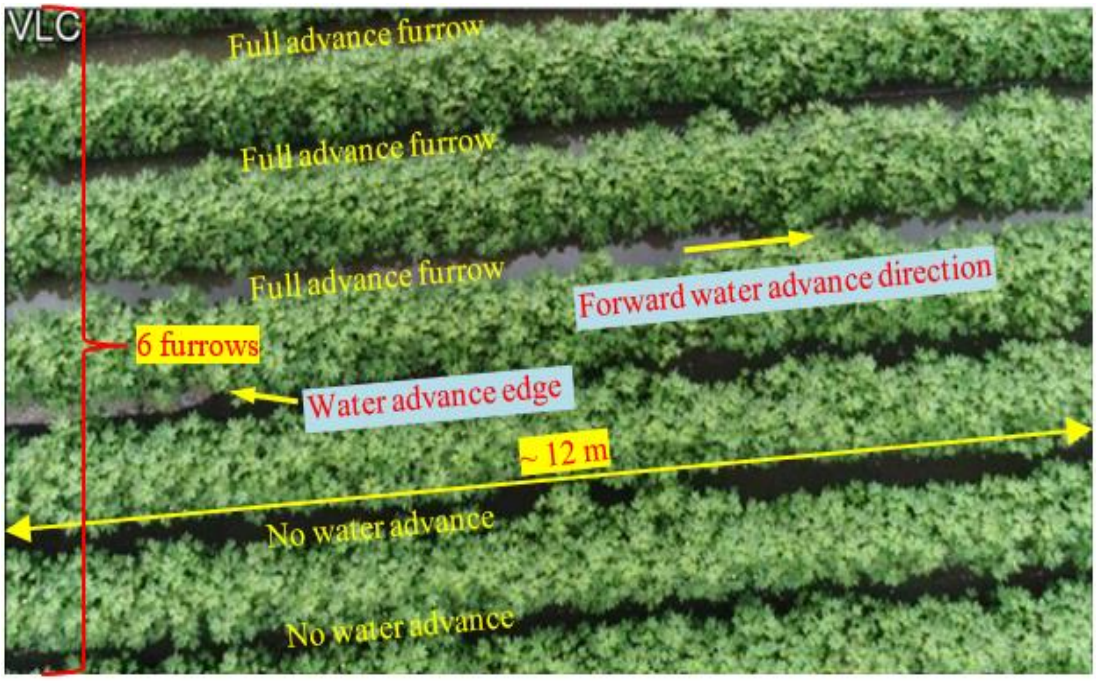

Figure 7.17 Forward water advance extracted from a video clip recorded during a flight mission with 8 metre altitude in Border 1 of Field 2, for irrigation on the 26-01-2018.

Table 7.3 contains a summary of the number of furrows where water advance can be detected according to the flight altitude and the time of the flight mission. In Table 7.3, it is obvious that at the higher flight altitude (25m) there is a greater chance to detect a higher number of the furrows that had actual water advance edges compared with the lower flight altitude (e.g. 8m). It was also noticed that completing the flight mission at an appropriate time of during the advance phase will provide a better chance to detect a higher number of actual water advance front edges in furrows. This is clear from comparison of comparing the first and second flight missions of the irrigation event on the 11-01-2018, where 62 and 7 furrows were detected, respectively.

Table 7.3 Number of furrows out of total of 312 and 300 furrows for Border 1 and 2, respectively, in which the water front advance was detected in each flight mission.

Event date	Border number	Flight mission number	Commencing supply /Open check gate time	Flight Mission time	Advance time, min.	Flight altitude, m	Number of furrows in which the advance front was detected
30-12-2017	2	1	*	12:01 PM	-	25	98
30-12-2017	2	2	*	1:46 PM	-	25	11
11-01-2018	1	1	5:25 AM	6:18 AM	53	25	91
11-01-2018	2	1	9:42 AM	11:00 AM	78	25	62
11-01-2018	2	2	9:42 AM	12:47 PM	185	25	7
26-01-2018	1	1	6:25 AM	8:19 AM	114	8	6
10-02-2018	2	1	10:20 AM	11:55 AM	95	8	2
17-02-2018	2	1	9:59 AM	11:17 AM	78	8	0

* Opening one sub gate of the top check gate at 9:56 AM, and then opening the second sub-gate at 10:08 AM, and then opening the remainder of the check gate at 11:10 AM was unusual. The supply to the field was stopped at 9:50 AM and resupply began at 11:06 AM.

7.6. Water recession measurements using UAV

The methodology adopted to extract water recession measurements from the UAV images was the same as that adopted for the advance measurements, as described in Section 6.6.3.2. However, the process to identify the water recession was less successful because of the difficulty in recognizing the part of the furrow that had water, and the part of the furrow where water had already receded. Flight altitude, sunlight angle and plant canopy density are the primary factors that impact the ability to extract reliable data from the recorded videos. Extracting the recession measurements from the UAV videos is harder than for advance measurements because the latter only requires the user to distinguish the difference between water and dry soil, whereas the former requires a difference between water and wet soil. Shallow water depths and ponded water in the undulations of the furrows considered as a receded furrow (Figure 7.18). One or more flight missions for each border of Field 2 were conducted for each irrigation event to cover the recession phase. For each recession flight, water recedes partly or completely along the furrow length. Then for the next recession flight, another part, or all the remaining length of the furrow had receded.

Figure 7.18 Example video screenshot during the recession captured with 15 metres altitude in Border 1 of Field 2. The flight mission commenced at 1:13 PM on 19-01-2018.

Figure 7.19 shows the recession time for two furrows (13 and 15) located in Border 1 of Field 2 during the irrigation event conducted on 19-1-2018. This sample of extracted data from three flight missions at 15 m flight altitude recorded recession measurements at three different times (356, 412, and 504 min.) after the water first entered the furrows. As shown in Figure 7.19, water had receded from each part of the furrow at different times logged by the flight mission, Table B-2 (Appendix B) shows the recession measurements collected from three flight missions conducted in Border 1 of Field 2 for the irrigation event conducted on the 19-01-2018.

Figure 7.20 shows the cumulative frequency distribution percentage for receded furrows at three recession times (356, 412, and 504 min.) for the event conducted on 19-01-2018 in Border 1 of Field 2. This figure shows the percentage of furrows which have receded past each distance during each of the UAV missions. For instance, it shows that at 356 minutes, 33% of furrows (102 out of 312 furrows) had receded past the first 150 m distance, and 23%, 2%, 0%, and 0% of furrows were receded from the 250, 350, 450, and 570 m, respectively. It also shows that the percentages of the receded furrows increased with increasing event time. It also shows, that the recession phase did not complete for 70% of the furrows at the 570 m distance from the furrow entrance by the time of the final mission.

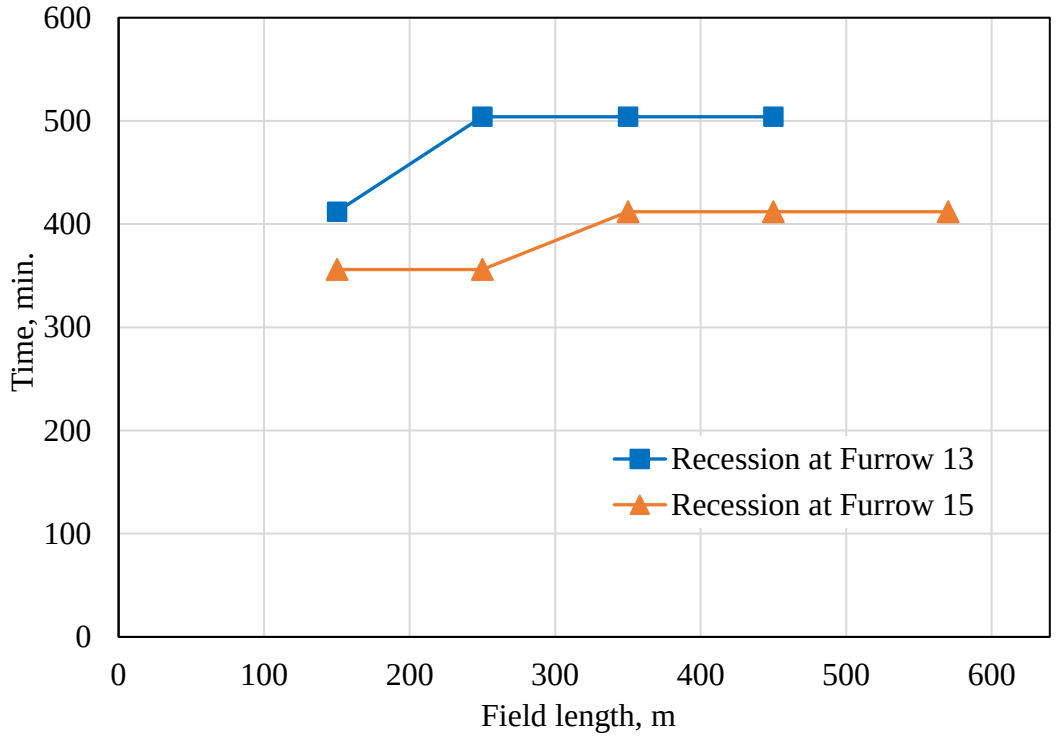

Figure 7.19 Recession time for two furrows (13 and 15) in Border 1 of Field 2 on 19-1-2018. This is a sample of the extracted data from three flight missions at a flight altitude of 15 m used to collect recession measurements.

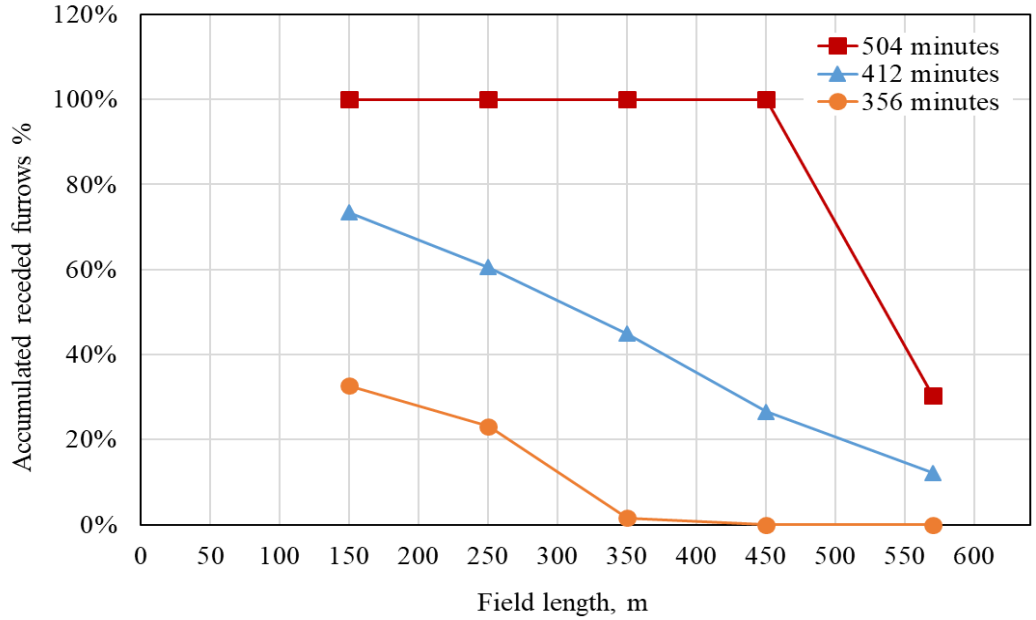

Figure 7.20 Cumulative frequency distribution for receded furrows percentage at three recession times for event conducted on 19-01-2018 in Border 1 of Field 2.

In fact, the actual flight paths were at 100, 200, 300, 400, and 500 metres. The actual recession times for the three flight recession missions were 356, 468, and 539 minutes, and they were calculated by subtracting the commencing time of entering furrows (5:25 AM) in Border 1, from the UAV recession flight times (11:21 AM, 1:13 PM, and 2:24 PM, respectively) for the irrigation event conducted on 19-01-2018. The reason for modifying the flight paths to be 150, 250, 350, 450, and 570 m, and the recession times to be 356, 412, and 504 minutes were explained in Section 6.6.3.2.

7.7. Water depth measurements in the furrows

Water depth measurement in furrow were collected via three different techniques in Season 2. Firstly, a new technique was trialled in order to capture water depth using a fixed camera. Secondly, a technique was developed in order to capture water depth using a float gauge. Finally, a new technique was trialled in order to collect a large number of peak water depth measurements using painted wooden stakes.

7.7.1. Fixed camera

Water depth measurements were conducted using wooden stakes painted with food colouring at approximately 55 metres from the furrow entrance. Figure 7.21 shows the water depth measurements on two furrows (WF and non-WF) located in Border 2 of Field 2 for irrigation event conducted on 26-01-2018. As shown in Figure 7.21, the water depth in the WF is larger than the non-WF. This figure also shows a variation in the water depth measurements of each furrow. The process of capturing the water depth measurements included cooling the camera to keep it working during the irrigation event. This is impractical because of the necessity to conduct other important measurements such as flying the UAV and measuring furrow flow rates. In addition, the high cost of the camera would restrict large scale measurements of this kind.

7.7.2. Float gauge

Peak water depth measurements in the furrow were conducted using a float gauge, at about 55 metres from the furrow entrance. Figure 7.22 shows the water depth measurements in three furrows (one is WF, and two are non-WFs) located in Border 1 of Field 2 for irrigation event conducted on 10-02-2018. As shown in Figure 7.22, the

water depth in the WF is larger than the non-WFs. It is believed that these measurements show lower reliability compared with the results obtained by the camera technique. There is a noticeable difference between the peak water depth of the non-WFs 4 and 5. This result could be from the poor performance of the float mechanism due to manufacturing. On the other hand, the high cost of the float gauge would restrict conducting large scale measurements using this technique.

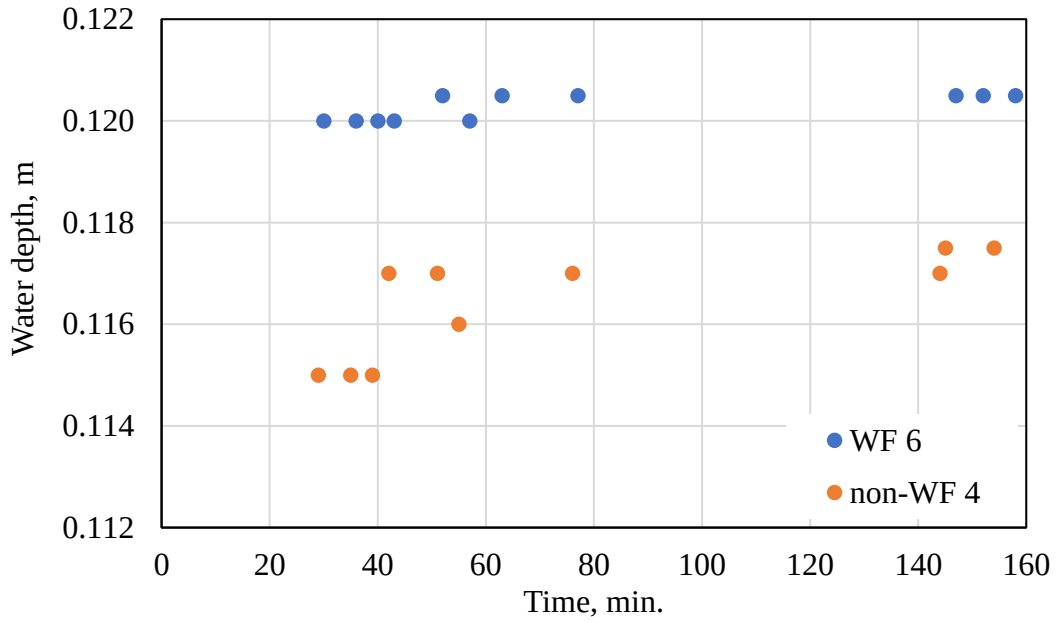

Figure 7.21 Water depths in furrows from fixed camera approximately 50 m from the top end of Border 2 in Field 2 for the irrigation event on 26-01-2018.

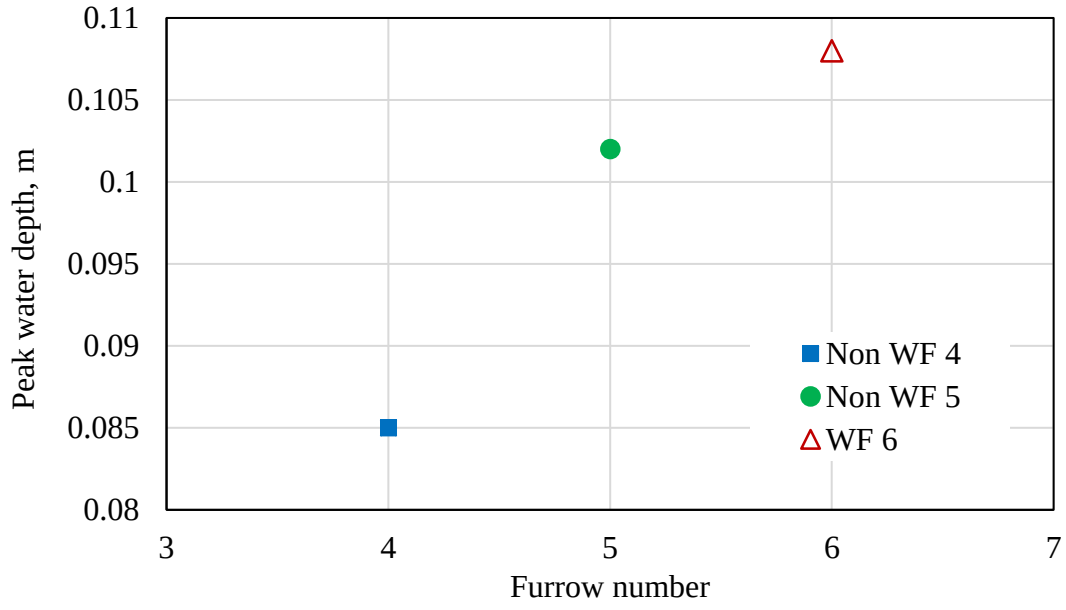

Figure 7.22 Peak water depths in furrows from float gauge approximately 55 m from the top end of Border 1 in Field 2 for the irrigation event on 10-02-2018.

7.7.3. Wooden Stakes painted with food colouring

Peak water depth measurements were conducted within both borders of Field 2 for four irrigation events in Season 2. The measurements covered 12, 24, or 36 adjoining furrows using painted wood stakes inserted approximately 52 m from the furrow entrance. Figure 7.23 shows the peak water depth measurements conducted on Border 1 of Field 2 for four irrigation events. The measurements covered a set of adjoining furrows from Furrow 13 Furrow number 36 or 48. Figure 7.24 shows the peak water depth measurements conducted on Border 2 of Field 2 for three irrigation events. The measurements covered sets of adjoining furrows from Furrow numbers 1 to 12 or 24.

Locations of the measured furrows are shown in Figure 4.3. As shown in Figure 7.23 and Figure 7.24, there are noticeable variations in the peak water depths between furrows. Generally, both figures show that the peak water depths in the WFs (numbers 6, 8, 18, 20, 30, 32, 42, and 44) are close to, but possibly higher than, the average depth. This variation will be investigated further in Section 10.2.2.

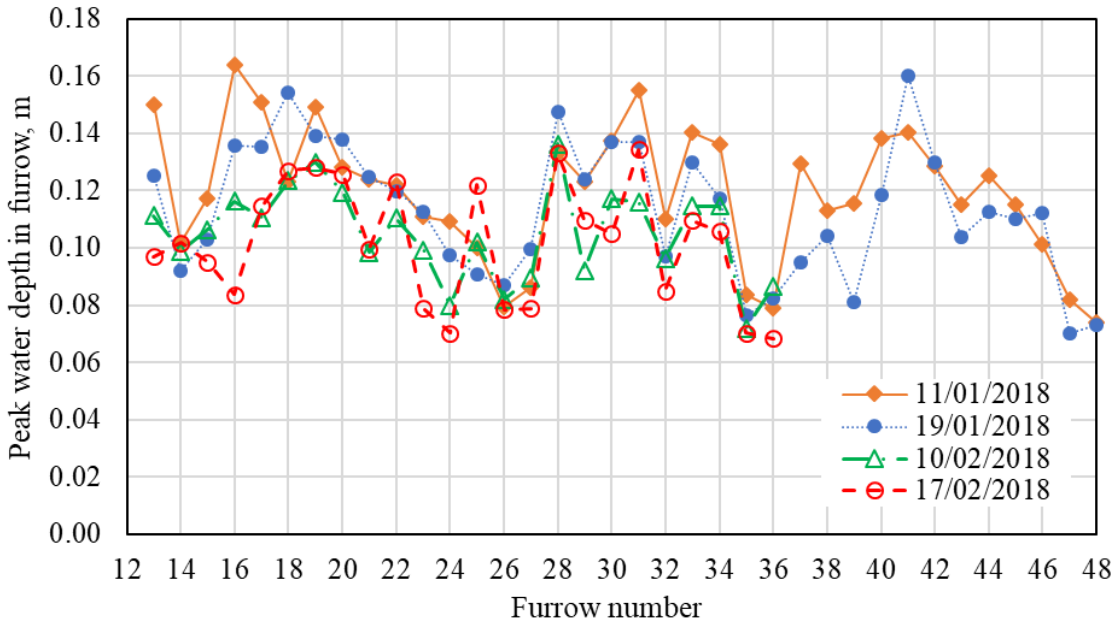

Figure 7.23 Peak water depths in furrows approximately 52 m from the top end of Border 1 in Field 2.

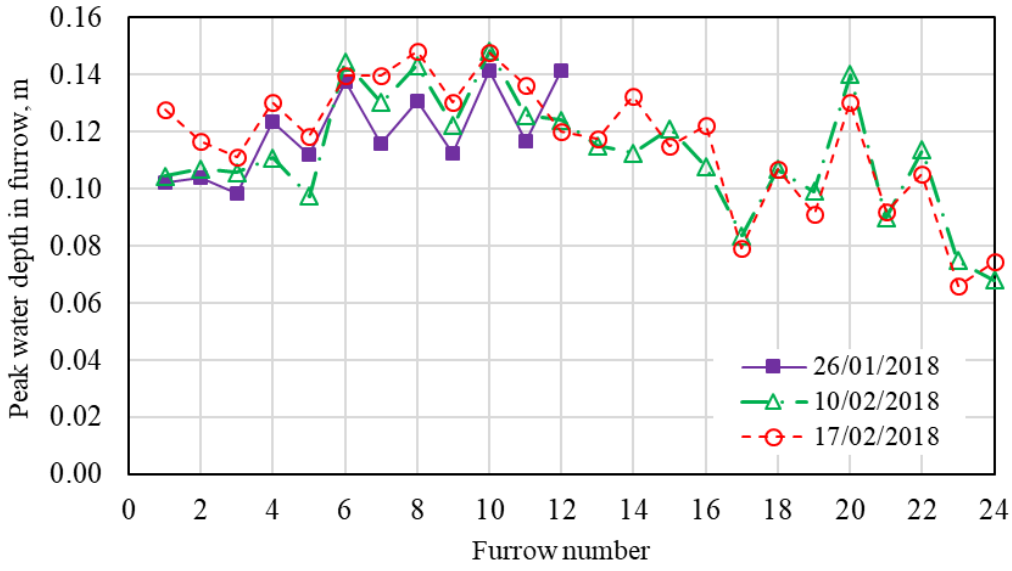

Figure 7.24 Peak water depths in furrows approximately 52 m from the top end of Border 2 in Field 2.

7.8. Soil water deficit estimation

Table 7.4 shows the summary of results for the soil water deficit (SWD) from IrriSAT (https://irrisat-cloud.appspot.com/) for Border 1 in Field 2, prior to each irrigation event throughout the whole of Season 2 (Table C-1 in Appendix C). Soil water deficits were not determined for Border 2 because it was difficult to conduct an accurate water balance without reliable runoff data from the tail drain.

Table 7.4 Soil water deficit at Border 1 of Field 2.

Irrigation event no.	Event date	SWD, mm
0	30-10-2017	-
1	15-12-2017	32.17
2	30-12-2017	77.11
3	11-01-2018	101.97
4	19-01-2018	113.72
5	26-01-2018	123.06
6	10-02-2018	130.73
7	17-02-2018	112.25

7.9. Conclusion

Hydraulic and surveying measurements were conducted in both borders of Field 2 in Season 2, 2017-2018. These measurements included conventional and unconventional

methodologies to capture the special hydraulic characteristics of FNSBO_Re irrigation system. A novel approach using UAV was employed to cover large scale measurements of advance and recession in the field. Modified furrow scale evaluations combined with large scale measurements create a methodology that can provide a good understanding of the irrigation performances of FNSBO_Re systems.

At the furrow scale, the furrow cross-sectional area, flow rate and advance rates showed noticeable variability between WFs and non-WFs. This variability highlights the difficulty of evaluating the FNSBO_Re irrigation system. However, peak water depths measurements also showed a variability between furrows, but this was not clearly explained by the position of the WF and non-WFs. Field scale advance measurements using UAV showed another form of variability between different sides of the borders. This variability means that more than one location in the border should be used to conduct measurements at the furrow scale.

The advance measurements using both IrriMATE ^{TM} advance sensors and UAV techniques showed a distinctive backward advance from the tail end for the water advance where water from faster furrows starts to back up from the bottom end of the border in the FNSBO_Re irrigation system. This distinctive behaviour adds some complexity to the field evaluation and analysis techniques. One potential approach is to avoid this bottom end of the field and concentrate on the advance measurements on that part of the field which does not experience backwards advance.

There were some limitations in the ability of the UAV technique to obtain good data for advance and recession. The ability to conduct a sufficient number of successful UAV flight missions was restricted by technical issues such as battery life and camera resolution, and site conditions such as the field size, plant growth stage (canopy) and sunlight angle. The necessity to conduct measurements of furrow flow rates was another reason there was weaknesses in the measurements. Trial flights were used to determine the appropriate flight features such as altitude and speed of the flights.

Chapter 8 and 9 focus on the evaluation procedures to model and evaluate the performance of FNSBO_Re systems. The data collected in Season 2 will be used to demonstrate these procedures.

CHAPTER EIGHT

Methodology to Model Performance of FNSBO_Re Irrigation Systems

8.1. Introduction

Initially, this chapter will examine the capability of a sample of hydraulic models to estimate soil infiltration parameters on a single furrow basis for a set of adjoining furrows in a FNSBO_Re irrigation system. Selecting the appropriate infiltration characteristics results will depend on the model reliability and the capacity to accommodate the higher quality of field measurements. The main aim of this chapter is to report on the development of a technique that can simulate the special irrigation process in the FNSBO_Re system that is required due to the special layout and irrigation management of this system. Finally, this technique will be used to simulate the results of trials and estimate the irrigation performance of the FNSBO_Re system at the furrow scale.

8.2. Estimation of infiltration parameters using different simulation models

This section will examine the volume balance method and some selected surface irrigation models for their capability to estimate soil infiltration parameters in near zero slope furrowed border irrigation systems with common water supply (FNSBO_Re). Unfortunately, most available models cannot accommodate all of the unique hydraulic characteristics of these irrigation systems.

8.2.1. Volume balance

Volume balance methods estimate the infiltration characteristic throughout the entire furrow length and the results represent the spatial average value of the infiltration parameters. Two notable examples are the Inflow-outflow method and the Two-Point method.

The special feature of the near zero slope furrowed border irrigation systems with common water supply is represented by hydraulic interactions between furrows at the top and bottom of each border. The Two-Point method was considered appropriate to complete this analysis. Normally, this method is designed to work during the advance phase, but may overcome the hydraulic complexity that occurs during the late stage of these irrigation events. This complexity is generated due to the backward flow off the top of the field, and flow entering furrows from the bottom of the field. Grabham (2012) stated that infiltration parameters can only be estimated based on field measurements during the advance phase. Runoff measurements during the drainage phase are difficult to capture due to the presence of a depth of water in the bankless channel (Grabham 2012).

8.2.1.1. Two-Point method

The Two-point method as described in section 3.5.4.2 depends on the inverse solution of the volume balance model to determine the infiltration parameters of the modified Kostiakov Equation 3.3 a, k and f_o from measurable quantities such as furrow inflow rate, water depth at the furrow entrance and water advance measurements (Elliott & Walker 1982). It was not feasible to measure water depths at the entrance to furrows because of the overflow happening between adjacent furrows. To overcome this, it was decided that furrow water depth, inflow rates and cross-sectional area would be measured just beyond the sill. Figure 8.1 shows the required measurable variables and their locations to apply the Two-Point method.

As the furrow outflow measurements were not conducted in this study, so the final infiltration rate (f_o) was not estimated. Therefore, the simple Kostiakov equation, as shown in Equation 3.1 was adopted. As shown in section 3.5.4.1 the water advance can be described using a power function (Equation 3.8). Usually, the two water advance measurements required for this method are taken at the middle ($0.5L$) and the end of the furrow (L) with their corresponding arrival times ($t_{0.5L}$ and t_L). Equations 8.1 and 8.2 are the formulae that are used to estimate the advance parameters, p and r, respectively:

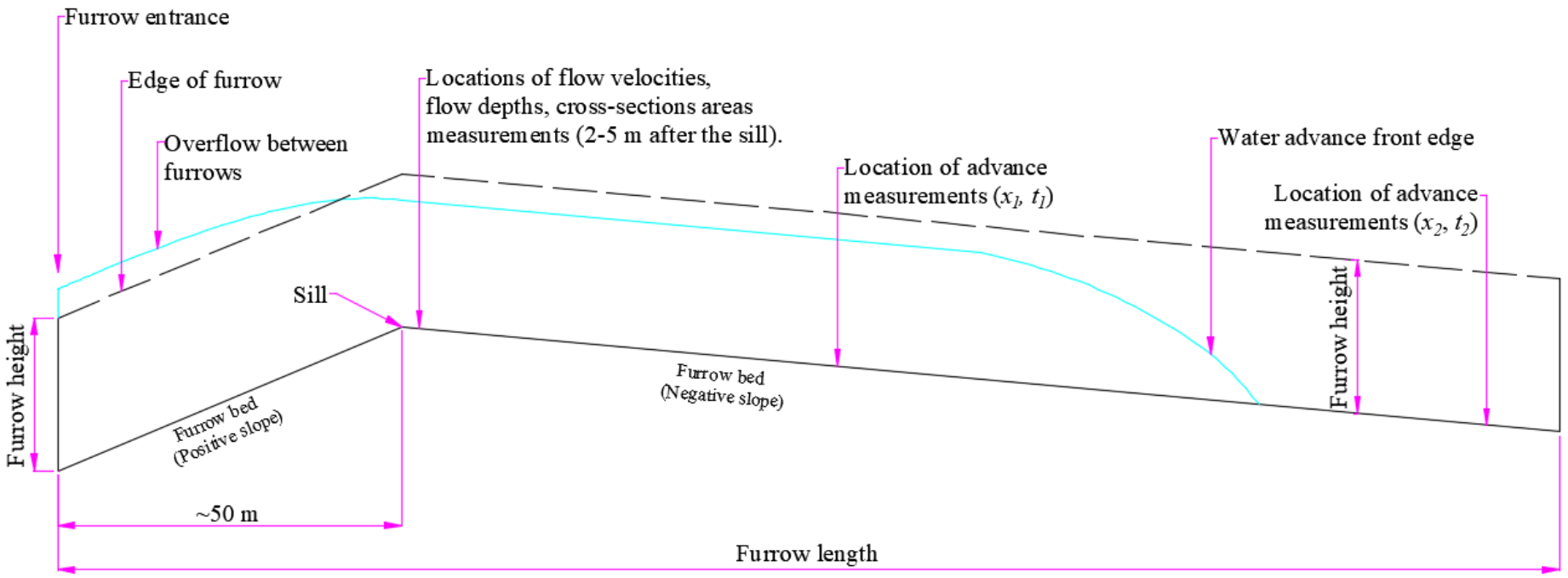

Figure 8.1 The required measurable variables and their locations to apply the Two-Point method.

$$r = \frac{\ln(\frac{0.5\ L}{L})}{\ln(\frac{t_{0.5L}}{t_L})} \quad 8.1$$

$$p = \frac{L}{t_L^r} \quad 8.2$$

In this study the advance measurements were not located precisely at the half and full length of the field and thus the closest measurements were used to estimate *p* and *r*.

The volume balance equation, Equation 3.13, without the runoff term and steady infiltration rate f_0 is expressed as:

$$Q_1 t = \sigma_s A_1 x + \sigma_{z1}\, k\, t^a x \quad 8.3$$

where Q_1 is the inflow rate of the furrow measured at the sill, A_1 is the area of flow at the sill, σ_{z1}, is as defined in Equation 3.10 and *t* is the elapsed time to reach the advance distance *x*.

Two advance points are chosen, usually, at the mid-distance, and the end, of the furrow. Thus for the mid-distance (0.5 L) of the furrow:

$$Q_1(t_{0.5L}) = \sigma_s A_1(0.5L) + \sigma_{z1}\, k\, (t_{0.5L})^a (0.5L) \quad 8.4$$

and for the end of the furrow:

$$Q_1 t_L = \sigma_s A_1 L + \sigma_{z1} k\, (t_L)^a L \quad 8.5$$

By solving these two Equations 8.4 and 8.5 simultaneously, it results in:

$$a = \frac{\ln(V_{0.5L}/V_L)}{\ln(t_{0.5L}/t_L)} \quad 8.6$$

where:

$$V_L = \frac{Q_1 t_L}{L} - \sigma_s A_1 \quad 8.7$$

$$V_{0.5L} = \frac{Q_1 t_{0.5L}}{0.5L} - \sigma_s A_1 \quad 8.8$$

Now *k* can be found by using σ_{z1} from Equation 3.10:

$$k = \frac{V_L}{\sigma_{z1}(t_L)^a} \quad 8.9$$

Table 8.1 shows the required information and inputs measured in the field to apply the Two-Point method.

Table 8.1 Information required to apply the Two-Point method.

General information			
Date	10-02-2018		
Season	2		
Event number	6		
Field number	2		
Border number	1		
Furrow number	17		
Furrow length	590 m		
Sill location	50 m from the furrow entrance		
Flow rate components			
Variable	**Unit**	**Value**	**Remark**
Water depth or depth of flow (y_1)	m	0.07	Measured on sill using ruler
Flow area (A_1)	m^2	0.019781	Cross-section on sill
Flow velocity (V)	m/s	0.204	Measured on sill using Flow-Tracker 2.
Flow rate (Q_1)	m^3/s	0.0040353	Calculated using $Q=VA$
Advance data			
0.5L	m	114.9	Mid-field advance distance
$t_{0.5L}$	min.	23	Advance time, mid-field
L	m	386.9	Advance distance from sill
t_L	min.	86	Advance time for *L*.

Table 8.2 shows the infiltration parameters *a* and *k* for a set of measured furrows, obtained by calculation with the Two-Point method. As shown in the Table 8.2, there

is considerable variation between the infiltration parameters which makes selection of representative infiltration a big challenge (Grabham 2012). Mathematically it is possible to find the equivalent (average) of infiltration parameters *a* and *k* which represent the whole set of measured furrows. This would help to achieve a better understanding of the irrigation performance at the border scale.

Table 8.2 Infiltration parameters *a* and *k* in 12 adjacent furrows estimated using the Two-Point method for Border 1 of Field 2 for irrigation on 10-2-2018.

Furrow no.	***a***	***k***
13	0.3683	0.0136
14	0.1287	0.0220
15	0.0155	0.0249
16	0.1740	0.0263
17	0.1133	0.0258
18	0.1354	0.0295
19	0.1719	0.0188
20	0.1629	0.0332
21	0.1257	0.0342
22	0.1397	0.0312
23	-0.0507	0.0690
24	-0.0602	0.0636

The process to determine the average infiltration parameters *a* and *k* for the whole set of instrumented furrows is as follows: Assume two values of infiltration time (τ_1 = 20 min., τ_2 = 150 min.) which represent the expected range of opportunity times. Substitute τ_1, *a* and *k* into Equation 3.1 to obtain the depth of infiltration for every furrow, then calculate the average of these $Z(\tau_1)$ values. Then, repeat the same procedure using τ_2, *a* and *k* to calculate the average of $Z(\tau_2)$. Then, find the average of the infiltration parameters *a* and *k* using the following Equations 8.10 and 8.11, respectively.

$$a_{average} = \frac{\log(z(\tau_1)) - \log(z(\tau_2))}{(log_{(\tau_1)} - log_{(\tau_2)})} \quad 8.10$$

$$k_{average} = 10^{(\log(z(\tau_1)) - a\log(\tau_2))} \quad 8.11$$

Table 8.3 shows the calculated values of Z (τ_1) and Z (τ_2). In this table, the values of the parameter *a* for the furrows numbered 23 and 24 are negative, which is outside the acceptable range for this Kostiakov parameter. A negative value for *a* means that accumulated depth of infiltration decreased with increased infiltration time, which is not logical. Results from Furrows 23 and 24 were not included in the calculation of the average infiltration parameters.

Table 8.3 Calculated individual values, and averages of $Z(\tau_1)$ and $Z(\tau_2)$ *a* and *k* for adjoining furrows in Border 1 of Field 2 for the irrigation event on 10-2-2018.

Furrow no.	***a***	***k***	***Z*** (20)	***Z*** (150)
13	0.3683	0.0136	0.0495	0.1039
14	0.1287	0.0220	0.0519	0.0672
15	0.0155	0.0249	0.0506	0.0522
16	0.1740	0.0263	0.0659	0.0936
17	0.1133	0.0258	0.0589	0.0741
18	0.1354	0.0295	0.0709	0.0931
19	0.1719	0.0188	0.0476	0.0673
20	0.1629	0.0332	0.0835	0.1159
21	0.1257	0.0342	0.0799	0.1030
22	0.1397	0.0312	0.0737	0.0976
23	-0.0507	0.0690	-	-
24	-0.0602	0.0636	-	-
Average	**0.16543**	**0.02479**	**0.0407**	**0.0568**

* Furrows with negative values of the infiltration parameters *a*, are not included in calculation of the averages of *a* and *k*.

From Table 8.3, $a_{average}$ was calculated using Equation 8.10 as $a_{average} = 0.16543$. Then, $k_{average}$ was calculated using Equation 8.11 as $k_{average} = 0.02479$. So, the average infiltration characteristic can be written as:

$$Z = 0.02479\,\tau^{0.16543} \qquad 8.12$$

8.2.1.2. IPARM model

The IPARM model estimates the infiltration parameters based on the same principles that are applied in the Two-Point method (Gillies & Smith 2005). IPARM completes calculations using more than two points, so the results should be more accurate than the Two-Point method. Figure 8.2 shows the inputs and results screen of the IPARM

model. This figure shows the inputs of Furrow 17 located in Border 1 of Field 2 for the irrigation event conducted on the 10-02-2018. The left side of the Figure 8.2 shows the main inputs (inflow, slope, field length, system type (furrow), furrow geometry dimensions, flow area at upstream (selected), and advance data (selected). The average longitudinal slope is calculated based on the elevation data of Furrow 17 (see Figure 8.5, table at the right) in the first 486 m, because there were slope changes in the field. Furrow geometry dimensions were extracted by ruler from the profile meter measurements collected around 55 m from the furrow entrance, on the sill.

The details and locations of these inputs are the same as that explained in the Two-Point method (Table 8.1). IPARM provides the ability to enter one of the following options for the upstream area used to calculate surface storage (value of Manning's *n*, measured upstream depth, measured upstream area (selected)). IPARM also provides the ability to select the input data for simulations (Advance data (selected), Advance and runoff data, Advance data with variable flow, and Advance and runoff data with variable flow). The right side of Figure 8.2, shows that the calculation of the parameters *a* and *k* can be executed by clicking the "Calculate" button. For Furrow 17, the value of *a* is 0.1146, while the value of *k* is 0.0256.

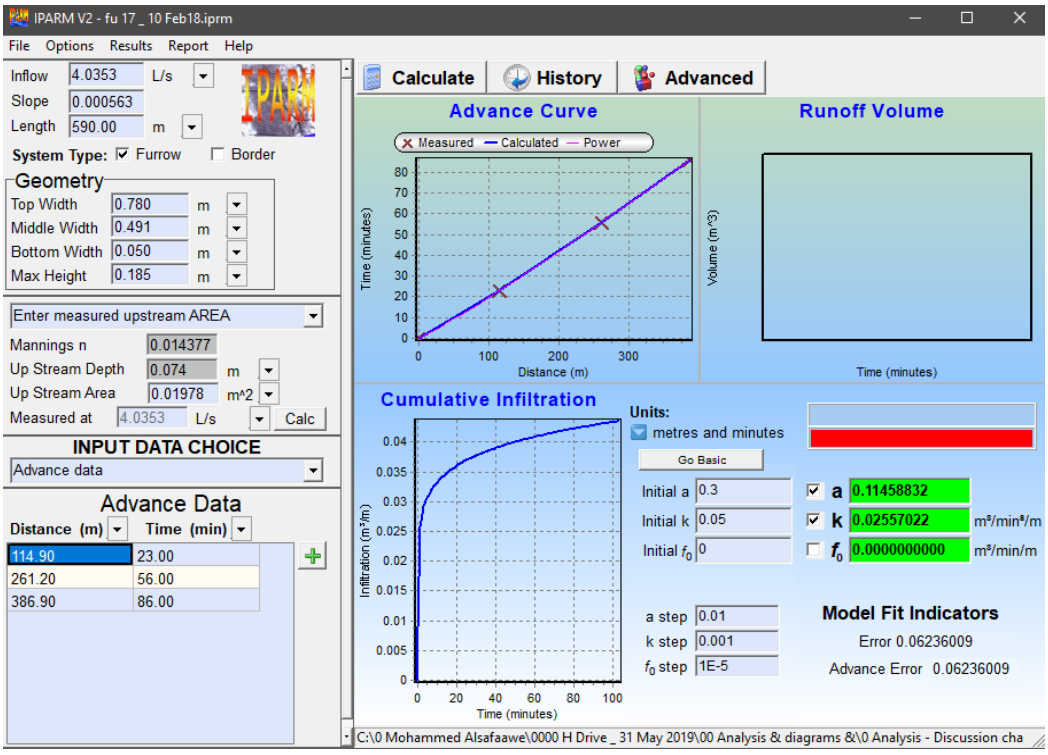

Figure 8.2 The input and results screen of IPARM for Furrow 17 in Border 1 of Field 2 for the irrigation on 10-02-2018.

Table 8.4 shows the infiltration parameters *a* and *k* calculated by IPARM for a set of adjoining furrows located in Border 1 of Field 2 for the irrigation event conducted on 10-2-2018. The values of the parameter *a* for the furrows 15, 23 and 24 are zeros, where IPARM unlike the Two-Point method does not allow *a* values to be negative. A zero value for *a* means that accumulated depth of infiltration does not change with increased infiltration time which is not logical. The averages values of the parameters *a* and *k* were found following the procedures explained in Section 8.2.1.1, specifically using Equations 8.10 and 8.11. The $a_{average}$ is 0.15577 and the $k_{average}$ is 0.02664. The furrows 15, 23 and 24 were not included in the calculation of the averages of the infiltration parameters.

Table 8.4 Infiltration parameters calculated by IPARM for Border 1 of Field 2 for the irrigation event conducted on 10-2-2018.

Furrow no.	***a***	***k***	*Z (20)*	*Z* (150)
13	0.3280	0.0154	0.0412	0.0799
14	0.0962	0.0247	0.0330	0.0401
15*	0.0000	0.0260	-	-
16	0.1615	0.0275	0.0445	0.0617
17	0.1146	0.0256	0.0360	0.0454
18	0.1041	0.0330	0.0450	0.0556
19	0.1902	0.0178	0.0290	0.0364
20	0.1040	0.0398	0.0543	0.0670
21	0.1500	0.0317	0.0497	0.0673
22	0.1243	0.0323	0.0469	0.0602
23*	0.0000	0.0582	-	-
24*	0.0000	0.0476	-	-
Average	**0.15577**	**0.02664**	0.0425	0.0581

* Furrows of zero values of the infiltration parameters *a* are not included in calculation of the averages of *a* and *k.*

8.2.2. SISCO

SISCO (Gillies & Smith 2015) provides an alternative method to estimate the infiltration parameters of the Kostiakov equation (*a* and *k*) from field measurements. SISCO differs from IPARM or the Two-point method in that it estimates the infiltration parameters using the full hydrodynamic model rather than the volume balance.

The following is an example of one of the simulation runs using SISCO. Figure 8.3 shows the input values for a Furrow 17 of Border 1 in Field 2 for the irrigation on 10-

2-2018 (Season 2). Generally, the details and locations of these inputs are the same as that explained in the Two-Point method (Table 8.1).

The Manning's *n* coefficient (0.012577) was calculated using the Manning equation calculator, circled in red in Figure 8.4. Manning's *n* was calculated based on upstream water depth, area of flow and flow rate at the sill (exact locations explained in Table 8.1), and the constant field slope entered in the input screen. The downstream furrow conditions, with options of a "Blocked" or "Free draining" selection does not impact on the calibration of the infiltration parameters *a* and *k*. Furrow cross-section dimensions were extracted with a ruler from the profile meter measurements collected at about 55 m from the furrow entrance, on the sill.

The furrow slope along the field length was input using variable values measured through the surveying (Figure 8.5). These data were entered as a table by clicking the "Bed Height data" button in the lower left corner of the input screen. Figure 8.5 shows furrows elevations at different distances along the field length. The left side data represents the original data, while the right side data represents the amended data to make the advance measurements commence from the sill by subtracting the nearest available distance (57.4) to the sill from the all distances. So, the original distance (57.4) amended to be zero, and so on. The amended data (the right side data) will be used in calibration of the parameters *a* and *k*, and in the simulation of the irrigation system.

SISCO provides four alternative approaches to estimate the infiltration parameters as shown in calibration screen (Figure 8.4). The appropriate option is selected to run the calibration based on the available measurements. The default option to run the calibration requires water advance measurements, while the other alternative methods require runoff measurements, recession measurements or water depth measurements, as shown in the check boxes top left of the calibration screen. The calibration was restricted to the parameters *a* and *k* by ticking the corresponding check boxes on the left side of the calibration screen. This restriction to two parameters was chosen firstly because of the short duration of the advance data but also to make the results comparable with Two-Point method. The value of the final infiltration (f_o) was set to be zero at the "Initial Values" part in the middle of "Calibration" screen.

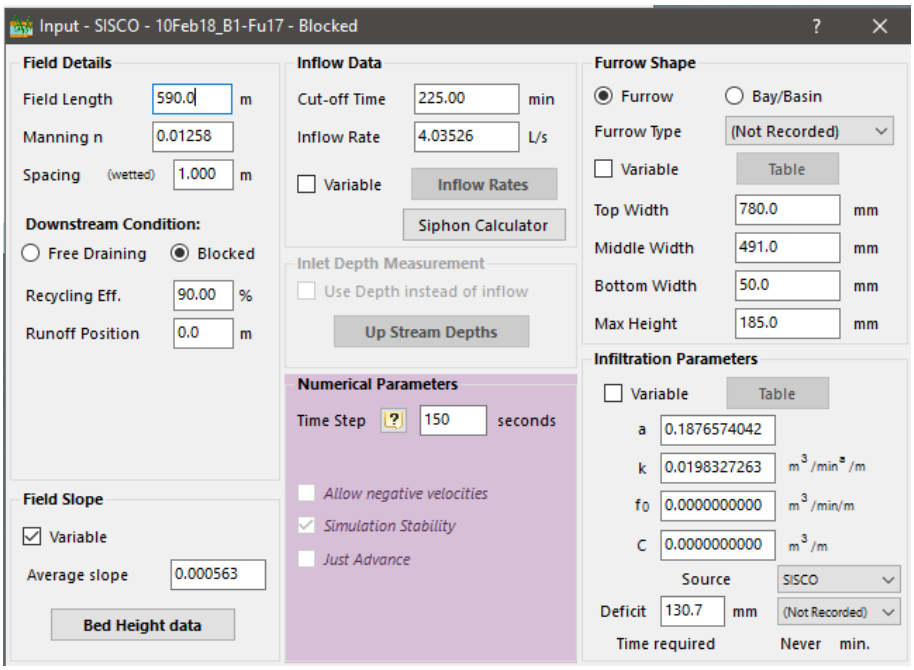

Figure 8.3 Input values for Furrow 17 located in Border 1 of Field 2 for the irrigation on 10-2-2018.

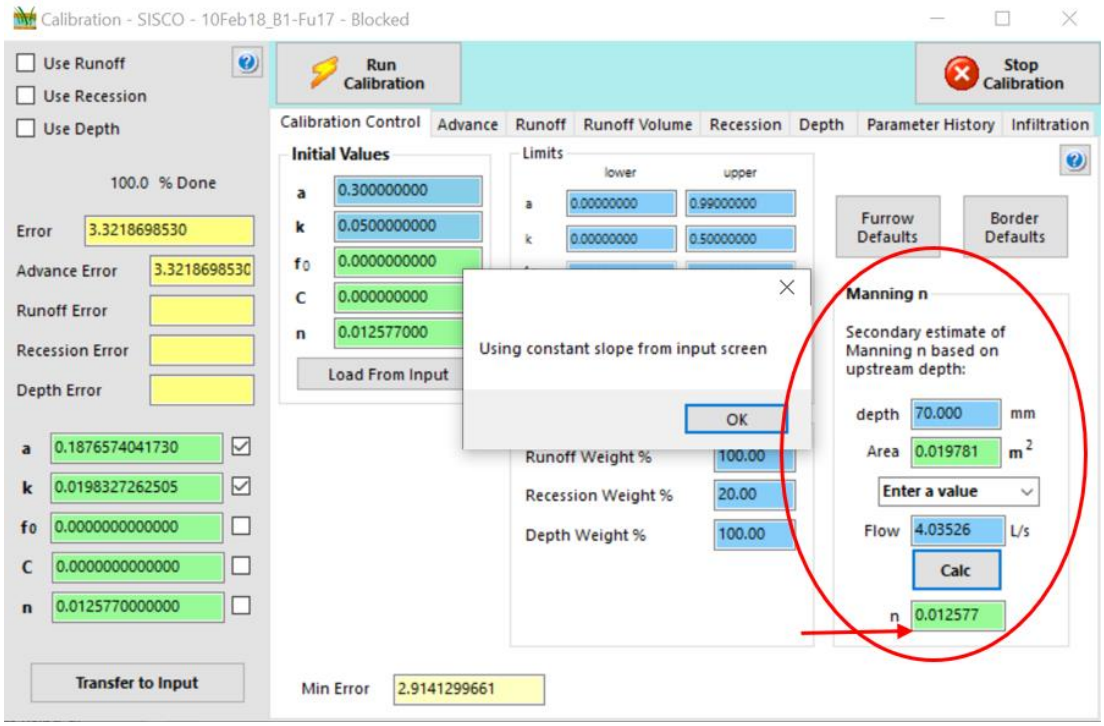

Figure 8.4 Calibration screen of SISCO, and the calculation of Manning's *n*.

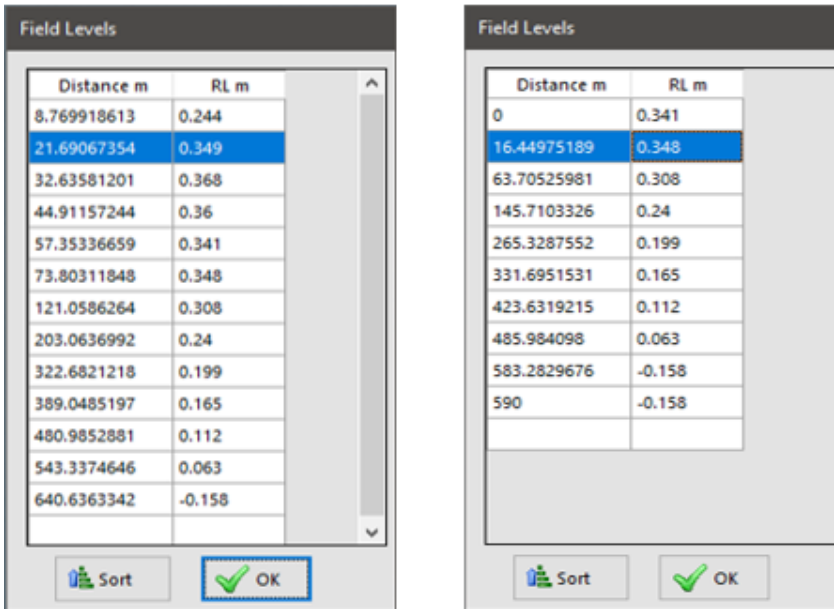

Figure 8.5 Furrows elevations along the field length. The left side data represents the original data, while the right side data represents the amended data to make the advance measurements commence from the sill.

Figure 8.6 shows water advance measurements for the current example entered into SISCO. This "Advance Data" table (Figure 8.6) is accessed by clicking the "Advance" button in the calibration screen. The advance distance and time measurements were amended as explained in the Two-Point method (Table 8.1).

The calibration process commences by clicking the 'Run Calibration' button in the calibration screen. The infiltration parameters (*a*, and *k*), are located at the left bottom of the calibration screen (Figure 8.7). For Furrow 17, the value of *a* is 0.18766 while the value of *k* is 0.01983.

This procedure is repeated for the adjoining furrows (13 to 24) of Border 1 of Field 2 for the irrigation event conducted on the 10-02-2018, to calculate the infiltration parameters *a* and *k* (Table 8.5). The values of the parameter *a* for Furrows 14, 18 and 20 are zeros, because the SISCO model does not allow *a* value to be negative. The average values of the parameters *a* and *k* were determined following the procedure explained in Section 8.2.1.1, specifically the Equations 8.10 and 8.11. The $a_{average}$ is 0.16151 and $k_{average}$ is 0.02341. Furrows 14, 18 and 20 were not used in the average calculation. So, the average infiltration characteristic can be written as:

$$Z = 0.02341\,\tau^{0.16151} \qquad 8.13$$

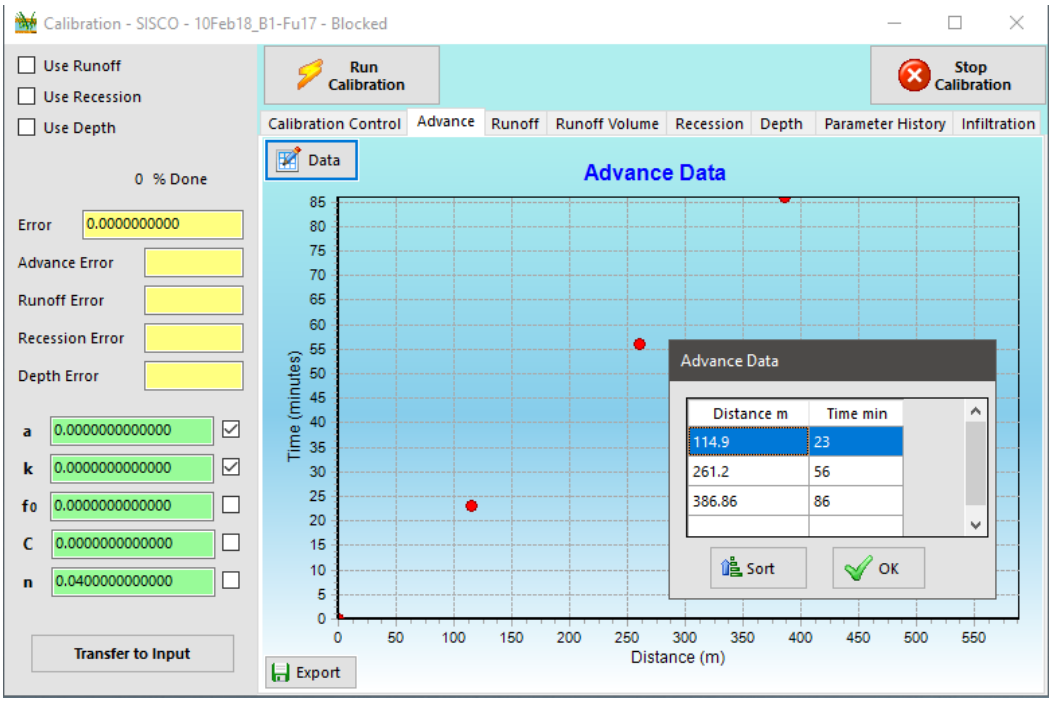

Figure 8.6 Water advance screen of SISCO with data from Furrow 17 in Border 2 of Field 2 for the event conducted on 10-02-2018.

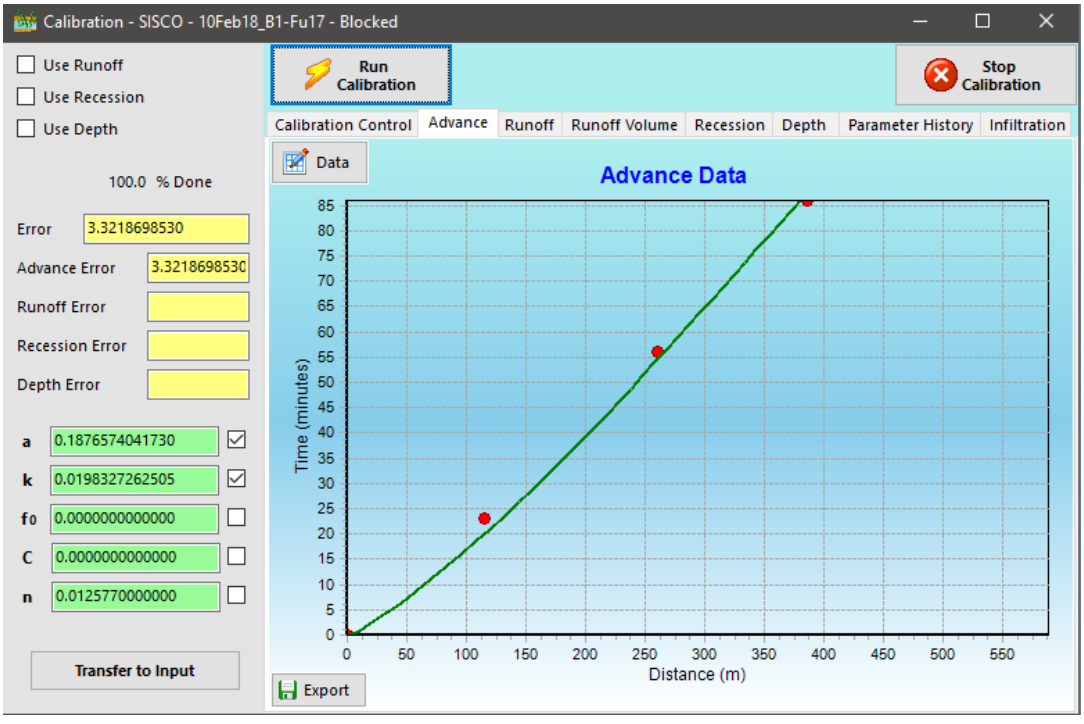

Figure 8.7 Calibration results of SISCO for Furrow 17 of Border 2 of the Field 2 for the event conducted on 10-02-2018.

Table 8.5 Infiltration parameters *a* and *k* calculated by SISCO for adjoining Furrows 13 to 24, located in Border 1 of Field 2, for the irrigation event conducted on 10-2-2018

Furrow no.	***a***	***k***	***Z* (20)**	***Z* (150)**
13	0.2825	0.0178	0.0415	0.0733
14*	0.0000	0.0306	-	-
15	0.0536	0.0183	0.0215	0.0239
16	0.1094	0.0308	0.0427	0.0532
17	0.1877	0.0198	0.0348	0.0508
18*	0.0000	0.0355	-	-
19	0.1065	0.0216	0.0297	0.0368
20*	0.0000	0.0478	-	-
21	0.0763	0.0372	0.0467	0.0545
22	0.2490	0.0177	0.0374	0.0617
23	0.1450	0.0310	0.0478	0.0641
24	0.1611	0.0245	0.0397	0.0549
Average	**0.16151**	**0.02341**	**0.0380**	**0.0526**

* Furrows with zero values of the infiltration parameters *a* are not included in the calculations of the averages of *a* and *k*.

A zero value for *a* means that the accumulated depth of infiltration does not change with increased infiltration time, which is not logical. Therefore, the infiltration parameters of Furrows 14, 18 and 20 will be estimated again based on the average value of *a*, as shown in Figure 8.8. For example, for Furrow 14 (Figure 8.8), the average value of *a* is 0.16151 and will be entered into the "*a*" field of the "Initial values" section and is unticked for the parameter *a* in the left side of the same figure; then "Run Calibration" is clicked to estimate the new value of *k*, which is equal to 0.01771. The same process was repeated to estimate the new values of *k* for Furrows 18 and 20, which were 0.02235 and 0.03000, respectively. Table 8.6 shows the final values of the "Infiltration parameters" *a* and *k* as calculated by SISCO for the adjoining furrows 13 to 24, located in Border 1 of Field 2 for the irrigation event conducted on the 10-2-2018.

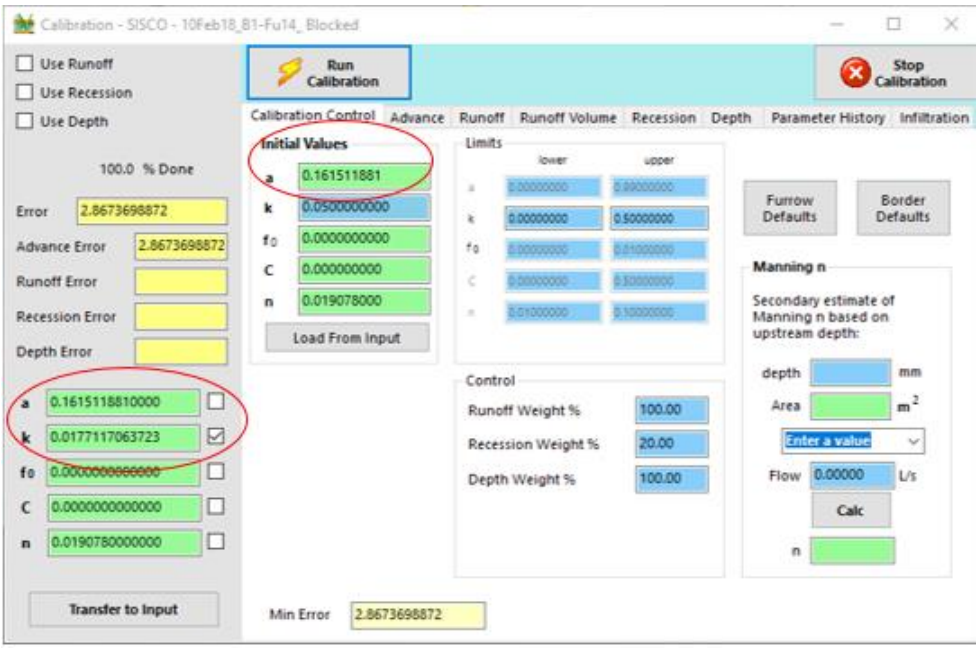

Figure 8.8 Estimating the infiltration parameter *k* when the *a* value is known (here, using $a_{average}$).

Table 8.6 Final values of Infiltration parameters *a* and *k* calculated by SISCO for adjoining furrows (13 to 24) located in Border 1 of Field 2 for the irrigation event conducted on 10-2-2018

Furrow no.	*a*	*k*
13	0.2825	0.0178
14	0.16151	0.01771
15	0.05363	0.01830
16	0.10944	0.03076
17	0.18766	0.01983
18	0.16151	0.02235
19	0.10649	0.02161
20	0.16151	0.03000
21	0.07628	0.03717
22	0.24897	0.01773
23	0.14505	0.03098
24	0.16107	0.02447

8.2.3. WinSRFR

The ability of WinSRFR to estimate the infiltration parameters of the Kostiakov equation (*a* and *k*) was evaluated. Figure 8.9 shows the main screen of the WinSRFR model. As explained in Section 3.6.3, “Event Analysis” is an evaluation function used

to estimate the infiltration parameters *a* and *k*. By clicking the button "Event Analysis", the "Evaluation" screen is displayed (Figure 8.10) where the user can enter inputs. As shown in Figure 8.10 there are several input footer tabs including: Start Event, System Geometry, Soil Crop Properties, Inflow / Runoff, Field Measurements, Execution, and Results. On the "Start Event" screen, there are two choices to perform the calibration of infiltration parameters: the Merriam-Keller post-irrigation volume balance analysis, and the Elliot-Walker Two-Point method of analysis. Both of the available options perform the calibration of the infiltration parameters using the volume balance model. The Elliot-Walker Two-Point method will be adopted in this study. The "Start Event" screen includes selecting the System Type (Basin / Border, or Furrow is selected) and the required depth of irrigation. Generally, the values, details and locations of these inputs are the same as that explained in SISCO (Figure 8.3). However, WinSRFR does not accept Manning's *n* value lower than 0.014. So, the Manning's *n* value is assumed to be 0.014, instead of the value suggested (n = 0.01258) from field measurements using SISCO.

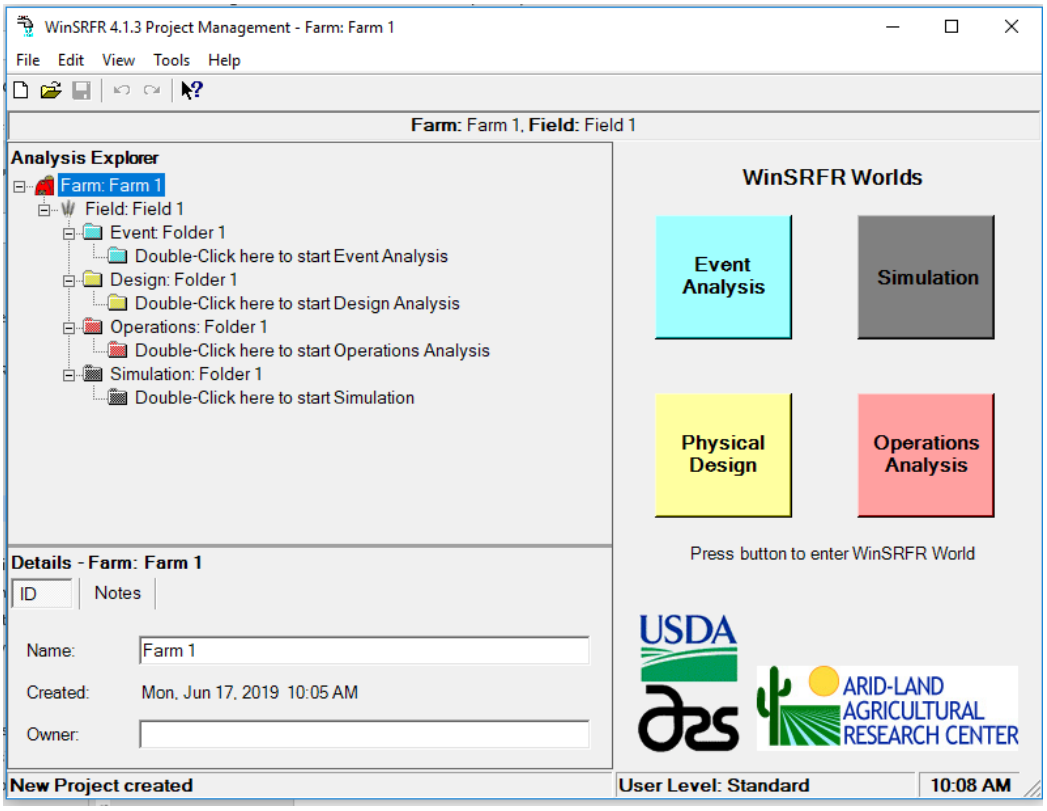

Figure 8.9 Main screen of WinSRFR 4.1.3

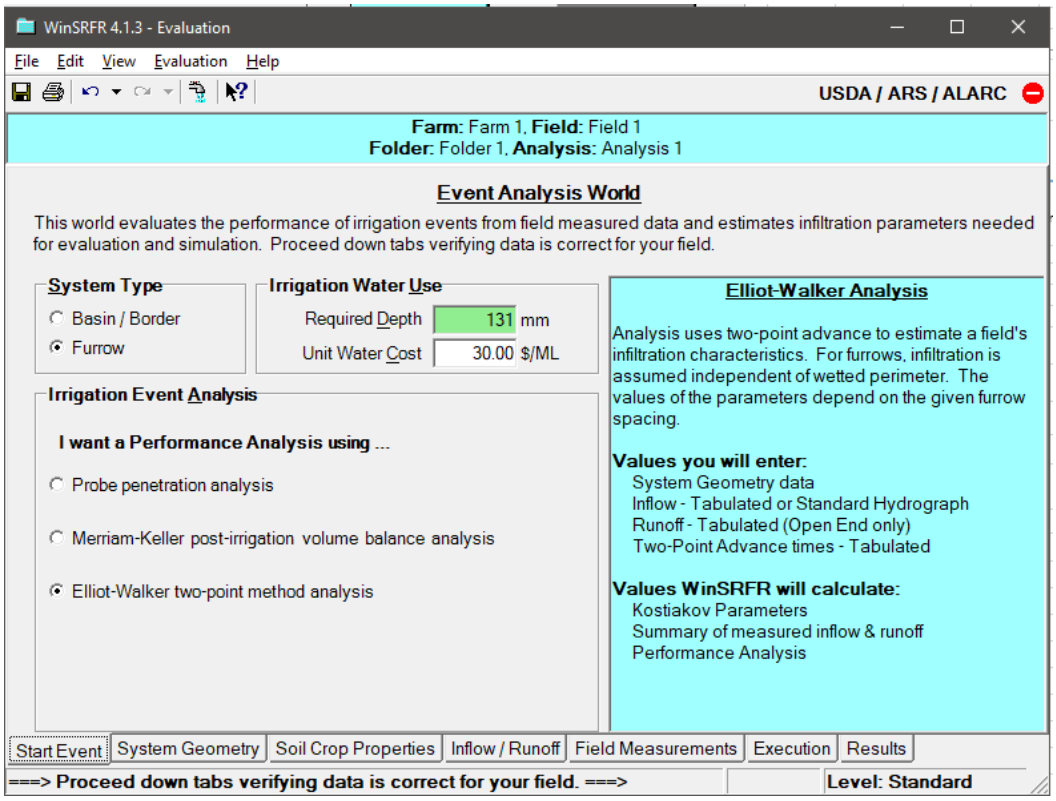

Figure 8.10 Evaluation screen of WinSRFR

Table 8.7 shows the summary of the other required inputs used to estimate the infiltration parameters *a* and *k* via WinSRFR, for Furrow 17 in Border 1 of Field 2 for the irrigation event held on the 10-2-2018.

The infiltration parameters were estimated by clicking the "Estimate *a* & *k*" button on the "Execution" tab. For this furrow the value of *a* is 0.085 while the value of *k* is 43.092 mm/hr[a]. The parameter *k*, converted to match the units of the other models, would be 0.0304 mm/min[a]. WinSRFR provides the ability to update the Surface shape factors at Point 1 and 2 (σ_{s1} and σ_{s2}, respectively) by calculating new values of them. The infiltration parameters (*a* and *k)* were estimated again by adopting these new calculated surface shape factors. This process is repeated three times, until the newly obtained infiltration parameters do change less than 1% between iterations.

Table 8.7 Required inputs used in WinSRFR model, for Furrow 17 in Border 1 of Field 2 for the irrigation event conducted on the 10-2-2018.

Tabs	Items	Inputs
Start Event	Type of irrigation analysis	Elliot-Walker Two-Point method
	System type	Furrow
Soil Crop Properties	Manning *n* (not accepted)	0.01258
	Manning *n* (used)	0.014
Field Measurements	Advance distance of Point 1, m	114.9
	Advance time of Point 1, hr	0.38
	Advance distance of Point 2, m	386.86
	Advance time of Point 2, hr	1.43
Execution for the first run of estimation the infiltration parameters	σ_{s1} for the first run	0.765 (Default)
	σ_{s2} for the first run	0.795 (Default)
	Infiltration parameter *a*	0.085
	Infiltration parameter *k*, mm/hr[a]	43.092
	Infiltration parameter *k*, mm/min[a]	0.0304
Execution for the second run of estimation the infiltration parameters	σ_{s1} for the second run	0.992 (Calculated)
	σ_{s2} for the second run	1.110 (Calculated)
	Infiltration parameter *a*	0.059
	Infiltration parameter *k*, mm/hr[a]	37.353
	Infiltration parameter *k*, mm/min[a]	0.0293
Execution for the third run of estimation the infiltration parameters	σ_{s1} for the third run	1.009 (Calculated)
	σ_{s2} for the third run	1.128 (Calculated)
	Infiltration parameter *a*	0.059
	Infiltration parameter *k*, mm/hr[a]	37.05
	Infiltration parameter *k*, mm/min[a]	0.0291

Table 8.8 shows the infiltration parameters *a* and *k* calculated by WinSRFR for a set of adjoining furrows (13 to 24) located in Border 1 of Field 2 for the irrigation event conducted on the 10-2-2018. The values of the parameter *a* for Furrows 15, 23 and 24 are negative. In these cases the Two-Point method does not work properly in the WinSRFR model because it results in illogical values of infiltration parameters. To find the averages values of the parameters *a* and *k* the procedures explained in Section 8.2.1.1 were applied, specifically the Equations 8.10 and 8.11. Furrows 15, 23 and 24 were not included in the calculation of the averages of the infiltration parameters. The $a_{average}$ is 0.08584 and the $k_{average}$ is 0.03058.

Table 8.8 Infiltration parameters *a* and *k* calculated by WinSRFR for Furrows 13 to 24 in Border 1 of Field 2 for the irrigation event conducted on the 10-2-2018.

Furrow no.	***a***	***k***	***Z** (20)*	***Z*** (150)
13	0.288	0.0180	0.0426	0.0761
14	0.056	0.0259	0.0307	0.0343
15*	-0.002	0.0273	-	-
16	0.097	0.0330	0.0441	0.0536
17	0.059	0.0291	0.0347	0.0391
18	0.004	0.0343	0.0347	0.0350
19	0.088	0.0224	0.0292	0.0348
20	0.016	0.0451	0.0474	0.0489
21	0.027	0.0429	0.0465	0.0491
22	0.061	0.0384	0.0461	0.0522
23*	-0.074	0.0750	-	-
24*	-0.064	0.0672	-	-
Average	**0.08584**	**0.03058**	**0.0395**	**0.0470**

* Furrows with negative values for the infiltration parameters *a* are not included in the calculations of the averages of *a* and *k*.

8.2.4. Fit of models to measured advance data

Both IPARM and SISCO were used to estimate soil infiltration parameters for most of the furrows measured. It was observed that both models provide good predictions of measured advance with similar levels of accuracy. From the example shown in Figure 8.11 for Furrow 17 it can be seen that both SISCO and IPARM are fitting closely to the measured data. IPARM and SISCO use a measure of fit termed the E_{Ad}, a non-dimensionalised value, expressed as a percentage which is given by Equation 8.14. In terms of E_{Ad}, IPARM (E_{Ad} = 0.0624) has a lower error than SISCO (E_{Ad} = 3.32157) but WinSRFR failed to predict the advance and has an unacceptable error (E_{Ad} = 13.58311). According to the fit of the advance data, both IPARM and SISCO are equally suitable, but SISCO offers the advantage that is based on a more robust theoretical model, and more importanty, provides the outputs necessary for the TBC method. Therefore, SISCO was adopted for estimating the infiltration parameters.

$$E_{Ad} = \sqrt{\frac{\Sigma\,(x_{measured} - x_{predicted})^2}{\Sigma\,(x_{measured})^2}} \qquad 8.14$$

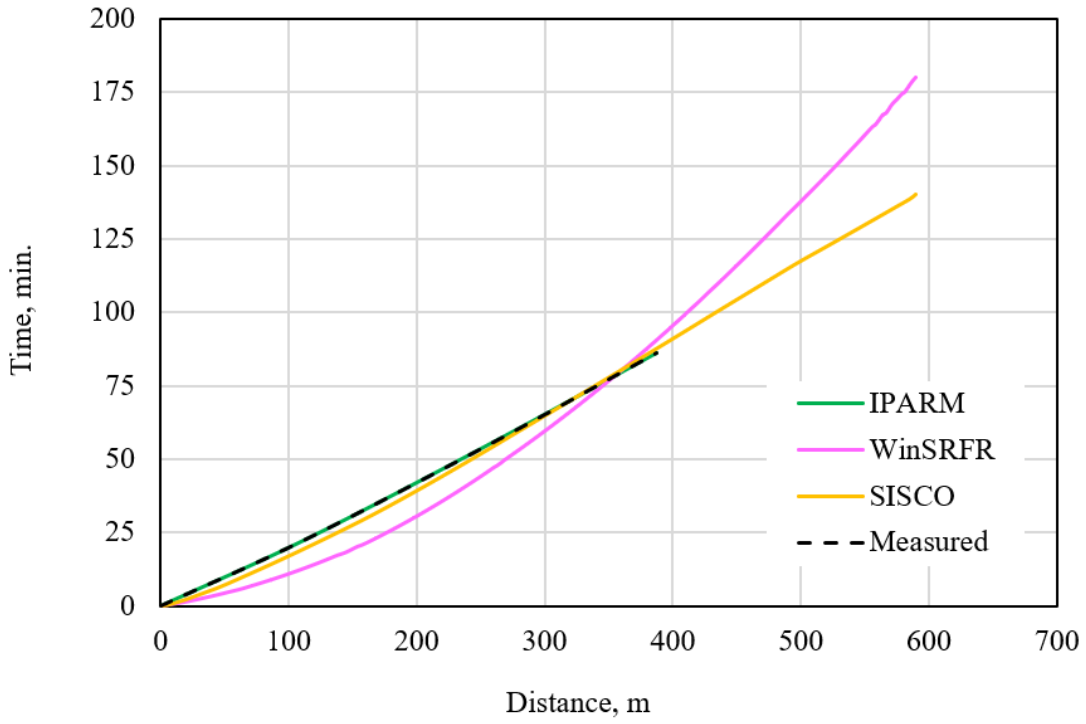

Figure 8.11 Measured and simulated advance distances

8.2.5. Conclusion

Table 8.9 shows the summary of the infiltration parameter averages calculated by all four models for a set of adjoining furrows in Border 1 of Field 2 for the same irrigation event. Figure 8.12 shows the average infiltration characteristics for the four models as presented in Table 8.9. The cumulative infiltration depth curves show the same behaviour of the infiltration characteristics in all models. This behaviour normally represents the infiltration into the soil with cracks (Novak et al. 2000). The cracks were noticed clearly in the furrows (Figure 4.4). As shown in Figure 8.12, the initial infiltration value, which is represented by the magnitude of the *k* parameter, was very significant compared with the steady infiltration value along the remainder of the IOT, which is represented by the magnitude of the *a* parameter. Because the initial infiltration is dominating the process, the irrigation performance is less impacted by the differences in the IOT between furrows.

Generally, it can be noticed that the accumulated infiltration depth values were close in all the models. However, SISCO's model results will be adopted in the analysis

because it based on the full hydrodynamic model which is considered to have the highest reliability compared with the other models (see Chapter 3). While only WinSRFR and SISCO can accommodate variable field slope, SISCO has the advantage of being able to accommodate many advance measurements, compared with only two advance measurements in WinSRFR. Hence, SISCO's results can be more reliable.

Table 8.9 Summary of the infiltration parameters averages for Border 1 of the Field 2 for the irrigation event conducted on the 10-2-2018.

	Two-Point	IPARM	SISCO	WinSRFR
a	0.16543	0.15577	0.16151	0.08584
k	0.02479	0.02664	0.02341	0.03058

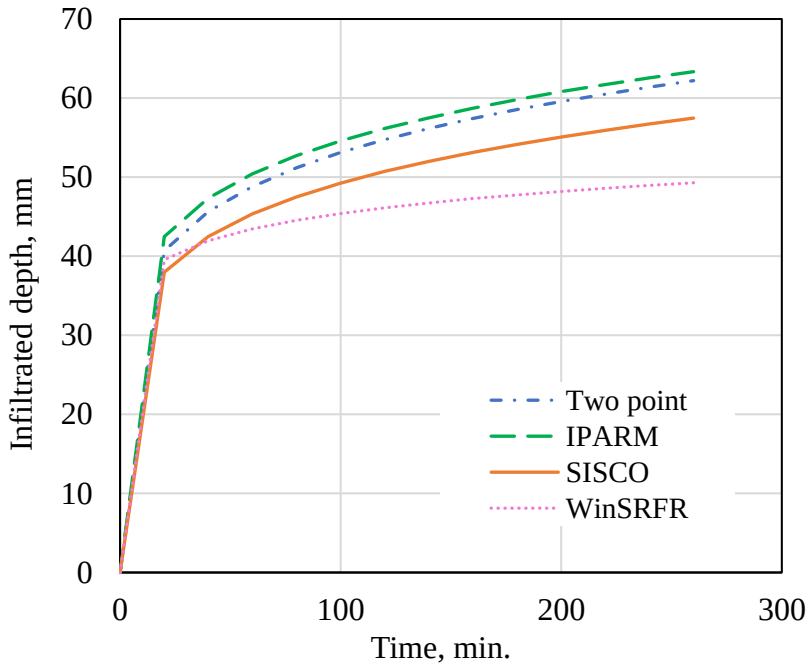

Figure 8.12 Average infiltration characteristics for Border 1 of Field 2 for the irrigation event conducted on the 10-2-2018

8.3. Estimating the irrigation performance using the SISCO model at the furrow scale

In this section, irrigation performance of events will be estimated using the SISCO model. The irrigation performance estimation will be conducted for a single furrow taking into consideration two different scenarios of downstream flow condition: Blocked end and Free draining. The reasoning behind using SISCO was the ability of

this model to stop the simulation process at any time, and extract the data to conduct manual calculations and determine the irrigation performance. This feature is not provided by any other models.

After estimating the infiltration parameters of Furrow 17, as explained in Section 8.2.2, the performance results were calculated by clicking 'Run Simulation' on the main screen of SISCO (Figure 3.2). A sample of the simulated results is shown in Figure 8.13. The simulated results displayed in Figure 8.13 are for Blocked downstream conditions. The simulated results for Free draining downstream conditions (Figure 8.14) can be generated by ticking the Free draining option shown in Figure 8.3.

The following terms will be considered in the ensuing discussion: Application Efficiency (AE%), Requirement Efficiency (RE%), Distribution Uniformity (DU%), and the volumetric proportions (Runoff%, Drainage%, and Storage%) as percentages of the total inflow volume (volume applied). Runoff volume refers to the drained water passing through the tail drain box. Drainage volume refers to the volume of infiltration that percolates deeply below the effective depth of the root zone. Storage volume refers to the volume of water stored on the soil surface.

Comparing the irrigation performance results between the two downstream conditions for Furrow 17 (Figure 8.13 and Figure 8.14) shows that the AE and RE in the Blocked condition are higher than the Free draining condition, while the DU in the Blocked condition is lower than the Free draining condition. This will be discussed for all studied furrows results, and are gathered in Table 8.10.

Table 8.10 shows the gathered simulated results of the irrigation performance for the set of adjoining Furrows 13 to 24 in Border 1 of Field 2 for the irrigation event conducted on the 10-2-2018, for both downstream Blocked and Free draining conditions. As shown in Table 8.10, for the Blocked condition there is a wide variation in the performance indices among the furrows, from 51.17 to 95.13% for AE, from 34.48 to 96.51% for RE, and from 38.66 to 73.94% for DU. Similarly, for the Free draining condition, the AE and RE varied widely from 28.44 to 73.76% and from 19.02 to 63.56%, respectively, while the DU values are more consistent with the average values that varied from 95.18 to 99.09%. Generally, it is clear to conclude that there is

a large variation in the irrigation performance among those adjoining furrows in this irrigation system, regardless of the downstream flow conditions.

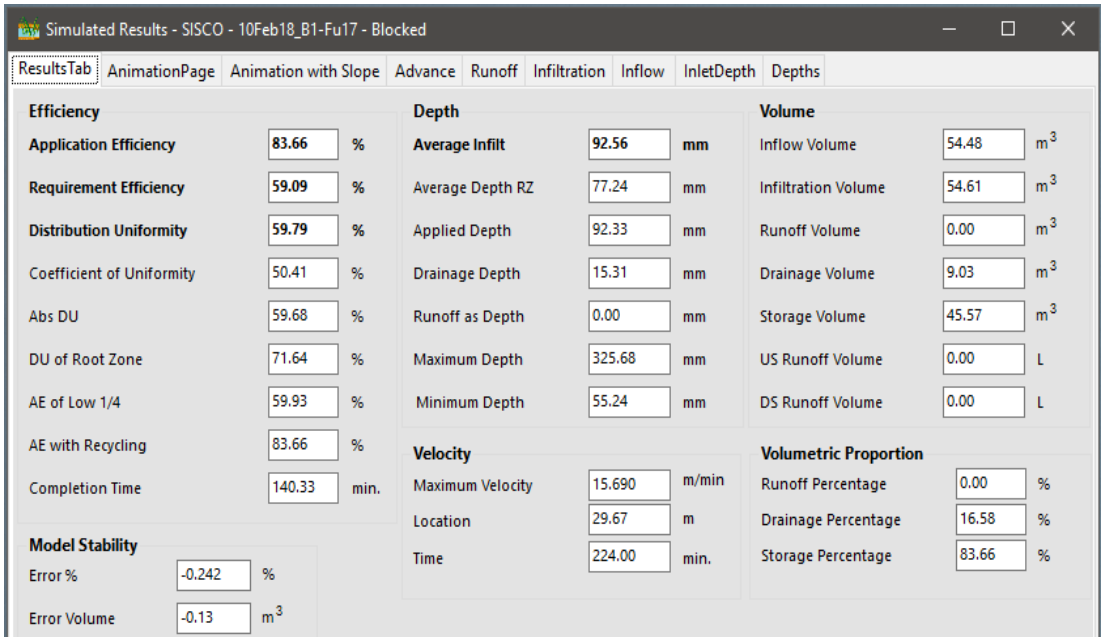

Figure 8.13 Simulation results for the blocked downstream condition for Furrow 17 of Border 1 of Field 2 on 10-02-2018.

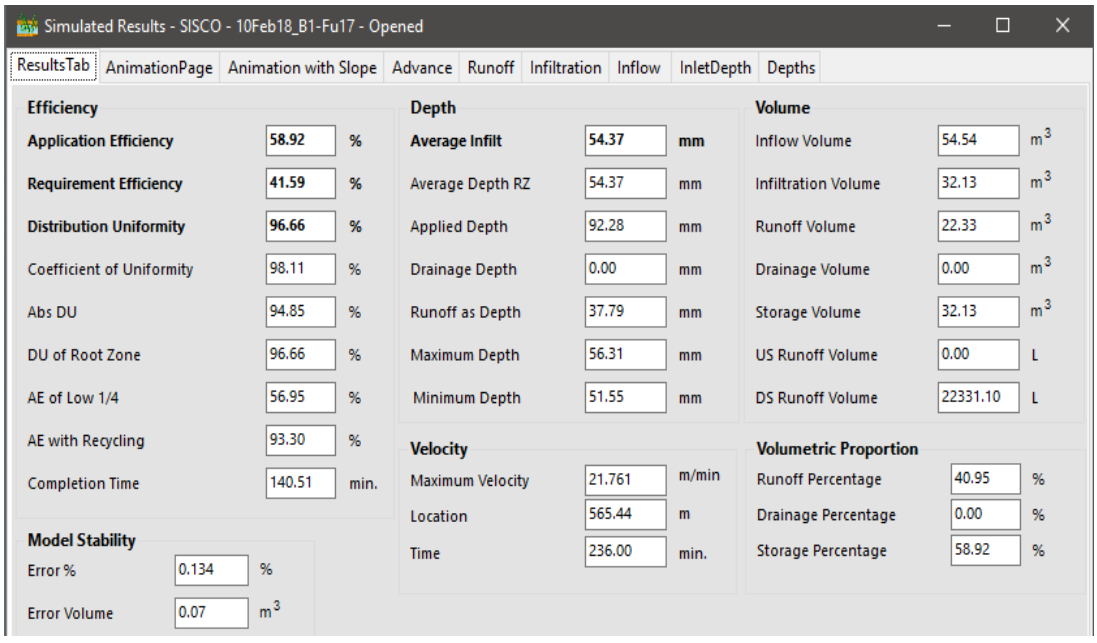

Figure 8.14 Simulation results for the free draining downstream condition for Furrow 17 of Border 1 of Field 2 on 10-02-2018.

Table 8.10 Simulated results of irrigation performance for furrows 13 to 24 in Border 1 of Field 2 on 10-2-2018.

Furrow #	Blocked						Free draining					
	AE %	RE %	DU %	Runoff Volume %	Drainage Volume %	Storage Volume %	AE %	RE %	DU %	Runoff Volume %	Drainage Volume %	Storage Volume %
13	70.03	83.81	53.76	0.00	30.28	73.03	53.19	63.56	96.80	46.67	0.00	53.19
14	80.62	54.27	49.13	0.00	19.88	80.62	49.40	33.20	99.01	50.49	0.00	49.40
15	83.81	34.48	45.56	0.00	16.89	83.81	46.32	19.02	99.09	53.55	0.00	46.32
16	75.73	72.14	45.87	0.00	24.59	75.73	45.51	43.28	99.07	54.39	0.00	45.51
17	83.66	59.09	59.79	0.00	16.58	83.66	58.92	41.59	96.66	40.95	0.00	58.92
18	60.01	90.80	42.40	0.00	39.36	60.01	28.44	42.96	98.13	71.49	0.00	28.44
19	79.19	70.67	38.66	0.00	20.58	79.19	33.76	30.10	98.96	66.04	0.00	33.76
20	51.17	96.51	47.67	0.00	48.33	51.17	30.33	57.10	98.51	69.49	0.00	30.33
21	75.86	83.87	50.90	0.00	23.73	75.86	40.41	44.61	97.59	59.65	0.00	40.41
22	77.31	70.57	50.94	0.00	22.98	77.31	50.85	46.38	98.41	48.97	0.00	50.85
23	95.13	73.76	67.75	0.00	4.85	95.13	66.47	51.58	97.13	33.39	0.00	66.47
24	90.75	54.10	73.94	0.00	9.53	90.75	73.76	43.97	95.18	26.18	0.00	73.76

Comparing the irrigation performance results between the two downstream conditions for the same furrows (Table 8.10) shows that the AE and RE in the Blocked condition are higher than the Free draining condition. This is because the summation of the estimated water losses for each furrow (runoff volume and drainage volume) in the Blocked condition are lower than the Free draining condition. However, the comparison between the two downstream conditions shows that DU under Blocked conditions is lower than for Free draining conditions. This is due to the overestimation in the infiltrated depth and drainage in the Blocked condition, especially at the bottom end of the furrow. Figure 8.15 shows the SISCO simulated results for the infiltrated depth along Furrow 17 for both downstream Blocked (top) and Free draining (bottom) conditions. The green line represents the soil water deficit (130.73 mm, see Table 7.4). As shown in Figure 8.15, there was an overestimation of the infiltrated depth in the lower part of the furrow for the Blocked condition, with infiltrated depths exceeding 300 mm at the very bottom end of the furrow.

(Grabham 2012) conducted simulations in WinSRFR and SISCO models by selecting a Blocked downstream condition, although the furrows ends were open Grabham noted that the water leaving the downstream end of the furrows accumulated and redistributed across other furrows within the border. It was assumed that the water re-entering furrows from their downstream ends behaved like a blockage at the end of those furrows. However, this assumption could imply an error in the calculated performance indices because it neglects the significant amount of runoff and overestimates the infiltrated depth of water (Table 8.10). Therefore, it is believed a better situation of the downstream condition in this field, is something between Blocked and Free draining conditions. The current simulation models do not provide the ability to accommodate the downstream end of the field being initially blocked, but then opened at some later time (temporarily blocked condition).

Figure 8.15 SISCO results of the infiltrated depth along Furrow 17 for both downstream Blocked (top) and Free draining (bottom) conditions, in Border 2 of Field 2 for 10-02-2018.

8.4. A technique to estimate the performance indices for the real downstream condition

As stated above, currently available models are unable to simulate the field irrigation management conditions observed at this field site.

In order to determine the performance indices that represent the real downstream condition (temporarily blocked condition), a method described below will utilise spreadsheet calculations based on the SISCO simulation results for Blocked conditions.

Figure 8.16 shows the "Animation with Slope" screen that displays the simulated results of SISCO for Furrow 17 located in Border 1 of Field 2 for the irrigation event conducted on the 10-2-2018 with a Blocked downstream condition. This window (Figure 8.16) also displays the value of the volume balance components at a particular time during the irrigation: the total inflow volume, the surface stored volume, and the infiltrated volume, in cubic metres. It also represents graphically the surface stored water as shown by the blue line, and the infiltrated water shown as the red line, both with respect to the reduced level of the furrow bed, shown in the brown line, along the furrow length. The "Export" button, as shown in the upper left corner of Figure 8.16, provides the ability to export this data as a spreadsheet file, at any selected time during the simulated irrigation. The form of the exported data is determined based on the option chosen for Area or Depth. The exported surface stored data represents the flow areas along the furrow length, when the "Area" option is ticked. And it represents the flow depths when the "Depth" option is ticked. In Figure 8.16 the "Area" option is ticked, as shown by the radio button at the lower right corner of this figure. The area or depth values for the surface storage are not limited to the height of the furrow. The infiltrated depth values are the same whether the "Area" or "Depth" options are ticked, where in both cases they represent the infiltrated volumes per unit length per unit width (furrow spacing). Also, the reduced level along the furrow length are the same for both options (Area or Depth).

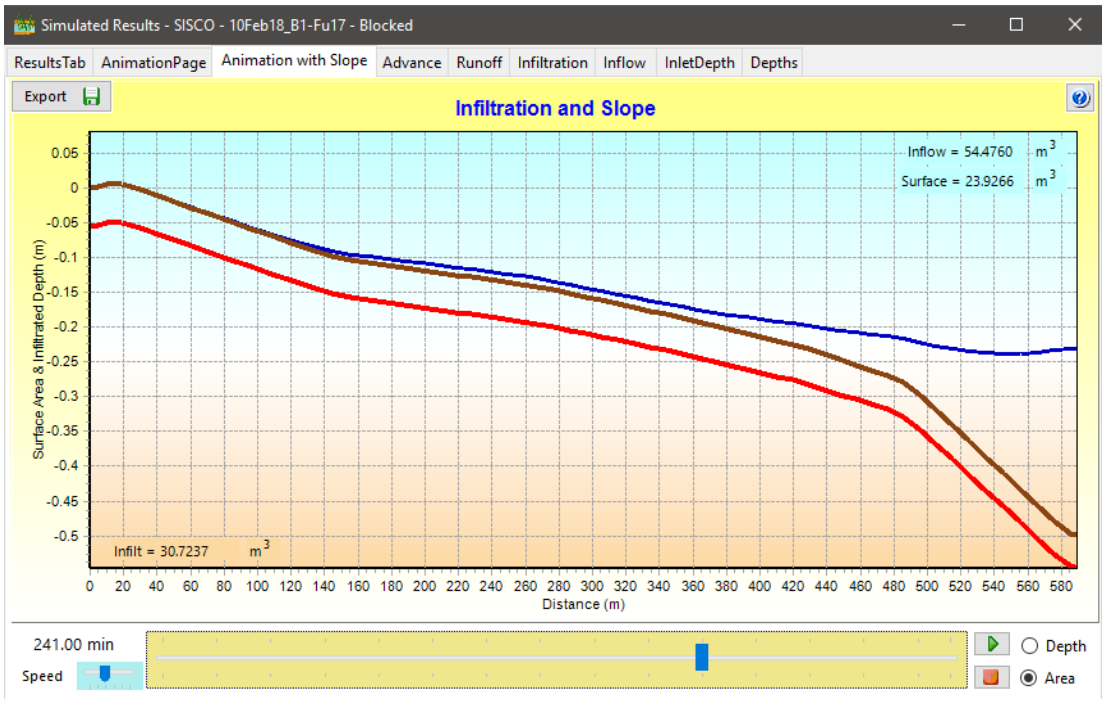

Figure 8.16 A screenshot of the SISCO "Animation with Slope" screen for Furrow 17 of Border 1 in Field 2 on the 10-2-2018 (Blocked downstream condition).

Figure 8.17 shows the "Animation Page" screen that displays the simulated results from SISCO for the same set of data as used in Figure 8.16. Figure 8.18 shows the SISCO "Advance" screen that displays the simulated results of the water front advance and recession in Furrow 17. The "Export" button at the upper left corner of Figure 8.18 provides the ability to export water advance and recession data as a spreadsheet file.

The suggested technique involves two calculations for runoff and infiltration, as shown in Figure 8.19 and Figure 8.20, respectively. These calculations are based on the surface storage, infiltration, water advance, and reduced ground level data along the furrow length, as exported from SISCO while running a simulation with a Blocked downstream condition.

The suggested manual calculations are based on real field practice to match the duration that the bottom check gate or tail drain box was blocked, before being opened. The term "temporarily blocked calculation" (TBC) will be used to refer to this suggested manual calculation process.

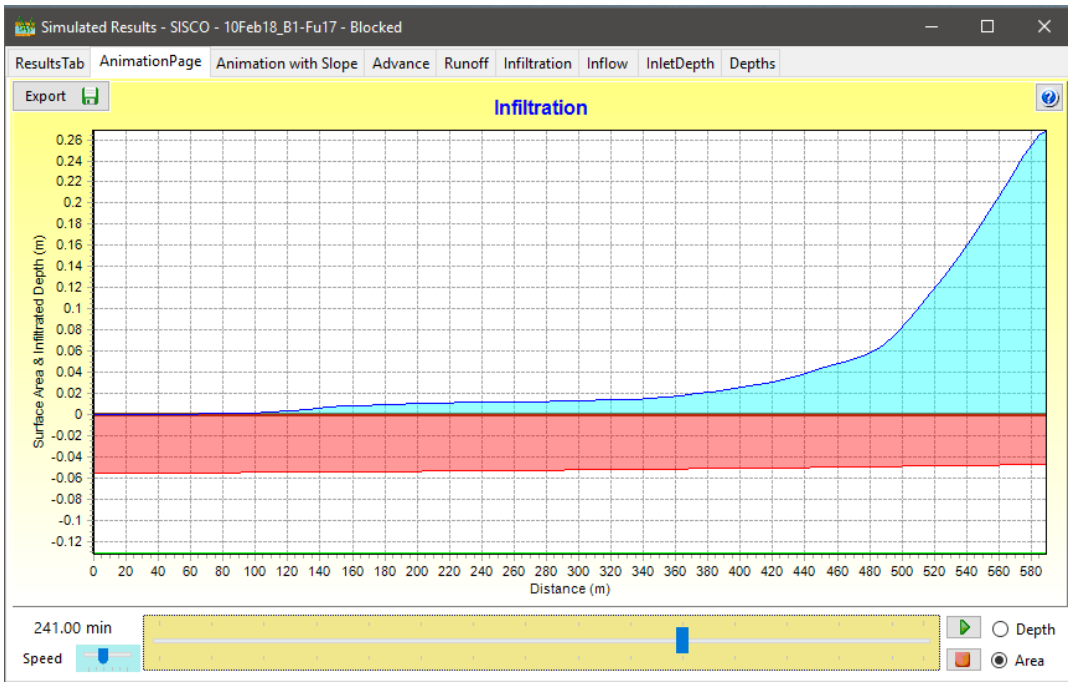

Figure 8.17 A screenshot of the SISCO "Animation Page" of Border 1 in Field 2 on the 10-2-2018 (Blocked downstream condition).

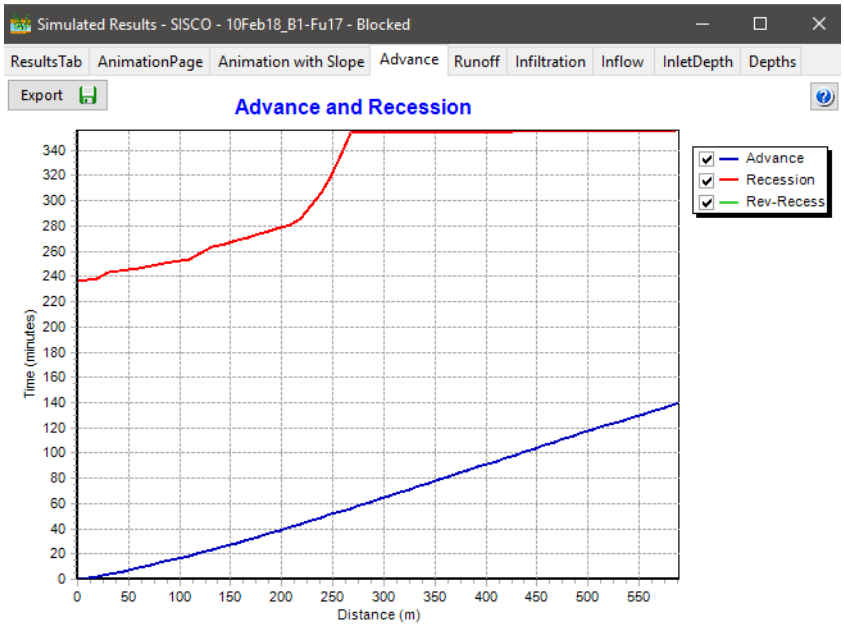

Figure 8.18 The SISCO "Advance" for Furrow 17 of Border 1 in Field 2 on the 10-2-2018 (Blocked downstream condition).

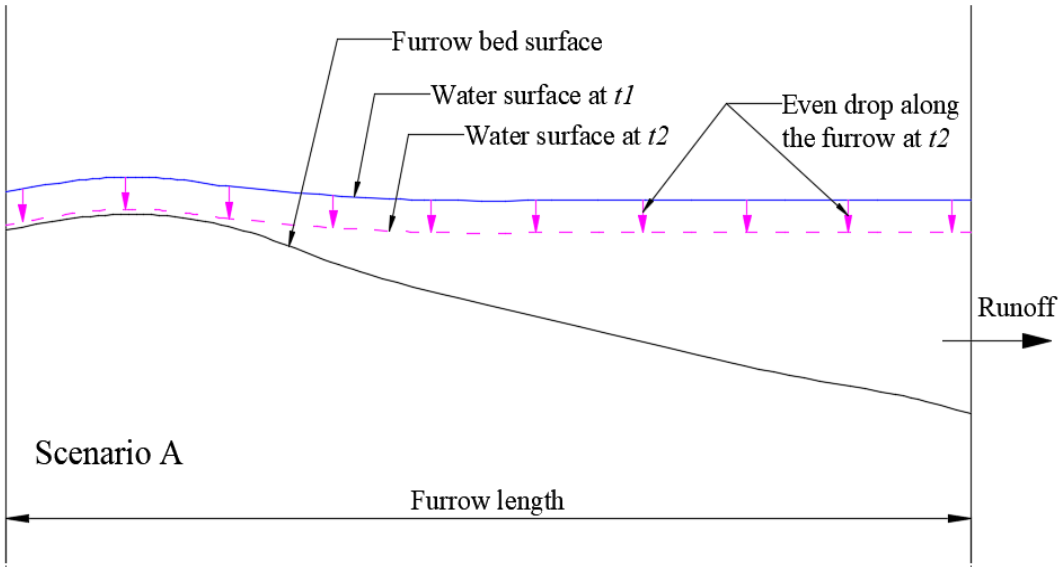

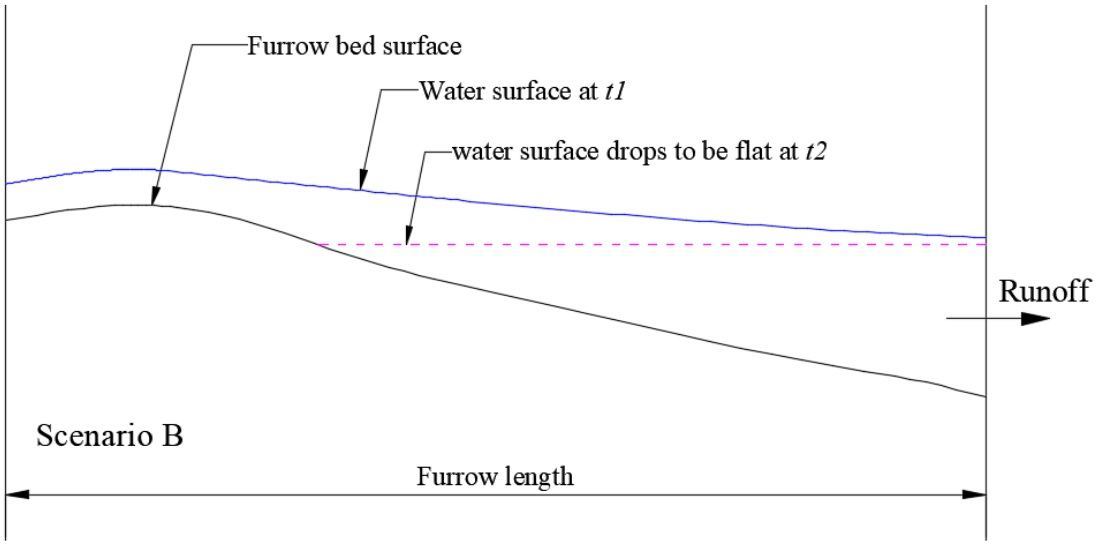

Figure 8.19 Runoff processes simulated when the temporarily blocked calculation (TBC) is used.

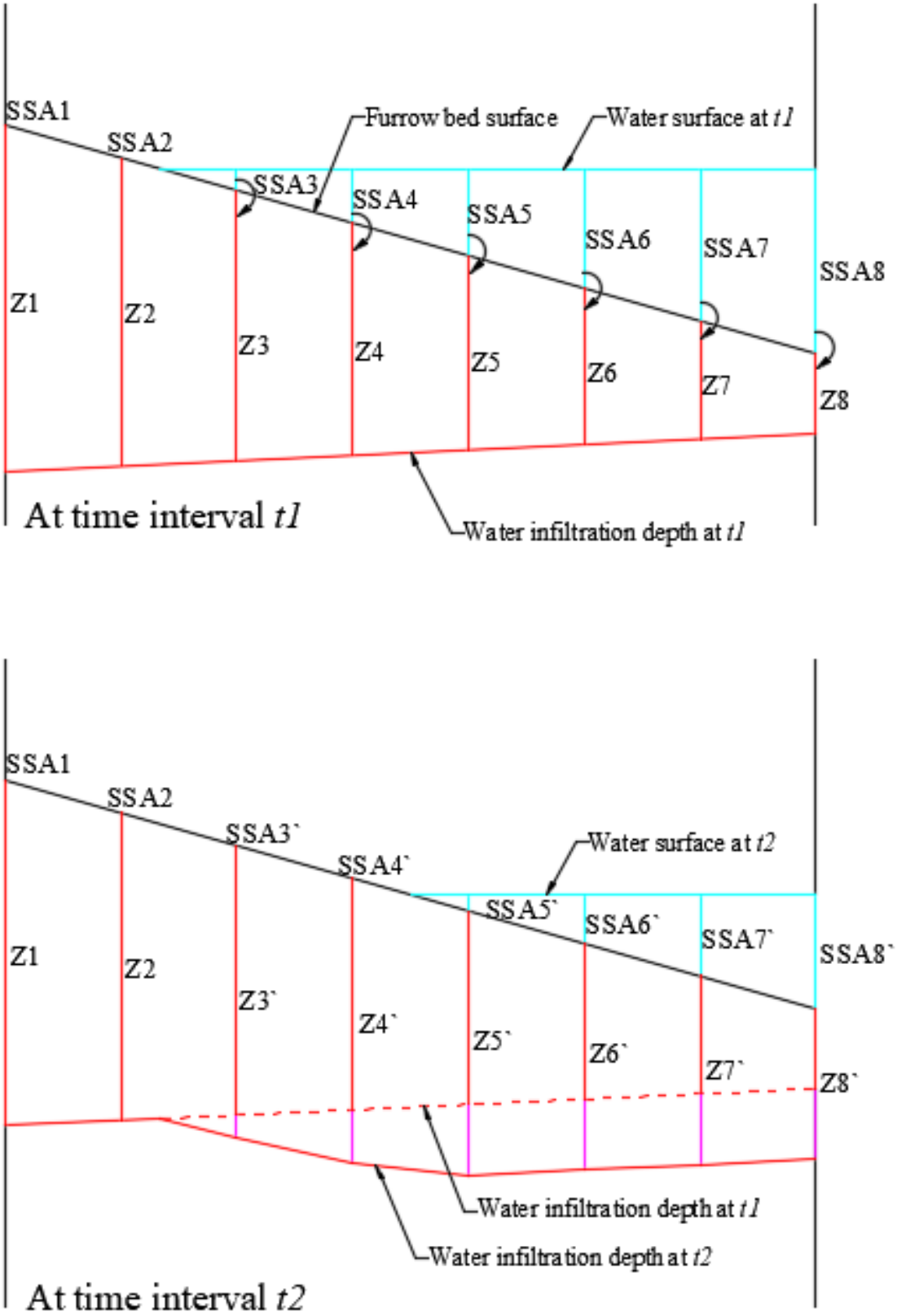

Figure 8.20 Infiltration process during the temporarily blocked calculation (TBC).

For a furrow located in Border 1 of Field 2, the runoff calculation will commence when the bottom check gate (located between the two borders bottom of the Field 2) is opened, and will finish when most of the water disappears from the furrow surface, by either flowing through the bottom check gate (runoff), or by infiltrating into the soil. For a furrow located in Border 2 of Field 2, the calculation will commence when the tail drain box is opened.

The TBC commences when runoff starts or when the SISCO simulation model reaches "Lateral Flow Regime" (which-ever occurs first).

In SISCO, the phrase "Lateral Flow Regime" means that the furrow flow velocity is very small and the infiltration is very low; therefore the simulation process ceases, to avoid convergence issues. Theoretically, with the 'Lateral Flow Regime simulation process, the entire water volume needs a very long time to be infiltrated into the soil profile.

If the SISCO simulation model reaches the "Lateral Flow Regime" condition before simulated runoff commences (by opening the bottom check gate or the tail drain box), the TBC will only involve calculation of infiltration for the period until runoff commences. This condition occurs in Furrow 20 where the simulation model reached the "Lateral Flow Regime" only four minutes before commencing runoff. Then both parts of the TBC (Infiltration and Runoff) were applied consecutively from the opening of the bottom check gate until all of the water disappeared from the furrow surface by draining or infiltrating. Selecting the "Blocked" downstream condition for the furrow is appropriate for simulation of real irrigation practice in this system, as it is initially blocked, but is then opened some later time, and the temporarily blocked calculation (TBC) is then most appropriate to simulate it.

Furrow 17 located in Border 1 of Field 2 will be used to explain the calculation steps. This furrow was selected because the results are close to the average, compared with the other furrows (see Section 8.8).

After simulation was completed, the CSV data files were exported from the plots on the "Animation with Slope" and "Animation Page" tabs of the SISCO model (Figure 8.16 and Figure 8.17Figure 8.17) at a time corresponding to the opening time of the

bottom check gate (240 minutes); the "Advance" tab data (Figure 8.18) can be exported at any time of the simulation. This point in the simulation time (240 minutes) calculated is based on the difference between the time were water commenced entry to the furrow (6:25 AM) and the opening time of the bottom check gate (10:25 AM). In this case the files were exported at 241 minutes, as this was the closest available simulated time step to the gate opening time. Once the bottom check gate is opened, the augmented infiltration along the furrow is estimated based on a combination of the TBC for runoff and infiltration in that furrow, as previously shown in Figure 8.19 and Figure 8.20, respectively. The infiltrated volume is estimated based on the calibrated infiltration parameters *a* and *k* for Furrow 17 (Table 8.5).

For the TBCs it was decided that a time step of 10 minutes would be both adequate and convenient to complete the runoff calculations.

As shown in Figure 8.19, there are two potential Scenarios (A and B) to estimate the redistribution of surface water storage along the furrow at each time interval after subtracting the runoff (or outflow) volume. The first scenario (A) assumes that water surface drops by the same amount along the furrow during each time step, while the second scenario (B) assumes that water surface along the furrow drops to be flat. In fact, the reality of redistribution water after running off or draining certain volume of water is neither in scenario (A) nor (B). In reality, the water flows and redistributes in a manner between these two scenarios, where the water takes some time to flow from point to another. Scenario A assumes a stagnant condition which is not true because water is flowing due to the presence of the field slope. Whilst in Scenario B it is assumed that water migrates towards the downstream end of the furrow in a manner which could not match the real flow velocity and the real micro-topography of the furrow, as water could accumulate in small separated ponds. In both scenarios the water runoff volume is the same but there is a difference present in the water distribution along the furrow. This difference impacts on the infiltration calculation through both the amount and the uniformity of the infiltrated depths along the furrow. An example of each scenario will be explained in Sections 8.5 and 8.6.

After completing the runoff calculation for the current time step, an infiltration calculation (Figure 8.20) is implemented based on the new distribution of the surface water storage areas (SSAs) along the furrow as a result of the runoff calculation. Using

the calibrated infiltration parameters *a* and *k* obtained from the SISCO model, the infiltrated depth can be estimated for each adopted time interval (10 minutes) as an increment of time of the total infiltration opportunity time. As shown in Figure 8.20, there are three possible cases of infiltrated depths that can be added to the previous accumulated depths of infiltration. The first case, when there is no infiltration, occurs because there is no water on the furrow surface as shown in Figure 8.20 at positions SSA1 and SSA2. In the second case, the infiltrated depth is limited to the surface storage area where the soil infiltration capacity is higher than the water available on the furrow surface, as shown at positions SSA3 and SSA4. For the third case, where there is a sufficient amount of the surface storage area on the furrow surface, the infiltrated depth is governed by the infiltration function during the interval times, as shown at positions SSA5, SSA6, SSA7 and SSA8 in Figure 8.20.

The runoff and infiltration calculations are repeated at ten minute time intervals until the water disappears from the furrow surface, or when the runoff logged via the Starflow at the bottom check gate ceases.

In the runoff calculations, the runoff volume from each furrow was calculated based on the flow rates that were logged by the Starflow through the bottom check gate, divided by the number of the furrows in the first border for the flow duration. However, in reality, there is actually a variance in the amount of runoff from each furrow, as some furrows contain large amounts of the surface water storage, such as the WFs, while the other furrows contain only small amounts of the surface water storage. In this situation the final estimated volume obtained from runoff calculations in individual furrows may not match the real volumes logged by the Starflow. Therefore, to reduce the possible errors, scaling of the runoff flow rates logged by the Starflow were completed according to the surface storage volume (SSV) ratio, represented by the surface storage volume (SSV) of each furrow divided by the average of the SSVs of the observed twelve adjoining furrows. These SSVs are obtained from SISCO before commencing the runoff and infiltration calculations, at 240 minutes in the adopted example.

The final volume balance can be calculated by adding the augmented infiltrated volume obtained from these calculations, to the last infiltrated volume before commencing these calculations. The final runoff volume is computed based on the

difference between the initial surface storage volume and the augmented infiltrated volume obtained from these calculations, or by accumulating the runoff volumes of the runoff calculations.

Then the performance indices RE and AE can be calculated based on the final estimated components of the volume balance, while the DU is calculated based on the final distribution of the infiltrated depths along the furrow.

8.5. Example of TBC technique developed - Runoff Calculations - Scenario A

This section will detail the volume balance procedure introduced above, for Scenario A, where water levels drop at a constant rate along the length of the field.

Table 8.11 shows the required inputs, and calculation procedure for the runoff calculation assuming that all water depth drops by the same amount along the furrow (Figure 8.19, Scenario A) in Furrow 17 of Border 1 in Field 2 for the irrigation event on the 10-02-2018 from ten minutes after the bottom check gate is opened (in the period from 240 to 250 minutes). The furrow distance intervals (Column 1), the SSA (Column 2), and the adjusted runoff volume per furrow (Column 3) are the required inputs to implement the runoff calculations (Scenario A). The SSA (Column 2) is exported from the SISCO model (Figure 8.17) at the time corresponding to the opening of the check gate so as to implement the first run of the runoff calculations, as shown in this calculation example. For the next time interval and subsequent time steps, the SSA is obtained from the infiltration calculation (Section 8.7) of the previous time interval.

The adjusted runoff volume per furrow (Column 3) is obtained from the real Starflow measurements at the bottom check gate (Table A-4 and Table A-5 in Appendix A) at a specific time, divided by the number of the furrows (312) in Border 1, and multiplied by the SSV ratio of that furrow as shown in Table 8.12. For convenience, the runoff calculation is repeated every ten minutes, but the Starflow was configured to log data every five minutes. So, the adjusted runoff volume per furrow used is the summation of the measured runoff volume during ten minutes. The runoff volume in this case was based on the average of the measurements of the two Starflows (with serial numbers

1645 and 1900, see Table A-4 and Table A-5 in Appendix A) mounted at the bottom check gate.

As explained in Section 8.4, the SSV ratio was used to adjust the runoff volume per furrow according to the amount of water stored in each furrow.

Table 8.13 shows the calculation of the SSV ratio for all furrows at the opening time of the bottom check gate (240 minutes) for the irrigation event conducted on the 10-02-2018. For this example, the SSV ratio of Furrow 17 is (23.9266/43.2266 = 0.553516). As a result, the adjusted runoff volume flowing through the bottom check gate between 240 and 250 minutes is 2.45048 m^3 × 0.553516 = 1.356379 m^3.

Column 4 of Table 8.11, the SSV, is computed using Equation 8.15, and represents the volume of surface storage between the next, and previous distances.

$$SSV = (Next\ distance - Previous\ distance) \times (Next\ SSA + Previous\ SSA)/2 \quad 8.15$$

For example, substituting the distance intervals 45.173 and 58.487 m and their corresponding SSAs, 0.000214 and 0.000555 m^2 respectively, into Equation 8.15, yields the SSV as shown below:

SSV = (58.487 – 45.173) * (0.000214 + 0.000555)/2 = 0.005118 m^3

The total SSV over this whole furrow length is found by computing the summation of the SSVs (23.9266 m^3).

The remaining SSV on the whole furrow surface of the end of the time interval (Column 5) is computed by subtracting the adjusted runoff volume per furrow (Column 3) from the summation of the previous SSV (Column 4), as shown below:

Remaining SSV = 23.9266 – 1.356379 = 22.5703 m^3.

Table 8.11 Temporarily blocked calculation (TBC) of runoff for Scenario A (water level dropping at a constant rate) for Furrow 17 in Border 1 of Field 2, for the irrigation event conducted on the 10-02-2018 between the time 240 and 250 minutes.

Furrow distance (m) (1)	SSA exported from SISCO or last infiltration calc. (m^2) (2)	Adjusted runoff volume per furrow (m^3) (3)	SSV at 240 min. (m^3) (4)	Remaining SSV at 250 min. (m^3) (5)	Depth of flow (*y*) at 240 min. (m) (6)	Estimated depth drop (m)(7)	Depth of flow after subtracting drop at 250 min. *y* (m) (8)	New SSA at 250 min. (m^2) (9)	New SSV at 250 min. (m^3) (10)
		1.356379	**Σ 23.9266**	**Σ 22.5703**					**Σ 22.5703**
0.0	0.000000				0.000000	0.005280	-0.005280	0.000000	
4.308	0.000000		0.000000		0.000000	0.005280	-0.005280	0.000000	0.000000
10.158	0.000000		0.000000		0.000000	0.005280	-0.005280	0.000000	0.000000
19.048	0.000000		0.000000		0.000000	0.005280	-0.005280	0.000000	0.000000
29.670	0.000000		0.000000		0.000000	0.005280	-0.005280	0.000000	0.000000
45.173	0.000214		0.001659		0.003000	0.005280	-0.002280	0.000000	0.000000
58.487	0.000555		0.005118		0.006400	0.005280	0.001120	0.000068	0.000450
71.350	0.000905		0.009390		0.009200	0.005280	0.003920	0.000297	0.002342
84.046	0.001267		0.013791		0.011800	0.005280	0.006520	0.000568	0.005489
96.471	0.001698		0.018420		0.014500	0.005280	0.009220	0.000901	0.009128
108.640	0.002335		0.024535		0.018100	0.005280	0.012820	0.001419	0.014118
120.607	0.003375		0.034161		0.023400	0.005280	0.018120	0.002320	0.022374
132.400	0.004939		0.049021		0.030200	0.005280	0.024920	0.003698	0.035486
144.033	0.006729		0.067865		0.037000	0.005280	0.031720	0.005306	0.052369
155.465	0.008009		0.084232		0.041500	0.005280	0.036220	0.006488	0.067408
166.533	0.008690		0.092414		0.043800	0.005280	0.038520	0.007128	0.075357
177.204	0.009303		0.096002		0.045700	0.005280	0.040420	0.007674	0.078976
187.657	0.009860		0.100163		0.047500	0.005280	0.042220	0.008206	0.082999
197.965	0.010363		0.104224		0.049000	0.005280	0.043720	0.008660	0.086921
208.139	0.010807		0.107693		0.050400	0.005280	0.045120	0.009092	0.090306
218.195	0.011189		0.110594		0.051500	0.005280	0.046220	0.009437	0.093165
228.149	0.011501		0.112915		0.052400	0.005280	0.047120	0.009724	0.095356
238.009	0.011732		0.114542		0.053100	0.005280	0.047820	0.009949	0.096991
247.785	0.011865		0.115339		0.053500	0.005280	0.048220	0.010078	0.097892
257.484	0.011873		0.115110		0.053500	0.005280	0.048220	0.010078	0.097745
267.111	0.011912		0.114488		0.053600	0.005280	0.048320	0.010111	0.097180
276.702	0.012189		0.115575		0.054400	0.005280	0.049120	0.010372	0.098226
286.331	0.012557		0.119131		0.055500	0.005280	0.050220	0.010736	0.101617

Furrow distance (m) (1)	SSA exported from SISCO or last infiltration calc. (m^2) (2)	Adjusted runoff volume per furrow (m^3) (3)	SSV at 240 min. (m^3) (4)	Remaining SSV at 250 min. (m^3) (5)	Depth of flow (y) at 240 min. (m) (6)	Estimated depth drop (m)(7)	Depth of flow after subtracting drop at 250 min. y (m) (8)	New SSA at 250 min. (m^2) (9)	New SSV at 250 min. (m^3) (10)
295.978	0.012923		0.122905		0.056500	0.005280	0.051220	0.011071	0.105187
305.608	0.013295		0.126231		0.057500	0.005280	0.052220	0.011410	0.108237
315.212	0.013687		0.129563		0.058600	0.005280	0.053320	0.011787	0.111388
324.788	0.014122		0.133156		0.059800	0.005280	0.054520	0.012204	0.114876
334.334	0.014722		0.137680		0.061400	0.005280	0.056120	0.012770	0.119210
343.861	0.015616		0.144513		0.063700	0.005280	0.058420	0.013601	0.125617
353.393	0.016764		0.154313		0.066700	0.005280	0.061420	0.014716	0.134949
362.915	0.018156		0.166251		0.070100	0.005280	0.064820	0.016021	0.146336
372.413	0.019794		0.180228		0.074000	0.005280	0.068720	0.017573	0.159541
381.885	0.021663		0.196333		0.078300	0.005280	0.073020	0.019350	0.174863
391.329	0.023741		0.214408		0.083000	0.005280	0.077720	0.021371	0.192295
400.745	0.026005		0.234203		0.087800	0.005280	0.082520	0.023518	0.211336
410.132	0.028431		0.255489		0.092800	0.005280	0.087520	0.025842	0.231665
419.489	0.031024		0.278174		0.098000	0.005280	0.092720	0.028352	0.253557
428.820	0.034196		0.304276		0.104100	0.005280	0.098820	0.031416	0.278836
438.170	0.038122		0.338119		0.111300	0.005280	0.106020	0.035195	0.311433
447.617	0.042284		0.379795		0.118700	0.005280	0.113420	0.039260	0.351683
457.074	0.046637		0.420463		0.126000	0.005280	0.120720	0.043445	0.391069
466.515	0.051159		0.461616		0.133400	0.005280	0.128120	0.047863	0.430992
475.938	0.055843		0.504160		0.140800	0.005280	0.135520	0.052455	0.472668
485.342	0.062394		0.555951		0.150600	0.005280	0.145320	0.058800	0.523120
494.840	0.074202		0.648704		0.167400	0.005280	0.162120	0.070357	0.613371
504.782	0.090906		0.820760		0.189400	0.005280	0.184120	0.086758	0.781027
515.061	0.109547		1.030205		0.212000	0.005280	0.206720	0.105055	0.985804
525.233	0.129325		1.214881		0.234300	0.005280	0.229020	0.124503	1.167511
535.316	0.150190		1.409242		0.256300	0.005280	0.251020	0.145009	1.358808
545.382	0.172227		1.622693		0.278300	0.005280	0.273020	0.166793	1.569267
555.429	0.195388		1.846612		0.300100	0.005280	0.294820	0.189611	1.790297
565.442	0.219603		2.077855		0.321800	0.005280	0.316520	0.213517	2.018455
575.424	0.244833		2.317983		0.343400	0.005280	0.338120	0.238472	2.255856
585.377	0.265316		2.538588		0.360300	0.005280	0.355020	0.258789	2.474454
590.0	0.268903		1.234914		0.363200	0.005280	0.357920	0.262345	1.204667

Table 8.12 A sample of the calculation used to obtain the adjusted runoff volume per furrow from two the Starflows between 240 and 250 minutes in Furrow 17 of Border 1 in Field 2 for the irrigation event conducted on the 10-02-2018.

Time	Time, min.	Remarks	Runoff volume obtained from Starflow measurements (m^3)		Average of the runoff volume obtained from two Starflows (m^3)	Runoff volume per furrow (m^3)	Adjusted volume per furrow (m^3) (SSV ratio =0.553516)
			SN 1645	SN1900			
10:25 AM	240	Open bottom check	-	-	-	-	-
10:30 AM	245	-	470.4682	230.4973	350.4827	1.12334	0.621787
10:35 AM	250	-	462.0077	366.1263	414.0670	1.32714	0.7345
						Σ2.45048	**Σ 1.356379**

Table 8.13 The calculation of the SSV ratio for all furrows at the opening time of the bottom check gate at 240 minutes, for the irrigation event conducted on the 10-02-2018.

Furrow no.	Closest available time on SISCO model of the opening bottom check gate from 240 min. (min.)	SSV at opening bottom check gate after 240 min. (m^3)	SSV ratio
13	241.00	46.7437	1.081365
14	241.02	28.2535	0.653614
15	241.02	17.7648	0.410969
16	241.00	41.8524	0.968210
17	241.00	23.9266	0.553516
18	241.02	85.3477	1.974426
19	241.00	46.8931	1.084821
20	241.00	103.1876	2.387133
21	239.58	52.8586	1.222826
22	241.00	36.2466	0.838526
23	241.00	21.7899	0.504086
24	241.00	13.8545	0.320509
		Σ 43.2266	

To find the new water depths along the whole furrow length (Column 8) an estimate of the drop in the water depth (Column 7) that occurred due to run-off is required (Column 3). The new water depths along the whole furrow length (Column 8) are calculated by subtracting this drop in water depth (Column 7) from the previous water depth (Column 6). The new water depths (Column 8) represent the new distribution of

the remaining SSV (Column 5) along the furrow length. Based on these new water depths (Column 8), the new SSA (Column 9) can be calculated. Then based on the new SSAs (Column 9) and their corresponding distances intervals (Column 1), the new SSVs can be calculated. The summation of the new SSVs along whole furrow length is then compared with the remaining SSV (22.5703 m^3, Column 5) where each should have the same volume (22.5703 m^3, Column 10). The exact value of the assumed drop in the water depth is obtained when the difference between the summation of the remaining SSVs and the summation of the new SSVs equals zero. The following will illustrate the steps explained above.

The depth of flow, *y*, (Column 6) at each distance interval can be calculated using the following formula:

$$SSA = W_B\, y + \frac{c\, y^{m+1}}{m+1} \qquad 8.16$$

where:

SSA is the surface storage area (Column 2), m^2,

W_B is the bottom width of the furrow, m, and

y is the flow depth in the furrow, m.

The geometry factors of the furrow shape, *c* and *m*, are obtained from the IPARM model (for convenience) for the specific dimensions of Furrow 17 (top width, middle width, bottom width and maximum height, which have the following values 0.78, 0.491, 0.05 and 0.185, respectively) to give *c*= 2.48986, *m*= 0.72712. The VLOOKUP function in Microsoft Excel was used to solve *y* efficiently (depth of flow, Column 6) for each SSA (Column 2).

The new water depth *y* (Column 8) can be found using the following equation:

$$y_{new} = y - Drop \qquad 8.17$$

where:

y_{new} is the new depth of flow (Column 8), in metres,

y is the previous depth of the flow before implementing the runoff calculation (Column 6), in metres, and

Drop is the estimated water depth drop in metres

For example, y_{new} at the distance interval 58.487 m (Column 1) is:

$y_{new} = 0.006400 - 0.005280 = 0.001120$ m.

Here, the depth drop of 0.005280 m is the solved value for the drop at this time step. Then, the new SSA (Column 9) can be calculated using Equation 8.16. For example, the new SSA at the distance of 58.487 m is:

$SSA_{new} = (0.05 * 0.001120) + (2.48986*(0.001120)^{0.72712+1}) / (0.72712 +1) = 0.000068$ m^2

If the y_{new} has a negative value, then the new SSA is equal to zero.

The new SSV (Column 10) can be calculated using Equation 8.15.

For example, substituting the interval distances 45.173 and 58.487 m and their corresponding SSAs, 0.0 and 0.000068 m^2, respectively, into Equation 8.15, yields the new SSV for this distance interval as shown below:

$SSV_{new} = (58.487 - 45.173) \times (0.000068 + 0.0)/2 = 0.00045$ m^3

Finally, summing the values of SSV_{new} across the length of the furrow gives the new total SSV of 22.5703 m^3.

The exact value of the assumed drop in water depth is obtained when the difference between the summation of the remaining SSV and the summation of the new SSV based on the calculated depths is equal to zero. Using the trial and error method, the depth drop can be estimated by assuming a random value that meets the equality between the remains SSV and the new SSV. The exact depth drop for each time interval was computed using the Solver tool in Microsoft Excel by setting the difference between the summation of the remaining SSV and the summation of the new SSV, as a minimum objective, and by changing the depth drop value.

Table 8.14 shows the main steps to estimate the depth drop using the measured runoff flowing from the bottom check gate at time 250 minutes.

This calculation procedure is repeated for each furrow until all water disappears from the furrow surface by run-off or infiltration in the furrow. Then, the performance indices can be computed.

Table 8.14 Main steps to estimate the drop depth using measured runoff from the bottom check gate at time 250 minutes.

Item	Value	Remarks
Summation of Previous SSV, m^3	23.9266	Obtained by compute the summation of the all SSVs at all distance intervals along the furrow length and their corresponding SSAs using the Equation 8.15 at the time 240 minutes.
Runoff volume obtained from Starflow at 250 minutes, m^3	1.12334 + 1.32714 = (2.450480)	Obtained by divided the flow volume passed through the bottom check gate at time from 240 to 250 minutes by the number of furrows at that border (1).
Adjusted runoff or flow out volume logged via Starflow, m^3	1.356379	Obtained by multiply 2.450480 by the SSV ratio (0. 553516) obtained from Table 8.13.
Summation of remains SSV, m^3	22.5703	Obtained by subtract the adjusted flow volume (1.356379) from the Summation of the previous SSV (23.926648).
Estimated depth drop, m	0.00528	Subtract this drop from the previous flow depths at each distances interval to obtain new flow depths.
Summation of new computed SSV, m^3	22.5703	Firstly Compute SSA at each distance intervals based on the new flow depths using the Equation 8.16, then compute SSV at each distance intervals based on the computed SSA and distances intervals Equation 8.15.
Difference between the summation of remaining SSV and the summation of the new computed SSV, m^3	0.0000	Set objective to be minimum using Solver tool in Microsoft excel

8.6. Example of the developed TBC technique- Runoff Calculations - Scenario B

In a similar manner to Section 8.5, this section will document the process of the developed volume balance procedure, TBC, according to Scenario B where water levels are maintained at a common horizontal level across the length of the field.

Table 8.15 shows the required inputs, and calculation results for runoff in Furrow 17 of Border 1 in Field 2 for the irrigation event conducted on the 10-02-2018 ten minutes after the bottom check gate is opened (period from 240 to 250 minutes), using the assumption that the water surface along the furrow drops to have the same level (Figure 8.19, Scenario B),. The furrow distance interval (Column 1), the furrow reduced level (Column 2), the SSA (Column 3), and the adjusted runoff volume per furrow (Column 4) are required inputs for the runoff calculations (Scenario B). The adjusted runoff volume per furrow (Column 4) is obtained from the Starflow measurements at the bottom check gate (Table A-4 and Table A-5 in Appendix A) at the specific time, divided by the number of furrows (312) in Border 1 (Table 8.12), and multiplied by the SSV ratio for each furrow (Table 8.13), as explained in Section 8.5.

In Table 8.15, the SSA (Column 3) is exported from the SISCO model (Figure 8.17) at the check gate opening time to implement the first step of the runoff calculation shown in this table. For the next time intervals, the SSA (Column 3) is obtained from the last infiltration calculation (Section 8.7) of the previous time interval.

Based on the SSA (Column 3) and their corresponding distance intervals (Column 1), the SSV (Column 5) is computed using Equation 8.15. The total SSV over the field length is found by computing the summation of the SSVs (23.9266 m^3).

The remaining SSV on the furrow surface (Column 6) is computed by subtracting the adjusted runoff volume per furrow (Column 4) from the previous SSV (Column 5), as shown below:

Remaining SSV = 23.9266 – 1.356379 = 22.5703 m^3.

Table 8.15 Temporarily blocked calculation (TBC) for runoff using scenario B, (water drop to a flat water surface level) for Furrow 17 located in Border 1 of Field 2 for the irrigation event conducted on the 10-02-2018 at the time 250 minutes.

Furrow distance, (m) (1)	Furrow reduced level (m) (2)	SSA exported from SISCO, or from last Infiltration calc. (m^2) (3)	Adjusted runoff volume per furrow (Starflow) (m^3) (4)	SSV (m^3) (5)	Remaining SSV, (m^3) (6)	Estimated flat water level, (m) (7)	New water depth, (m) (8)	New SSA, (m^2) (9)	New SSV (m^3) (10)	Depth of flow (y) – Vlookup, (m) (11)	Water level (water depth + reduced level), (m) (12)
			1.356379	**Σ 23.9266**	**Σ 22.5703**				**Σ 22.5703**		
0.0	0.0	0.0				-0.126426	-0.126426	0.0		0.0	0.0
4.308	0.001833	0.0		0.0		-0.126426	-0.128259	0.0	0.0	0.0	0.001833
10.158	0.004323	0.0		0.0		-0.126426	-0.130748	0.0	0.0	0.0	0.004323
19.048	0.004439	0.0		0.0		-0.126426	-0.130864	0.0	0.0	0.0	0.004439
29.670	-0.003018	0.0		0.0		-0.126426	-0.123408	0.0	0.0	0.0	-0.003018
45.173	-0.016140	0.000214		0.001659		-0.126426	-0.110285	0.0	0.0	0.003000	-0.013140
58.487	-0.027402	0.000555		0.005118		-0.126426	-0.099024	0.0	0.0	0.006400	-0.021002
71.350	-0.038189	0.000905		0.009390		-0.126426	-0.088237	0.0	0.0	0.009200	-0.028989
84.046	-0.048717	0.001267		0.013791		-0.126426	-0.077709	0.0	0.0	0.011800	-0.036917
96.471	-0.059020	0.001698		0.018420		-0.126426	-0.067406	0.0	0.0	0.014500	-0.044520
108.640	-0.069110	0.002335		0.024535		-0.126426	-0.057315	0.0	0.0	0.018100	-0.051010
120.607	-0.079034	0.003375		0.034161		-0.126426	-0.047392	0.0	0.0	0.023400	-0.055634
132.400	-0.088813	0.004939		0.049021		-0.126426	-0.037613	0.0	0.0	0.030200	-0.058613
144.033	-0.097666	0.006729		0.067865		-0.126426	-0.028759	0.0	0.0	0.037000	-0.060666
155.465	-0.103752	0.008009		0.084232		-0.126426	-0.022673	0.0	0.0	0.041500	-0.062252
166.533	-0.107546	0.008690		0.092414		-0.126426	-0.018879	0.0	0.0	0.043800	-0.063746
177.204	-0.111204	0.009303		0.096002		-0.126426	-0.015222	0.0	0.0	0.045700	-0.065504
187.657	-0.114787	0.009860		0.100163		-0.126426	-0.011639	0.0	0.0	0.047500	-0.067287
197.965	-0.118320	0.010363		0.104224		-0.126426	-0.008106	0.0	0.0	0.049000	-0.069320
208.139	-0.121807	0.010807		0.107693		-0.126426	-0.004619	0.0	0.0	0.050400	-0.071407
218.195	-0.125254	0.011189		0.110594		-0.126426	-0.001172	0.0	0.0	0.051500	-0.073754
228.149	-0.128665	0.011501		0.112915		-0.126426	0.002240	0.000150	0.000747	0.052400	-0.076265
238.009	-0.132045	0.011732		0.114542		-0.126426	0.005619	0.000468	0.003049	0.053100	-0.078945
247.785	-0.135396	0.011865		0.115339		-0.126426	0.008970	0.000868	0.006533	0.053500	-0.081896
257.484	-0.138720	0.011873		0.115110		-0.126426	0.012295	0.001338	0.010701	0.053500	-0.085220
267.111	-0.142467	0.011912		0.114488		-0.126426	0.016041	0.001948	0.015818	0.053600	-0.088867
276.702	-0.147073	0.012189		0.115575		-0.126426	0.020647	0.002804	0.022788	0.054400	-0.092673
286.331	-0.152006	0.012557		0.119131		-0.126426	0.025580	0.003844	0.032006	0.055500	-0.096506

Furrow distance, (m) (1)	Furrow reduced level (m) (2)	SSA exported from SISCO, or from last Infiltration calc.(m^2) (3)	Adjusted runoff volume per furrow (Starflow) (m^3) (4)	SSV (m^3) (5)	Remaining SSV, (m^3) (6)	Estimated flat water level, (m) (7)	New water depth, (m) (8)	New SSA, (m^2) (9)	New SSV (m^3) (10)	Depth of flow (y) – Vlookup, (m) (11)	Water level (water depth + reduced level), (m) (12)
295.978	-0.156948	0.012923		0.122905		-0.126426	0.030522	0.005006	0.042692	0.056500	-0.100448
305.608	-0.161881	0.013295		0.126231		-0.126426	0.035456	0.006281	0.054345	0.057500	-0.104381
315.212	-0.166801	0.013687		0.129563		-0.126426	0.040376	0.007661	0.066947	0.058600	-0.108201
324.788	-0.171707	0.014122		0.133156		-0.126426	0.045282	0.009142	0.080457	0.059800	-0.111907
334.334	-0.176788	0.014722		0.137680		-0.126426	0.050363	0.010783	0.095108	0.061400	-0.115388
343.861	-0.182199	0.015616		0.144513		-0.126426	0.055773	0.012646	0.111605	0.063700	-0.118499
353.393	-0.187693	0.016764		0.154313		-0.126426	0.061268	0.014658	0.130126	0.066700	-0.120993
362.915	-0.193183	0.018156		0.166251		-0.126426	0.066757	0.016784	0.149696	0.070100	-0.123083
372.413	-0.198658	0.019794		0.180228		-0.126426	0.072232	0.019020	0.170035	0.074000	-0.124658
381.885	-0.204118	0.021663		0.196333		-0.126426	0.077692	0.021359	0.191226	0.078300	-0.125818
391.329	-0.209563	0.023741		0.214408		-0.126426	0.083137	0.023800	0.213248	0.083000	-0.126563
400.745	-0.214991	0.026005		0.234203		-0.126426	0.088565	0.026339	0.236048	0.087800	-0.127191
410.132	-0.220402	0.028431		0.255489		-0.126426	0.093976	0.028972	0.259594	0.092800	-0.127602
419.489	-0.225840	0.031024		0.278174		-0.126426	0.099415	0.031721	0.283967	0.098000	-0.127840
428.820	-0.232066	0.034196		0.304276		-0.126426	0.105641	0.034991	0.311234	0.104100	-0.127966
438.170	-0.239415	0.038122		0.338119		-0.126426	0.112989	0.039018	0.346022	0.111300	-0.128115
447.617	-0.246839	0.042284		0.379795		-0.126426	0.120413	0.043265	0.388661	0.118700	-0.128139
457.074	-0.254271	0.046637		0.420463		-0.126426	0.127845	0.047696	0.430109	0.126000	-0.128271
466.515	-0.261689	0.051159		0.461616		-0.126426	0.135264	0.052293	0.471965	0.133400	-0.128289
475.938	-0.269095	0.055843		0.504160		-0.126426	0.142669	0.057054	0.515206	0.140800	-0.128295
485.342	-0.278913	0.062394		0.555951		-0.126426	0.152487	0.063626	0.567435	0.150600	-0.128313
494.840	-0.295700	0.074202		0.648704		-0.126426	0.169274	0.075535	0.660880	0.167400	-0.128300
504.782	-0.318282	0.090906		0.820760		-0.126426	0.191856	0.092858	0.837088	0.189400	-0.128882
515.061	-0.341628	0.109547		1.030205		-0.126426	0.215203	0.112292	1.054344	0.212000	-0.129628
525.233	-0.364732	0.129325		1.214881		-0.126426	0.238306	0.133001	1.247533	0.234300	-0.130432
535.316	-0.387635	0.150190		1.409242		-0.126426	0.261210	0.154941	1.451725	0.256300	-0.131335
545.382	-0.410498	0.172227		1.622693		-0.126426	0.284073	0.178209	1.676713	0.278300	-0.132198
555.429	-0.433317	0.195388		1.846612		-0.126426	0.306892	0.202764	1.913715	0.300100	-0.133217
565.442	-0.456063	0.219603		2.077855		-0.126426	0.329637	0.228534	2.159502	0.321800	-0.134263
575.424	-0.478735	0.244833		2.317983		-0.126426	0.352309	0.255484	2.415712	0.343400	-0.135335
585.377	-0.496663	0.265316		2.538588		-0.126426	0.370237	0.277670	2.653064	0.360300	-0.136363
590.0	-0.499704	0.268903		1.234914		-0.126426	0.373278	0.281510	1.292616	0.363200	-0.136504

The calculations in Table 8.15 are based on the assumption that the water on the soil in the furrow will have a flat horizontal surface along the whole furrow length. The new water depths along the whole furrow length (Column 8) are found by subtracting the furrow reduced level (Column 2) from the estimated flat water level (Column 7). The new water depths (Column 8) represent the new distribution of the remaining SSV (Column 6) along the furrow length. Based on these new water depths (Column 8) and the furrow geometry, the new SSA (Column 9) can be calculated. Then based on the new SSAs (Column 9) and their corresponding distances intervals (Column 1), the new SSVs (Column 10) can be calculated. The summation of the new SSVs (Column 10) along whole furrow length are compared with the remaining SSV (Column 5), where it should have the same volume (Column 10). The exact value of the assumed drop in the water depth is obtained by minimising the difference between the summation of the remaining SSV and the summation of the new SSV. The following will provide an example of the steps explained above.

The new water depths (Column 8) along the furrow, can be found using the following equation:

$$y_{new} = WL_{estimated} - RL \qquad 8.18$$

where:

y_{new} is the new depth of the flow in metres,

$WL_{.estimated}$ is the estimated flat water level in metres, and

RL is the furrow reduced level in metres.

For example, the y_{new} at the distance interval equals to 228.149 m (Column 1) is:

y_{new} = -0.126426 – (-0.128665) = 0.00224 m.

Here, the water level is assumed to be -0.126426 m which is actually the final value of the water level at this time step.

Based on the new water depths (Column 8) along the furrow, the new SSA (Column 9) is computed using Equation 8.16.

For example, the new SSA at the distance interval 228.149 m is:

$SSA_{new} = (0.05 \times 0.00224) + (2.48986 \times (0.00224)^{0.72712+1}) / (0.72712 + 1) = 0.000150$ m^2

If the y_{new} is negative, then the new SSA is equal to zero.

Based on the new SSAs (Column 9) and their corresponding distances intervals, the new SSV (Column 10) is computed using Equation 8.15.

For example, substituting the distance intervals 228.149 and 218.195 m, and their corresponding SSAs, 0.00015 and 0.0 m^2, respectively, into Equation 8.15 yields the SSV as shown below:

$SSV = (228.149 - 218.195) \times (0.00015 + 0.0)/2 = 0.000747$ m^3

The new SSVs are assumed over the field length (22.5703 m^3, Column 10) and are compared with remaining SSV (22.5703 m^3), where the estimated flat water level when correct, should have the same volume. The exact water level for each time intervals is computed using the Solver tool in Microsoft Excel by setting the difference between the summation of the remaining SSV (Column 6) and the summation of the new SSV (Column 10), as a minimum objective. The exact value of the flat water level is obtained when the difference between the summation of remaining SSV and the summation of the new SSV is equal to zero.

Figure 8.21 illustrates the runoff calculation (Scenario B) using the current example data of Furrow 17 in Border 1 of Field 2 for the irrigation event conducted on the 10-02-2018, between the time 240 minutes (water level) and 250 minutes (estimated or new water level). Figure 8.21 shows the following components: the furrow reduced level (Column 2), the water level (Column 12), and the estimated water level (Column 7), as recorded in Table 8.15.

However, unlike reality, the runoff process according to Scenario B assumes that the water flows very quickly towards the downstream end of the furrow very quickly,

compared with the anticipated real situation. Also, this scenario ignores the possibility of water accumulating in small separated ponds due to the micro-topography of the furrow.

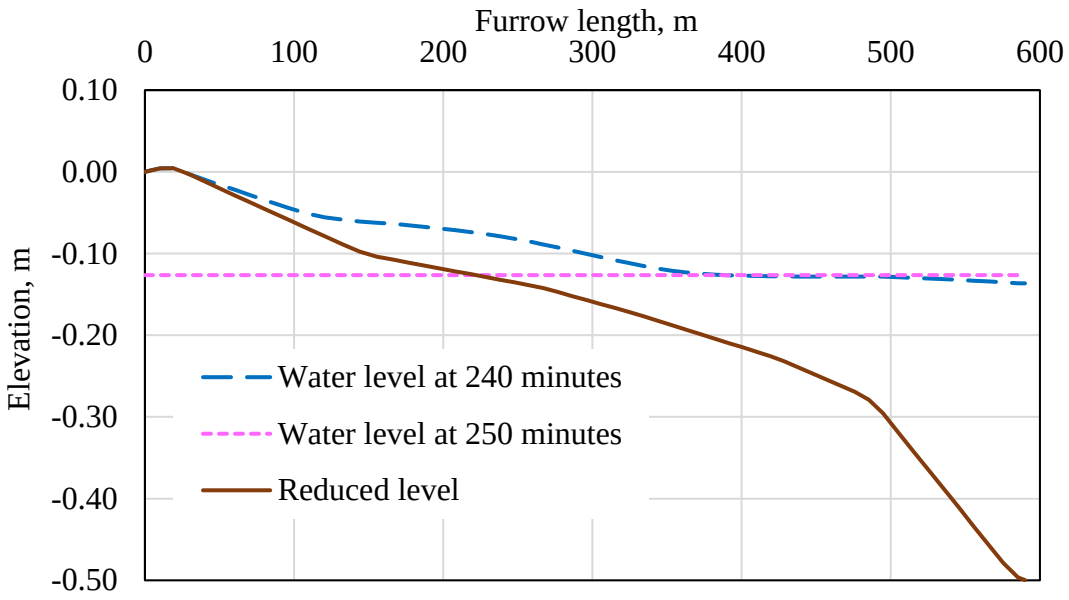

Figure 8.21 Calculation of the new water level at 250 minutes based on the water level at 240 minutes using Scenario B for Furrow 17 in Border 1 of Field 2 on the 10-02-2018.

8.7. Example of the developed TBC technique-Infiltration Calculations

As is known in reality, runoff and infiltration processes occur simultaneously. However, as was suggested earlier the runoff calculation will be implemented first for a specific time interval, and then the infiltration calculation will be implemented second, for the same specific time interval, based on the SSAs from that runoff calculation. Table 8.16 shows the TBC for infiltration in Furrow 17 of Border 1 in Field 2, for the irrigation event conducted on the 10-02-2018, between the time of 240 and 250 minutes. The furrow distance intervals (Column 1), the infiltration depth (Column 2), the SSA (Column 3), and the water front advance time (Column 4) are the required inputs to implement these infiltration calculations. The infiltration depth (Column 2) is exported from SISCO (Figure 8.17) at the opening of the check gate time to implement the first pass of the infiltration calculation as shown in this table. For the next time interval and so on, the infiltrated depth (Column 2) is obtained from

the TBCs for the previous time interval. The SSA (Column 3) is obtained from the runoff calculation for the same time interval. The water front advance time (Column 4) is obtained from the exported data set out of the SISCO model (Figure 8.18).

The fifth and sixth columns represent the infiltration opportunity time (IOT) at time 240 and 250 minutes, respectively. They are calculated by subtracting the water front advance time (Column 4) at each distance interval from the time elapsed since the start of the event (240 or 250 minutes).

For instance, the IOT at the time of 240 minutes and the distance 4.308 m is (240 – 0.1875 = 239.8125 minutes), while the IOT at the time 250 minutes and the distance 4.308 m is (250 – 0.1875 = 249.8125 minutes).

The potential infiltrated depth (Column 7) is calculated based on the infiltration parameters *a* and *k* obtained from the SISCO model, which are 0.18766 and 0.01983, respectively. For example, the potential infiltrated depth, Z_p, at the distance 4.308 m occurs from the IOT at the time 240 minutes to the IOT at the time 250 minutes is:

Potential infiltration depth, Z_p =

$(0.01983\times (249.8125)^{0.18766}) - (0.01983\times (239.8125)^{0.18766}) = 0.000427$ m.

The potential infiltrated depth represents the capacity of the soil to infiltrate water in a specific period, if there is a sufficient amount of water on the furrow surface (SSA, Column 3).

The actual infiltration depth (Column 8) is equal to the potential infiltration depth (Column 7) if the previous SSA (Column 3) is greater than or equal the potential infiltration depth (Column 7), otherwise it will be equal to the previous SSA (Column 3).

Table 8.16 TBC of the infiltration for Furrow 17 located in Border 1 of Field 2 for the irrigation event conducted on 10-02-2018 between the times 240 and 250 minutes.

Furrow distance, m (1)	Infiltration volume / meter length / furrow spacing, m (2)	SSA (obtained from runoff calculation for the same time interval), m^2 (3)*	Water front advance time, min. (4)	IOT at 240 min. (5)	IOT at 250 min. (6)	Potential Infiltration Depth (Z_p), m (7)	Actual Infiltration Depth, m (8)	Infiltration volume / meter length / furrow spacing, m (9)	SSA, m^2 (10)	Infiltration volume, m^3 (11)
										Σ 31.0332
0.0	0.055909	0.0	0.0	240.00	250.00	0.000427	0.0	0.055909	0.0	
4.308	0.055826	0.0	0.1875	239.8125	249.8125	0.000427	0.0	0.055826	0.0	0.240681
10.158	0.055548	0.0	0.8750	239.1250	249.1250	0.000428	0.0	0.055548	0.0	0.325762
19.048	0.055313	0.0	2.0625	237.9375	247.9375	0.000429	0.0	0.055313	0.0	0.492783
29.670	0.055349	0.0	3.7500	236.2500	246.2500	0.000432	0.0	0.055349	0.0	0.587742
45.173	0.055239	0.0	6.2500	233.7500	243.7500	0.000436	0.0	0.055239	0.0	0.857186
58.487	0.055128	0.000068	8.7500	231.2500	241.2500	0.000439	0.000068	0.055195	0.0	0.735150
71.350	0.055016	0.000297	11.2500	228.7500	238.7500	0.000443	0.000297	0.055313	0.0	0.710741
84.046	0.054903	0.000568	13.7500	226.2500	236.2500	0.000447	0.000447	0.055350	0.000121	0.702514
96.471	0.054789	0.000901	16.2500	223.7500	233.7500	0.000451	0.000451	0.055240	0.000450	0.687048
108.640	0.054674	0.001419	18.7500	221.2500	231.2500	0.000455	0.000455	0.055130	0.000964	0.671533
120.607	0.054559	0.002320	21.2500	218.7500	228.7500	0.000459	0.000459	0.055018	0.001861	0.659083
132.400	0.054442	0.003698	23.7500	216.2500	226.2500	0.000463	0.000463	0.054905	0.003235	0.648165
144.033	0.054323	0.005306	26.2500	213.7500	223.7500	0.000468	0.000468	0.054791	0.004838	0.638051
155.465	0.054204	0.006488	28.7500	211.2500	221.2500	0.000472	0.000472	0.054676	0.006016	0.625668
166.533	0.054084	0.007128	31.2500	208.7500	218.7500	0.000477	0.000477	0.054560	0.006651	0.604549
177.204	0.053962	0.007674	33.7500	206.2500	216.2500	0.000481	0.000481	0.054443	0.007193	0.581584
187.657	0.053839	0.008206	36.2500	203.7500	213.7500	0.000486	0.000486	0.054325	0.007720	0.568494
197.965	0.053715	0.008660	38.7500	201.2500	211.2500	0.000491	0.000491	0.054206	0.008169	0.559341
208.139	0.053590	0.009092	41.2500	198.7500	208.7500	0.000495	0.000495	0.054086	0.008596	0.550901
218.195	0.053464	0.009437	43.7500	196.2500	206.2500	0.000500	0.000500	0.053964	0.008937	0.543280
228.149	0.053336	0.009724	46.2500	193.7500	203.7500	0.000506	0.000506	0.053842	0.009218	0.536509
238.009	0.053207	0.009949	48.7500	191.2500	201.2500	0.000511	0.000511	0.053718	0.009438	0.530304
247.785	0.053076	0.010078	51.2500	188.7500	198.7500	0.000516	0.000516	0.053592	0.009562	0.524537
257.484	0.052944	0.010078	53.7500	186.2500	196.2500	0.000522	0.000522	0.053466	0.009557	0.519160
267.111	0.052811	0.010111	56.2500	183.7500	193.7500	0.000527	0.000527	0.053338	0.009583	0.514109
276.702	0.052676	0.010372	58.7500	181.2500	191.2500	0.000533	0.000533	0.053209	0.009839	0.510953
286.331	0.052540	0.010736	61.2500	178.7500	188.7500	0.000539	0.000539	0.053079	0.010197	0.511695
295.978	0.052402	0.011071	63.7500	176.2500	186.2500	0.000545	0.000545	0.052947	0.010526	0.511435

Furrow distance, m (1)	Infiltration volume / meter length / furrow spacing, m (2)	SSA (obtained from runoff calculation for the same time interval), m^2 (3)*	Water front advance time, min. (4)	IOT at 240 min. (5)	IOT at 250 min. (6)	Potential Infiltration Depth (Z_p), m (7)	Actual Infiltration Depth, m (8)	Infiltration volume / meter length / furrow spacing, m (9)	SSA, m^2 (10)	Infiltration volume, m^3 (11)
305.608	0.052262	0.011410	66.2500	173.7500	183.7500	0.000551	0.000551	0.052813	0.010858	0.509215
315.212	0.052121	0.011787	68.7500	171.2500	181.2500	0.000557	0.000557	0.052679	0.011230	0.506563
324.788	0.051978	0.012204	71.2500	168.7500	178.7500	0.000564	0.000564	0.052542	0.011641	0.503818
334.334	0.051834	0.012770	73.7500	166.2500	176.2500	0.000571	0.000571	0.052405	0.012199	0.500937
343.861	0.051688	0.013601	76.2500	163.7500	173.7500	0.000578	0.000578	0.052265	0.013023	0.498592
353.393	0.051539	0.014716	78.7500	161.2500	171.2500	0.000585	0.000585	0.052124	0.014131	0.497495
362.915	0.051390	0.016021	81.2500	158.7500	168.7500	0.000592	0.000592	0.051981	0.015429	0.495640
372.413	0.051238	0.017573	83.7500	156.2500	166.2500	0.000599	0.000599	0.051837	0.016974	0.493037
381.885	0.051084	0.019350	86.2500	153.7500	163.7500	0.000607	0.000607	0.051691	0.018744	0.490287
391.329	0.050928	0.021371	88.7500	151.2500	161.2500	0.000615	0.000615	0.051543	0.020757	0.487485
400.745	0.050770	0.023518	91.2500	148.7500	158.7500	0.000623	0.000623	0.051393	0.022895	0.484613
410.132	0.050610	0.025842	93.7500	146.2500	156.2500	0.000631	0.000631	0.051241	0.025211	0.481699
419.489	0.050447	0.028352	96.2500	143.7500	153.7500	0.000640	0.000640	0.051087	0.027712	0.478764
428.820	0.050283	0.031416	98.7500	141.2500	151.2500	0.000649	0.000649	0.050931	0.030767	0.475951
438.170	0.050116	0.035195	101.2500	138.7500	148.7500	0.000658	0.000658	0.050774	0.034537	0.475514
447.617	0.049946	0.039260	103.7500	136.2500	146.2500	0.000667	0.000667	0.050614	0.038592	0.478899
457.074	0.049774	0.043445	106.2500	133.7500	143.7500	0.000677	0.000677	0.050451	0.042768	0.477885
466.515	0.049600	0.047863	108.7500	131.2500	141.2500	0.000687	0.000687	0.050287	0.047176	0.475501
475.938	0.049422	0.052455	111.2500	128.7500	138.7500	0.000698	0.000698	0.050120	0.051758	0.473082
485.342	0.049242	0.058800	113.7500	126.2500	136.2500	0.000708	0.000708	0.049951	0.058091	0.470530
494.840	0.049059	0.070357	116.2500	123.7500	133.7500	0.000720	0.000720	0.049779	0.069638	0.473619
504.782	0.048873	0.086758	118.7500	121.2500	131.2500	0.000731	0.000731	0.049604	0.086027	0.494037
515.061	0.048684	0.105055	121.2500	118.7500	128.7500	0.000743	0.000743	0.049427	0.104312	0.508961
525.233	0.048492	0.124503	123.7500	116.2500	126.2500	0.000756	0.000756	0.049247	0.123747	0.501849
535.316	0.048296	0.145009	126.2500	113.7500	123.7500	0.000768	0.000768	0.049064	0.144240	0.495661
545.382	0.048097	0.166793	128.7500	111.2500	121.2500	0.000782	0.000782	0.048879	0.166011	0.492938
555.429	0.047894	0.189611	131.2500	108.7500	118.7500	0.000796	0.000796	0.048690	0.188815	0.490108
565.442	0.047687	0.213517	133.7500	106.2500	116.2500	0.000810	0.000810	0.048498	0.212706	0.486616
575.424	0.047477	0.238472	136.2500	103.7500	113.7500	0.000825	0.000825	0.048302	0.237646	0.483124
585.377	0.047262	0.258789	138.7500	101.2500	111.2500	0.000841	0.000841	0.048103	0.257948	0.479730
590.000	0.047124	0.262345	140.3310	99.6690	109.6690	0.000852	0.000852	0.047975	0.261493	0.222098

*SSA obtained from runoff calculation Scenario A

The new infiltration depth (Column 9) depends on the value of previous SSA (Column 3) and the potential infiltration depth (Column 7). If the previous SSA (Column 3) equals zero, the new infiltration depth (Column 9) will be equal to the previous infiltration depth (Column 2). And, if the actual infiltration depth (Column 8) is greater than the previous SSA (Column 3) then the new infiltration depth (Column 9) will be equal to the previous infiltration depth (Column 2) plus the previous SSA (Column 3). Otherwise it will be equal to the previous infiltration depth (Column 2) plus the actual infiltration depth (Column 8).

The new SSA (Column 10) will be equal to the previous SSA (Column 3) minus the actual infiltration depth (Column 8). The new SSAs (Column 10) will be inputs for the next runoff calculation.

The infiltrated volume can be calculated using the following equation:

$$\begin{aligned} &Inifiltration\ volume \\ &= (Next\ distance - Previous\ distance) \\ &\times (Next\ infiltration\ depth + Previous\ infiltration\ depth)/2 \end{aligned} \tag{8.19}$$

For instance, the calculation for the infiltrated volume at the distance intervals of 4.308 and 10.158 m, and their corresponding new infiltrated depths of 0.055826 and 0.055548 m, respectively, are:

Infiltrated Volume = (10.158 – 4.308) × (0. 055548 + 0. 055826) /2 = 0.325762 m^3.

Then the summation of the infiltrated volume can be computed at this interval time, which is 31.0332 m^3 (Table 8.16).

The final step is to calculate the additional infiltrated volume which occurs after the bottom check gate is opened.

Additional Infiltrated Volume = (Final infiltrated volume from TBC*) – (Infiltrated volume when bottom check gate is opened)*

Infiltration Volume = 32.5958 – 30.7237 = 1.8721 m^3

Alternatively, this can be calculated by subtracting the summation of the adjusted runoff volume (Column 3 in Scenario A, or Column 4 in Scenario B) for all of the TBC for runoff, from the SSV ((Column 4 in Scenario A, or Column 5 in Scenario B) at the check gate opening time (23.9266 m^3 in the current example).

Additional Infiltration Volume = (SSV – Σ adjusted runoff volumes)

Infiltration Volume = 23.9266 - 22.0545 = 1.8721 m^3. (based on Scenario A)

8.8. Comparison between TBC results for Scenarios A and B

As explained in Section 8.4, there are two possible scenarios (A and B) for redistribution of the stored surface water (new SSA) along the furrow length, which impacts the amount of infiltration and its distribution along the furrow.

Comparing the values of the new SSA (Column 9) in Table 8.11 and Table 8.15 for both scenarios of the runoff calculations (Scenarios A and B, respectively), highlights the different distributions of the SSA. In the first time step of the runoff calculation (the period between 240 and 250 minutes) using Scenario A, the surface water disappeared (SSAs = 0) from the first 45.173 m of furrow, as shown in Column 9 of Table 8.11. Whilst in Scenario B (Table 8.15, Column 9) the surface water disappeared (SSAs = 0) from the first 218.195 m during the same period. This difference in water recession along the furrow length will alter the opportunity times and provide different infiltrated depths along the furrow in each scenario. Thus, the difference in the SSA distribution between both scenarios will impact on all of the performance indices.

Figure 8.22 shows the final infiltrated depths at the end of the irrigation event for Furrow 17, when adopting Scenarios A and B for runoff calculations. Generally, Figure 8.22 shows that the estimated infiltrated depths associated with Scenario A are larger than the ones for Scenario B at the top end of the field (in this case up to 350 m). As a result, it is found that after completing all of the runs for runoff and infiltration, generally Scenario A has a larger infiltrated volume (1.8721 m^3) compared with Scenario B (1.5451 m^3). This is explained by the fact that Scenario A has a longer part of the furrow length that is submerged with surface water, which in turn increases

the opportunity time for infiltration along this part of furrow length, compared with Scenario B. However, both scenarios have very similar values for the added infiltrated volume (as Furrows 18, 19, 20 and 21), as shown in Table 8.17.

Table 8.17 shows that the difference in the total infiltrated volumes in both scenarios range between 0.1% and 2.1%. Therefore, it can be concluded that there is no significant difference in the total infiltrated volume between Scenarios A and B.

Table 8.17 shows that the reason for selecting Furrow 17 as an example to explain the TBC, is that the added infiltrated volume in it was close to the average of the other furrows.

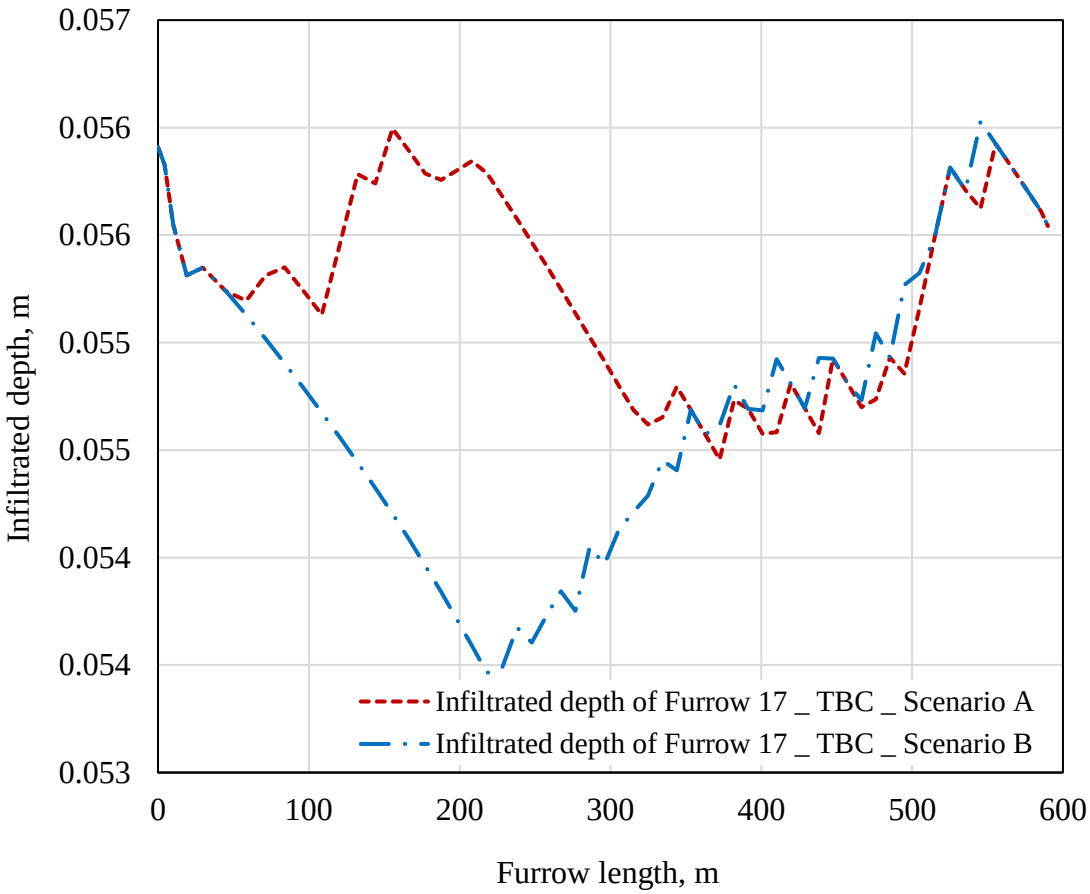

Figure 8.22 Final infiltrated depths from Scenarios A and B for the runoff calculation.

Table 8.17 Calculated infiltrated depths from Scenarios A and B.

Furrow #	Added Infiltrated Volume_ Scenario A (m^3)	Total infiltrated volume_ Scenario A (m^3)	(Added infiltrated volume) / (total infiltrated volume), % Scenario A	Added Infiltrated Volume_ Scenario B (m^3)	Total infiltrated volume_ Scenario B (m^3)	(Added infiltrated volume) / (total infiltrated volume), % Scenario B	Difference between the Percentage of the total infiltrated volume of Scenario A & B	Difference in the added infiltrated volume between Scenarios A and B (m^3)
13	4.0511	49.9876	8.1%	3.6195	49.5560	7.3%	0.8%	0.4316
14	1.3687	25.2977	5.4%	1.0475	24.9765	4.2%	1.2%	0.3212
15	0.2937	14.4760	2.0%	0.1718	14.3541	1.2%	0.8%	0.1219
16	1.3479	33.2792	4.1%	1.1927	33.1240	3.6%	0.4%	0.1552
17	1.8721	32.5958	5.7%	1.5451	32.2688	4.8%	1.0%	0.3270
18	2.1527	33.1068	6.5%	2.1073	33.0614	6.4%	0.1%	0.0454
19	0.9979	23.2754	4.3%	0.9890	23.2665	4.3%	0.0%	0.0089
20	2.9906	44.5371	6.7%	3.0338	44.5803	6.8%	-0.1%	-0.0432
21	1.1998	33.7188	3.6%	1.2017	33.7207	3.6%	0.0%	-0.0019
22	1.6740	36.0675	4.6%	1.4767	35.8702	4.1%	0.5%	0.1973
23	2.4392	40.4380	6.0%	2.2079	40.2067	5.5%	0.5%	0.2313
24	1.8399	34.0604	5.4%	1.0998	33.3203	3.3%	2.1%	0.7401

8.9. Estimation the performance indices for the furrow distance after the sill

Furrow 17 of Border 1 in Field 2 for the irrigation event conducted on the 10-02-2018 will be used as an example to explain how to estimate the performance indices for the distance between the sill and the end of the field (furrow). Table 8.18 shows the inputs required to estimate the performance indices. Based on the calculated values of the additional infiltrated and runoff volumes that were obtained using the TBC (using Scenario A as an example), a new set of volume balance components were estimated. The required volume in the root zone were estimated from the soil water deficit (SWD) prior to each irrigation event throughout the whole season using the simple water balance approach of IrriSAT (Appendix C). The SWD for Border 1 of Field 2 for the irrigation event conducted on the 10-02-2018 is 130.73 mm (Table 7.4). The drainage volume was calculated by subtracting the SWD from all the infiltrated depths along

the furrow length, previously obtained from the final time step of the TBC, then calculating the infiltrated volume of deep drainage based on the depth results and their corresponding distances, using Equation 8.19. AE and RE were estimated using Equations 8.20 and 8.21, respectively.

Table 8.18 The information required for calculation of the performance indices, for Scenario A, across the distance between the sill and the end of Furrow 17 located in Border 1 of Field 2 for the irrigation event conducted on the 10-02-2018.

Item	Value
Total inflow volume (m^3)	54.4760
Drainage volume (m^3)	0.0
Infiltrated volume (m^3) before commencing the TBC (at 240 minutes), see Figure 8.16.	30.7237
Added infiltration volume (m^3) obtained from the TBC (based on Scenario A)	1.8721
Final infiltration volume (m^3) at the furrow length part after the sill (590 m), (30.7237 + 1.8721) m^3.	32.5958
Required volume at the root zone (m^3) = (SWD × Distance from the sill to the end of the furrow × Furrow spacing) = ((130.73/1000) ×590×1) = 77.11 m^3	77.11

$$AE\% = \frac{(Infiltrated\ volume - Drainage\ volume)}{Total\ inflow\ volume} \qquad 8.20$$

AE% = (32.5958 – 0.0) / (54.4760) ×100 = 59.84%

$$RE\% = \frac{(Infiltrated\ volume - Drainage\ volume)}{Required\ volume} \qquad 8.21$$

RE% = (32.5958 – 0.0) / (77.11) × 100 = 42.27%

The distribution uniformity was calculated using Equation 2.2 and the infiltrated depth results from the final step of the TBC for both Scenarios A and B. The linear interpolation function in Excel was used to obtain the values of the infiltrated depths at equal distance intervals from the suggested values, as the files exported from SISCO were at uneven distance intervals. Then the values of the infiltrated depths were sorted in ascending order and the average of the lowest quarter number of values was

computed, along with the average of all depth values, before substituting them into the uniformity equation introduced previously. The DU value for Furrow 17 was 98.93% in Scenario A.

DU% = (0.05466 / 0.05525) ×100 = 98.93% (using Equation 2.2).

Table 8.19 summarises the volume balance components and the performance indices estimated using the TBCs (Scenarios A and B) and SISCO results (see Table 8.10) for "Blocked" and "Free draining" downstream conditions for Furrow 17 in Border 1 of Field 2 for the irrigation event conducted on the 10-02-2018. Runoff volume refers to the total runoff water passing through the bottom check gate, which is the summation of adjusted runoff volumes for all of the TBC time steps calculation (from the bottom check gate is opened until there is no SSV remains at the furrow surface, or remaining SSV = 0).

It can be noticed that there is only a slight difference in the volume balance components and the performances indices obtained from Scenarios A and B. Therefore, to a large degree it depends on the scenario chosen when conducting the TBC. However, the domination of the initial infiltration and the field layout (vertical step) in the current irrigation system would decrease the impact of the TBC compared with other systems that could have soils with higher final infiltration rates, and longer recession phases (see Sections 8.2.4 and 11.3.2). Also, in current field studied, high flow rates and furrow sizes had impacted significantly on the irrigation performance (see Section 10.2.7) which would not be the case in other systems. Comparing the TBC (Scenarios A or B) with the Free draining condition shows small differences in the results, while large differences are shown in the Blocked condition.

Table 8.20 shows the performance results of the TBC using both Scenarios A and B for Furrows 13 to 24 in Border 1 of Field 2 on 10-2-2018. The volumetric proportions (runoff volume%, drainage volume% and storage volume%) as percentages of the total inflow volume. Runoff volume% is the propotion of the summation of the adjusted runoff volumes to the total inflow volume. Similarly, this table shows slight differences in the performances indices obtained from both Scenarios A and B. This table shows high DU results, ranging between 96.59% and 99.5% for Scenario A, and ranging between 96.61% and 99.34% for Scenario B. The AE ranges between 28.37%

and 74.08% for Scenario A, and between 28.33% and 72.47% for Scenario B. The values of RE varies between 18.77% and 64.82% for Scenario A, and between 18.61% and 64.26% for Scenario B.

These variations in the AE and RE values result from the considerable variation in diverted flows, water advance, and cross sectional areas between furrows. The low values of AE and RE are caused by considerable runoff losses due to the high applied inflow rates, the low final infiltration characteristic of this soil, and the relatively short opportunity time used in the irrigation practice for this field.

Table 8.19 Volume balance components and performance indices for both standard downstream conditions and the TBC for Furrow 17 located in Border 1 of Field 2 of the irrigation event conducted on the 10-02-2018.

Item	TBC _ Scenario A	TBC _ Scenario B	Blocked	Free draining
Total inflow volume (m^3)	54.4760	54.4760	54.4760	54.5373
Infiltrated volume (m^3)	32.5958	32.2688	54.61	32.1333
Runoff Volume (Σ *adjusted runoff volumes*) (m^3)	22.0545	22.3815	0	22.33
Storage in the root zone (m^3)	32.5958	32.2688	45.57	32.13
Drainage volume (m^3)	0	0	9.03	0
Error volume (m^3)	-	-	-0.13	0.07
Required volume at the root zone (m^3)	77.11	77.11	77.11	77.11
AE%	59.84	59.23	83.66	58.92
RE%	42.27	41.85	59.09	41.59
DU%	98.93	98.33	59.79	96.66

Comparing the TBC results for all adjoining furrows (13 to 24) in both scenarios (Table 8.20) with SISCO simulated results under the downstream "Free draining" condition (Table 8.10) shows small differences, while shows large differences are shown in the Blocked downstream condition.

Similarly, Figure 8.23 shows a significant difference in the infiltrated depth in the Blocked condition compared with the Free draining condition and the TBC. It shows a very slight difference between the Free draining condition and the TBC (Scenario A). So, it is concluded that it would not be worth completing the TBC for the current irrigation system. However, conducting the TBC would be more useful under different circumstances (see Section 11.3.2).

Table 8.20 TBC results of irrigation performance for Furrows 13 to 24 in Border 1 of Field 2 on 10-2-2018.

Furrow no.	Scenario A						Scenario B					
	AE %	RE %	DU %	Runoff volume %	Drainage volume %	Storage volume %	AE %	RE %	DU %	Runoff volume %	Drainage volume %	Storage volume %
13	54.15	64.82	98.93	46.25	0.00	54.15	53.68	64.26	97.86	46.72	0.00	53.68
14	48.73	32.81	98.51	51.79	0.00	48.73	48.11	32.39	98.75	52.40	0.00	48.11
15	45.62	18.77	99.24	55.06	0.00	45.62	45.24	18.61	99.16	55.44	0.00	45.24
16	45.29	43.16	99.50	55.13	0.00	45.29	45.08	42.96	99.28	55.34	0.00	45.08
17	59.84	42.27	98.93	40.48	0.00	59.84	59.23	41.85	98.33	41.09	0.00	59.23
18	28.37	42.93	97.50	71.29	0.00	28.37	28.33	42.87	98.45	71.33	0.00	28.33
19	33.81	30.18	98.76	66.67	0.00	33.81	33.80	30.17	98.71	66.68	0.00	33.80
20	30.62	57.76	98.73	68.88	0.00	30.62	30.65	57.81	98.91	68.85	0.00	30.65
21	39.54	43.73	99.34	60.58	0.00	39.54	39.54	43.73	99.34	60.58	0.00	39.54
22	51.23	46.77	99.40	49.11	0.00	51.23	50.95	46.52	98.92	49.39	0.00	50.95
23	67.62	52.44	99.01	32.36	0.00	67.62	67.23	52.14	98.75	32.74	0.00	67.23
24	74.08	44.17	96.59	26.13	0.00	74.08	72.47	43.21	96.61	27.74	0.00	72.47

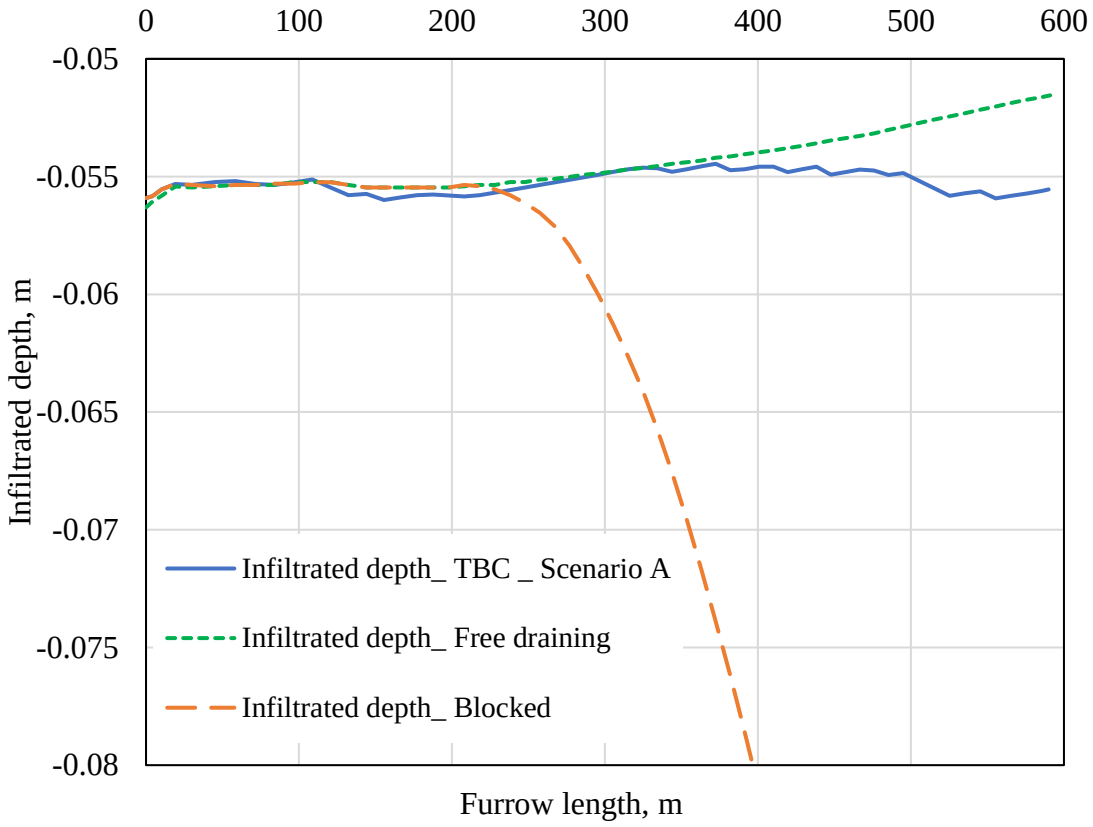

Figure 8.23 Infiltrated depth obtained by the TBC (Scenario A), and Blocked and Free draining condition for Furrow 17 located in Border 1 of Field 2 of the irrigation event conducted on 10-02-2018.

8.10. Estimation of the infiltrated volume for the upstream part of the furrow, before the sill.

The true performances indices for the entire furrow length requires an estimation of the infiltrated volume for the upstream section (50 metres) of the furrow before the sill.

As explained in the previous sections, all the estimations of the infiltration parameters *a* and *k* for the furrows ignored the distance from the furrow entrance to the sill according, to the considerations explained in Section 8.2.1.1.

The estimation of the infiltrated volume for that part of the furrow upstream of the sill (50 metres) requires an assumption of the IOT, based on field observations. It was observed during the irrigation events that a large amount water drains-back from this

upstream part of the furrow, within approximately 30 minutes of the check gate at the top of Field 2 being opened. The IOT can be calculated based on this assumption and the water advance Equation 3.8. To simplify the infiltration calculation at this upstream distance, it is assumed that this drains over this entire distance at the same time. This can be justified from field observations, where water receded rapidly due to the presence of the vertical step and the wide check gate between the adjoining borders which passes large amount of water in a short period of time. For convenience, the advance equation parameters *p* and *r* were obtained from IPARM while the infiltration parameters *a* and *k* were obtained from SISCO. Table 8.21 shows the required inputs and information to estimate the infiltrated volume for the most upstream 50 metres of Furrow 17.

Table 8.22 shows the calculation of the infiltrated volume of the most upstream 50 metres of Furrow 17 in Border 1 of Field 2 for the irrigation event conducted on the 10-02-2018. In this table, it was decided to divide the distance from the furrow entrance to the sill into increments of ten metres to obtain an acceptable accuracy for the infiltration calculation. The advance time (Column 2) is calculated using Equation 3.8. The IOT (Column 4) is the difference between the total time to drain-back all of the water from this 50 metres upstream of the sill (Column 3), and the advance time (Column 2). The infiltrated depth was calculated using Equation 8.13.

Table 8.21 The information required to calculate the infiltrated volume on the most upstream 50 m of Furrow 17 in Border 1 of Field 2 for the irrigation event conducted on the 10-02-2018.

Item	value
Time water commenced entry to furrow	6:25 AM
Top check gate opening time	10:25 AM
Time between water entry to furrow and top check gate opening	240 min
Time duration for drain-back after top check gate opened	30 min.
Total time duration between water entry into furrow and completion of drain-back	270 min.
Water advance parameter *p*, obtained from IPARM model	6.44525
Water advance parameter *r*, obtained from IPARM model	0.91937
Infiltration parameter, *a*, obtained from SISCO model	0.18766
Infiltration parameter, *k*, obtained from SISCO model	0.01983

Table 8.22 Calculation of the infiltrated volume in the most upstream 50 m of Furrow 17 located in Border 1 of Field 2 for the irrigation event conducted on the 10-02-2018.

Distance, m (1)	Advance time, min (2)	Total time to drain-back, min. (3)	IOT, min (4)	Infiltrated depth (Z), m (5)	Infiltrated volume, m^3 (6)
0	0.00	270.0	270.0	0.05671	
10	1.61	270.0	268.39	0.05664	0.56676
20	3.43	270.0	266.6	0.05657	0.56608
30	5.33	270.0	264.7	0.05650	0.56534
40	7.28	270.0	262.7	0.05642	0.56457
50	9.28	270.0	260.7	0.05634	0.56377
					Σ 2.8265

For example, the infiltrated depth, *Z*, (Column 5) at a distance of 10 m, with *a* and *k* values obtained from Table 8.21, can be calculated as shown below:

$Z = 0.01983 \times (268.39)^{0.18766} = 0.05664$ m.

The infiltrated volume (Column 6) can be calculated using Equation 8.19, as shown below (for the distance 0 to 10 m):

Infiltration volume = $(10 - 0) \times (0.05664 + 0.05671) / 2 = 0.56676$ m^3.

The total infiltrated volume on this most upstream 50 metres of the furrow can be found by computing the summation, as shown in Table 8.22.

8.11. Estimation of the performance indices for the entire furrow length

Furrow 17 located in Border 1 of Field 2 during the irrigation event conducted on the 10-02-2018 will be used as an example to explain how to estimate AE and RE for the entire furrow length. Table 8.23 shows the inputs required to estimate the AE and RE. In this table, the total inflow volume is assumed to be the same value as that adopted for calculation of the performance indices across the distance between the sill and the end of the furrow (see Table 8.18). In fact, this assumption is not true because the inflow rate measurements were conducted at the sill instead of the furrow entrance. Therefore, the value of the total inflow volume that was used in calculation of the

performance indices across the entire length of the furrow (Table 8.23) potentially includes an under-estimation compared with the real situation in the field. However, the relatively small length of the furrow from the entrance to the sill (50 m) in comparison with the entire length of the furrow (640 m) may lessen the influence of that assumption. As discussed earlier it was not possible to conduct individual furrow measurements at the furrow entrance due to the overflow between adjacent furrows that occurs at this part in the field.

Table 8.23 The information required to calculate the AE and RE for the entire length of Furrow 17 located in Border 1 of Field 2 for the irrigation event conducted on the 10-02-2018.

Item	Value
Total inflow volume	54.4760 m^3
Drainage volume	0.0 m^3
Required volume at the root zone = (SWD × Furrow length × Furrow spacing) = ((130.73/1000) ×640×1) =	83.6672 m^3
Infiltrated volume in the most upstream 50 metres of the furrow (see Section Table 8.22).	2.8265 m^3
Infiltrated volume before commencing the TBC (at 240 minutes), see Figure 8.16	30.7237 m^3
Added infiltration volume obtained from the TBC (based on Scenario A)	1.8721 m^3
Final infiltration volume at the furrow length part after the sill (590 m), (30.7237 + 1.8721) m^3.	32.5958 m^3
Gross infiltration volume at the entire furrow length (640 m), (2.8265 + 32.5958) m^3	35.4224 m^3

The required volume in the root zone was estimated based on the simple water balance approach of IrriSAT (Appendix C), where the soil water deficits (SWD) prior to each irrigation event throughout the whole season were calculated. The SWD for Border 1 of Field 2 of the irrigation event conducted on 10-02-2018 was 130.73 mm (Table 7.4). The drainage volume was calculated by subtracting the SWD from all of the infiltrated depths obtained from the final time step of the TBC along the furrow length, and then calculating the infiltrated volumes of deep drainage based on the depth results and their corresponding distances, using the Equation 8.19. AE and RE were estimated using Equations 8.20 and 8.21, respectively.

AE% = (35.4224 – 0.0) / (54.4760) ×100 = 65.02% (using Equation 8.20).

RE% = (35.4224 – 0.0) / (83.6672) ×100 = 42.34% (using Equation 8.21).

Table 8.24 and Table 8.25 show the volume balance components and the estimated AE and RE values for the entire length of Furrows 13 to 24 in Border 1 of Field 2 for the irrigation event conducted on the 10-02-2018. Table 8.24 shows values of AE ranging between 30.73% and 80.59% for Scenario A, while Table 8.25 shows values of AE between 30.69% and 78.98% for Scenario B. These tables contain a similar variance for RE, between 18.78% and 64.90% for Scenario A, and between 18.63% and 64.39% for Scenario B. Similarly, as discussed in Section 8.9, these variations in the AE and RE values are caused by the considerable variation in diverted flows, water advance, and cross sectional areas between furrows. And, the low ranges of AE and RE result from considerable runoff losses due to the high applied inflow rates, the low final infiltration characteristic of this soil, and the relatively short opportunity time used in the irrigation practice for this field.

8.12. TBC flowchart

This purpose of this section is to summarise the steps of TBC, including the required inputs to implement the process. These steps have been described previously in the relevant sections above but is best explained using a series of flowcharts.

Figure 8.24 shows the steps for obtaining the inputs required to implement TBC. Figure 8.25 shows Subroutine 1, used to determine the cessation time of simulation, which initially equals the commencement time of runoff. Figure 8.26 shows Subroutine 2, used for the calculation of the adjusted runoff volume per furrow. Figure 8.27 shows Subroutine 3, used to calculate the geometry factors of the furrow shape (c and m). Figure 8.28 shows Subroutine 4, the main process for the TBC calculation. Figure 8.29 shows Subroutine 5 which impements Scenario A of the TBC runoff calculation for one time step, while Figure 8.30 shows Subroutine 6, the same process following Scenario B. Figure 8.31 shows Subroutine 7, the infiltration calculation for one time step.

Table 8.24 Results of the entire furrow length using Scenario A.

furrow # (1)	Inflow volume, m^3 (2)	Required volume, m^3 (3)	Drainage volume, m^3 (4)	Infiltrated volume at U/S part of furrow (50 m), m^3 (5)	Infiltrated volume before commencing TBC (at 240 minutes), m^3 (6)	Added infiltration volume obtained from TBC, m^3 (7)	Final infiltration volume at the furrow length part after the sill (590 m), m^3 (8) = 6+7	Gross infiltration volume at the entire furrow length, m^3 (9) = 5+6+7	AE% (10) = 9/2	RE% (11) = 9/3
13	92.3092	83.6672	0.0	4.3157	45.9365	4.0511	49.9876	54.3033	58.83	64.90
14	51.9156	83.6672	0.0	2.1809	23.9290	1.3687	25.2977	27.4786	52.93	32.84
15	31.7319	83.6672	0.0	1.2339	14.1823	0.2937	14.4760	15.7099	49.51	18.78
16	73.4765	83.6672	0.0	2.8339	31.9313	1.3479	33.2792	36.1131	49.15	43.16
17	54.4760	83.6672	0.0	2.8265	30.7237	1.8721	32.5958	35.4224	65.02	42.34
18	116.6969	83.6672	0.0	2.7548	30.9541	2.1527	33.1068	35.8616	30.73	42.86
19	68.8394	83.6672	0.0	1.9590	22.2775	0.9979	23.2754	25.2344	36.66	30.16
20	145.4594	83.6672	0.0	3.6984	41.5465	2.9906	44.5371	48.2355	33.16	57.65
21	85.2763	83.6672	0.0	2.8451	32.5190	1.1999	33.7189	36.5640	42.88	43.70
22	70.4005	83.6672	0.0	3.0874	34.3935	1.6740	36.0675	39.1549	55.62	46.80
23	59.8031	83.6672	0.0	3.4758	37.9988	2.4392	40.4380	43.9138	73.43	52.49
24	45.9782	83.6672	0.0	2.9955	32.2205	1.8399	34.0604	37.0559	80.59	44.29

Table 8.25 Results of the entire furrow length using Scenario B.

furrow # (1)	Inflow volume, m^3 (2)	Required volume, m^3 (3)	Drainage volume, m^3 (4)	Infiltrated volume at U/S part of furrow (50 m), m^3 (5)	Infiltrated volume before commencing TBC (at 240 minutes), m^3 (6)	Added infiltration volume obtained from TBC, m^3 (7)	Final infiltration volume at the furrow length part after the sill (590 m), m^3 (8) = 6+7	Gross infiltration volume at the entire furrow length, m^3 (9) = 5+6+7	AE% (10) = 9/2	RE% (11) = 9/3
13	92.3092	83.6672	0.0	4.3157	45.9365	3.6194	49.5559	53.8716	58.36	64.39
14	51.9156	83.6672	0.0	2.1809	23.9290	1.0475	24.9765	27.1573	52.31	32.46
15	31.7319	83.6672	0.0	1.2339	14.1823	0.1719	14.3542	15.5881	49.12	18.63
16	73.4765	83.6672	0.0	2.8339	31.9313	1.1926	33.1239	35.9578	48.94	42.98
17	54.4760	83.6672	0.0	2.8265	30.7237	1.5450	32.2687	35.0952	64.42	41.95
18	116.6969	83.6672	0.0	2.7548	30.9541	2.1072	33.0613	35.8162	30.69	42.81
19	68.8394	83.6672	0.0	1.9590	22.2775	0.9890	23.2665	25.2255	36.64	30.15
20	145.4594	83.6672	0.0	3.6984	41.5465	3.0337	44.5802	48.2787	33.19	57.70
21	85.2763	83.6672	0.0	2.8451	32.5190	1.2016	33.7206	36.5658	42.88	43.70
22	70.4005	83.6672	0.0	3.0874	34.3935	1.4767	35.8702	38.9576	55.34	46.56
23	59.8031	83.6672	0.0	3.4758	37.9988	2.2079	40.2067	43.6825	73.04	52.21
24	45.9782	83.6672	0.0	2.9955	32.2205	1.0998	33.3203	36.3158	78.98	43.41

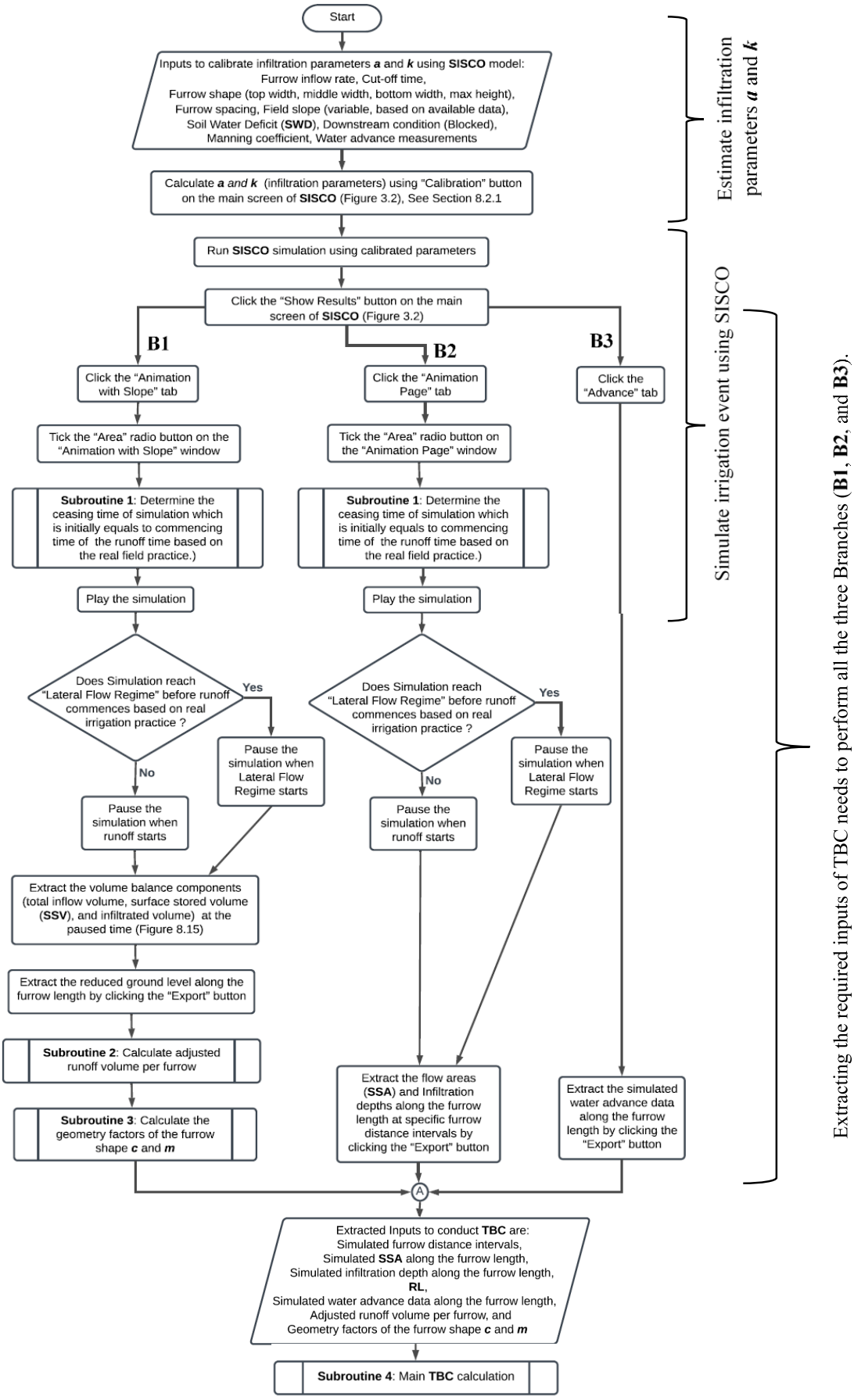

Figure 8.24 Obtaining the inputs required to implement TBC.

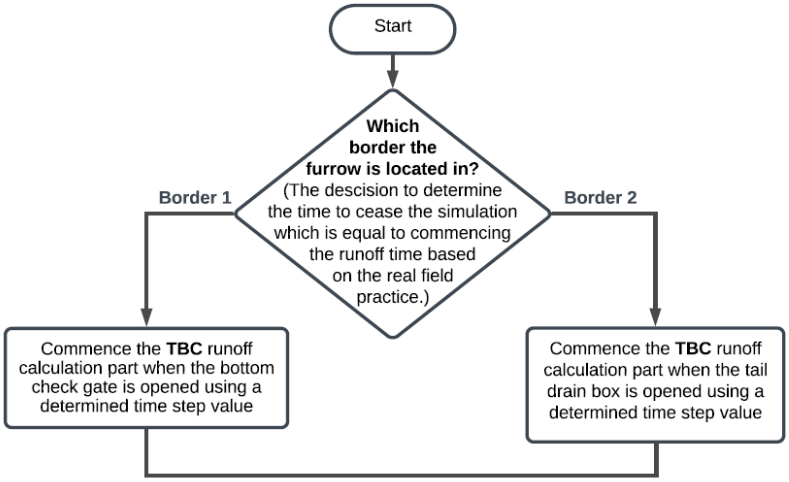

Figure 8.25 Determine the ceasing time of simulation which is initially equals to commencing time of the runoff time based on the real field practice (Subroutine 1).

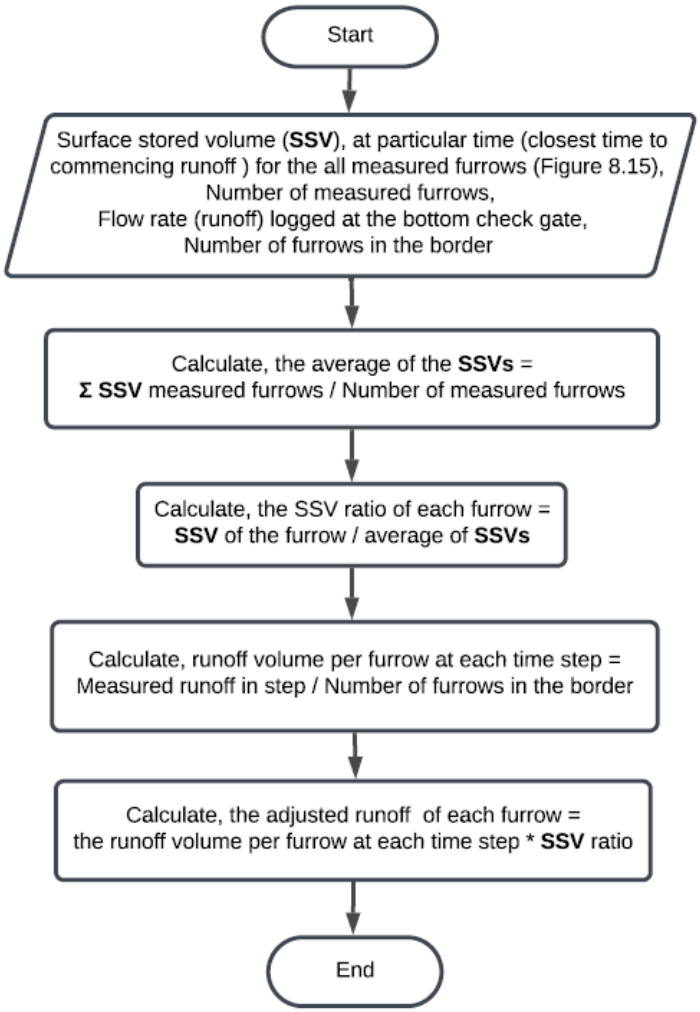

Figure 8.26 Calculating the adjusted runoff volume per furrow (Subroutine 2).

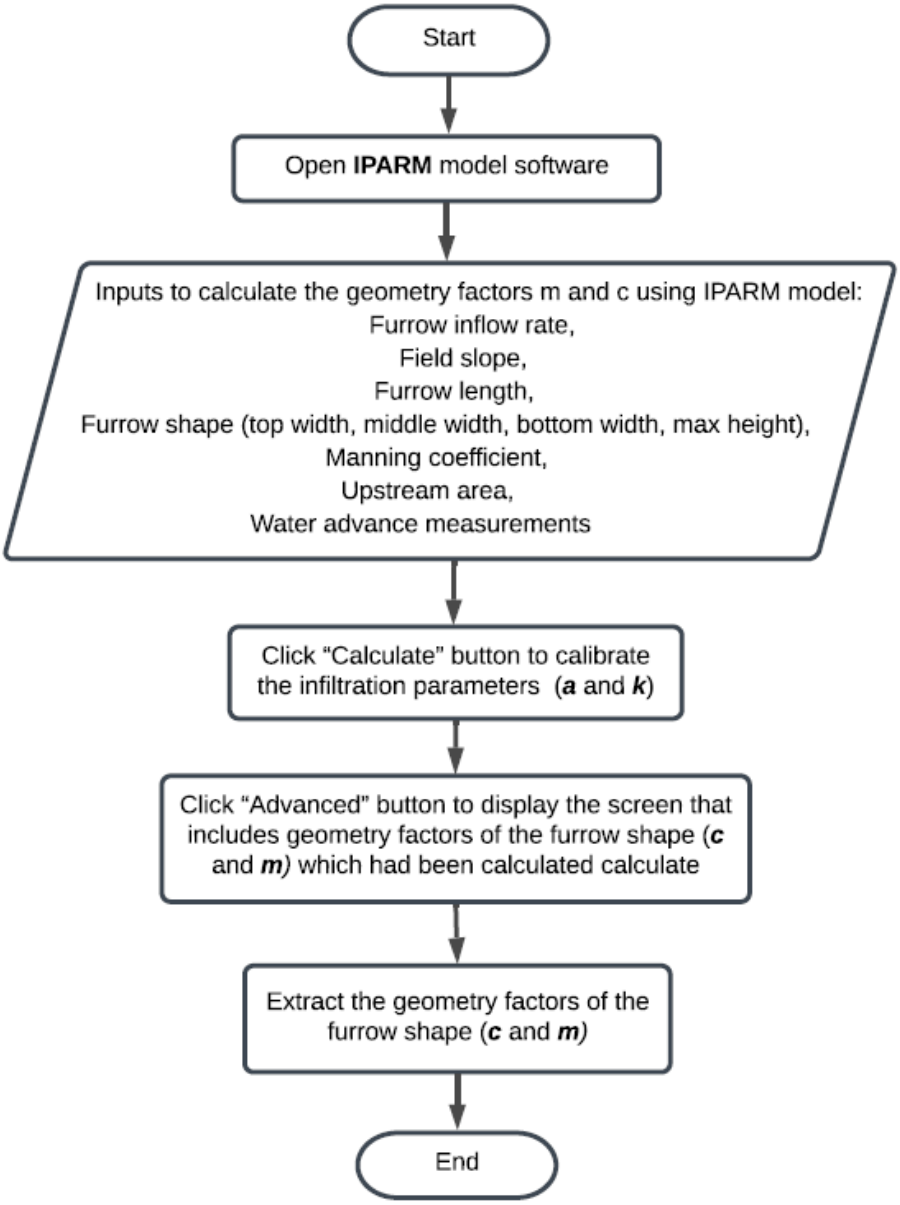

Figure 8.27 Calculating the geometry factors of the furrow shape c and m (Subroutine 3).

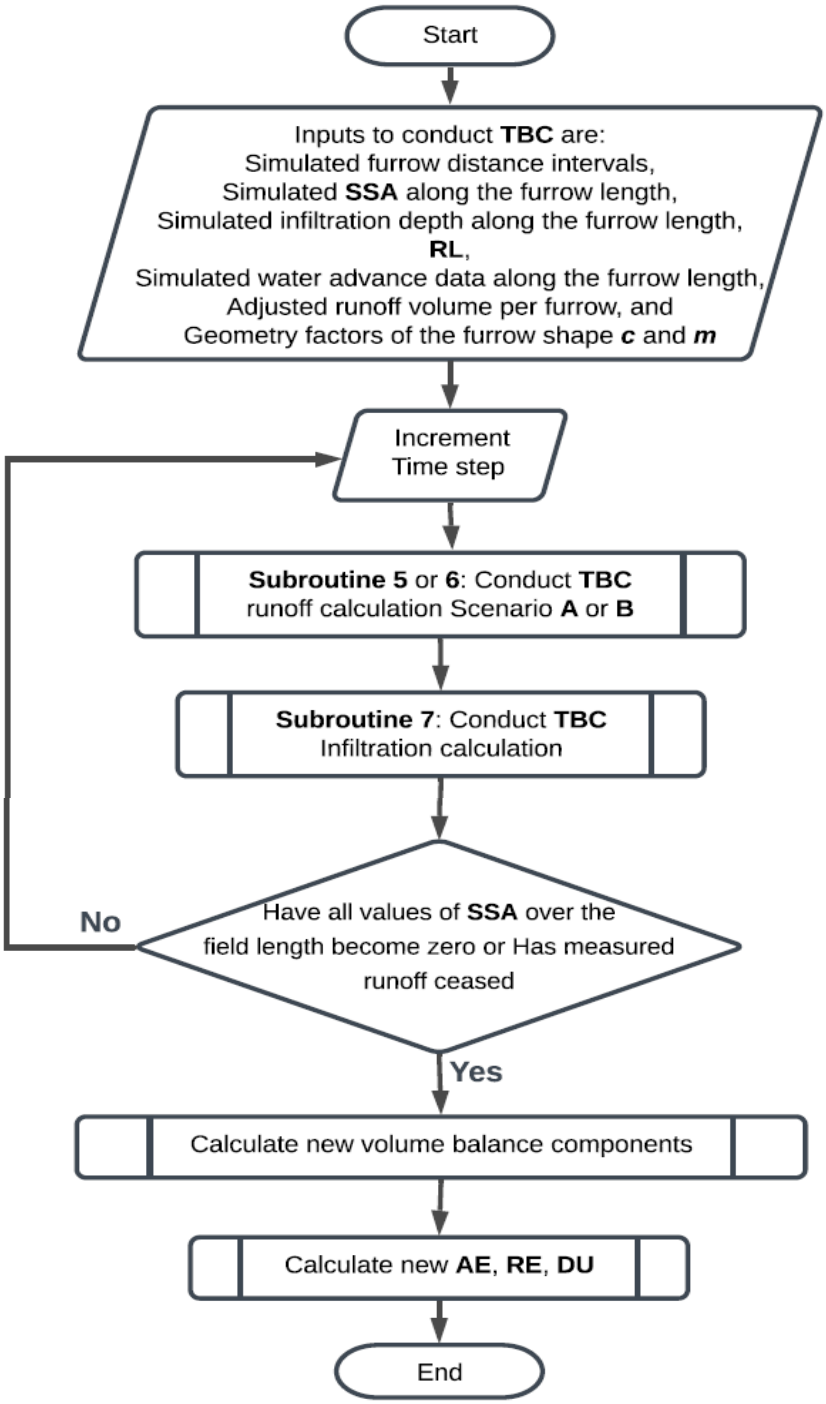

Figure 8.28 Main TBC calculation (Subroutine 4).

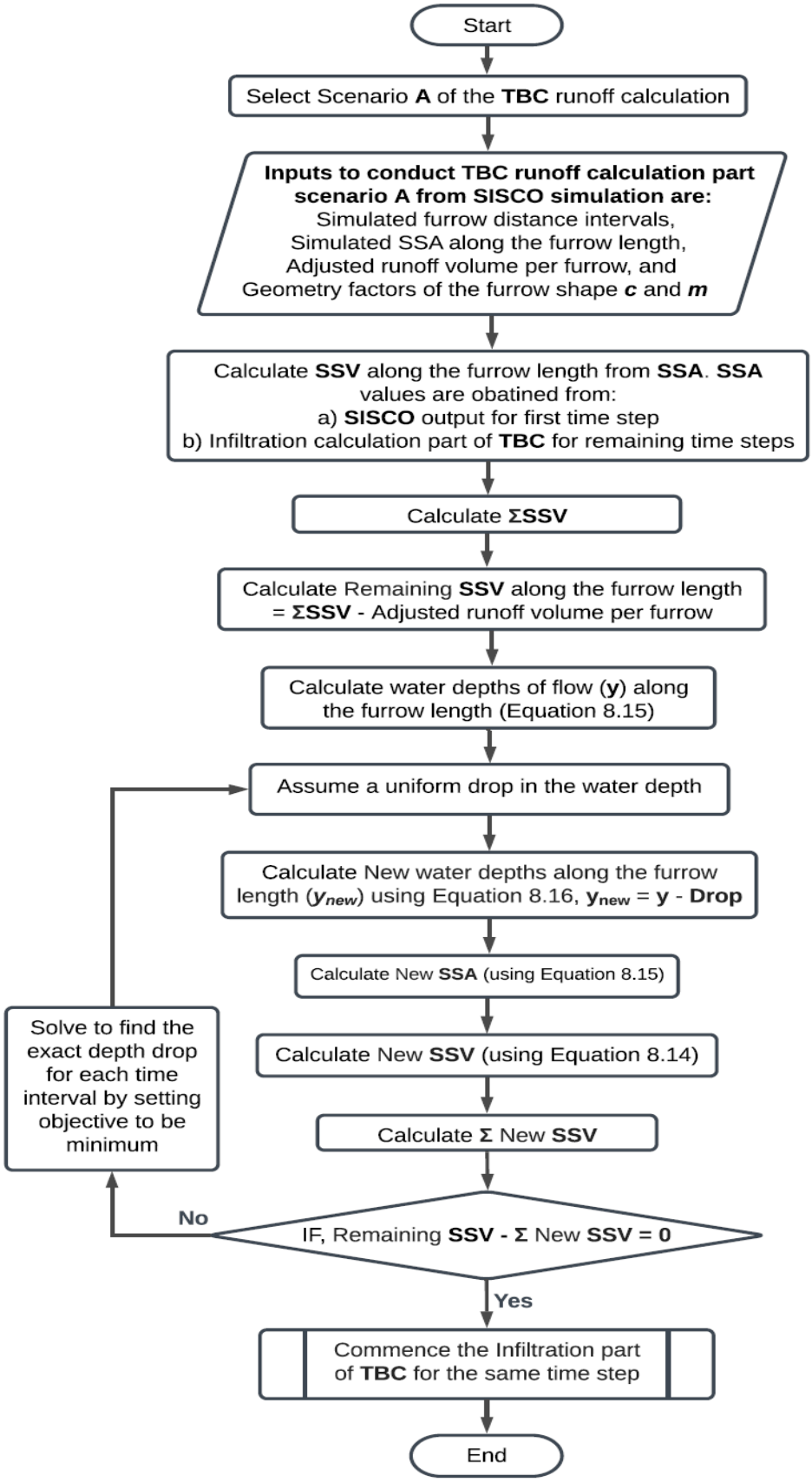

Figure 8.29 Scenario A of the TBC runoff calculation, for one time step (Subroutine 5).

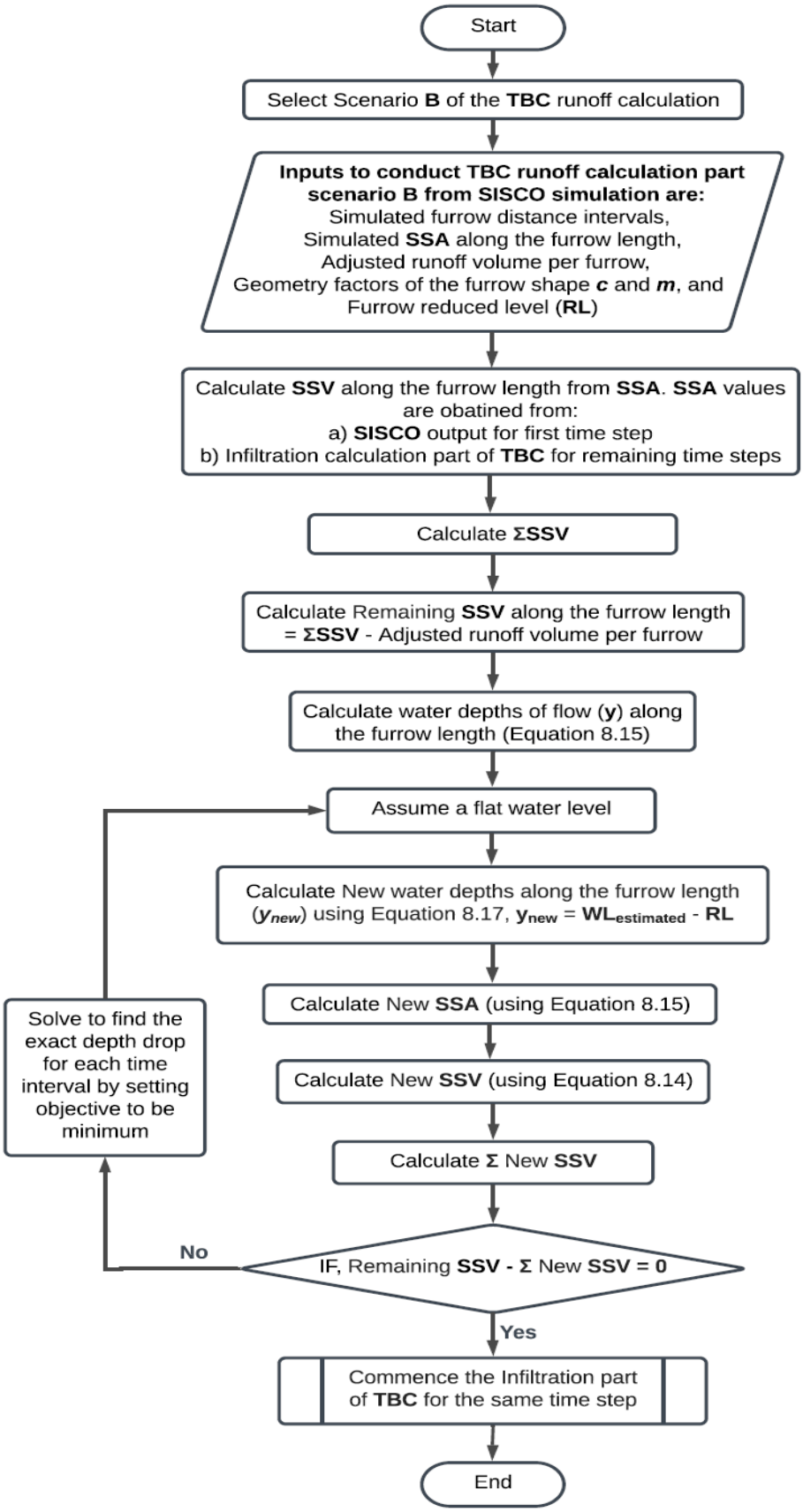

Figure 8.30 Scenario B of the TBC runoff calculation, for one time step (Subroutine 6).

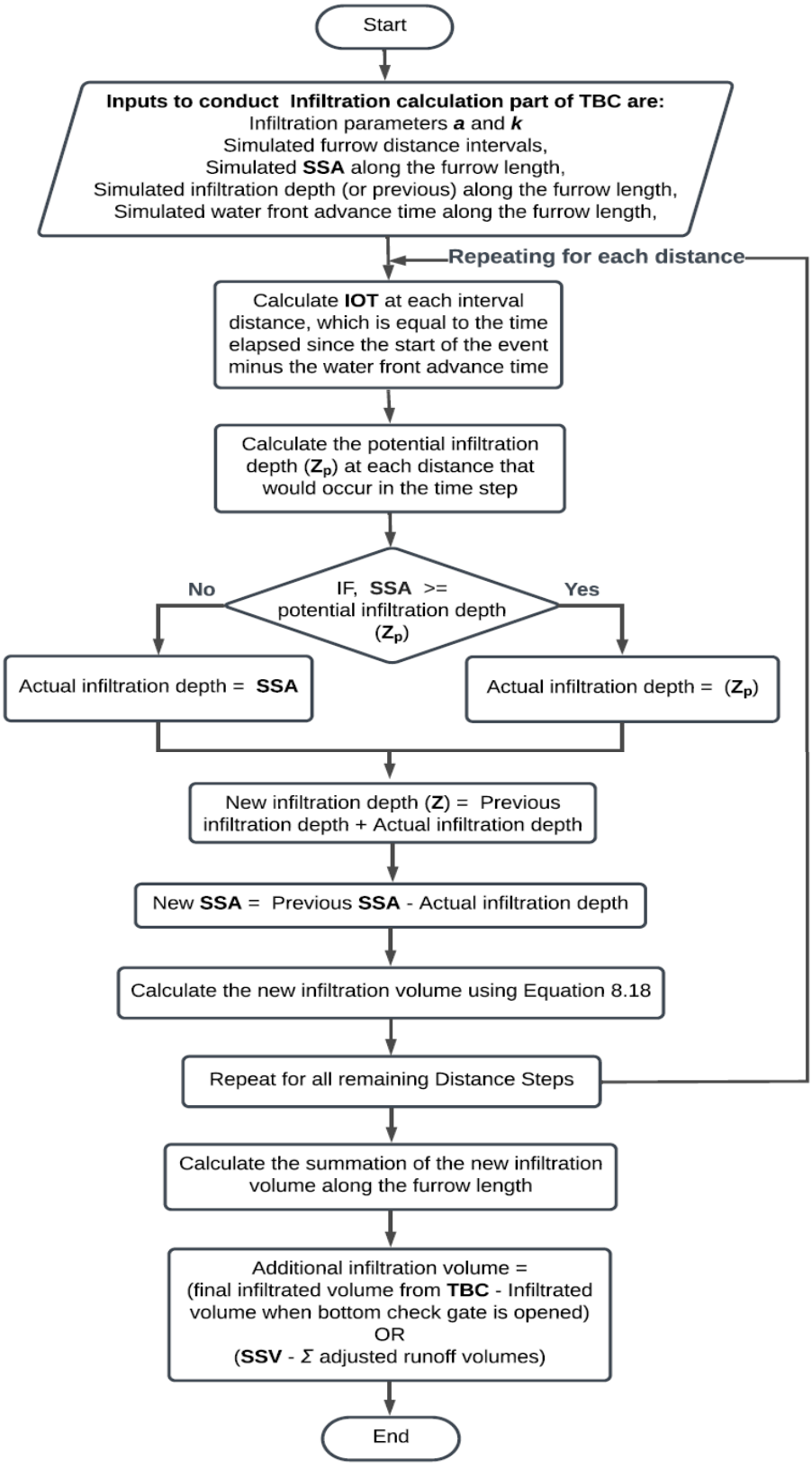

Figure 8.31 Infiltration calculation part of TBC, for one time step (Subroutine 7).

8.13. Conclusion

The infiltration characteristics were estimated using a sample of common surface irrigation models that are based on a range of theoretical hydraulic models with different levels of reliability and complexity.

These methods were applied initially omitting that part of the field upstream of the sill. The results obtained from these selected models showed approximately the same behaviour for the infiltration characteristics, with a high initial infiltration compared with a low steady infiltration value for the remainder of the IOT. This indicates the possibility of adopting any of these models for estimating the infiltration characteristics. However, the SISCO model was adopted for the estimation of the infiltration characteristics, because it based on the most reliable hydraulic model (full hydrodynamic), and its capacity to accommodate a higher quantity of field measurements. Conducting the field evaluation measurements (flow rate, water advance, and cross-sectional area of furrow) at the sill for the purpose of estimating the infiltration parameters was a good approach to avoid some measurement limitations (overflow observed between furrows at the most upstream part of the furrow close to the furrow entrance, and the change in the furrow shape and size at the furrow entrance due to erosion). In addition, selecting the measurement position at the sill was critical because of its hydraulic importance as a management feature diverting flow between furrows in this FNSBO_Re system.

The available hydraulic models were capable of simulating the irrigation process for blocked or free draining conditions at the downstream end, but this was not actually the case for the FNSBO_Re system. Therefore, a new approach was developed to simulate the irrigation process in the FNSBO_Re system, accommodating the "temporarily blocked condition" (TBC) in this system. Accordingly, this calculation approach developed, was named the temporarily blocked calculation (TBC) process. The TBC was developed based around the SISCO model due to its ability to stop the simulation at any time and extract the data to conduct this partly manual calculation process. The TBC process utilised a spreadsheet program to conduct evaluations based on some SISCO simulation results for blocked downstream conditions. The results obtained were used to determine the performances indices that reflect the real downstream conditions of the field. The TBC results suggested two potential scenarios

to predict the redistribution of water surface storage along the furrow length, after subtracting the runoff volume. The first scenario assumes that water surface drops by the same amount along the entire furrow length during each time step, while the second scenario assumes that water surface along the furrow drops to be horizontal. Each scenario implies a different redistribution of the stored surface water along the furrow length, and hence different amounts of infiltrated depth and distribution of these along the furrow length, providing different estimations of the performance indices. In fact, the reality of the redistributed water depths after run-off is not represented perfectly in either scenario. The results obtained from the TBC showed that the estimated infiltrated depth using the first scenario was slightly larger to the results obtained by the second scenario. In terms of the total infiltrated volumes, there were only slight differences (ranged between 0.1% and 2.1%) between both scenarios for results calculated in twelve furrows. Accordingly, there were insignificant differences in the volume balance components and performance indices between both scenarios. Therefore, it can be concluded that adopting either of these scenarios would be sufficient, to a large degree.

However, the domination of the initial infiltrated depth and the field layout (vertical step) in the current irrigation system could decrease the impact of the TBC results, compared with other systems that have soils with higher final infiltration rates, and longer recession phases. Therefore, it can be conclude that the TBC could be more useful under different circumstances.

The TBC results for Furrows 13 to 24 in Border 1 of Field 2 on 10-2-2018 (Table 8.20) are characterised by a high DU, from 97% to 99% for both Scenarios A and B. This is caused by low steady infiltration rate and rapid advance. The values of AE varied between 28% and 74% for Scenario A, and between 28% and 72% for Scenario B. RE ranged between 19% and 65% for Scenario A, and ranged between 19% and 64% for Scenario B. It was believed that this variation in the efficiencies indices are due to the considerable variation in the diverted flow, water advance and cross sectional areas between furrows. The low AE and RE resulted from the large runoff losses which caused by the large applied flow rate and low infiltration characteristics of the soil.

Comparing the TBC (Scenarios A or B) with the Free draining condition showed a small difference in the results, and a large difference with the Blocked condition.

Though the performance results obtained by the TBC were very close to the Free draining condition, generally, this does not undermine the importance of the TBC process, where these results could be due to the behaviour of the special infiltration characteristics and the particular field layout of the system studied.

Practically, it is worth adopting the TBC approach because it requires a relatively small extra amount of data over that required conduct calculations with either the Blocked or the Free draining conditions.

A complimentary upstream calculation was developed to estimate the infiltrated volume for the upstream part of the field prior to the sill, before combining this with the results for whole field, so as to estimate the performance indices for the whole field (furrow). In fact, this upstream complimentary calculation was based on an assumption that assumed water drains-back over this entire short distance (from the furrow entrance to the sill) at the same time. This assumption was based on real observations from that part of the field. It was observed that the water drained-back quickly from that portion of the field (from the furrow entrance to the sill) due to the presence of a vertical step between the adjoining borders and the wide check gate between the adjoining borders, which have the capacity to pass large amounts of water in a relatively short period of time. The combined results obtained from the TBC process and this complimentary upstream calculation process estimated the volume balance components and the performance indices for the entire length of the furrow when adopting both scenarios (A and B) very well.

The results for entire furrow length (13 to 24) in Border 1 of Field 2 on 10-2-2018 (Table 8.24 and Table 8.25) showed same trend of variations but higher AE values compared with the furrow length after the sill, ranging between 31% and 81% for Scenario A, and ranged approximately between 31% and 79% for Scenario B. Similarly, the results of RE for entire furrow range from 19% and 65% for Scenario A, and from 19% and 64% for Scenario B.

The methodology and results presented in this chapter demonstrate a novel technique to determine the irrigation performance of FNSBO_Re irrigation systems. However, the significant variation in results between individual furrows in the same border

highlight the importance to collect measurements in a sufficient number of furrows in each border.

CHAPTER NINE

Developing a UAV Technique to Determine the IOT

9.1. Introduction

The chapter mainly aims to develop a new technique to determine infiltration opportunity times (IOTs) from UAV advance and recession flight missions. This will allow application of the intensive evaluation results from a few furrows to the whole border, to allow estimation of the DU for the border scale. The other performance indices (AE and RE) at the border scale can be estimated based on the existing tool (IrriSAT) to estimate the soil water deficit (SWD), and flow rate measurements at the field scale which yields the net volume applied to the border.

9.2. Technique to extract infiltration opportunity time from UAV data

In the following Sections 9.2.1 to 9.2.4 the technique which was developed to estimate the DU from UAV data will be discussed. An example for one of the irrigation events will be used to explain the steps in this technique. The steps are as follows:

1. Find the average infiltration parameters (Equation 8.12) using SISCO, as explained in Section 8.2.2.
2. Extract the UAV advance data from the irrigation event conducted on 19-01-2018, at the UAV flight time for the following distances: 150, 250, 350, 450, and 570 m.
3. Select a sample of UAV advance distance data (24 furrows), as shown in Table 9.1.
4. Replace the farthest advance distance of each furrow with one advance time, and delete the other results from advance distance data (Table 9.2).

5. Extract the UAV recession time from the UAV recession flight missions (a sample of 24 furrows is shown in Table 9.3).
6. Obtain the IOTs by subtracting the advance times from the recession times for the corresponding location in each furrow (Table 9.4).
7. Because an only small number of data (IOT) can be extracted from the available data (about 17%), a complementary methodology (Section 9.2.2) will be used to provide more data representing a larger proportion of the field.
8. Estimate the parameters p and r for water advance Equation 3.8 based on IrriMATE ^{TM} advance sensor measurements, using the Solver tool in Microsoft Excel (Table 9.5).
9. Hypothesise that the parameter r is constant between furrows, while p is varying, and so determine $r_{average}$ from furrows with sufficient advance data (Table 9.5).
10. Estimate the parameter p for each individual furrow based on UAV advance data (Table 9.1) and $r_{average}$ (Table 9.5), as shown in Table 9.6.
11. Use the water advance parameters ($r_{average}$ and p) obtained in Steps 9 and 10, respectively, to estimate the time of advance along all furrows distances (150, 250, 350, 450, 570 m in Table 9.7.
12. Estimate IOTs by subtracting the advance time (obtained in Step 11) from the recession time (from Step 5), at the equivalent distances along the furrow (Table 9.8).
13. Estimate the infiltrated water depths at the distances that have IOTs (Step 12) using the cumulative infiltration Equation 8.13.
14. Estimate the DU using Equation 2.2, as explained in Section 9.2.3.
15. Estimate AE and RE, as explained in Section 9.2.4.

9.2.1. Extraction infiltration opportunity time (IOT) from UAV videos.

This section will explain the process of obtaining infiltration opportunity times (IOTs) from UAV advance and recession flight missions. The irrigation event on the 19-1-2018 is used as an example, because it includes one good advance flight mission and three good recession flight missions.

Table 9.1 shows a sample of extracting the advance data from the UAV Flight Mission #1 conducted at Border 1 of Field 2 for irrigation event conducted on 19-1-2018. The sample shows only 24 furrows out of 312 furrows of the Border 1. The actual flight paths were located at distances of 100, 200, 300, 400 and 500 metres from the furrows entrance at the top end of Border 1 of Field 2, while the adopted distances are 150, 250, 350, 450, and 570 metres, as explained in Section 6.6.3.2. While this is not ideal, with the available data set, this was the best possible choice to complete analyses.

Table 9.1 mean that the water advance did not reach this distance at that time of the flight mission. The flight mission to chase the advancing water front was conducted at 6:46 AM. This was about 81 minutes after water commenced entering the furrows at the top of the border at 5:25 AM. The irrigation event commenced at 12 minutes earlier at 5:13 AM with light application from the supplying pipe to reduce the potential erosion which could occur when starting with high flow rates. In this field water normally commences entering the furrows after about 10-15 minutes after the start of the irrigation. Furrows with numbers 6, 8, 18 and 20 are WFs while the rest are non-WFs. As shown in Table 9.2 there is one advancing time value for each furrow which represents the edge of the water advance front. In most irrigation events there was only one UAV flight mission for advance because there were many other measurements to be conducted during the irrigating, such as measuring the flow rates using Flow Tracker2 for twelve of adjoining furrows at every border which consumes about one hour alone. In some occasions, these flow rate measurements were conducted twice for each border which requires about two hours. Normally, the required time to irrigate each border is approximately 3.5 hours. Typically, the flight mission required about 20 minutes (about 12 minutes for the flight and the rest time required for the preparing to the flight). Moreover, battery life was another constraint limiting the chance to have

more flight missions during the advance phase of the irrigation events. While it would have been ideal to conduct larger numbers of UAV flight missions, it was decided that the priority to collect a range of data from each event including both the advance and flow.

Table 9.1 Sample of the extraction of UAV advance data of the Flight mission #1 conducted at Border 1 of Field 2 for the irrigation event conducted on 19-1-2018.

Furrow no.	UAV's flight mission paths at specific distances, m				
	x_1 = 150	x_2 = 250	x_3 = 350	x_4 = 450	x_5 = 570
1	150	250			
2	150	250			
3	150	250			
4	150	250	350		
5	150	250	350		
6*	150	250	350	450	
7	150	250	350		
8*	150	250	350	450	
9	150	250	350		
10	150	250	350		
11	150	250			
12	150	250			
13	150	250	350		
14	150	250	350		
15	150	250			
16	150	250	350		
17	150	250	350		
18*	150	250	350	450	570
19	150	250	350		
20*	150	250	350	450	570
21	150	250	350		
22	150	250	350		
23	150	250			
24	150	250			

* Wheeled furrows

Table 9.2 Sample of the UAV advancing time from Flight Mission #1 conducted at Border 1 of Field 2 of the irrigation event conducted on 19-1-2018

	UAV flight mission advancing time at specific distances, min.				
Furrow no.	x_1 **= 150**	x_2 **= 250**	x_3 **= 350**	x_4 **= 450**	x_5 **= 570**
1		81			
2		81			
3		81			
4			81		
5			81		
6*				81	
7			81		
8*				81	
9			81		
10			81		
11		81			
12		81			
13			81		
14			81		
15		81			
16			81		
17			81		
18*					81
19			81		
20*					81
21			81		
22			81		
23		81			
24		81			

* Wheeled furrows

Table 9.3 shows part of the UAV recession data captured over three flight missions in Border 1 of Field 2 for the irrigation event conducted on 19-1-2018. The actual recession times were 356, 468, and 539 minutes, but the adopted ones are 356, 412, and 504 minutes, as explained in Section 6.6.3.2. The empty cells in the Table 9.3 refer to the parts of the furrows that have not receded in that mission. Three flight missions were possible because most of the intensive activities cease once recession phase commences.

Table 9.3 Sample of the recession time data collected from three UAV flight missions in Border 1 of Field 2 for the irrigation event conducted on 19-1-2018.

	UAV's flight mission recession time at specific distances, min.				
Furrow no.	x_1 **=150 m**	x_2 **= 250 m**	x_3 **= 350 m**	x_4 **= 450 m**	x_5 **= 570 m**
1	356	356	504	504	
2	356	356	504	504	
3	412	412	412	412	
4	412	412	412	412	
5	412	412	412	412	412
6*	504	504	504	504	
7	412	412	412	412	412
8*	356	356	504	504	
9	356	412	412	412	412
10	504	504	504	504	
11	356	412	412	412	412
12	356	412	412	412	412
13	412	504	504	504	
14	356	356	412	412	
15	356	356	412	412	412
16	356	356	412	412	
17	356	356	412	412	
18*	356	356	504	504	
19	356	356	412	504	
20*	412	412	504	504	
21	356	412	412	504	
22	356	356	504	504	
23	356	356	412	504	
24	356	412	412	504	

* Wheeled furrows

Table 9.4 shows estimated infiltration opportunity times (IOT) from UAV advance and recession data for a sample of furrows located in Border 1 of Field 2 for the irrigation event conducted on 19-1-2018. The IOT values were estimated by subtracting the advance time from the recession time for each corresponding cell of Table 9.2 and Table 9.3, respectively. Based on the availability of UAV advance and recession data at the same corresponding locations, there are only a few locations where the IOT can be estimated, as shown in Table 9.4. Based on this procedure for this irrigation event, the IOT can be estimated for only 17% of the total cells. The total number of cells is 1560, which represents the whole border area, while the number of cells where the IOT can be estimated is 271. It was only possible to estimate the IOT in 9% and 4% of the border area for the irrigation events of the 11-1-2018 and 26-01-2018, respectively, in Border 1 of Field 2.

Table 9.4 Sample of estimated IOTs from UAV advance and recession data for a sample of furrows located in Border 1 of Field 2 for the irrigation event conducted on 19-1-2018.

	Estimated IOT from UAV data, min.				
Furrow no.	x_1 **=150 m**	x_2 **= 250 m**	x_3 **= 350 m**	x_4 **= 450 m**	x_5 **= 570 m**
1		275			
2		275			
3		331			
4			331		
5			331		
6*				423	
7			331		
8*				423	
9			331		
10			423		
11		331			
12		331			
13			423		
14			331		
15		275			
16			331		
17			331		
18*					
19			331		
20*					
21			331		
22			423		
23		275			
24		331			

* Wheeled furrows

The depth of infiltration can be estimated by substituting the IOT into the Kostiakov Equation 8.13. Distribution uniformity (DU) can be estimated using the Equation 2.2. However, as most of the IOT data is missing, this DU will not provide a good understanding of the irrigation performance of the entire border. Therefore, a technique is required to generate advance data over a large part of the field to obtain more IOT data, more estimated infiltration depths, and a better understanding of the irrigation performance for that border.

9.2.2. Developing a technique to interpolate IOT from UAV data

Finding IOTs for any distance along the border of every furrow will provide the opportunity to estimate infiltrated depths applied to that border at the corresponding locations. Substituting these IOTs into the Kostiakov Equation 8.13 will yield the infiltrated water depths at these locations, so that the irrigation performance can be predicted for these parts of the border. This section will outline a new approach to obtain IOTs from the UAV advance and recession flight missions.

Usually the field measurements only included one effective flight mission in each border during the advance phase. Usually, this mission was conducted after about one third of the time required to irrigate that border. This flight mission captured most of the advance phase data in each border, while the next mission captured less data because the advance was completed in most furrows.

As a result, the advance data extracted from the UAV only included one point for each furrow, but this point may be located at different downstream distances between furrows. To overcome this lack of advance measurements the following complementary methodology was developed. Based on the IrriMATE ^{TM} advance sensors measurements, the parameters p and r for the water advance Equation 3.8 will be estimated using the Solver tool in Microsoft Excel. It was hypothesised that parameter r can considered constant, while p is varying. Theoretically, the parameter r depends more heavily on the soil properties, while parameter p depends on the water application rate.

Table 9.5 shows the calculation process to estimate the parameters p and r. In this table, there are four groups of data. The first group includes the advance times from the IrriMATE ^{TM} sensors at actual advance distances, for a set of selected furrows in Border 1 of Field 2 for the irrigation event held on the 10-2-2018. The second group represents the calculated advance distances (x_c) in metres, while the third group represents the squared error of the distances and the last group are the advance parameters p and r. Firstly, values are estimated for p and r. Then the advance distances (x_c) are calculated by substituting the corresponding initial estimates of p and r, and the corresponding actual advance time into Equation 3.8. The distance squared error

is calculated at each corresponding advance distance using ((*calculated advance distances* – actual *advance distances*)^2). Then the distance squared errors are calculated from the sum of all cells.

The advance parameter *p* for each individual furrow will also be estimated using the Solver tool, based on the available UAV advance data (Table 9.2), and $r_{average}$ from Table 9.5, as shown in Table 9.6. The value of *p* is solved for each furrow by using the Excel Solver to minimise the difference between the measured advance distance, and the calculated advance distance. This process is repeated twice more to make sure that the solved *p* values have reached a constant value. As a result there will be now one value of the parameter *p* for each individual furrow, and one value of *r* representing all furrows in the border. To estimate the calculated time of advance for a given distance (Table 9.7) the transformed formula of Equation 3.8, as shown below, can be used:

$$t = \left(\frac{x}{p}\right)^{1/r_{average}} \qquad 9.1$$

The IOTs can then be estimated by subtracting the advance times from the recession times (Table 9.3), as shown in Table 9.8. However, in Table 9.8 there are empty cells which represent the locations where the water had not receded by the final measurement flight. However, the process outlined here, has significantly increased the number of cells where the IOT can be estimated. In this case it has increased the number of cells from 17% to 86% of the total number.

Figure 9.1 shows the calculated advance based on the advance and recession data measured by the UAV for Furrows 13 and 15 in Border 1 of Field 2, for the irrigation event conducted on 19-1-2018.

Table 9.5 The calculation process to estimate the parameters *p* and *r* using the advance times from the IrriMATE ™ sensors installed in Border 1 of Field 2 for the irrigation event on 10-2-2018.

Furrow no.	Actual advance time, min				Calculated advance distance (x_c) from Equation 3.8, m				Distance Squared errors				Advance parameters	
	x_1 = 166.5	x_2 = 312.8	x_3 = 438.4	x_4 = 542.8	x_{c1}	x_{c2}	x_{c3}	x_{c4}	(x_{c1} – 166.5)^2	(x_{c2} – 312.8)^2	(x_{c3} – 438.46)^2	(x_{c4} – 542.8)^2	*p*	*r*
13	25	53	81	105	168.11	310.59	439.22	542.95	2.593	4.863	0.580	0.022	12.1213	0.8169
14	34	70	100	126	163.44	316.39	438.44	541.65	9.392	12.857	0.001	1.326	6.4936	0.9147
15	39	76	109	134	164.63	312.85	442.63	539.92	3.488	0.002	17.357	8.275	4.8471	0.9623
16	31	64	93	119	165.86	314.35	437.07	543.22	0.404	2.388	1.934	0.176	8.0250	0.8820
17	33	66	96	87	168.58	341.44	500.03	452.34	4.319	820.053	3791.278	8182.27	4.7935	1.0182
18	21	44	62	79	162.77	318.84	435.47	542.77	13.913	36.483	8.945	0.001	10.2256	0.9090
19	27	53	76	98	169.34	312.46	433.48	546.07	8.086	0.115	24.828	10.663	8.4875	0.9082
20	21	44	63	79	161.95	317.34	439.85	540.36	20.671	20.654	1.922	5.934	10.1605	0.9094
21	31	62	89	115	165.80	313.92	437.93	No data	0.491	1.247	0.284	No data	7.0165	0.9209
22	32	No	94	119	166.37	0.00	438.80	542.56	0.016	97843.8	0.118	0.057	7.3521	0.9000
23	43	83	116	146	166.36	314.74	435.40	544.17	0.018	3.755	9.360	1.872	4.3399	0.9695
24	48	92	131	147	156.84	315.87	462.03	523.03	93.364	9.401	555.501	390.944	2.4335	1.0761
25	47	95	135	142	151.40	325.23	476.45	503.35	228.078	154.610	1442.996	1556.39	2.3084	1.0865
26	54	108	152	146	157.16	337.84	492.69	471.27	87.191	626.963	2941.362	5117.07	1.9215	1.1041
27	43	84	119	142	160.52	315.28	447.90	535.23	35.731	6.139	89.122	57.274	3.6215	1.0081
28	30	62	90	115	165.59	314.55	437.26	543.03	0.827	3.051	1.449	0.054	8.1939	0.8838
									Sum of all squared errors (SSE) = 124274.4					***r average* = 0.95436**

Table 9.6 A sample of the calculation results from using the Excel Solver tool to estimate the advance parameter *p* for each furrow based on the average *r* from Table 9.5 ($r_{average}$ = 0.95436).

Furrow no.	UAVs flight mission advance times (min.) at specific distances (m).					*p*	Distance Squared error
	x_1 = **150**	x_2 = **250**	x_3 = **350**	x_4 = **450**	x_5 = **570**		
1		81				3.772	0
2		81				3.772	0
3		81				3.772	0
4			81			5.281	0
5			81			5.281	0
6*				81		6.789	0
7			81			5.281	0
8*				81		6.789	0
9			81			5.281	0
10			81			5.281	0
11		81				3.772	0
12		81				3.772	0
13			81			5.281	0
14			81			5.281	0
15		81				3.772	0
16			81			5.281	0
17			81			5.281	0
18*					81	8.600	0
19			81			5.281	0
20*					81	8.600	0
21			81			5.281	0
22			81			5.281	0
23		81				3.772	0
24		81				3.772	0
							SSE = 0

* Wheeled furrows

Table 9.7 Calculated advance times for specific distances along furrows from Equation 9.1, using the fitted values of *p* from Table 9.6

Furrow no.	Calculated time of advance min.) at specific distances (m).				
	x_1 =**150**	x_2 = **250**	x_3 = **350**	x_4 = **450**	x_5 = **570**
1	47	81	115	150	192
2	47	81	115	150	192
3	47	81	115	150	192
4	33	57	81	105	135
5	33	57	81	105	135
6*	26	44	62	81	104
7	33	57	81	105	135
8*	26	44	62	81	104
9	33	57	81	105	135
10	33	57	81	105	135
11	47	81	115	150	192
12	47	81	115	150	192
13	33	57	81	105	135
14	33	57	81	105	135
15	47	81	115	150	192
16	33	57	81	105	135
17	33	57	81	105	135
18*	20	34	49	63	81
19	33	57	81	105	135
20*	20	34	49	63	81
21	33	57	81	105	135
22	33	57	81	105	135
23	47	81	115	150	192
24	47	81	115	150	192

* Wheeled furrows

Table 9.8 Sample of estimated IOTs from UAV data, including both measured and calculated advance and recession data for a sample of furrows located in Border 1 of Field 2 for the irrigation event conducted on 19-1-2018.

Furrow no.	Estimated IOTs from UAV data, min.				
	x_1 = **150** m	x_2 = **250** m	x_3 = **350** m	x_4 = **450** m	x_5 = **570** m
1	309	275	389	354	
2	309	275	389	354	
3	365	331	297	262	
4	379	355	331	307	
5	379	355	331	307	277
6*	478	460	442	423	
7	379	355	331	307	277
8*	330	312	442	423	
9	323	355	331	307	277
10	471	447	423	399	
11	309	331	297	262	220
12	309	331	297	262	220
13	379	447	423	399	
14	323	299	331	307	
15	309	275	297	262	220
16	323	299	331	307	
17	323	299	331	307	
18*	336	322	455	441	
19	323	299	331	399	
20*	392	378	455	441	
21	323	355	331	399	
22	323	299	423	399	
23	309	275	297	354	
24	309	331	297	354	

* Wheeled furrows

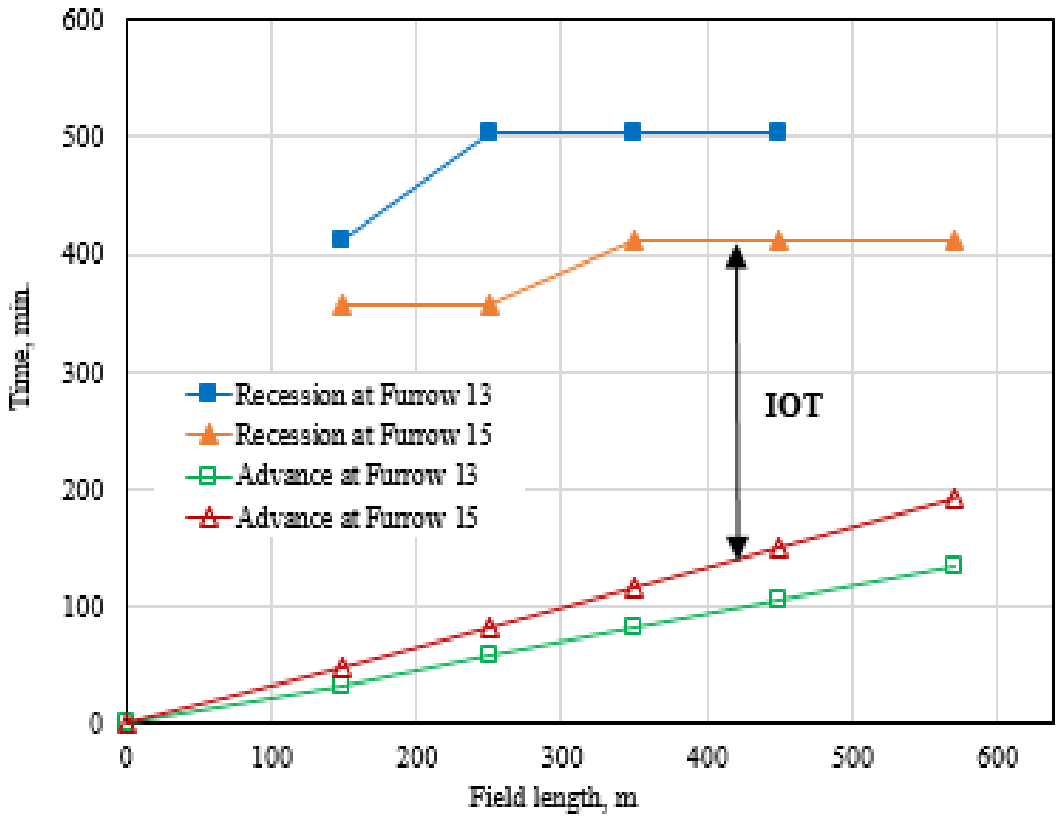

Figure 9.1 Plot of calculated advance, based on advance and recession data from the UAV for Furrows 13 and 15, in Border 1 of Field 2 for the irrigation event conducted on the 19-1-2018.

9.2.3. Estimation of border scale distribution uniformity (DU) from UAV data

Using IOTs estimated with the developed technique (Section 9.2.2), infiltrated water depths can be estimated by substituting the IOTs (Table 9.8) into Equation 8.13 (Table 9.9). Distribution uniformity (DU) can be estimated using Equation 2.2. The infiltrated water depth can be estimated for 1343 cells out of a total 1560 cells in this border. A count of one quarter of the available data is 336 cells. The average of the lowest quarter number of values from the available cells containing infiltrated water depths, is 58.7 mm. The average of all infiltrated water depths is 60.8 mm. So, the lowest quarter DU is equal to 96.6%.

As a result of the many missing cells at the farthest advance distance of 570 m and the total sample including many cells with greater IOTs, there is probably an overestimation of the DU in this case.

Table 9.9 A sample of calculated infiltrated water depths based on the estimated IOTs from UAV data in Border 1 of Field 2 for the irrigation event conducted on 19-1-2018.

Furrow no.	Estimated infiltrated water depths based on UAV data, mm.				
	x_1 = **150**	x_2 = **250**	x_3 = **350**	x_4 = **450**	x_5 = **570**
1	59	58	61	60	
2	59	58	61	60	
3	61	60	59	58	
4	61	60	60	59	
5	61	60	60	59	58
6*	63	63	63	62	
7	61	60	60	59	58
8*	60	59	63	62	
9	60	60	60	59	58
10	63	63	62	62	
11	59	60	59	58	56
12	59	60	59	58	56
13	61	63	62	62	
14	60	59	60	59	
15	59	58	59	58	56
16	60	59	60	59	
17	60	59	60	59	
18*	60	59	63	63	
19	60	59	60	62	
20*	61	61	63	63	
21	60	60	60	62	
22	60	59	62	62	
23	59	58	59	60	
24	59	60	59	60	

* Wheeled furrows

9.2.4. Estimation of application efficiency (AE) and requirement efficiency (RE) at the border scale

Based on the water flow rates measured at the field scale (Sections 6.6.1 and 7.4.1), the net applied volume for each Border (1 and 2) of Field 2 was calculated. Then, the net applied water depth in each border was calculated based on the area in each border. Table 9.10 shows the summary of the flow rate measurements at the field scale showing the net applied depth (mm) in Borders 1 and 2 of Field 2, for seven measured irrigation events.

The first event which is denoted with 0 (zero) was not measured but it was assumed that the applied depth was equal to the average applied depth from the measured events (1 to 7).

Table 9.10 Net applied water depth (mm) in each border

Irrigation event no.	Event date	Applied water depth in Border 1, mm	Applied water depth in Border 2, mm
0	30-10-2017	68.4*	n/a
1	15-12-2017	73.2	n/a
2	30-12-2017	69.6	n/a
3	11-01-2018	66.6	n/a
4	19-01-2018	59.7	n/a
5	26-01-2018	72.2	n/a
6	10-02-2018	77.0	81.2
7	17-02-2018	60.7	n/a

* Applied water depth proposed as an average of all other measured irrigation events.

To estimate AE% and RE% from total water volumes, in this case, an assumption was made that no deep drainage will occur until the field average SWD has been replenished. Therefore, if the depth of infiltration is less than this average SWD, there is no deep drainage, and the depth of water stored in the root zone will be equal to the depth of infiltration. If the depth of infiltration is greater than the field average SWD, then deep drainage will occur, and the amount of drainage will be equal to the depth of infiltration minus the SWD. In this case, the depth of water stored in the root zone will be equal to the SWD.

The applied irrigation depth for Border 1 of Field 2 is obtained from the inflow volume at the main supply pipe (logged by Starflow) from the commencement of the irrigation event, to the opening the top check gate of Field 2, divided by the border area. For example, for the irrigation event conducted on the 10-02-2018, the applied irrigation volume equals the inflow volume at the main supply pipe from the start of the irrigation event (10-02-2018 at 6:15 AM) to the opening of the top check gate of Field 2 (10-02-2018 at 10:20 AM), which is 27224.7 m^3 (see Table A-2 in Appendix). The applied irrigation depth for Border 1 in this event can be calculated by dividing the applied irrigation volume to Border 1 by the area of that border ((27224.7 / (640×312)) ×1000 = 136.3 mm. In this example, the infiltrated depth is 77.0 mm (Table 9.10) and is less than SWD of 130.73 mm (Table 7.4), so that the depth of water stored in the root zone is equal to the infiltrated depth, as explained in the assumption provided above. To estimate AE for this example the water depth stored in the root zone of 77.0 mm and the applied irrigation depth of 136.3 mm was substituted into Equation 2.1, as shown below:

AE% = (77.0 / 136.3) ×100 = 56.5%

To estimate RE for the same example, the water depth stored in the root zone of 77.0 mm, and the SWD prior to the event, 130.73 mm, were substituted into Equation 2.3, as shown below:

RE% = (77.0/ 130.73) × 100 = 58.9%.

Table 9.11 shows the summary of the irrigation performance indicators, AE and RE, for Border 1 in Field 2, for the irrigation events conducted in Season 2.

To calculate the SWD after the irrigation event on the 26-01-2018:

SWD (after the event of 26-01-2018) = (SWD before the event (9-02-2018)) + (ET_c_daily of 10-02-2018) – (Irrigation depth) – (Rainfall depth)

SWD (after the event of 26-01-2018) = 130.73 + 9.44 – 77.0 – 0.0 = 63.17 mm.

Table 9.11 Summary of AE and RE results for Border 1 of Field 2, for the irrigation events conducted during Season 2.

Event No.	Event date (Season 2)	Infiltrated depth in Border 1, mm	SWD of Border 1, mm	Volume applied to Border 1 from the main supply pipe till open the top check gate, m3	Depth applied to Border 1 from the main supply pipe till open the top check gate, mm	AE (%)	RE (%)
1	15/12/2017	73.2	32.17	27534.7	137.9	53.1	100
2	30/12/2017	69.6	77.11	28804.9	144.3	48.2	90.2
3	11/01/2018	66.6	101.97	30592.4	153.2	43.5	65.3
4	19/01/2018	59.7	113.72	24022.2	120.3	49.6	52.5
5	26/01/2018	72.2	123.06	26995.9	135.2	53.4	58.6
6	10/02/2018	77.0	130.73	27224.7	136.3	56.5	58.9
7	17/02/2018	60.7	112.25	25666.8	128.5	47.3	54.1

As shown in Table 9.11 the AE for irrigation events in Border 1 of Field 2 were relatively low and ranged between 43.5% and 56.5%. Large runoff volumes contributed to the low AE results. This runoff essentially resulted from large incoming flow rates in this FNSBO_Re system, which are necessary to overcome the reverse and near zero slopes along the field and to complete the advance phase in a shorter time, thus reducing the deep percolation losses at the top of the field. This table also shows low RE for most irrigation events (third to the seventh irrigation event, which ranged from 52.5% to 65.3%). This could have resulted from the low final infiltration rate characteristic of this field, and the relatively short opportunity time used in the irrigation practice for this field.

9.3. Conclusion

It is impractical to conduct evaluation measurements for all the furrows in the border, in the same way the sample of twelve furrows were measured, due to the massive effort and resources. Combining the UAV data to obtain IOTs for estimations of the infiltration characteristics in the twelve evaluated furrows provided a novel approach to obtain irrigation performance (uniformity) at the border scale. A technique to

interpolate IOT from UAV data was developed to overcome the shortage of UAV data. The limited number of UAV advance flight missions led to a shortage in the number of IOTs. The technique developed, which was based on advance sensor measurements, succeeded in raising the number of IOT data from 17% to 86%, in one example. It is believed that there was an overestimation of the DU due to the shortage of IOTs (which resulted from the shortage in recession measurements from the UAV) at the farthest part of the field.

AE and RE were estimated at the border scale based on the average net depth applied in each border, obtained from the flow rate measurements at the field scale, and the SWD, which was estimated from the simple water balance tool (IrriSAT). These estimations were based on the assumption that no deep drainage will occur until the soil water deficit has been replenished. Adoptiong of this technique meant the current study did not involve measuring soil moisture. The results showed low values of AE and RE in the FNSBO_Re system at the border scale, where results ranged from 43.5% to 56.5% for AE, and from 52.5% to 100% for RE. These low efficiency indices result from the considerable runoff losses due to the large applied inflow rates, and the low final infiltration characteristic of this soil.

Conducting soil moisture content measurements and determining other soil physical characteristics, such as the field capacity, would provide more reliable results for AE and RE in the border, instead of adopting this water balance approach.

CHAPTER TEN:

Factors Influencing Variability in FNSBO_Re systems

10.1. Introduction

Observations during the field trials indicated that there was significant variation in the behaviour of water flow between furrows across each irrigated border. This variation poses a challenge for the measurement and modelling techniques developed in this thesis. The speed of water advance provides a simple way to quantify the variation, and as described in the previous chapter, the water advance determines the infiltration characteristic and therefore the modelling predictions for each furrow. This chapter will discuss the factors that influence the variability of water advance in the FNSBO_Re irrigation system.

The discussion will cover the measurements conducted in both seasons but the focus will be on the measurements of Season 2. The measurements in Season 2 were specifically designed to provide a better understanding of the variability in diverting flow at the border scale through employing the UAV technique. The data in Season 2 is also of greater quality because of the efforts to avoid the mistakes and limitations associated with Season 1.

10.2. Investigation of factors influencing the variability of water advance

Compaction as a result of machinery traffic is known to have an impact on the speed of water advance. This section will investigate the other furrow characteristics some of which are related to the wheel traffic.

It is difficult to pick out the wheel compacted furrows in Figure 7.14 so the results have been separated into two plots; Figure 10.1 (a) with the data from the wheeled tracked furrows (WFs) and Figure 10.1 (b) for the non-wheeled tracked furrows (non-

WFs). These results represent the data from a single flight mission in the second border of Field 2. This irrigation event commenced at 5:25 AM on 11-1-2018, and the check gate opened at 9:42 AM. The flight mission commenced at 10:56 AM, 74 minutes after water started entering the furrows. The majority of infield operations are conducted using 12 m wide machinery and therefore the WFs follow a standard repeating pattern as follows: 6, 8, 18, 20, 30, 32, .. 294, and 296). In total there are 50 WFs and 250 non-WFs in the second border. As it is shown in Figure 10.1 (a) the front of the forward water advance had already reached the bottom end of the second border in 42% (21 out of 50) of WFs by the time of this first flight mission. In contrast, as shown in Figure 10.1 (b) there is no completed forward advance for any of the non-WFs at this flight mission.

The aim of field levelling preparations is to provide uniform field slopes both laterally across the field and down each furrow. Providing a zero slope across the width of the border between furrows should improve the uniformity of flows between furrows and therefore improve the uniformity of advance rates. However, a variation in the water advance (Figure 10.1) was evident in the data collected by the UAV technique. There appears to be a trend with those furrows with lower start numbers having faster advance rates. This trend may be a result of problems in the field levelling or cultivation practices or may be part of the field design to improve water drainage. Despite the cause, this variation in advance rate is an issue for irrigation management of these large borders.

The main trend observed in the data is that the fastest water advance is associated with WFs as compared with non-WFs. Although it is clear that WFs had the faster water advance compared with non-WFs, it is not obvious which factors cause that difference. The factors investigated include furrow elevations, cross-sectional areas, peak water depths and flow rates.

The following sections attempt to identify the reasons why the WFs have faster water advance and demonstrate (show) the relationship (or the correlation) between these factors and the water advance.

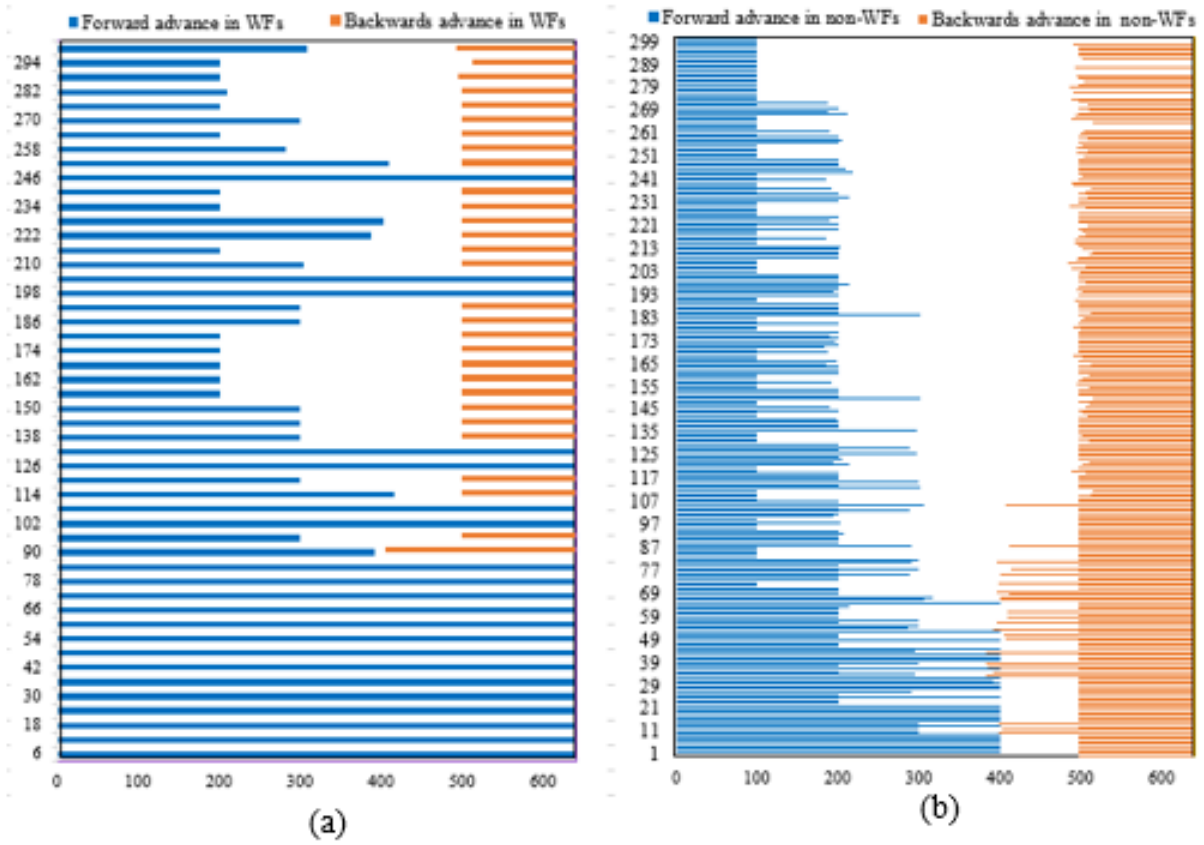

Figure 10.1 Water advance of wheeled tracked furrows (a) and non - wheeled tracked furrows (b), for the first flight mission at the second border of the Field 2. Irrigation event was held on 11-1-2018, the check gate opened at 9:42 AM, and the flight mission commenced at 10:56 AM

10.2.1. Furrow elevation

Elevations of WFs and non-WFs (along whole the field length, and near the divergence distance of the longitudinal slope along the field length (sill) were compared using the independent samples t-test. This test determines if there is any statistically significant difference ($p<0.05$) between WFs and non-WFs or if the variation is random. In other words, the t-test will show the impact of machinery operations on the furrow elevations. The null hypothesis is that there is no statistically significant difference between the WFs and non-WFs elevations. T-test calculations were conducted via IBM SPSS Statistics 25. Application of this t-test requires an assumption of equal variances between the two sample groups, which is supported through the application of the Levene's test for equal variance. A Levene's test P value of < 0.05 indicates that the variances of the two populations are different and any differences are unlikely to have occurred by chance while a P value of > 0.05 indicates that the variance of the two populations are equal.

Table 10.1 shows the independent-sample t-test (equal variances assumed) for all elevation data along the whole length of the non-WFs and WFs located in the first and second border of Field 2, and the second border of Field 3. For the first border along the whole length of the Field 2, an independent-sample t-test was conducted to compare the elevations of the WFs with non-WFs. The non-WFs elevation data as the first variable group of t-test comparison, included the surveyed furrows numbered 12, 13, 14, 15, 16, 17, 19, 21, 22, 23, and 24. The WFs elevation data as the second variable group included the surveyed furrows 18 and 20. The Levene's test, with a P value = 0.816 greater than $\alpha = 0.05$ indicated that the variances of the two group are equal. Thus the test is completed with equal variances assumed. Here, the independent-sample t-test results showed that there is no statistically significant difference between the WF and non-WF elevations. Here the null hypothesis had been rejected because the one tailed P-value (0.407) is greater than α (0.05). Although the mean of the WFs elevations (0.235 m) is lower than the non-WFs elevations (0.242 m), statistically, there is no significant difference between the elevations of the WFs and non-WFs. The one tailed P value was adopted for this comparison because it was hypothesised that elevation of non-WFs is greater than wheeled furrows.

Similarly, for the second border along the whole length of the Field 2, an independent-sample t-test was conducted to compare the elevations of the WFs with non-WFs. This time the analysis included 24 sequential furrows numbered 1 to 24 which included 4 WFs (6, 8, 18, and 20).

Table 10.1 Independent-sample t-test (equal variances) for elevation data of the non-WFs and WFs, located in the first and second border of Field 2, and the second border of Field 3.

	Field 2				Field 3	
	Border 1		Border 2		Border 2	
	Non-WF	WF	Non-WF	WF	Non-WF	WF
Mean (m)	0.242	0.235	0.046	0.016	0.9559	0.9639
Standard deviation	0.14507	0.14518	0.1307	0.1275	0.2595	0.2711
Observations	137	28	277	58	372	70
Degree of freedom	163		333		440	
Levene's test* P-Value	0.816		0.493		0.746	
t value	0.236		1.59		-0.234	
P-value (one-tail)	0.407		0.0565		0.4075	
Result	Not Significant		Not Significant		Not Significant	

* The Levene's test indicates whether the variance of two groups are equal where a P value of < 0.05 indicates that the variances are not equal.

The Levenne's test shows that the P value of 0.493 is greater than α (0.05) and the variances of the two group are equal. Thus, it is valid to apply the t-test based on equal variances assumed. The summary of the t-test results of the second border of Field 2 (Table 10.1) showed that there is no statistically significant difference between the WFs and non-WFs' elevations where the P-value (0.0565, one tailed) is greater than α (0.05). However, this difference does become significant if we adopt the level of significant was (α = 0.1).

For the second border along the whole length of the Field 3, an independent-sample t-test was conducted to compare the elevations of the WFs with non-WFs (Table 10.1). This test considered the surveyed furrows from number 3 to 13 inclusive, where numbers 6 and 8 were the WFs. The Levenne's test P value of 0.746 is greater than α (0.05) and therefore the variances of the two group are equal and so the t-test can be applied. The summary of the t-test results of the second border showed that there is no statistically significant difference between the WFs and non-WFs' elevations where the P-value (0.4075, one tailed) is greater than α (0.05).

As shown in Table 10.1, the means of WFs elevations were 7 and 30 mm lower than the non-WFs in Border 1 and 2, respectively in Field 2, while in Border 2 of Field 3 WFs were 8 mm higher than the non-WFs. It would be expected that the machinery traffic would deform and compact the soil such that the furrow bed would be lower in the WFs compared to the non-WFs. This was observed in two out of the three measured borders. All t-test results (Table 10.1) showed that there are no statically significant difference between the WFs and non-WFs' elevations in any of the three tested borders.

One-way ANOVA analysis was used to compare the elevations of the non-WFs of each border, to determine if there is any statistically significant difference ($p<0.05$) between them. For Border 1 of Field 2, the one-way ANOVA results showed that the average of all furrows are not significant where the P value (0.956) is greater than α (0.05). This means, statistically, that the average elevations of all furrows are the same. Since the average of all furrows are the same there was no value in a comparison between different furrows. Similarly, for Border 2 of Fields 2 and 3, the one-way ANOVA results also showed that there is no statistically significant difference among the elevations of the non-WFs' themselves where P-values (1.000, and 0.944, respectively) were greater than α (0.05).

The surveying showed that the first 50 m from the furrow entrance of Field 2 and 3 had slight positive slopes followed by negative slopes for the rest of the length of the field. Because of the larger impact of this positive (reverse) slope on controlling the water advance rate uniformity in the furrows, t-tests were used to compare the elevations of the WFs and non-WFs at the closest available distance to the sill positioned approximately 50 to 57 m from the furrow entrance (Table 10.2). The sets of the tested furrows are the same as mentioned above (Table 10.1). For Border 1 of Field 2, an independent-sample was conducted to compare the elevations of the WFs and non-WFs. The closest available elevations measurements were at about 57 m from the furrow entrances. As shown in Table 10.2, the t-test result showed that there is no statistically significant difference between the furrow elevations (P-value one tailed (0.124) is greater than α (0.05)). For the Border 2 of Field 2, an independent-sample t-test was conducted to compare the elevations of the WFs and non-WFs. The closest available elevations from surveying measurements at the sill were located

approximately 54 m from the furrow entrances. As shown in Table 10.2, the t-test result showed that there is a statistically significant difference between the furrow elevations at the sill (P-value one tailed (0.000) is smaller than α (0.05)). For Border 2 of Field 3, an independent-sample t-test was conducted to compare the elevations of the WFs and non-WFs. The closest available elevations measurements were at about 50 and 56 m from the furrow entrances. The summary of the t-test results (Table 10.2) showed that there is no statistically significant difference between the WF and non-WF elevations where the P-value (0.1385, one tailed) is greater than α (0.05).

Table 10.2 Independent-sample t-tests (equal variances) for elevation data of the non-WFs and WFs at the sill, located in Border 1 and 2 of Field 2, and Border 2 of Field 3.

	Field 2				Field 3	
	Border 1*		Border 2**		Border 2***	
	Non-WF	WF	Non-WF	WF	Non-WF	WF
Mean (m)	0.3646	0.38	0.1949	0.1550	1.1747	1.1865
Standard deviation	0.1706	0.000	0.01223	0.01816	0.0198	0.0176
Observations	10	2	20	4	22	4
Degree of freedom	10		22		24	
Levene's test* P-Value	0.107		0.375		0.569	
t value	-1.228		5.524		-1.112	
P-value (one-tail)	0.124		0.000		0.1385	
Result	Not Significant		Significant		Not Significant	

* The Levene's test indicates whether the variance of two groups are equal where a P value of < 0.05 indicates that the variances are not equal.

The means of WF elevations close to the sill were 15.4 and 11.8 mm higher than the non-WFs in Border 1 of Field 2 and Border 2 of Field 3, respectively. Whilst the mean of the WF elevations in Border 2 of Field 2 was 39.9 mm lower than the non-WFs. So, there were varying trends, where in some borders the WFs have lower elevation compared with the non-WFs while in others they have the higher elevation. The higher elevation in the WFs comparing with the non-WFs differs from the general expectation regarding the impact of machinery operations on the furrow elevations. For example, Grabham (2012) found that the elevation in the WFs entrance were 16 to 18 mm lower than the non-WFs, and statistically a significant difference between WFs and non-WFs, in all tested borders.

Figure 10.2 and Figure 10.3 shows the relation between the non-dimensionalised water advance in the furrows and furrow elevations of the same furrows located in Border 1

and 2, respectively, of Field 2. The data of Figure 10.2 were gathered from the elevation surveys close to the sill of twelve adjoining furrows located in Border 1 of Field 2, and the corresponding UAV advance data from three available irrigation events conducted on 11-01-2018, 19-01-2018, and 26-01-2018. The data of Figure 10.3 was gathered from the elevation surveys close to the sill of twenty four adjoining furrows located in Border 2 of Field 2, and the corresponding UAV advance data from four available irrigation events conducted on 30-12-2017, 11-01-2018, 10-02-2018, and 17-02-2018. The non-dimensionalised values were determined by dividing furrow elevation and water advance by the mean of the values from the same event. Figure 10.2 and Figure 10.3 show weak correlations (R^2=0.013 and R^2=0.2001, respectively) between the advance and the furrow elevation which means that the furrow elevation does not have a strong impact on the advance variability between furrows.

This weak correlation disagrees with Grabham (2012), where he found that the furrow elevation is the governing factor that reflects the variability in the water advance between WFs and non-WFs. He considered that improving the performance within borders was "somewhat limited to maintenance of furrow elevation". In addition, De Sousa et al. (1995) used a simulation approach to show that for near zero slope furrows that receive water from a common supply channel, the elevation of the furrow entrance has a significant impact on DU. They found that DU decreased from 91% to 43% when the variation in the furrow entrance expressed by the standard deviation (SD) of the entrance elevations changed from SD = 0 mm to SD = 30 mm. (De Sousa et al. 1995) also concluded that the impact on DU is higher for longer furrows compared to shorter furrows.

One key difference between these previous studies and the current work is the design of the field. Both Grabham (2012) and De Sousa et al. (1995) studied the impact of the furrow elevation at the furrow entrance on a level field while this study focusses on a layout which includes the sill at some distance from the entrance as an important design feature. This difference could be insignificant where the sill is positioned at a relatively short distance from the furrow entrance, but for the fields studied this sill was located at a distance of 50 m down a 640 or 1340 m long field. This sill is also less prone to erosion, which may cause changes in furrow shape, compared to the furrow entrance.

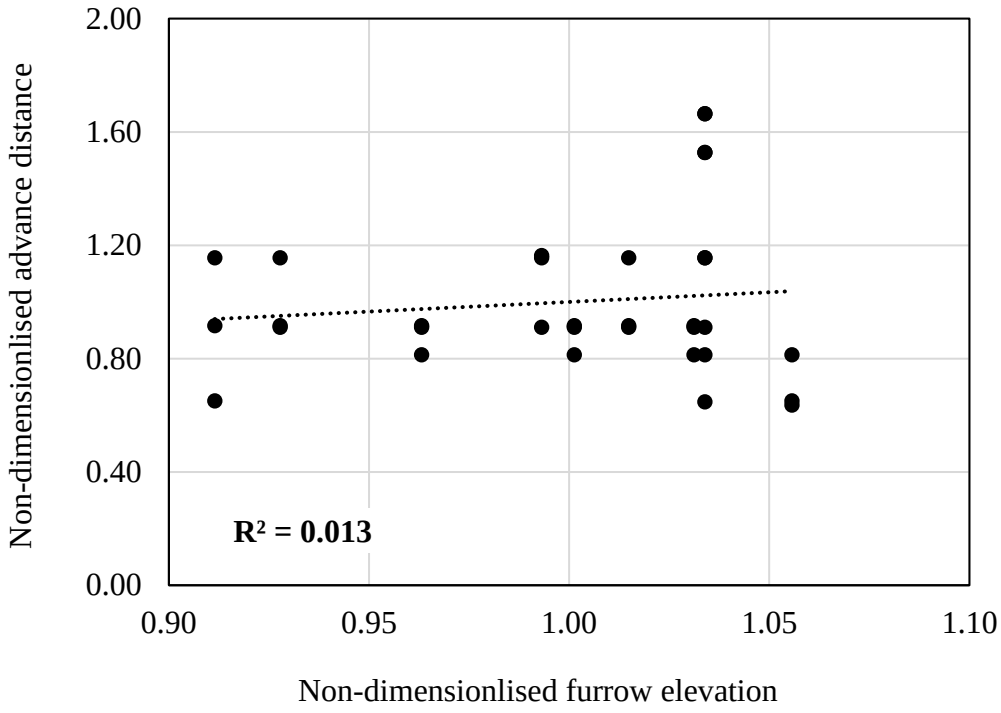

Figure 10.2 The relationship between the non-dimensionalised water advance and the non-dimensionalised furrow elevations in Border 1 of Field 2.

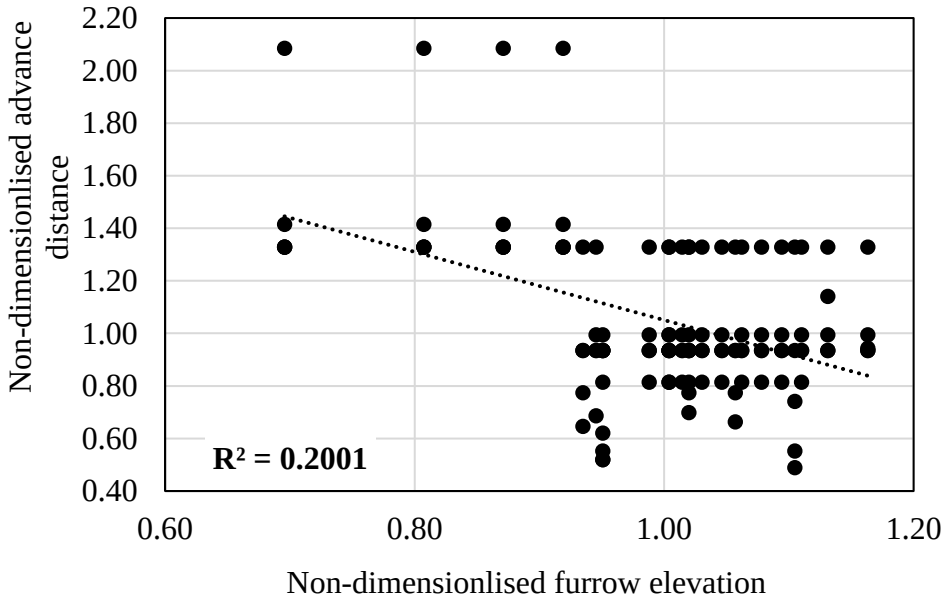

Figure 10.3 The relation between the non-dimensionalised water advance and the non-dimensionalised furrow elevations in Border 2 of Field 2.

Based on the analysis presented above, it can be concluded that furrow elevation is not the dominant factor affecting water advance rate and its variation. To explain the possible factors behind the water advance variation, a number of variables will be tested by studying their relationship with the advance and determining whether they are contributing to this variation. Peak water depth, cross-sectional area, and flow rate in the furrow are the variables that will be examined. The measurements of these variables were conducted at or around the sill due to its importance for this particular field design.

10.2.2. Peak water depths

Peak water depth measurements at about 52 m from the furrow entrance were analysed using the independent-sample t-test to determine if there is any statistically significant difference ($p<0.05$) between the WFs and non-WFs (Table 10.3). This independent-sample t-test encompassed peak depth measurements from four events (11-1-2018, 19-1-2018, 10-2-2018, and 17-2-2018) in Border 1 of Field 2 (Figure 7.23). A total of 36 adjacent furrows (No. 13 - 48) were measured on events conducted on 11-1-2018, and 19-1-2018, and 24 adjacent furrows (No. 13 - 36) on the 10-2-2018, and 17-2-2018. As a result this data includes 20 WFs and 100 non-WFs. The results of this test (Table 10.3) for the first border of Field 2 show a statistically significant difference between the peak water depths of WFs and non-WFs (P-value one tailed (0.005) is smaller than α (0.05)).

A similar analysis was conducted on the peak water depths measurements collected during three irrigation events 26-01-2018, 10-2-2018, and 17-2-2018 from Border 2 of Field 2 (Figure 7.24). These measurements include 12 adjacent furrows (No. 1 – 12) from the event on the 26-01-2018, and 24 adjacent furrows (No. 1 – 24) from the events on the 10-2-2018 and 17-2-2018. The resulting data includes 10 WFs and 50 non-WFs. The results from Border 2 (Table 10.3) demonstrate a statistically significant difference between the peak water depths of wheeled and non-wheeled furrows (P-value one tailed (0.0015) is smaller than α (0.05)), which is in agreement with Border 1.

Table 10.3 Independent-sample t-tests, for peak water depth measurements of the non-WFs and WFs, located in the first border and second border of Field 2.

	Border 1*		Border 2**	
	Non- WF	WF	Non- WF	WF
Mean (m)	0.1091	0.1210	0.1121	0.1328
Standard deviation	0.0230	0.0164	0.0198	0.0147
Observations	100	20	50	10
Degree of freedom	35.8		58	
Levene's test P-Value	0.046		0.344	
t value	-2.737		-3.129	
P-value (one-tail)	0.005		0.0015	
Result	Significant		Significant	

Figure 10.4 and Figure 10.5 show the relationship between the non-dimensionalised water advance from UAV flight missions and peak water depth at the sill of the same furrows located in Border 1 and 2, respectively, of Field 2. The data for Border 1 (Figure 10.4) was gathered from irrigation events conducted on 11-01-2018, and 19-01-2018. Similarly the data for Border 2 (Figure 10.5) was gathered from irrigation events conducted on 10-02-2018, and 17-02-2018. The non-dimensionalised values were determined by dividing peak water depth and water advance by the mean of the values from the same event. Both Figure 10.4 and Figure 10.5 show weak correlations (R^2= 0.2433 and R^2= 0.2917, respectively) between the advance and the peak water depth which means that the peak water depth does not explain the advance variability between furrows.

These results agree with the relationships between furrow elevation and water advance (Figure 10.2 and Figure 10.3), where peak water depth and elevation surveying data should be directly related and inversely proportional if the elevation of the water surface is consistent between furrows.

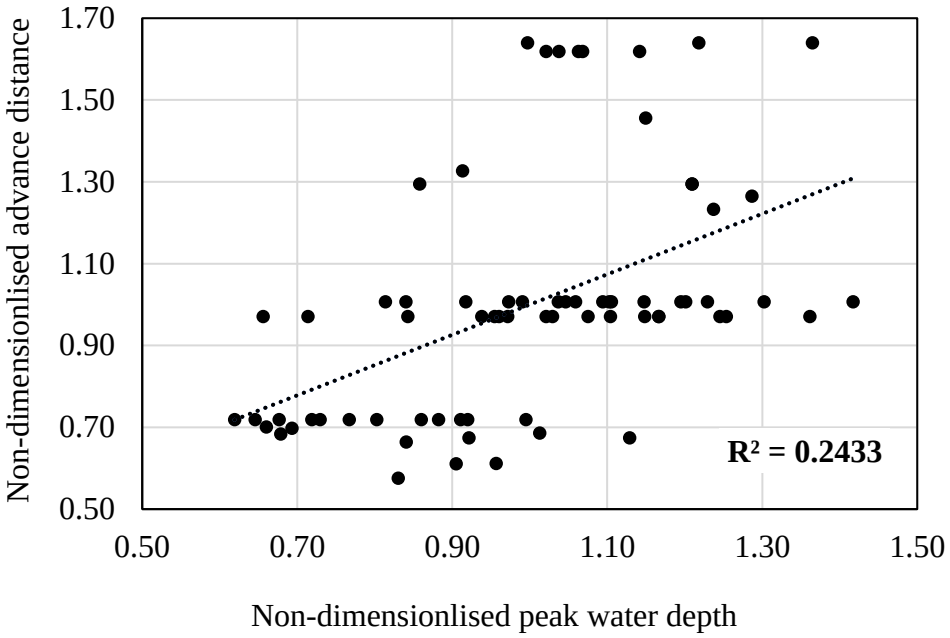

Figure 10.4 The relationship between the non-dimensionalised water advance and the non-dimensionalised peak water depth at the sill in Border 1 of Field 2.

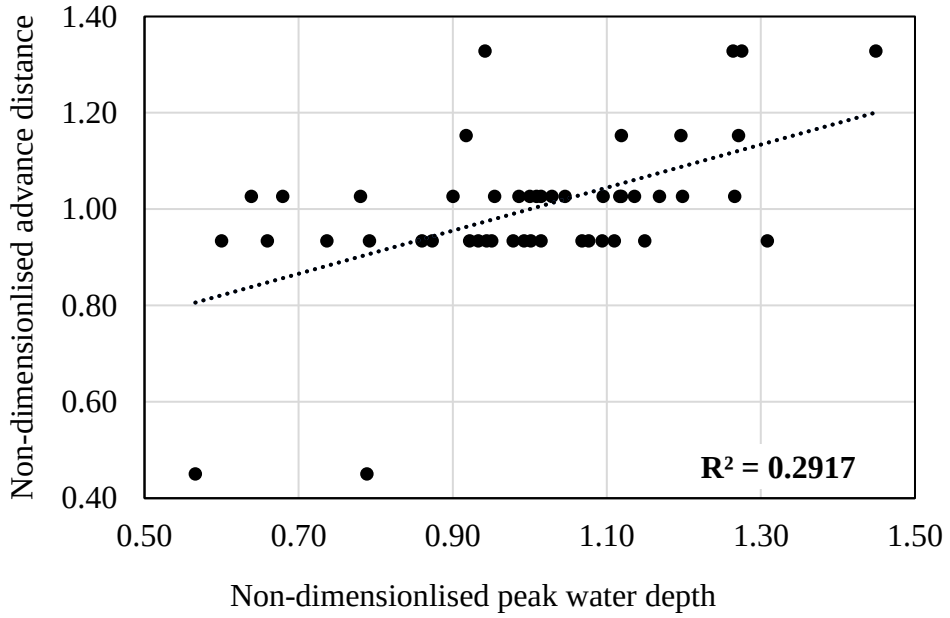

Figure 10.5 The relationship between the non-dimensionalised water advance and the non-dimensionalised peak water depth at the sill in Border 2 of Field 2.

10.2.3. Cross-sectional area

Cross-sectional area of flow was collected at a location close to the sill (about 50-54 m from the furrow entrance) and at a similar location to the peak water depths. This data was analysed using an independent-sample t-test to determine if there is any statistically significant difference ($p<0.05$) between cross sectional areas of the WFs and non-WFs. Measurements were collected from 12 adjacent furrows (No. 13 - 24) from two events (10-1-2018 and 18-1-2018 (Figure 7.5)) resulting in a total of 4 WFs and 20 non-WFs. The t-test results for the first border (Table 10.4) showed a statistically significant difference between the cross-section areas of WFs and non-WFs (P-value one tailed (0.000) is smaller than α (0.05)).

Table 10.4 Independent-sample t-test (equal variances assumed*) for cross-sections areas of the non-wheeled furrows and wheeled furrows, located in Border 1 of Field 2.

	Non- WF	WF
Mean (cm^2)	853.59	1172.47
Standard deviation	66.35	56.26
Observations	20	4
Degree of freedom	22	
Levene's test P-Value	0.808	
t value	-8.947	
P-value (one-tail)	0.000	
Result	Significant	

As shown in Table 10.4, the mean cross-sectional areas of WFs is 27.2% higher than the non-WFs. This can be attributed to the machinery movement which causes furrow compaction and results in a change in the furrow shape. Grabham (2012) found that on average the cross-sectional area on the WFs was 12% greater than non-WFs, and attributed that to an average 17 mm lower elevation in the WFs. However, the measurements collected in Border 1 show that the elevation of the WFs is slightly higher than the non-WFs (Table 10.2) and hence this increase in cross sectional area is not simply explained by wheel traffic making the furrow deeper. Instead, it is proposed that the wheel changes the shape making the furrow wider.

UAV advance data was collected from this same border (Border 1 of Field 2) during the two events on the 11-01-2018 and 19-01-2018. Figure 10.6 shows the relationship

between the non-dimensionalised water advance and cross-section area of these same 12 furrows across the two events. The non-dimensionalised values were determined by dividing each value of cross-section area and water advance by the mean of the values from the same event. Figure 10.6 shows a good correlation (R^2=0.7038) between the advance and the cross-section area which means that the cross-sectional area has an important impact on the advance variability between furrows. In other words, a variability in water advance can be predicted by the cross-sectional area of the furrows. Although measuring the cross-sectional areas is not an easy task compared with other measurements such as furrow elevation, it provides far more useful information regarding the likely variability in water advance.

The analyses presented in this chapter have indicated that other factors such as furrow cross section could combine with furrow elevations regarding the water advance rate.

Less obstacles to the water stream in the furrows are expected in the WFs comparing with the non-WFs. There should be fewer soil clods and plant remains that cause blockage to the flow in the WFs compared with the non-WFs.

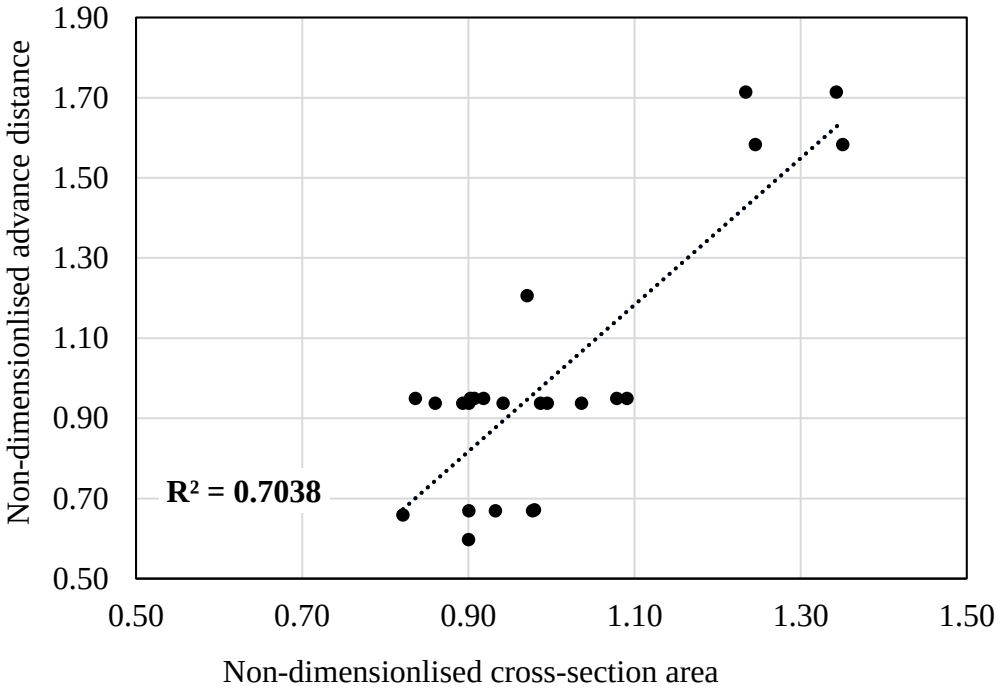

Figure 10.6 The relationship between the non-dimensionalised water advance and the non-dimensionalised cross-section area of the same furrows.

10.2.4. Flow rates of furrows

Furrow flow rate measurements were collected between 55 to 57 m from the furrow entrances to coincide with the location of the sill and the depth and cross-sectional area measurements. These measurements were analysed using an independent sample t-test to investigate the behaviour of the WFs and non-WFs and the relationship with advance (Table 10.5). For the Border 1, this analysis considered the 12 furrows (No. 13 - 24) which included 2 WFs. The flows were collected from all irrigation events in these same furrows. The results of the t-test for Border 1 (Table 10.5) showed a statistically significant difference between the furrow flow rate measurements between the WFs and non-WFs (P-value one tailed (0.000) is smaller than α (0.05)). The mean of the flows of the WFs was almost double that of the non-WFs (0.01140 m^3/s compared with 0.00579 m^3/s).

Regarding Border 2 of Field 2, the independent-sample t-test considered 12 adjacent furrows (No. 1 – 12) with flows collected over the entire season. The t-test for Border 2 (Table 10.5) showed a statistically significant difference between the flow rates of WFs and non-WFs (P-value one tailed (0.000) is smaller than α (0.05)). The mean flow rate in this border exhibited a similar relationship between the WFs and non-WFs as the first border. The mean flow rate of the WFs of 0.01839 m^3/s is much higher than the non-WFs of 0.00656 m^3/s. This variation in the furrow flow rates between WFs and non-WFs agrees with the results of Grabham (2012) which found that the average flow rates in the WFs was 37% greater than the non-WFs.

Table 10.5 Independent-sample t-test for furrow flow rate measurements of the non-WFs and WFs, located in Border 1 and 2 of Field 2.

	Border 1*		Border 2**	
	Non- WF	WF	Non- WF	WF
Mean (m^3/s)	0.00579	0.01140	0.00656	0.01839
Standard deviation	0.00178	0.00287	0.00252	0.00511
Observations	57	12	99	20
Degree of freedom	67		20.9	
Levene's test P-Value	0.129		0.000	
t value	-8.862		-10.096	
P-value (one-tail)	0.000		0.000	
Result	Significant		Significant	

Figure 10.7 shows the relation between the non-dimensionalised water advance and non-dimensionalised flow rate in these furrows. The data of this figure represents data collected from all irrigation events across both borders of Field 2. Figure 10.7 shows a moderate correlation (R^2=0.6477) between the advance and the flow rate, which means that the flow rate has an important impact on the advance variability between furrows.

Although the flow rate is an essential component of the evaluation of the surface irrigation systems, conducting these flow rate measurements for large numbers of furrows is a complex and time consuming process, and is more difficult compared with furrow elevation and cross-sectional area.

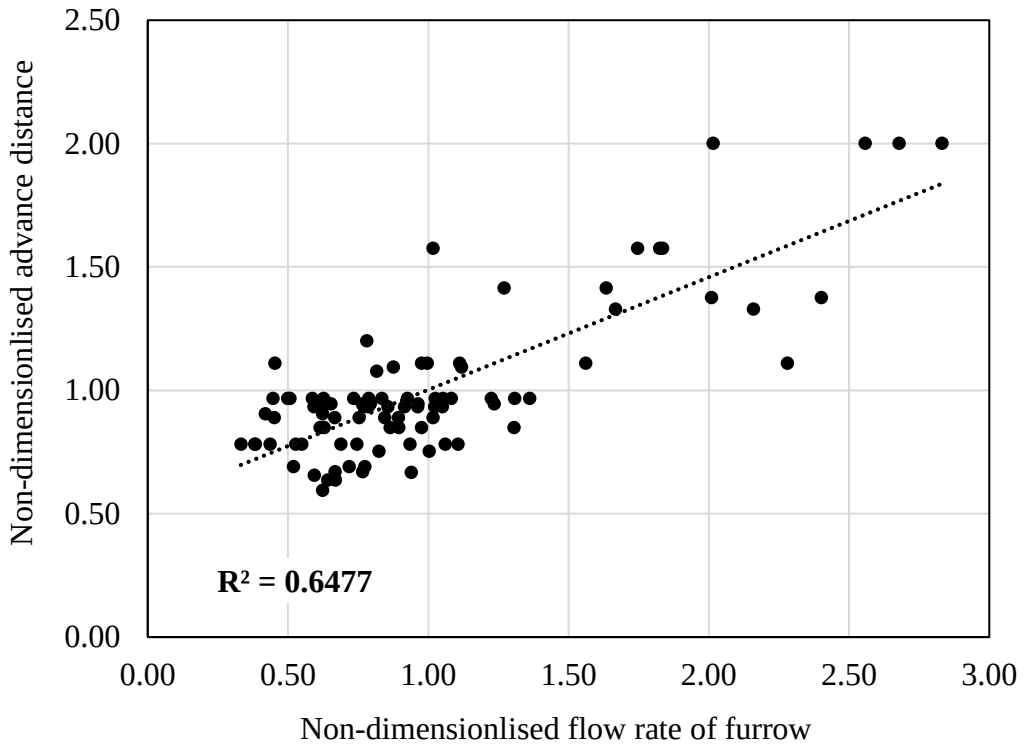

Figure 10.7 The relationship between the non-dimensionalised water advance and the non-dimensionalised flow rates of the same furrows.

10.2.5. Infiltration

It is expected the higher water advance rate in WFs compared with non-WFs is partly the result of changes in infiltration associated with soil compaction. Soil compaction

leads to a reduction in the infiltration capacity, which should result in faster advance rates. Unlike the previous factors, the estimated infiltration rates are dependent on field measurements of water advance, flow rate, and cross-sectional area. The following analysis is presented in order to examine the strength of the relationship between water advance and infiltration compared to the other factors.

Infiltration parameters of each furrow were estimated using SISCO, based on the field measurements conducted on 10-02-2018 in Border 1 of Field 2 (Table 8.5) in 12 adjacent furrows (No. 13 – 24). The accumulated infiltrated depths in each furrow were estimated using an opportunity time of 200 minutes using Equation 8.13. The infiltration depths were analysed using the same methodology as described for the other factors. The independent-sample t-test showed that there is no statistically significant difference between the accumulated infiltrated depths of WFs and non-WFs where the P-value (0.2675, one tailed) is greater than α (0.05). Unexpectedly, the mean of accumulated infiltrated depths of the WFs is higher than the non-WFs.

Table 10.6 Independent-sample t-test results for infiltration depth at 200 minutes between the WFs and non-WFs located in Border 1 of Field 2.

	Non- WF	WF
Mean (mm)	53.83	61.59
Standard deviation	15.89	12.73
Observations	10	2
Degree of freedom	10	
Levene's test P-Value	0.742	
t value	-0.643	
P-value (one-tail)	0.2675	
Result	Not Significant	

Figure 10.8 shows the relation between the non-dimensionalised water advance and the non-dimensionalised accumulated infiltrated depth in the same furrows. The data gathered for this figure include the accumulated infiltrated depths calculated at a constant time (200 minutes) and the infiltration parameters obtained by the SISCO model for the event conducted on 10-02-2018 in Border 1 of Field 2 (Table 8.5), and UAV advance data collected from three events (11-01-2018, 19-01-2018 and 26-01-2018) conducted at the same border. The non-dimensionalised values were determined by dividing each value of accumulated infiltrated depth and water advances by the

mean of the values from the same event. Figure 10.6 shows a weak correlation between the advance and the accumulated infiltrated depth which means that the accumulated infiltrated depth does not have a strong relationship with the advance variability between furrows (R^2=0.0022). In other words, a variability in water advance cannot be predicted by the infiltration characteristics.

As explained in the Section 8.2.4, when the initial infiltrated depth dominates the total accumulated infiltrated depth (Figure 8.12), the variability in the water advance has less significance, especially when the advance phase is short as for the events measured. Based on these results, it can be concluded that the infiltration characteristics do not have a dominating impact on the irrigation process as expected in conventional irrigation systems.

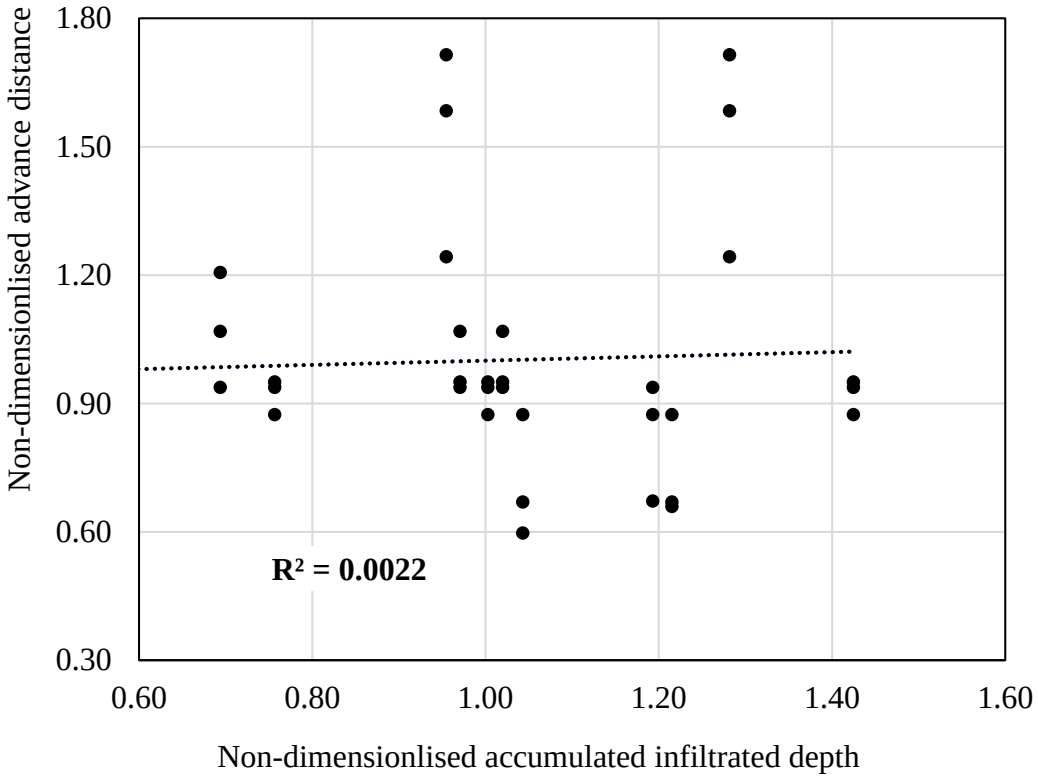

Figure 10.8 The relation between the non-dimensionalised water advance and the non-dimensionalised accumulated infiltrated depth in the same furrows.

10.2.6. Factors influencing performance indices

Water advance measurements at the border scale (from UAV data) succeeded in capturing the impact of the variation in diverting flow between furrows in the FNSBO_Re irrigation system (see Chapter 9). Also, water advance measurements are considered a vital piece of data used to evaluate the infiltration characteristics which are required for modelling surface irrigation (see Chapter 8). As a result, water advance rate is a vital parameter in determining the irrigation performance of these surface irrigation systems. Previously, sections 10.2.1 to 10.2.5 have highlighted the factors that influence the variability of water advance in this FNSBO_Re irrigation system. Therefore, it can be concluded that factors such as furrow cross sectional area, and furrow flow rates, which were correlated with water advance also have a strong influence on the irrigation performance.

10.2.7. Conclusion

A number of factors including elevation, peak water depth, cross sectional area, flow rate, and infiltration were statistically examined using an independent-sample t-test to compare values between WFs and non-WFs. These tests showed that the wheel traffic has a clear impact on some of these factors, most notably the cross-sectional area and flow rate. It was clear that there is a difference in the water advance between WFs and non-WFs, but it is not obvious as to which of these factors have a significant impact on the advance. The strength of the correlation between these factors and the advance rate was investigated by non-dimensionalising each quantity and then determining the R-squared value. The correlation results showed that the studied aspects impact the advance with different degrees of significance.

Based on previous studies, the furrow elevation was expected to have the largest impact and therefore a high correlation with the water advance, and a large impact on irrigation performance through the distribution uniformity. Unexpectedly, it was found that the furrow elevation and peak water depth have an insignificant impact on the water advance. Infiltration characteristics, expressed as a infiltrated depth at a single opportunity time also was found to have an insignificant impact on the water advance. Both the cross-sectional area and flow rate were found to have strong correlations with the water advance, and thus have a significant impact on the irrigation performance.

Therefore, it can concluded that in the current field, the variation in irrigation performance across the border is governed by the shape of each furrow and the variation in flow rate. The impact of the infiltration process on the irrigation performance was somewhat limited to the initial infiltration value (or a crack fill volume).

Commonly, growers believe that the elevation is the main factor governing the irrigation performance, and so they adopt a sill for instance, as a practice to improve the performance through reducing the advance variability. Perhaps, because the current studied field has good land grading (elevation), other factors such as furrow shape and flow rate have a larger impact on the advance variability. Improving the performance of this irrigation system can be achieved by reducing the difference between the dimensions of the non-WFs and WFs. Using narrower tyres on the agricultural machinery could be an appropriate way to reduce the difference between non-WFs and WFs, but this would require field measurements to prove the benefits of such a practice.

Examining these aspects statistically (using a t-test) and determining the degree of their correlations with the water advance provides an understanding as to which factors have a significant impact on the irrigation performance through affecting the advance rate. This analysis also provides guidance as to what should be measured in the future to characterise the variability in performance. The significance of each aspect and the capability to measure it at the large scale determines which aspects could be adopted for routine field measurement. Based on the current results, cross-sectional area of the furrow appears to be the most valuable and appropriate measurement for FNSBO_Re systems

.

CHAPTER ELEVEN:

A Technique to Evaluate FNSBO_Re systems

11.1. Introduction

This chapter will discuss the measurement techniques applied in this study including surveying and geometry measurements, and irrigation evaluation measurements. The outcomes of this discussion will inform the suggested procedure to conduct these measurements in future studies. Secondly, this chapter will discuss the developed analysis techniques at the furrow and border scales to evaluate this system. The main purpose of this chapter is to describe the new methodology to measure and evaluate FNSBO_Re systems.

11.2. Discussion of measurements

Field measurements were conducted in a number of irrigation events throughout two seasons to evaluate two fields characterised with near zero slope furrowed border irrigation systems with common water supply (FNSBO_Re). The measurements include the components which are required to apply the volume balance concept, and other important measurements that determine the geometry of the field. The discussion will cover the measurements conducted in both seasons but will focus on the measurements of Season 2, because of the limitations with Season 1 explained in Section 5.7.

11.2.1. Field surveying

Determining the longitudinal slopes down the furrows and the vertical separation between adjoining borders is important to understand the irrigation process and the hydraulic interaction behaviour within and between borders in FNSBO_Re systems. Such measurements were collected in Field 2, as described in previous chapters.

The relationship between the non-dimensionalised water advance in the furrows and furrow elevations showed that the furrow elevation does not affect the advance

variability between furrows. However, this is contrary to De Sousa et al. (1995) and Grabham (2012), where they considered that the elevation at the entrance as a governing factor influencing the advance variability between furrows, and hence also having a significant impact on the irrigation performance. In this study, it was found that the cross-sectional area and the flow rate of the furrow were the significant factors influencing the water advance. This does not undermine the importance of the elevation factor in governing the irrigation performance. The fields studied in this research are well graded and have minimal differences in elevation between furrows meaning that other factors, such as cross-sectional area are more significant. It is proposed that differences in furrow elevation have a larger impact on field performance in circumstances with poor field levelling.

In this study, the elevation surveying covered a small numbers of furrows from each border. Between 13 and 24 adjoining surveyed furrows out of about 300 and 180 furrows of the borders of Field 2 and 3, respectively, were sampled in this study. This could be deemed poor in representing these kind of irrigation systems which are characterised by variability in diverting water to the furrows and in the water advance. However, conducting the elevation survey for all furrows along the whole length could be a difficult task. For the FNSBO_Re system the most important location to capture in terms of hydraulic performance are the sill, where the furrow transitions from a positive to negative grade. Therefore, it is suggested that future field measurements capture the sill elevation in a large number of furrows (perhaps 25%); and include the elevation survey along the entire field length for a small numbers of furrows (e.g. 6 to 12 furrows).

In this study, all surveyed furrows in both fields were located close to one side of each border. As a result it is possible that the elevation measurements fail to properly represent the variation across the border. This problem can be noticed in Figure 10.1 where there appears to be a trend in the water advance rates across the border in the low numbered furrows having faster advance rates than the other furrows. As a result, it is suggested that future studies should select the furrows based on observed variation in the advance rates across the border. A simple approach to select furrows from different locations in the border and to conduct the elevation surveys and other measurements will be explained in Section 11.2.8.

In this study, selecting furrows at the side of the borders for surveying and the other measurements, was for ease of accessibility. Measurements in the middle of the border when the soil was wet, during or following irrigation, or in later stages of crop growth would have been impractical. The selection of adjoining furrows for these measurements was to provide a representative sample capturing random variability and to capture the pattern of non-WFs and WFs. Manual selection of individual furrows might have resulted in some form of bias towards a particular type of furrow. The measurement collecting should capture the advance rate variability between furrows resulting from machinery traffic.

11.2.2. Furrow geometry

Simple furrow cross-sectional area measurements were conducted by measuring top width, middle width, bottom width, and the maximum depth of the furrows at four intervals along twelve adjoining furrows in Border 2 of Field 3. These measurements reflect the standard dimensions used by common simulation models to describe the furrow shape. Furrow cross-sectional area measurements were conducted at a higher level of accuracy using a profile meter near the sill for twelve adjoining furrows located in Border 1 of Field 2.

The significant correlation between the cross-sectional areas and the water advance discussed in Chapter 9 means that it might be advisable to conduct these measurements in a larger number of the furrows of each border with a good level of accuracy. Conducting these measurements across the entire border is impractical considering the large numbers of furrows in each border (e.g. 300 furrows in each border of Field 2). Furthermore, the measurement process requires more time and effort compared with elevation surveying. Because of the hydraulic importance of the sill and it being less subject to change in furrow shape due to erosion compared with the furrow entrance, it could be sufficient to conduct these measurements only at the sill instead of many intervals along furrows. This single measurement in each furrow is supported by the fact that the values of the cross-sectional areas did not change significantly along the field length during measurements in Border 2 of Field 3 in Season 1, 2017. Selection of the furrows that can represent the whole border will be explained in Section 11.2.8.

11.2.3. Flow rate measurements at field scale

Flow rate measurements at the field scale can be used to estimate the net water volume and depth applied to each border. Flow measurements are also crucial in the estimation of AE and RE for the border scale.

Focussing on Season 2, Field 2, Starflow instruments were used to conduct the field scale flow rate measurements at the supply pipe (by logging water velocities and flow areas), the check gates between borders (by logging the water depths and velocities), and the drain boxes (by logging the water depths). The flow areas at the check gates were determined by multiplying the logged water depths by the check gate width. The flow rates at the supply pipe and check gates were estimated by multiplying the flow areas by water velocities. Flow rates at the head and tail drain boxes were estimated from water depths using the pipe energy equations, and sharp-crested weir equation, respectively.

Two Starflow instruments were mounted on the supply pipe and each check gate, while one Starflow was mounted on each drain box of Field 2. The purpose of mounting two Starflow instruments was to obtain a high reliability in the measurements and to raise the probability of at least one good dataset in case any damage or faults occur with a device. In each case the average of the correctly functioning Starflow measurements was adopted. The use of two Starflows was justified in two occasions where one of the Starflows that was mounted in the supply pipe did not work for the whole season and some of Starflows in the check gates did not function correctly in some events.

Instantaneous flow rate measurements conducted at the check gates using the SonTek FlowTracker2 generally showed a uniform distribution of water depths and velocities across the check gates. Hence, they show the suitability of using one Starflow measuring the velocity at one point at the gate to infer the flow through the entire gate. However, there was a noticeable overestimation in the flow rates values obtained by Starflows compared with the SonTek FlowTracker2. The Starflow flow rate measurements were corrected based on SonTek FlowTracker2 measurements.

The suspected reason behind the difference between the Starflow and SonTek FlowTracker2 flow rate measurements was the fact that the Starflow measures velocity

at a point and the discharge is found by assuming a uniform distribution for the water depths and velocities across the check gate. In reality, the water depths and velocity distribution across the check gates were not perfectly uniform. There is a blocking factor resulting from the obstacle of flow caused by the check gate pylons. The Starflows were positioned in the middle of two pylons which probably corresponds to the highest velocity across the width of the gate. Starflow instruments can provide an acceptable level of reliability for flow rate measurements at the field scale. However, these measurements should be validated against independent instantaneous flow rate measurements such as those performed with the SonTek FlowTracker2 instrument. Instantaneous flow rate measurements should be conducted for each check gate and if possible each event, to either validate or calibrate the Starflow flow rate measurements.

Adopting an independent set of measurements that can be linked to field scale flow rate measurements such as the estimation of the net applied volume or depth through soil moisture probes is advisable. While this kind of measurement is too inaccurate for calibration of inflow rates they can be used as a reference to decide whether the net depth held in the soil profile calculated from flow rate measurements is logical. Flow rate measurements at the field scale conducted in Season 1, in Field 3 show a low estimated value of the net applied depth held in the border, especially in the last two irrigation events. As discussed in Section 5.5.2, though this net applied depth held in the border was unexpected, there was no specific reason to doubt the flow rate measurements. As adopted in Season 2, mounting more than one Starflow can reinforce the reliability of the flow rate measurements at the field scale. However, the presence of such independent measurements (such as using moisture content probes) can help in reinforcing the reliability of the field scale flow rate measurements.

The flow rates in the head channel drain box were estimated based on the total head losses along the pipe using pipe energy equations, whilst the flow rates in the tail drain box were estimated based on the weir equation. The difficulty of applying the weir equation in this situation is that the top crest of the tail drain box was neither broad nor sharp-crested. It was believed that the structure it closest to the sharp-crested weir condition and it was adopted in this research. The approach adopted in estimating the flow rate in the head and tail drain boxes could have lower reliability compared with logging the water velocities and flow areas directly from the pipe. The difficult

conditions in both drain boxes prevent mounting of Staflows in these pipes. Finding other technical solutions to mount flow measuring instruments in drain pipes should provide better results in regards to the reliability of the measurements, than was achieved in this study.

11.2.4. Flow rate measurements at furrow scale

Flow rate measurements at the furrow scale, coupled with other evaluation measurements (water advance, and cross-sectional area) were used to estimate the infiltration parameters based on well-known evaluation methods, and to study the variation in diverted flows between furrows.

The FlowTracker 2 instrument was used to conduct flow rate measurements for individual furrows. The portable nature of this instrument provides the flexibility to conduct the measurements for many furrows within different borders and fields. The flow rate measurements were conducted close to the sill to avoid the overflow between furrows which occurs close to the furrow entrance. Flow velocities are also likely to be highest at this point meaning that error relative to the magnitude of the flow is minimised. The sill has hydraulic importance in controlling the diverting water to the furrows. Therefore it was considered that this would be a relevant location to collect data.

Focussing on the second season of results, the flow rate measurements were conducted on twelve adjoining furrows in each border of Field 2. It was impractical to cover a larger number of furrows during the inflow time, which was about three hours for each border of Field 2, as this measurement in 12 furrows consumed about one hour. In some occasions, the flow rate measurements were conducted twice for each border at two different times. This second set of measurements was performed to make sure that there was no significant difference in the instantaneous measured values of the flow rates. The necessity to conduct other measurements, such as flying the UAV, was another constraint preventing further flow rate measurements. The results showed a considerable variability in the flow rate values between the twelve measured furrows Table 10.5. A similar pattern in flow rates was noticed when these measurements for the same furrows were conducted twice during the same irrigation event.

Although the selected set of furrows could not represent the variability in the whole border properly, it can be assumed that it is still a good sample to understand the differences in diverted flows between furrows. In fact, the advance data in Figure 10.1 suggests more variability, where the flow rates could be lower for the furrows in the outer part of the border (at the opposite end to the measured section) because they have lower advance rates. As shown in Section 10.2.4 there is a good correlation between the flow rate and the water advance (R^2=0.6477). Therefore it is suggested that observations of the advance across the border could be used to inform the choice of furrows for individual flow measurements. A technique recommended to select furrows for flow rate measurement, will be explained in Section 11.2.8.

Four Starflow instruments were installed within the field to capture flow rate measurements of the furrow throughout the whole inflow time for one of the irrigation events. These instruments were mounted close to the sill, 60 metres from the furrow entrance. These instruments were capable of exhibiting reliable flow rate measurements though there is some concern in that they have relatively large size compared with the small size of the flow stream in the furrow. Two out of the four Starflow instruments succeeded to log the flow rate measurements, where the other two Starflows logged bad data, possibly due to plant residue covering the transducer eyes of the instruments. These flow rate measurements showed steady behaviour of flow rate values throughout the whole irrigation event, which reinforces the approach for measuring the instantaneous flow rate once or twice during the irrigation event.

The high cost of devices such as the Starflow limits the number of furrows that can be measured. The portability, reliability and flexibility of the Flow-Tracker2 instrument means that it is well suited for instantaneous measurements and validating the data provided by Starflow instruments.

11.2.5. Advance and recession measurements

The advance measurements were conducted using IrriMATE advance sensors and a UAV technique. While advance sensors provide the ability to conduct accurate advance measurements for many intervals at determined distances along the field, it was unable to cover enough furrows to capture the anticipated variability in water advance between furrows associated with the FNSBO_Re system. The cost and the

considerable field work involved with these sensors made adoption of this technique inappropriate to study the performance at the large scale. However, this technique did successfully provide robust sets of advance data that were used in the evaluation of the current irrigation system. Based on the UAV advance data, a technique recommended for selection of the instrumented furrows that represent the whole border, will be explained in Section 11.2.8. Advance measurements using the conventional (e.g. IrriMATE) advance sensors, in addition to other required measurements to estimate the infiltration parameters, will be conducted in these selected furrows.

The UAV technique developed was adopted to conduct advance and recession measurements in Field 2 during Season 2. Two main kinds of flight missions were used in these measurements: the flight paths across the furrows (Figure 6.14) and flight paths along the field length, parallel to the furrows (Figure 6.15). The flight missions crossing the border at determined interval distances proved to be very useful because of the ability to provide advance and recession measurements accurately for all furrows in the border. However, this kind of flight mission has some constraints, which are discussed later in this section. On the other hand, the flight mission with the longitudinal paths covered a small number of furrows and was unable to determine the location of the water front edge accurately. Therefore, this kind of flight mission was not adopted for advance/recession measurements. However, longitudinal flights can provide a quick impression about the nature of water advance and recession along whole field length.

The UAV technique provided a better understanding of the variability of the water advance between furrows at the border scale. The UAV data obtained from one flight mission during the advance phase indicated the variability in the water advance between furrows, but not the advance rates in these furrows. Conducting more than one successful flight mission can create a set of water advance data for all furrows in a border that can then be used in estimating the infiltration parameters. However, this advance data should be associated with other evaluation measurements in the same furrows (flow rate and cross-sectional area) to conduct on evaluation analysis (see Sections 11.3.2, 11.3.4).

The number of possible flight missions in each event was restricted because of the limited resources. The number of flight missions are governed by the battery life,

number of available batteries, accessibility to recharge the used batteries, travel speed, dimensions of the border, number of flight paths per mission and the total time available, considering that other measurement tasks must be conducted during the irrigation event. Therefore, in this study, there was generally one flight mission to cover the advance phase, and two or three of flight missions to cover the recession phase in each border. It was possible to conduct more than one flight mission to record the recession phase because there are no other required measurements after the inflow into the border ceases. The flight missions for the water advance were conducted when the water advance front reached about half the length of the field. Sometimes there were two flight missions during the advance phase. However, the second advance flight mission was not able to record a significant amount of the advance when the water advance in most furrows had already reached the end of the field (Table 7.3).

To implement multiple good flight missions, it is suggested the first mission is conducted when the water front is in the first quarter of the field length and three to six missions are completed before the advance in most furrows is finished. At least three flight missions should be conducted before the advance in WFs has reached the end.

Improving the quality of advancing water front detection in a greater numbers of furrows can be achieved by increasing the number of the flight paths that cover the field (Figure 6.14). In the current study, the adopted interval distance between the flight paths was 100 metres. For analysis, an advance distance midway between two flight paths was assumed whenever the advance front edge was not detected by the UAV, because it was located somewhere between the two paths. This approach may introduce a significant error in the resulting advance data. This error depends on the flight altitude as the error margin is increased with a low flight altitude as the UAV camera covers a narrower strip of the field and therefore detect less water fronts. With a higher UAV altitude, the width of covered strip increases, and should reduce the error margin. Reducing the interval distance between the paths from 100 m to 50 m can reduce the error significantly (for advance front edges not detected by UAV) and improve the advance data quality by increasing the chance to catch actual water advance edges. A suggested strategy to implement more missions is to adopt different flight missions during the advance phase. For example, at the early stages of the

advance phase, adopt small distance intervals between the flight paths, and cancel any paths at the downstream part of the border, which the water advance front has not yet reached. This strategy was adopted in the current study by manually stopping the flight mission early when there were no more water fronts in the remaining flight paths by clicking the RTH (Return to Home) button on the remote control of the drone. Another strategy to implement more missions at later stages of the advance phase, is to alter the mission so that flight paths for the top of the field are removed, if it is anticipated that the water advance has already exceeded this distance. Adopting such strategies can also reduce the effort and time for extracting the advance data from the recorded video recordings.

The most efficient flight missions can be conducted in the early stage of plant growth, where the plant canopy has less impact, and the UAV can be flown at a higher altitude thereby covering larger parts of the field. At a later growth stages, the shadow and canopy impact the ability to detect the water advance front. The flight missions close to midday are more efficient in detecting water advance because the sunlight is perpendicular and water can be easily distinguished from the soil. Detecting recession is more difficult than the advance because reflections on the water surface can occur from the wetted soil even without water depth. Conducting flight missions with low altitude provides good quality UAV video recordings to which can detect the receded furrows.

Conducting frequent flights missions during the advance phase is a time consuming task, and therefore a dedicated person should be allocated for this process leaving other staff to conduct the additional measurements.

11.2.6. Peak Water depth

Water depth in the furrow is an important variable that can be used to quantify the surface storage component of the volume balance. The surface storage is necessary in evaluating surface irrigation systems. In this measured FNSBO_Re irrigation system, the measurement showed a fast water advance and high flow rate, and low estimated infiltration characteristics, thus large surface storage volumes (SSV). This suggests a significant role of SSV in furrows during the irrigation process, which poses a high

consideration for SSV measurements (perhaps represented by flow depths) to obtain a reliable estimate of the infiltration parameters (*a* and *k*).

The high cost of instruments that can log water depths dynamically during the whole irrigation event led to the adoption of alternative techniques to measure peak water depths. A simple and inexpensive approach involving the use of wooden stakes painted by food colouring was adopted to measure the peak flow depth in the furrows. This approach provided the capacity to cover between 24 and 48 furrows in each border.

The peak water depth measurements showed noticeable variation between furrows, in general. Statistically, results showed the peak water depths in WFs were higher than non-WFs. However, there was only a weak correlation between the peak water depths and water advance. Though this weak correlation could undermine the influence of this variable on the irrigation process, the peak water depth still represents an important variable in understanding the irrigation process in surface irrigation systems.

As the SSV in the current irrigation system is so important, there may be a requirement to conduct water depth measurements at many locations along the furrow instead of at just one location as was adopted in this study where peak water depths were collected at the sill only. It is a useful aid in understanding the irrigation process and the volume balance. However, water depths are not required in the measurement and evaluation process developed in this study.

11.2.7. Unsuccessful methodologies

There were some unsuccessful trials completed of alternative techniques to collect field measurements during the first and second seasons. These trials were completed to accommodate some unusual circumstances and to provide additional or alternative sorts of measurements.

The design of the hydraulic structures and field conditions in these systems poses difficulties for installation of flow measuring equipment. Channels and structures often remain submerged prior to and throughout the season meaning that alternative approaches are required. Attempts were made to mount a Starflow instrument in the supply pipe of Field 3 during Season 1 using a using a heavy piece of flat steel (Figure

4.23) instead of using the pipe expansion ring used in Season 2. With the main channel full of water the inlet pipe was completely submerged during installation of the measuring equipment. This technique failed because the high water velocities during the irrigation lifted or pushed the flat piece of steel from its original position inside the pipe resulting in problems with the measured velocities.

The capture of water depths and velocities using fixed cameras was tested during a limited number of irrigation events. These cameras were found to have a sensitivity to high temperatures in the field. They successfully captured the measurements for a few minutes, but then stopped because of overheating. Attempts were made to cool these cameras so they could continue working, but it was impractical to continue with these efforts because of the necessity to conduct other important measurements, such as piloting the UAV and measuring furrow flow rates. In addition, the high cost of these cameras also limits any large scale measurement using this technique. Detecting water velocity in the furrows was also trialled using the UAV and dye tracer technique. Dispersion and movement of the dye restricted this technique. Tracking the dye movement using the UAV was better than walking on saturated furrows.

Water advance measurements are important for the surface irrigation evaluation process. Attempts were made to collect advance data using a smartphone GPS app (MotionX-GPS). The significant variation in the water advance front between furrows, most notably between the WFs and non-WFs, made this technique difficult. The GPS technique was very time consuming and involved walking long distances in a zig-zag pattern, while only covering a relatively small number of furrows. Conducting these types of advance measurements,repeatedly for several distance intervals, left no time available to conduct other important measurements. Another downside of this technique was the inaccuracy in these measurements, in particular, when determining the furrow number. Walking through the field to collect the advance measurements was difficult because of the height and density of the cotton plants. To cause further complication, it was difficult to observe the irrigation advance front, unless standing directly in the furrow being observed, because of the density of the crop, especially at the latter stages of plant growth.

Measuring peak water depth in the furrows was also trialled using the float depth gauge. The relatively high cost of this gauge compared with the wooden stakes painted with food colouring restricted use of this technique.

11.2.8. Selection of furrows for instrumentation and measurements

Evaluation of the irrigation performance in FNSBO_Re systems requires the conduct of large numbers of field measurements to cover the anticipated field variability. These irrigation systems consist of a large numbers of furrows in each border, with multiple interconnected borders in each field. Completing large numbers of measurements is very difficult and impractical in some cases. Some of these measurements must be conducted during the irrigation event, such as furrow flow rate and UAV water advance. Other measurements can be collected prior to or after the irrigation event such as advance times using advance sensors, furrow cross-sectional areas, and elevation surveying. For example, completing flow rate measurements for a large number of furrows using the portable Flow-Tracker2 instrument during the irrigation event, is impractical. Setting up the Flow-Tracker2 and conducting the instantaneous measurements consumes approximately five minutes for each furrow. On the other hand, using instruments that can be set in the field before commencing the event such as Starflows or flumes is ideal, as they can be installed before the event but the number of devices required involves a high cost and a large effort for installation and subsequent data collection. New techniques such as analysis of short video recordings of the stream taken by a smart phone camera, to calculate the flow rate (see Section 3.2.1), are promising, but will likely have lower reliability than traditional techniques.

The time of the day when the irrigation occurs impacts on the types of possible measurements and the quality of the measured data. Most measurements which are collected during the event are difficult to conduct during darkness. Measurements such as the UAV advance are best collected at certain times during the day for ease of water detection in furrows. This is an important consideration as many farmers may choose to operate surface irrigation systems 24 hours per day. There is the possibility that because bankless systems facilitate faster irrigation times, a greater proportion of events occur during daylight hours. The constraint that some measurements must be

collected in daylight, requires consideration of the location and border choice for intensive measurements.

(Grabham 2012) suggested the survey of furrow elevations would aid in selection of furrows to measure flow rates, water depths, and water advance measurements. As a result, the measurements were able to capture the impact of different furrow elevations, and the effect of WFs and non-WFs. In that study the elevations of furrow entrances was considered to be the governing factor causing variation in water advance between furrows. For FNSBO_Re systems this same importance can be transferred to the sill, which serves at the control point for furrow flows.

It was initially thought that measuring furrow characteristics would help identify the range of furrow variability and inform the selection of irrigation measurement positions. Furrow elevation, peak water depth, flow rate and cross-sectional area were examined to determine the most important governing factors affecting the advance variability in the current system. The results did not clearly identify the factors that could be measured to explain the advance variability at the field scale. Therefore, it is proposed that a better and more efficient approach is to use the results of the UAV advance data capture, instead of relying on elevations and other measurements. The UAV technique provides the ability to accurately understand the variability in the advance across the border, with less effort compared to elevation surveys. The main limitation is that the UAV data from the current irrigation is used to determine the measurement locations for subsequent events, rather than the current event.

The recommended approach to understand the water advance variability is based on using UAV advance data obtained from a flight at the beginning of the irrigation season to identify those furrows within the border which are representative of the variation in water advance. The resulting set of furrows will represent the range of factors which may be influencing this variation rather than focussing on one factor at a time. For example, let us assume that the advance data of Figure 7.14 is for a flight conducted at the beginning of the season. This data would used to determine which furrows should be considered for further evaluation measurements. It is clear from Figure 7.14, that the furrows can be split visually to six groups based on the water advance distances. The first group represents the furrows that have water advance less than 150 m, the second group of furrows have an advance distance greater than 150 m

but not exceeding 250 m, the third group of furrows have advanced further than 250 m but not exceeding 350 m, and so on. For the same example, it can be observed that there is no advance data for the fifth group in which advance distance is greater than 450 m and less than 550 m. The next step involves selection of between three to five furrows in each group for furrow flow rate measurement, water depth, cross-sectional area, and water advance. The observations during field trials have indicated that three to five furrows should be sufficient to characterise each group. This furrow selection process takes into account the ease of accessing these furrows, and the degree that they represent the whole border.

Selecting adjoining furrows in each of these advance groups is desirable as the measurement process will require less time and effort compared to separate furrows. In addition, the selection of adjacent furrows is likely to capture the variability that results from normal practices like machinery traffic. The problem with choosing adjacent furrows is that these measurements may not be able to represent the potential variation across the border. It is suggested that furrows be selected from more than one location across the border, for example at both sides, or the side and the middle of the border. This should improve the representation of possible soil characteristics in the sample across the border.

To conclude, selection of furrows or groups of furrows for instrumentation, based on the variability of advance, is the first priority. Secondly, these furrows should be situated in more than one location across the border to appropriately sample any variability across the border. If possible, these furrows should be located in one or two adjoining sets of furrows for convenience. Observations during the field trials have indicated that between three and five furrows in each group is a good compromise between accuracy and practical effort. The total number of WFs and non-WFs selected, should reflect the percentage of WFs and non-WFs in the border.

Grower notes and researcher field observations are another important source of information, which should be consulted, when selecting furrows for instrumentation. This form of information can provide details of locations that have weak plants, different soil characteristics, or a shortage or surplus of applied water.

11.3. Discussion of analysis

This section will discuss the analyses presented in Chapter 8, with the aim of developing a methodology for the analysis of FNSBO_Re systems.

11.3.1. Estimation of infiltration parameters

A sample of available surface irrigation computer models were tested for their ability to accommodate the characteristics of FNSBO_Re systems. Most of these models include some form of inverse solution for infiltration parameters based on field measurements. As discussed in Section 3.6, the inverse approach is more practical, simple, and reliable, compared with the direct approach of measuring the infiltration characteristic. None of these models had the capacity to accommodate all of the special hydraulic aspects of FNSBO_Re systems. As explained in Section 3.6.7, each model offered a different level of reliability and capacity to accommodate these special aspects. In addition, the quality and form of the collected data, such as variable or constant field slopes or flow rates, may influence the selection of the most appropriate model.

Although each model offered different capacities to accommodate different input data, the infiltration results were close in all models. For example, the Two-Point method and WinSRFR accommodated only two advance points for the inverse solution, while IPARM and SISCO can accommodate many points. The Two-Point method and IPARM only accommodate a constant slope due to their reliance on the volume balance model, while WinSRFR and SISCO can accommodate a variable slope. In terms of inflow data, the measured data was limited to a single average flow rate, but WinSRFR, SISCO and IPARM can accommodate variable inflow. Based on the accuracy and capacities of these models to accommodate higher quality inputs, it was decided to adopt the infiltration parameters obtained from SISCO.

Field measurements were collected in such a way as to overcome the limitations associated with the FNSBO_Re irrigation system. Unlike conventional methodologies for estimation of infiltration parameters, the geometry and the hydraulic measurements were conducted on or close to the sill rather than at the furrow entrance. The main reason for this modification was to avoid the overflow between furrows which was

observed at the furrow entrances at the beginning of the furrows. Conducting these measurements close to the sill should provide more stability and reliability, because the shape of the furrows is less subject to erosion, and hence the cross-sectional area and flow rate measurements would be at more controlled conditions, compared with the furrow entrance. In addition, starting the measurements at the sill permits the application of the inverse solution for infiltration from advance, which has been developed for conventional furrow irrigation. The distance to the sill (~50 metres) is relatively small compared to the entire field length (640 metres for Field 2), and therefore the furrow downstream of the sill should provide a good representation of the results for the whole field.

For calculations purposes, the water advance measurements were amended by making the sill position the start point for water advance assuming the time to reach the sill is equal to zero. This practice overcomes the difficulty of the wetting of this first part of the field, occurring either gradually or rapidly, depending on grower management of each irrigation event.

The estimated infiltration parameters were similar between the different inverse modelling approaches. The infiltration characteristics illustrated a high initial infiltrated depth, followed by a lower steady infiltration rate for the remainder of the IOT. This behaviour was attributed to the governing role of cracks in the soil profile, where most of the infiltrated depth occurs in a short time compared with the whole IOT.

The significant variability observed between furrows for furrow flow rate, water advance and cross-sectional area, support the practice of completing the evaluation using a small number of furrows to represent the whole border properly. There is a possibility that conducting the evaluation in only 12 furrows out of 300 furrows in each border, as performed in this research, may not properly represent the infiltration characteristics of the whole border. Taking water advance variability as an indicator of uniformity, the UAV advance data showed a large variation in between furrows in general, and a clear difference between non-WFs and WFs. To obtain a representative sample for the field, the measurements should be conducted on a number of furrows of both types (non-WFs and WFs) at different locations across each border, as

explained in Section 11.2.8. Each of these furrows should be analysed separately, without combining advance data or flow from multiple furrows.

11.3.2. Irrigation performance at furrow scale

As mentioned in the previous section (11.3.1), none of the models studied had the capacity to simulate all of the special characteristics of FNSBO_Re systems. However, each model offered a different level of capacity to accommodate these special aspects. Theoretically, SISCO is based on the most accurate hydraulic model, the full hydrodynamic model. The main reason to adopt SISCO was its ability to stop the simulation at any time and extract the data for water depths, which were required to complete the temporarily blocked calculation (TBC) and obtain the irrigation performance. This feature does not exist in any of the other models.

There are two main constraints that impact the reliability of performance results obtained form SISCO in FNSBO_Re systems. The first constraint is the incapacity of SISCO to accommodate the real downstream conditions, where SISCO assumes either a Blocked or Free draining condition at the downstream end of the furrow. The second constraint relates to the measurement location in the proposed methodology, which involves inflow measurements close to the sill. Hence, the modelling and performance results neglect the first 50 metres of the field.

Regarding the downstream condition, field observations showed that the real downstream conditions are a mixture of Blocked and Free draining (opened) conditions. The downstream condition in the current field was initially blocked at the end of the advance, but was opened some later time. Consequently, there was an overestimation in the infiltration and an underestimation of the runoff volumes when adopting the blocked condition. The reverse is true if the opened condition is assumed.

A spreadsheet was developed to perform the TBC calculations to replicate the temporarily blocked downstream condition observed in the field. This spreadsheet requires the results extracted from the SISCO simulation, assuming Blocked conditions, and then allows calculation of runoff and infiltration based on the real field practice. These calculations commence when the bottom check gate is opened for a

furrow located in the first border, or when the tail drain box is opened for a single furrow located in the last border in the field.

There were two possible scenarios tested that describe the redistribution of surface storage water along the furrow, during runoff. The first scenario (A) assumes that water surface drops by a constant rate along the furrow during each time step. The second scenario (B) assumes the water surface drops to be horizontal along the furrow during each time step. However, in reality, the water flow is redistributed in a manner between these two scenarios. Scenario A assumes that runoff is extracted from all parts of the field simultaneously, while Scenario B assumes the water can redistribute itself perfectly at an infinite rate during each time step. Although both scenarios result in the same volume of runoff, the distribution of surface storage water and infiltrated depth along the furrow is different. Generally, Scenario A has a larger added infiltrated depth compared with Scenario B, except in four furrows where the added infiltrated depth were very close in both scenarios (Table 8.17). However, these differences were not significant in all the furrows in term of total infiltrated volume (or depth) during the whole irrigation event (ranged between 0.1 and 2.1%). Thus, there were no significant differences in relation to the other volume balance components and the irrigation performance indices between both scenarios. Therefore, either of these scenarios can be used for the TBC.

The results of both scenarios showed that the infiltrated depths based on the TBC results of the real downstream condition, were very close to the Free draining condition. This is partly due to the soil infiltration characteristics, where the majority of the infiltrated depth occurs in a relatively short time due after wetting. On these soils a small change in IOT would not significantly alter the infiltrated depth as most of the infiltration has already occurred.

Under different circumstances, the differences between the TBC results and the Free draining condition may be much larger, and hence the TBC approach would be more useful. For instance, if the final infiltration rate is higher or the recession time is longer, there would be more infiltration expected during the storage phase and the results would differ more significantly with the Free draining results. Longer recession times may occur on fields which do not have an adequate vertical step between borders

causing water to pond on the lower end of the field, thereby increasing infiltrated depths at the bottom end of the field.

Comparison of the volume balance components and the irrigation performance indices of both scenarios (A and B) with the Free draining condition, showed slight differences, while large differences were found with the Blocked condition. Although the performance results obtained by the TBC were very close to the Free draining condition, these calculations are a valid tool to understand the performance of FNSBO_Re systems.

Conducting the TBC requires minimal extra effort compared with the blocked or open conditions. The only extra requirement is that runoff measurements for the border must be available. Knowing how quickly the water drains from the field could be another simple alternative source of additional data for the TBC, instead of runoff measurements. It can be concluded that this TBC should be used whenever this runoff or drainage time data is available.

Estimating the performance indices for the entire furrow length was conducted by separately estimating the infiltration volume for the first 50 metres located upstream of the sill, based on the measured IOT, and combining this with the results of the TBC for the furrow length after the sill. The infiltration estimation process relies on the assumption that the majority of water drains back from this upstream part of the furrow within approximately 30 minutes after opening the top check gate of Field 2 allowing water to flow into the next border. This assumption is based on field observations during the events measured in this research. The vertical step between adjoining borders and the large size of the check gates in the head channel allows water to drain quickly from this part of the field. FNSBO_Re systems with smaller vertical steps or more restrictive structures may require larger drainage times. To simplify the infiltration calculation it was assumed that water drains from this entire upstream part of the furrow (50 metres) at the same time (see Section 8.10). This assumption has a minimal impact on the results because of the low final infiltration rate and the small length of this drainage time (30 minutes) in relation to the total IOT.

11.3.3. Estimation of DU, AE and RE at the furrow scale

Estimation of the performance indices for the furrow length downstream of the sill were completed based on the volume balance components from the TBC technique (Scenarios A or B). DU was calculated based on the infiltrated depth results from the final step of the TBC using Equation 2.2. Both the AE and RE indices require an estimation of the soil water deficit (SWD). A simple water balance tool, IrriSAT, was used to estimate the SWD prior to each irrigation based on remote sensing, reference evapotranspiration, rainfall and net applied depth from previous events. Estimation of the AE% and RE% was based on the assumption that no deep drainage will occur until the water deficit has been replenished. This technique suited the available field measurements in the current study, which did not involve measuring soil moisture.

11.3.4. Irrigation performance at border scale

It is likely that evaluation of about twelve adjacent furrows out of 300 furrows is insufficient in order to represent the irrigation performance of the entire border, particularly considering the degree of variability present within FNSBO_Re systems. On the other hand, conducting a full evaluation for all furrows in the border is impractical. A technique was developed to combine the UAV data (represented by the IOT) collected over the entire border with the infiltration characteristics estimated from intensive measurements on a small number of furrows, to obtain the irrigation performance at the border scale. If the furrows for intensive measurements are chosen carefully and represent the range of infiltration characteristics across the whole border, then the combination with the UAV data should provide a process that will be able to determine the uniformity across the whole border with good reliability. Therefore, the selection of the instrumented furrows as described in Section 11.2.8 is a crucial stage in the evaluation process.

Through this study of factors that influence the variability of the water advance it was found that the flow rate and the cross-sectional areas, are the most important, and not the infiltration. Therefore if possible, field observations should attempt to identify any obvious differences in flow rate or furrow cross section across the border.

Generally, if the variability in the water advance across the border results from differences in flow rate or cross-sectional area, this approach of combining UAV data with measured furrow data is valid. However, if the variability is largely due to the differences in the soil infiltration characteristics, the approach of combining the UAV data with the evaluation results of the measured furrows may not provide valid results.

11.3.5. Technique to estimate uniformity at the border scale

Water advance and recession measurements at the border scale were conducted using the UAV technique to estimate the IOT at predetermined locations in the borders. The infiltrated depths at these predetermined locations were estimated based on these IOTs and the averages of the infiltration parameters from the measurements in the 12 adjacent furrows. The UAV data allows these accurate results for the 12 adjoining furrows to be extrapolated to the whole border scale. The distribution uniformity (DU) of the entire border can then be determined using Equation 2.2.

Within the UAV data there were many undetected locations in the water advance and recession flight missions. As a result, the IOTs could only be calculated for 17% of the locations covered by the UAV flight missions in the border. A complementary methodology was developed to estimate the advance and recession times for all locations based on the available measured data. This complementary methodology succeeded in compensating for the shortages in the UAV data by raising the proportion of locations with available IOT data from 17% to 86% in one example event. The complementary methodology involves the prediction of the advance trajectory using a single or small number of advance times for each furrow from the UAV, and detailed advance data from a small number of furrows collected with IrriMATE advance sensors. Volume balance techniques commonly describe the advance trajectory using a power function with the coefficient p and exponent r. It was hypothesised that parameter r can considered constant between furrows while p is varying (see Section 9.2.2). In this way advance times for each furrow can be estimated using Equation 3.8, where there will be one value for the parameter p for each individual furrow, and one value of r representing all furrows in the border. Once these advance trajectories have been defined, the IOTs can be estimated for any location along the furrow length.

As mentioned above, the complementary methodology succeeded in obtaining IOTs at more locations than using the raw UAV data, but there were still locations with missing IOTs. The missing IOTs were due to shortages in the available recession data. Limited time availability to fly more recession flight missions, and the onset of darkness were the main reasons behind these shortages. It is believed that there was overestimation of the DU when the missing data tended to be located at the farthest part of the border (570 metres), which probably included the greater IOTs.

The reliability of estimated DU can be improved by increasing the quality and quantity of UAV measurements and advance measurements. There were shortages in the advance data obtained from the UAV technique due to only completing a single flight mission during the advance phase. Conducting greater numbers of flight missions during the advance phase would provide better advance data instead of depending on only one flight mission to cover this phase. Similarly, conducting more flight missions during the recession phase would improve the recession data. Field observation (by walking to monitor the receding furrows) can be another source of recession data especially when darkness, UAV batteries or other restrictions prevent completion of more flight missions. Regarding the estimated infiltration parameters, better selection of the measured furrows following the guidelines explained in Section 11.2.8, should provide more representative infiltration characteristics and therefore a higher reliability in the estimated DU.

11.3.6. Estimation of AE and RE at the border scale

As explained in Section 11.3.3, estimating the AE and RE at the border scale requires an estimation of the SWD using IrriSAT. Similarly, it was assumed that no deep drainage will occur until the water deficit has been replenished. The applied irrigation depth was estimated based on the flow rate measurements at the field scale.

Conducting moisture content measurements including the soil physical characteristics (e.g. field capacity) would provide a realistic situation of the real amount of water required to bring the soil moisture content back to the desired full point. Soil moisture measurements might increase the reliability of estimation of the efficiencies, but this approach was not tested in these trials. Alternatively, as explained in Section 5.7, conducting soil moisture content measurements prior to and post irrigation events can

be used as an independent data set that can be used to check the results from the irrigation analysis, thus reinforcing their reliability. Even if soil moisture data is available it is suggested that better estimations of soil water deficit can be achieved through use of a soil water balance tool such as IrriSAT.

11.4. Recommended evaluation technique

A primary outcome of this study is to define a new technique for measurement and evaluation of FNSBO_Re irrigation systems. This section will summarise this recommended technique. The suggested evaluation technique is as follows:

1. Select the study field before commencing the season so installation of instruments (e.g. Starflow) can be conducted in appropriate conditions; for instance during the maintenance time when the main channel or the drain is empty.
2. Conduct a field investigation and elevation surveys at an early stage before commencing the season to determine the main layout features of the field, such as the existence and position of the sill.
3. Conduct a more intensive field survey focussing at the sill for a large number of furrows (e.g. 25% of the total number of furrows in the border), while only conducting elevation surveys along the entire length of the field for several furrows.
4. Ask the farm manager how they usually manage the irrigation system regarding when and how check gates are opened and closed, and if there are any conditions where this practice may change, such as a decline the water level in the main channel.
5. Identify any challenges to installing flow measurement devices in the hydraulic structures in the field, and find technical solutions to these challenges

6. Install flow measuring devices (e.g. Starflow) at the hydraulic structures. If available, mount two instruments to reinforce the reliability, and to reduce the chance of losing data.
7. Collect preliminary observations for one of the early irrigation events completed, ideally the first irrigation event. Measurements during this event should include:
    a. UAV flight mission covering the advance phase
    b. Flow rate measurement at check gates
    c. Observation of backwards advance
    d. Observations of grower management of the irrigation

    These observations will provide a good understanding of the irrigation process, and locations in the field with excess or inadequate application of water. The UAV mission will be used to identify the variability and determe the best furrows in which to conduct the evaluation measurements, as explained in Section 11.2.8.
8. Select furrows that can represent the whole border based on the suggested methodology explained in Section 11.2.8. Suggestions for choosing the furrows are to:
    a. Include both types of furrows (WFs and non-WFs).
    b. Select the furrows from both sides of the border, and the middle of the border if applicable.
    c. Select furrows that represent the water advance variability between furrows, (earlier referred to as groups).
    d. Select between three and five furrows from each group for intensive measurement.
    e. Consider ease of access to selected furrows, and the convenience of measuring adjoining furrows, during the selection process.

9. Install flags and signs on important locations and the selected furrows, so they can be found easily during future measurements.
10. Conduct soil moisture content measurements which might be used to validate the results for AE and RE.

The following steps (from point 11 to 13) will be carried out for those events where detailed evaluation measurements are collected:

11. Install the advance sensors in the furrows selected in Step 8. These sensors will be placed at several locations down the length of the field starting at the sill and ending before the end of the field or at the point which is not likely to experience backward advance.
12. Conduct accurate flow rate and cross-sectional area measurements of the furrows at the sill for these selected furrows. If there was no sill, conduct the flow rate and cross-sectional area measurements at the furrow entrance or at a distance where no overflow between the adjoining furrows occurs.
13. Conduct the water advance, flow rate, and cross-sectional area measurements for the selected furrows. Repeat the furrow flow rate measurements if possible.
14. Conduct UAV flight missions during the irrigation event using software which can program the UAV to follow predefined paths. The following points should help to improve the quality of this data:
    a. It is suggested that more than one flight scheme is created to maximise the efficient use of the resources for example:
        i. One scheme for the early stages of the advance phase with small distance intervals between the flight paths, omitting the downstream end of the field.
        ii. A second scheme for later in the advance phase, which focusses the flight paths on the downstream end of the border.

b. Conduct the flight missions at the early stage of plant growth, when the plant canopy has less impact.
c. Conducting the first flight mission of each event when the water front is in the first quarter or less of the field.
d. Conduct more than one flight mission (between three and six) covering the advance phase, and about three missions to capture the recession phase.

The following steps outline the process for evaluation the FNSBO_Re irrigation system:

15. Estimate the infiltration characteristics for the intensively measured furrows according to Chapter 8.
16. Simulate the irrigation process for these furrows according to Chapter 8.
17. Apply the TBC calculations to the results from Step 16 according to Chapter 8.
18. Estimate the irrigation performance indices at the furrow scale according to the details in Chapter 8.
19. Use the UAV technique to interpolate IOTs across the border according to the processes outlined in Chapter 9.
20. Estimate the irrigation performance indices at the border scale according to the processes detailed in Chapter 9.

CHAPTER TWELVE

Conclusion and Recommendations

12.1. Introduction

Unconventional features of the FNSBO_Re irrigation system such as the variability in the flow diverted to furrows from the common irrigation supply system, the presence of a positive field slope for the top part of the field, and the existence of hydraulic interactions between the adjoining borders, require the adoption of novel irrigation performance methodologies. A combination of existing conventional and new techniques were adopted to conduct the measurements and the analysis of the FNSBO_Re irrigation system.

The main aim of this study was to develop an appropriate performance measurement methodology that can accommodate these special features of the FNSBO_Re irrigation system.

12.2. Conclusions

Near zero slope, furrowed border irrigation systems with common water supply referred to as bankless irrigation systems, or connected borders systems, are commonly used in Australia. However, a review of the literature indicates that there is limited information available on the performance of these systems. This is a result of the small numbers of measurements conducted and the lack of a robust technique to evaluate these systems.

The possible range of furrowed border irrigation systems designs, and the available performance results were reviewed in Chapter Two. This review identified several factors that influence the performance of surface irrigation systems. Throughout the literature review, it became clear that there is a lack of consistency in the way in which unconventional surface irrigation systems are defined. For this reason, Chapter 2 attempts to classify all surface irrigation systems using a standardised set of terms describing the field slope, bed configuration, water supply, and drainage condition.

This new terminology should serve as a convenient way to define surface irrigation systems into the future.

Field measurements were undertaken on a commercial cotton farm in northern New South Wales, Australia. These measurements were collected for two entire seasons and for two fields in each season. Field surveys showed the existence of a positive slope in approximately the first fifty metres at the top of the field, then a slight negative slope, sloping down with distance from the supply channel along the rest of the field. The surveying also identified the presence of a vertical step between the adjoining borders at the head and tail of the bankless channels.

Flow rate measurements at the field scale were conducted using a direct approach (measuring flow velocity and flow area) and indirect approaches (such as pipe energy and weir equations). These measurements were employed to estimate the net volume or depth of water held in each border, hence enabling the estimation of the AE and RE at the border scale. The estimated net depths of water applied to each border were smaller than expected, especially in Border 2 of Field 3. However, there was no specific reason to doubt these measurements.

Flows were also measured at the individual furrow scale. Conventional devices to measure the furrow flow rate such as weirs were not appropriate for the hydraulic conditions associated with flows on reverse or near-zero slopes. Instruments such as the SonTek FlowTracker2 hand-held acoustic doppler velocimeter were appropriate because they permit measurement of velocity without altering water flow. The furrow flow rate measurements conducted in the furrow for the whole irrigation supply time indicated that the discharge was relatively stable. This supports the concept of using average flow rate measurements to represent the whole irrigation duration.

Water front advance measurements were collected using a variety of techniques including IrriMATE sensors, fixed cameras, GPS tracking and UAV flights. Advance measurements in the furrows showed a distinctive behavior of FNSBO_Re systems where waters simultaneously advanced from both ends of the field. The data showed a rapid advance rate and a significant variation in the water advance between furrows, especially between WFs and non-WFS. A variation in the water advance was also present between the furrows located at the two sides of the border. The significant

variation between furrows combined with the backward advance from the bottom of the field present difficulties for evaluating this system. To minimize these difficulties, the advance measurements, using the advance sensors, in Season 2, were conducted on a part of the field that experiences minimal backwards advance. On the other hand, the limited number of advance sensors restricted the ability to understand this distinctive behaviour of the water advance as installation of the sensors was at greater distance intervals. Furrow flow rate, peak water depth and cross-sectional area measurements showed the same variability between furrows.

Conventional field evaluation measurements were modified to suit the layout of the FNSBO_Re system. Field evaluation measurements (flow rate, and cross-sectional area of furrow) were conducted at the sill to avoid the hydraulic and geometry limitations resulting from the special characteristics of this system. It was observed that water overflow occurs between furrows at the very top part of the furrow close to the furrow entrance. It was also found that the shape and size of the furrow changed significantly due to the erosion at the furrow entrance, while being more stable in the lower part of the furrow. Water advance data collection commenced from the sill toward the bottom of the field.

Some other new techniques were trialled, but they either failed to provide data, or were deemed to be impractical. These approaches included using an action camera, and UAV and food colouring techniques to record the water depth and velocities in the furrow, the MotionX-GPS app installed on a smartphone to record the advance measurements in the furrows manually, and a float gauge to measure the water depth in the furrow.

Infiltration characteristics were estimated based on the inverse solution approach using field measurements of advance. The inverse approach is the most reliable approach because of its capacity to represent the infiltration characteristics of the whole furrow compared with direct physical measurement at some positions.

The infiltration characteristics were estimated using a sample of common surface irrigation models. These models represent a range of reliability and complexity. These methods were applied for the part of the field between the sill and the bottom end of the field because the flow in this initial part of the field upstream of the sill is unknown

and most models cannot accommodate positive uphill grades. The estimated infiltration characteristics exhibit a high initial infiltrated depth, followed by a low steady infiltration rate for the remainder of the IOT. The results obtained from the software models and the Two-Point method showed similar estimates of the infiltration characteristics. This indicates that the choice of the estimation method was not crucial when applied to the section of the field downstream of the sill. The SISCO model was chosen for the estimation of the infiltration characteristics because it is based on the full hydrodynamic model which has the highest reliability compared with the other models. Infiltration parameters averages were calculated for twelve adjacent furrows in Border 1 of Field 2 for the same irrigation event.

The available hydraulic models were not able to accommodate the real field management observed at the field site. For instance, the available models cannot simulate when the bottom check gate, or tail drain box is initially blocked at the end of the advance phase, and is then opened after a period of ponding. The available hydraulic models simulate the irrigation assuming either blocked or free-draining conditions, whereas the system studied is operated under both these conditions at different times. Therefore, a new approach, called Temporarily Blocked Calculation (TBC) was developed to simulate the irrigation process of the FNSBO_Re system for the real downstream condition. The TBC was developed based on the SISCO model because of its ability to stop the simulation at any time and export transects of water depths and infiltrated depths from along the field length. The TBC method starts with a snapshot of the irrigation event assuming blocked conditions, and then conducts a volume balance type approach to describe the recession of the surface water once the runoff starts occurring.

Development of the TBC method suggested two potential scenarios to predict the redistribution of surface water storage along the furrow length during each time step, after subtracting the runoff volume. The first scenario assumes that the water surface drops by the same amount along the furrow length during each time step, while the second scenario assumes that water surface along the furrow drops to achieve a flat horizontal surface. The scenario chosen will alter the manner by which water is redistributed along the furrow length, hence also changing the distribution of infiltrated depths and having an impact on the performance indices. In reality, the true

redistribution of surface water is likely somewhere between these two scenarios. The results obtained from the TBC showed that the estimated infiltration depth using the first scenario was larger and closer to the measured results compared to the second scenario. Considering the total infiltrated volume, there were slight differences (ranging from 0.1% to 2.1%) between both scenarios for the twelve calculated furrows. Accordingly, there were insignificant differences in the volume balance components and performance indices between both scenarios. Therefore, it can concluded that either of these scenarios is satisfactory.

The TBC results for Furrows 13 to 24 in Border 1 of Field 2 on 10-2-2018 showed high uniformity, ranging between 96.59% and 99.5% for Scenario A, and ranging between 96.6% and 99.3% for Scenario B. The AE results ranged between 28.4% and 74.1% for Scenario A, and between 28.3% and 72.5% for Scenario B. The high inflow rates and low infiltration characteristic resulted in low RE, but there was significant variation between furrows with values ranging between 18.8% and 64.8% for Scenario A, and ranging between 18.6% and 64.3% for Scenario B.

The results of the TBC method were found to be similar to the model results for the free draining condition but vastly different to the blocked furrow condition. Although the performance results obtained by the TBC method were very close to the free-draining condition, this does not undermine the importance of this new approach. The measured field is characterised by a low final infiltration rate which means a lower infiltrated depth will enter the soil during this extra opportunity time. Also, the measured field is characterised by a large vertical step between borders which causes a rapid recession phase and means shorter opportunity times for water to infiltrate into the soil. Both of these factors (low final infiltration rate and large vertical step between borders) diminish the importance of the TBC and the scenario choice compared with other fields. The TBC technique will have greater value for those soils with higher final infiltration rates and for those layouts with a longer recession phase.

Adoption of the TBC approach is practical because it only involves a small extra amount of data in addition to that required to complete the calculations for blocked or free draining conditions.

A complementary upstream calculation was developed to estimate infiltrated volume for the upstream part of the field before the sill, which can then be combined with the results from the TBC to estimate the performance indices for the entire length of the furrow. This upstream complementary calculation was based on the assumption that the water drains from this upstream part of the field at the same time. This assumption is based on observations of the measured field. It was observed that the water drained-back quickly from that portion of the field between the furrow entrance and the sill due to the presence of an adequate vertical step between adjoining borders and wide check gates between the adjoining borders which have the capacity to pass large amount of water in a short time.

The results for the entire field length (Furrows 13 to 24) in Border 1 of Field 2 on 10-2-2018 showed AE results ranging between 30.7% and 80.6% for Scenario A, and between 30.7% and 79.0% for Scenario B between individual furrows. The RE results ranged between 18. 8% and 64.9% for Scenario A, and between 18.6% and 64.4% for Scenario B in the same furrows.

It is impractical (expensive and time consuming) to conduct the evaluation measurements for all furrows in the border using the intensive methods employed for the twelve furrows. A technique was developed to combine UAV data (represented by the IOT) with the estimated infiltration characteristics of a small number of intensively measured furrows, allowing evaluation of irrigation performance at the border scale. This technique includes the interpolation of IOT across the border from UAV data which may contain significant spatial gaps. The large size of the field, the limited quantity of UAV flight missions, and the difficulty in correctly identifying the water front, led to shortages in available IOTs. In one example the technique developed succeeded in raising the available IOT data from 17% to 86% of the field area, compared to the use of the raw UAV data alone.

While it was stated as an objective to characterise performance at the border and field scale, the measurements were not sufficient to provide good quality results for the entire field. The measurements were largely concentrated in one of the two borders within the field, hence that's why the performance results are only determined at this whole of border scale. Importantly the techniques described in this thesis would allow future studies to properly measure and evaluate the whole field performance.The AE

and RE were estimated at the border scale based from the net depth applied in each border using flow rate measurements at the field scale, and the SWD from the simple water balance tool, IrriSAT. The estimation was based on the assumption that no deep drainage will occur until the water deficit has been replenished at that position in the field. The use of a water balance tool suited the available field data where no information was available on soil moisture. Conducting soil moisture content measurements and other soil physical characteristics such as the field capacity may provide more reliable results regarding the estimation of the AE and RE of the border instead of adopting the water balance approach, but it is often difficult and impractical to obtain this data given the significant spatial variability of most soils. The results showed low values of AE and RE in the FNSBO_Re system at the border scale, which ranged from 43.5% to 56.5% for AE, and from 52.5% to 100% for RE. These low efficiencies indices result from the considerable runoff losses due to the high applied inflow rates, and the low infiltration characteristics. The border scale uniformity calculated using data from the UAV technique yielded high values of DU (up to 96.6%). It is believed that there was overestimation in the DU due to the absence of UAV measurements for the end of the recession phase at the bottom end of the field.

Statistical analyses indicated that machinery wheel traffic affects many aspects such as peak water depth, cross-sectional area, and flow rate. Investigating the factors that influence the variability of the water advance showed that the main driving factors for this variability were the flow rate and the cross-sectional areas. Unexpectedly, this investigation showed that the furrow elevation, and peak water depth have insignificant impact on the water advance, and thus have insignificant impact on the irrigation performance. Therefore, it can be concluded that in the current system, the irrigation performance is governed by the shape of the furrow and flow rate. The impact of the infiltration process on the variation of irrigation performance between furrows was somewhat limited to the initial infiltration value.

As mentioned above, it is impractical to measure large numbers of furrows in each border. A simple approach was developed which can be used to select the furrows instrumented for the evaluation measurements. This selection technique is based on understanding the water advance variability at the border scale through analysing UAV advance data from an event early in the season.

Chapter 11 outlines a recommended procedure for measurement and evaluation of FNSBO_Re irrigation systems. This procedure should also be useful for a range of surface irrigation systems including both traditional and alternative field layouts.

12.3. Limitations

There were a number of limitations which impacted the ability to conduct more intensive and reliable measurements. One issue is that some of the measurements must be conducted manually which limits the quantity of measurements which can be collected during an irrigation event in these systems. Allocating more than one qualified person to the task, or investigating automation of selected measurements could solve this limitation.

High instrument costs restricted the number of measurements which could be conducted and forced the adoption of alternative techniques with lower quality results, such as measuring peak water depths with a wooden stake. High instrument costs are also a concern for future studies, and hence the development of techniques to reduce the number of required measurements as described above.

12.4. Recommendations for further work

This study focusses on measurements and observations collected on a small number of fields on a single property during two seasons. The field layout on this farm is likely to be representative of many designs throughout the Australian Cotton Industry and therefore the developed measurement and analysis techniques should be applicable across other farms. While the performance results provide valuable insights into the behaviour of these systems, there is no guarantee that they provide a representative sample of these systems. It is recommended that similar studies are performed across fields from other properties in order to improve the quality of the findings.

Analysis of UAV data, in particular the detection of the advance and recession water fronts was conducted manually by reviewing video recordings collected during the flight missions. Automating the process of identifying the water front and the subsequent calculations of the developed approaches would reduce the significant

effort required for analysis. Automation of these techniques would encourage future evaluation measurements of these systems.

The modelling conducted in this PhD used a combination of existing computer models, manual calculations and computer spreadsheets. Developing a computerised hydraulic model which incorporates the techniques described in this project and can accommodate the special hydraulic features of these bankless irrigation systems would be of great value to the industry.

The methodology adopted in this study was labour intensive and required a large number of instruments. The measurements in this study are suitable for research purposes and may not be practical for commercial evaluation purposes. In this regard, simplifying this methodology by adopting only UAV measurements, and the flow rates between the borders, can significantly reduce the effort for field work without necessarily reducing the quality of the analysis.

Reference

ABS 2008, *Irrigation on Australian farms*, Australian Bureau of Statistics, cat. no 1301.1, Canberra, Australia, <http://www.abs.gov.au/ausstats/abs@.nsf/Previousproducts/1301.0Feature%20Article16012008?opendocument&tabname=Summary&prodno=1301.0&issue=2008&num=&view=>.

ABS 2018, *Increased agricultural water use in 2016-17* 21/05/2018 <file:///H:/000%20Writing%20+%20Sources%20+%20EndNote/000%20References%20+%20Sources/0000%202019%20new%20used%20reference/4618.0%20-%20Water%20Use%20on%20Australian%20Farms,%202016-17.html>.

ABS 2019a, *Water Account, Australia, 2016-17*, 12/02/2019 <http://www.abs.gov.au/ausstats/abs@.nsf/mf/4610.0>.

ABS 2019b, *Gross Value of Irrigated Agricultural Production, 2017-18*, 31/05/2019 <https://www.abs.gov.au/ausstats/abs@.nsf/mf/4610.0.55.008>.

ABS 2019c, *Value of Agricultural Commodities Produced, Australia, 2017-18*, 30/04/2019 <https://www.abs.gov.au/ausstats/abs@.nsf/mf/7503.0>.

Adrianov, BV & Mantellini, S 2013, Ancient Irrigation Systems of the Aral Sea Area: Ancient Irrigation Systems of the Aral Sea Area, 634, Oxbow Books, Limited.

Alejo, LA 2020, 'Evaluation of the SIRMOD model for optimum furrow irrigation performance', *Agricultural Engineering International: CIGR Journal*, vol. 22, no. 1, pp. 30-9.

Allen, R & Musick, J 1997, 'Furrow irrigation infiltration with multiple traffic and increased axle mass', *Applied engineering in agriculture*, vol. 13, no. 1, pp. 49-53.

Allen, R, Walter, I, Elliott, R, et al. 2005, 'The ASCE standard reference evapotranspiration equation', *ASCE, Reston*.

APSIM 2019, *Apsoil Database*, <https://www.apsim.info/apsim-model/apsoil />.

ASAE, E 2008, *Evaluation of Irrigation Furrows*, MI, USA, ASAE EP419.1 FEB1993 (R2008).

Austin, NR & Prendergast, JB 1997, 'Use of kinematic wave theory to model irrigation on cracking soil', *Irrigation Science*, vol. 18, no. 1, pp. 1-10.

Bakker, D, Plunkett, G & Sherrard, J 2006, 'Application efficiencies and furrow infiltration functions of irrigations in sugar cane in the Ord River Irrigation Area of North Western Australia and the scope for improvement', *Agricultural water management*, vol. 83, no. 1, pp. 162-72.

References

Bautista, E, Clemmens, A & Strelkoff, T 2009, 'Structured application of the two-point method for the estimation of infiltration parameters in surface irrigation', *Journal of irrigation and drainage engineering*, vol. 135, no. 5, pp. 566-78.

Bautista, E, Strelkoff, T & Clemmens, A 2012, 'Improved surface volume estimates for surface irrigation volume-balance calculations', *Journal of irrigation and drainage engineering*, vol. 138, no. 8, pp. 715-26.

Bautista, E, Schlegel, J, Strelkoff, TS, et al. 2006, 'An integrated software package for simulation, design, and evaluation of surface irrigation systems', in *Proceedings of the World Water and Environmental Resources Congress*.

Beat, L, Philippe, T & Peña-Haro, S 2014, 'Mobile device app for small open-channel flow measurement'.

Ben-Hur, M, Shainberg, I, Bakker, D, et al. 1985, 'Effect of soil texture and CaCO 3 content on water infiltration in crusted soil as related to water salinity', *Irrigation Science*, vol. 6, no. 4, pp. 281-94.

Benami, A & Ofen, A 1983, Irrigation engineering. Sprinkler, trickle, surface irrigation principles and agricultural practices, 806, Irrigation Engineering Scientific Publications, Haifa, Israel.

Booher, L 1974, 'Surface irrigation, Development paper, No.95

', *FAO United Nations*.

Bos, MG, Kselik, RA, Allen, RG, et al. 2009, Water requirements for irrigation and the environment, 633, Springer Science & Business Media.

Brater, EF, King, HW, Lindell, JE, et al. 1996, Handbook of hydraulics: for the solution of hydrostatic and fluid flow problems, 7th edn, 813, McGraw-Hill.

Burt, CM 1995, The surface irrigation manual, 1st Edn, 803, Waterman Industries Inc., Exeter, CA.

Burt, CM, Clemmens, A, Bliesner, R, et al. 1999, Selection of irrigation methods for agriculture: committee report / On-Farm Irrigation Committee, Water Resources Division, 804, American Society of Civil Engineers.

Burt, CM, Clemmens, AJ, Strelkoff, TS, et al. 1997, 'Irrigation performance measures: Efficiency and uniformity', *Journal of Irrigation & Drainage Engineering*, vol. 123, no. 6, p. 423.

Chadwick, A & Morfett, J 2013, Hydraulics in civil and environmental engineering, 5th edn, 811, Crc Press.

Chaudhry, MH 2007, Open-channel flow, 810, Springer Science & Business Media.

References

Chavez, C & Fuentes, C 2019, 'Design and evaluation of surface irrigation systems applying an analytical formula in the irrigation district 085, La Begoña, Mexico', *Agricultural water management*, vol. 221, pp. 279-85.

Clemmens, A 1983, 'Infiltration equations for border irrigation models'.

Clemmens, A 2000a, 'Measuring and improving irrigation system performance at the field level', *Irrigation Association of Australia, Melbourne*, pp. 190-9.

Clemmens, A 2000b, 'Level-basin irrigation systems: adoption, practices, and the resulting performance', in *National irrigation symposium. Proceedings of the 4th Decennial Symposium, Phoenix, Arizona, USA, November 14-16, 2000.*, American Society of Agricultural Engineers, pp. 273-82.

Clemmens, A 2007a, 'Simple approach to surface irrigation design: Spreadsheet applications', *e-Journal of land and water*.

Clemmens, A 2007b, 'Simple approach to surface irrigation design: theory', *e-Journal of land and water*.

Clyma, W & Clemmens, A 2000, 'Farmer management strategies for level basins using advance distance criteria', in *National irrigation symposium. Proceedings of the 4th Decennial Symposium, Phoenix, Arizona, USA, November 14-16, 2000.*, American Society of Agricultural Engineers, pp. 573-8.

CottonInfo 2014, *Bankless channels: The Cook family case study*, viewed 18 August 2015, <http://www.cottoninfo.com.au/sites/default/files/documents/CottonInfo%20bankless%20channels%20case%20study%20-%20March%202014.pdf>.

Dalgliesh, N, Cocks, B & Horan, H 2012, 'APSoil-providing soils information to consultants, farmers and researchers', in *16th Australian Agronomy Conference, Armidale, NSW*.

De Sousa, P, Dedrick, A, Clemmens, A, et al. 1995, 'Effect of furrow elevation differences on level-basin performance', *Transactions of the ASAE*, vol. 38, no. 1, pp. 153-8.

Dedrick, AR & Clemmens, AJ 1988, 'Hydraulic studies of surface drainage from level furrows', in *Planning now for irrigation and drainage in the 21st century*, ASCE, pp. 125-32.

DEEDI 2011, *Bankless channels - Bullamon plains*, Australian government viewed 10 March 2016, <https://moreprofitperdrop.files.wordpress.com/2012/01/wueinvhh_bankless-channels-case-study_final-_2_.pdf>.

Edraki, M, Humphreys, E, O'Connell, N, et al. 2003, 'Determination of irrigation efficiency and deep drainage for irrigated maize with a shallow watertable', *CSIRO Land and Water Technical Report*.

References

El-Dine, TG & Hosny, MM 2000, 'Field evaluation of surge and continuous flows in furrow irrigation systems', *Water resources management*, vol. 14, no. 2, pp. 77-87.

Eldeiry, A, Garcia, L, El-Zaher, A, et al. 2005, 'Furrow irrigation system design for clay soils in arid regions', *Applied engineering in agriculture*, vol. 21, no. 3, pp. 411-20.

Elliott, R & Walker, W 1982, 'Field evaluation of furrow infiltration and advance functions', *Transactions of the ASAE*, vol. 25, no. 2, pp. 396-0400.

Erie, LJ & Dedrick, AR 1979, Level-basin irrigation: a method for conserving water and labor, vol. 2261, 604, Dept. of Agriculture, Science and Education Administration: for sale by the Supt. of Docs., US Govt. Print. Off.

Fadul, E, Masih, I, De Fraiture, C, et al. 2020, 'Irrigation performance under alternative field designs in a spate irrigation system with large field dimensions', *Agricultural water management*, vol. 231, p. 105989.

Fangmeier, DD, Clemmens, AJ, El-Ansary, M, et al. 1999, 'INFLUENCE OF LAND LEVELING PRECISION ON LEVEL-BASIN ADVANCE AND PERFORMANCE', vol. 42, no. 4.

Feyen, J & Zerihun, D 1999, 'Assessment of the performance of border and furrow irrigation systems and the relationship between performance indicators and system variables', *Agricultural water management*, vol. 40, no. 2-3, pp. 353-62.

Gillies, M, Smith, R, Williamson, B, et al. 2010, 'Improving performance of bay irrigation through higher flow rates', in *Australian Irrigation Conference and Exibition 2010: Proceedings*, Irrigation Australia Ltd.

Gillies, MH 2008, 'Managing the effect of infiltration variability on the performance of surface irrigation', University of Southern Queensland.

Gillies, MH & Smith, R 2005, 'Infiltration parameters from surface irrigation advance and run-off data', *Irrigation Science*, vol. 24, no. 1, pp. 25-35.

Gillies, MH & Smith, RJ 2015, 'SISCO: surface irrigation simulation, calibration and optimisation', *Irrigation Science*, vol. 33, no. 5, pp. 339-55.

Gillies, MH, Smith, RJ & Raine, SR 2008, 'Measurement and management of furrow irrigation at the field scale'.

González, C, Cervera, L & Moret-Fernández, D 2011, 'Basin irrigation design with longitudinal slope', *Agricultural water management*, vol. 98, no. 10, pp. 1516-22.

Grabham, M, Hornbuckle, J, Raine, S, et al. 2008, 'Observations from initial evaluation trials of bankless channel irrigation systems', in *Irrigation Association of Australia National Conference*.

References

Grabham, M, Hornbuckle, J, Raine, SR, et al. 2009, 'Bankless channel irrigation systems: irrigation performance assessment', in *Irrigation Australia 2009: Irrigation Australia Irrigation and Drainage Conference: Proceedings*, Irrigation Australia Ltd.

Grabham, MK 2012, 'Performance evaluation and improvement of bankless channel surface irrigation systems', University of Southern Queensland.

GVIA 2016, *Grower Led Irrigation System Comparison in The Gwydir Valley*, CRDC1606 Technical Research Report.

GVIA, IA, CottonInfo 2019, *Siphon-less Irrigation Systems Guide 2019*, <https://www.cottoninfo.com.au/sites/default/files/documents/Irrigation%20Guide_2019%20NEW%20Exec%20PRINT.PDF>.

Holzapfel, E, Jara, J, Zuniga, C, et al. 2004, 'Infiltration parameters for furrow irrigation', *Agricultural water management*, vol. 68, no. 1, pp. 19-32.

Holzworth, DP, Huth, NI, deVoil, PG, et al. 2014, 'APSIM–evolution towards a new generation of agricultural systems simulation', *Environmental Modelling & Software*, vol. 62, pp. 327-50.

Hood, S & Carrigan, E 2006, 'Siphon-less irrigation project', in *Product, production, profit: progressing our natural advantage 13th Australian Cotton Conference'. Broadbeach, QLD*.

Hornbuckle, J, Montgomery, J & Vlesshouwer, J 2016, *A quick guide to the use of the cloud based IrriSAT app*, <https://irrisat-cloud.appspot.com/doc/IrriSAT_QuickGuide_20052016.pdf>.

Hunsaker, DJ, Bucks, D.A,Jaynes, D.B. 1991, 'Irrigation uniformity of level basins as influenced by variations in soil water content and surface elevation', *Agricultural Water Management,*, vol. 19, no. 4, pp. 325-40.

Israelsen, O & Hansen, VE 1962, Irrigation principles and practices, 3 edn, 802, John Wiley and Sons, New York.

Izadi, B & Wallender, W 1985, 'Furrow hydraulic characteristics and infiltration', *Transactions of the ASAE American Society of Agricultural Engineers*.

James, LG 1988, Principles of farm irrigation systems design, 805, John Wiley and Sons, Inc.

Jensen, ME 1980, Design and operation of farm irrigation systems, 3 edn, 801, American Society of Agricultural Engineers, Michigan.

Kaur, S, Raheja, A & Aggarwal, R 2019, 'Performance evaluation and optimization studies of border irrigation system for wheat in the Indian Punjab', *Water SA*, vol. 45, no. 1, pp. 41-7.

References

Khalid, M & Smith, JL 1978, 'Control of furrow infiltration by compaction', *Transactions of the ASAE*, vol. 21, no. 4, pp. 654-0657.

Khanna, M & Malano, HM 2006, 'Modelling of basin irrigation systems: A review', *Agricultural water management*, vol. 83, no. 1, pp. 87-99.

Khanna, M, Malano, HM, Fenton, JD, et al. 2003, 'Design and management guidelines for contour basin irrigation layouts in southeast Australia', *Agricultural water management*, vol. 62, no. 1, pp. 19-35.

Kindsvater, CE & Carter, RW 1959, 'Discharge characteristics of rectangular thin-plate weirs', *Transactions of the American Society of Civil Engineers*, vol. 124, no. 1, pp. 772-801.

Koech, R, Smith, R & Gillies, MH 2010, 'Automation and control in surface irrigation systems: current status and expected future trends', in *Proceedings of the 2010 Southern Region Engineering Conference (SREC 2010)*, Engineers Australia.

Koech, R, Smith, R & Gillies, M 2015, 'Trends in the use of surface irrigation in Australian irrigated agriculture: An investigation into the role surface irrigation will play in future Australian agriculture', *Water: Journal of the Australian Water Association*, vol. 42, no. 5, p. 84.

Kruse, EG 1978, 'Describing irrigation efficiency and uniformity', *Journal of the Irrigation and Drainage Division*, vol. 104, no. 1, pp. 35-41.

Lipiec, J, Kuś, J, Słowińska-Jurkiewicz, A, et al. 2006, 'Soil porosity and water infiltration as influenced by tillage methods', *Soil and Tillage Research*, vol. 89, no. 2, pp. 210-20.

Liu, K, Jiao, X, Guo, W, et al. 2020, 'Improving border irrigation performance with predesigned varied-discharge', *Plos one*, vol. 15, no. 5, p. e0232751.

Long, D, McCarthy, C & Jensen, T 2016, 'Row and water front detection from UAV thermal-infrared imagery for furrow irrigation monitoring', in *2016 IEEE International Conference on Advanced Intelligent Mechatronics (AIM)*, IEEE, pp. 300-5.

Mailhol, J-C & Gonzalez, J-M 1993, 'Furrow irrigation model for real-time applications on cracking soils', *Journal of irrigation and drainage engineering*, vol. 119, no. 5, pp. 768-83.

Martin, E & Eusuff, T 2000, 'Saving water using drain-back level basins', in *National irrigation symposium. Proceedings of the 4th Decennial Symposium, Phoenix, Arizona, USA, November 14-16, 2000.*, American Society of Agricultural Engineers, pp. 567-72.

McClymont, D & Smith, R 1996, 'Infiltration parameters from optimisation on furrow irrigation advance data', *Irrigation Science*, vol. 17, no. 1, pp. 15-22.

References

McKenzie, DC 1998, SOILpak, 3rd edn, NSW Agriculture, NSW, Australia, <https://www.cottoninfo.com.au/sites/default/files/documents/SOILpak.pdf>.

Merriam-Webster 2020, *Irrigation. In Merriam-Webster.com dictionary.*, <https://www.merriam-webster.com/dictionary/irrigation>.

Montgomery, J, Hornbuckle, J, Hume, I, et al. 2015, 'IrriSAT—Weather based scheduling and benchmarking technology', in *Proceedings of the 17th ASA Conference, Hobart, Australia*, pp. 20-4.

Moravejalahkami, B 2020, 'METHODS OF INFILTRATION ESTIMATION FOR FURROW IRRIGATION', *Irrigation and Drainage*, vol. 69, no. 1, pp. 52-62.

Morbidelli, R, Saltalippi, C, Flammini, A, et al. 2018, 'Role of slope on infiltration: a review', *Journal of Hydrology*, vol. 557, pp. 878-86.

Morris, MR, Hussain, A, Gillies, MH, et al. 2015, 'Inflow rate and border irrigation performance', *Agricultural water management*, vol. 155, pp. 76-86.

Nasseri, A, Neyshabori, M & Abbasi, F 2008, 'Effectual components on furrow infiltration', *Irrigation and Drainage*, vol. 57, no. 4, pp. 481-9.

Nasseri, A, Neyshabori, MR, Fard, AF, et al. 2004, 'Field-Measured Furrow Infiltration Functions', *Tarla Kosullarinda Ölçülmüs Karik Infiltrasyon Fonksiyonlari.*, vol. 28, no. 2, pp. 93-9.

North, S 2008, 'A review of Basin (Contour) Irrigation Systems I: Current design and management practices in the Southern Murray-Darling Basin, Australia', *CRC for Irrigation Futures*.

Novak, V, Šimåunek, J & Genuchten, MTv 2000, 'Infiltration of water into soil with cracks', *Journal of irrigation and drainage engineering*, vol. 126, no. 1, pp. 41-7.

NRCS 1997, *'National Engineering Handbook; [Part 652], Irrigation Guide*, USDA, Natural Resources Conservation Service:, Washington, DC.

Patin, J, Mouche, E, Ribolzi, O, et al. 2012, 'Analysis of runoff production at the plot scale during a long-term survey of a small agricultural catchment in Lao PDR', *Journal of Hydrology*, vol. 426, pp. 79-92.

Peña-Haro, S, Lüthi, B & Philippe, T 2015, 'Smartphone for measuring river discharge', in *EGU General Assembly Conference Abstracts*.

Pereira, L, Goncalves, J, Dong, B, et al. 2007, 'Assessing basin irrigation and scheduling strategies for saving irrigation water and controlling salinity in the upper Yellow River Basin, China', *Agricultural water management*, vol. 93, no. 3, pp. 109-22.

PIA 2013, Australian pipe friction handbook, 4th edn, 812, McPherson's Printing Group, <aryborough, VIC, Australia.

References

Pink, B 2010, *Water Account, Australia 2008–09*, Australian bureau of statistics, 29 NOV 2010, <https://www.ausstats.abs.gov.au/Ausstats/subscriber.nsf/0/D2335EFFE939C9BCCA2577E700158B1C/$File/46100_2008-09.pdf>.

Playan, E & Faci, JM 1996, 'Modeling microtopography in basin irrigation', *Journal of Irrigation & Drainage Engineering*, vol. 122, no. 6, p. 339.

Playán, E, Walker, W & Merkley, G 1994, 'Two-dimensional simulation of basin irrigation. I: Theory', *Journal of irrigation and drainage engineering*, vol. 120, no. 5, pp. 837-56.

Playán Jubillar, E & Martínez-Cob, A 1999, 'Simulation of basin irrigation scheduling as a function of discharge and leveling', *Investigación agraria. Producción y protección vegetales*, vol. 14, no. 3, pp. 545-54.

Postel, S 1999, Pillar of sand: can the irrigation miracle last?, 814, WW Norton & Company.

Raine, S & Walker, W 1998, 'A decision support tool for the design, management and evaluation of surface irrigation systems', in *Irrigation Association of Australia National Conference*.

RISC, RISC 2009, 'Manual of British Columbia Hydrometric Standards', *British Columbia Ministry of Environment, Province of British Columbia, Version*, vol. 1, p. 204.

Rojas-Ponce, S, Smith, R & Gillies, M 2011, 'Improved evaluation of bay (and furrow) irrigation', in *Proceedings of Irrigation 2011-New Horizons, Fresh Ideas Regional Conference and Exhibition*, Irrigation Australia Ltd., pp. 1-2.

Salahou, MK, Jiao, X & Lü, H 2018, 'Border irrigation performance with distance-based cut-off', *Agricultural water management*, vol. 201, pp. 27-37.

Sanchez, C, Zerihun, D, Strelkoff, T, et al. 2008, 'Development of management guidelines for efficient irrigation of basins on sandy soils', *Applied engineering in agriculture*, vol. 24, no. 2, pp. 215-24.

Saxon, SL & Dye, CW 1995, 'A simple, inexpensive peak water-level gauge', *Hydrobiologia*, vol. 315, no. 3, pp. 231-3.

Sayari, S, Rahimpour, M & Zounemat-Kermani, M 2019, 'Assessment of straight and meandering furrow irrigation strategies under different inflow rates', *Water SA*, vol. 45, no. 4, pp. 685-90.

Scaloppi, EJ, Merkley, GP & Willardson, LS 1995, 'Intake parameters from advance and wetting phases of surface irrigation', *Journal of irrigation and drainage engineering*, vol. 121, no. 1, pp. 57-70.

References

Sivarajan, S, Maharlooei, M, Bajwa, S, et al. 2018, 'Impact of soil compaction due to wheel traffic on corn and soybean growth, development and yield', *Soil and Tillage Research*, vol. 175, pp. 234-43.

Smith, R 2014, Irrigation Science, *USQ study book*, 809, USQ campus, Australia, QLD, Toowoomba.

Smith, R & Uddin, M 2020, 'Selection of flow rate and irrigation duration for high performance bay irrigation', *Agricultural water management*, vol. 228, p. 105850.

Smith, R, Raine, SR & Minkevich, J 2005, 'Irrigation application efficiency and deep drainage potential under surface irrigated cotton', *Agricultural water management*, vol. 71, no. 2, pp. 117-30.

Smith, R, Uddin, M & Gillies, M 2018, 'Estimating irrigation duration for high performance furrow irrigation on cracking clay soils', *Agricultural water management*, vol. 206, pp. 78-85.

SonTek 2016, *FlowTracker2 User"s Manual*, <http://www.geotechenv.com/Manuals/SonTek_Manuals/sontek_flowtracker2_manual.pdf>.

Strelkoff, T & Clemmens, A 2007, 'Hydraulics of surface systems', *Design and operation of farm irrigation systems/Glenn J. Hoffman...{et al.]*.

Strelkoff, T, Clemmens, A, El-Ansary, M, et al. 1999, 'Surface-irrigation evaluation models: Application to level basins in Egypt', *Transactions of the ASAE*, vol. 42, no. 4, pp. 1027-37.

Tadele, D, Taddesse, F & Bekele, M 2019, 'Evaluation of hydraulic performance a case study of etana small scale irrigation scheme wolaita zone Ethiopia', *International Journal of Hydrology*, vol. 3, no. 3.

Trout, TJ 1992, 'Flow velocity and wetted perimeter effects on furrow infiltration', *Transactions of the ASAE*, vol. 35, no. 3, pp. 855-63.

Unidata 2013, *Manual Starflow ultrasonic doppler instrument with micrologger, Model 6526*, issue 4.0, Unidata Pty Ltd, Western Australia.

USDA 1974a, *Furrow Irrigation*, 5, John Wiley and Sons, New York, <ftp://ftp.wcc.nrcs.usda.gov/wntsc/waterMgt/irrigation/NEH15/ch5.pdf>.

USDA 1974b, *Border Irrigation*, 4, National Technical Information Service, Washington, DC, <ftp://ftp.wcc.nrcs.usda.gov/wntsc/waterMgt/irrigation/NEH15/ch4.pdf>.

USDA 2012, *Surface irrgatiom*, Natural resources conservation service,, Washington, DC, <http://directives.sc.egov.usda.gov/OpenNonWebContent.aspx?content=32940.wba>.

References

Valiantzas, JD 1997, 'Volume balance irrigation advance equation: Variation of surface shape factor', *Journal of irrigation and drainage engineering*, vol. 123, no. 4, pp. 307-12.

Van Dijck, S & Van Asch, TW 2002, 'Compaction of loamy soils due to tractor traffic in vineyards and orchards and its effect on infiltration in southern France', *Soil and Tillage Research*, vol. 63, no. 3-4, pp. 141-53.

Voorhees, W, Young, R & Lyles, L 1979, 'Wheel traffic considerations in erosion research', *Transactions of the ASAE*, vol. 22, no. 4, pp. 786-0790.

Walker, WR 2003, *SIRMOD III: Surface irrigation simulation, evaluation and design*.

Walker, WR & Skogerboe, GV 1987, Surface irrigation. Theory and practice, 808, Prentice-Hall, Inc.

Walker, WR, Prestwich, C & Spofford, T 2006, 'Development of the revised USDA–NRCS intake families for surface irrigation', *Agricultural water management*, vol. 85, no. 1-2, pp. 157-64.

Wall, D 1996, 'open channel flow measurement devices', Brigham Young University, Provo, Utah.

WATERpak 2015, 'WATERpak – a guide for irrigation management in cotton and grain farming systems', in http://www.cottoncrc.org.au/industry/Publications/Water/WATERpak>.

Xu, J, Cai, H, Saddique, Q, et al. 2019, 'Evaluation and optimization of border irrigation in different irrigation seasons based on temporal variation of infiltration and roughness', *Agricultural water management*, vol. 214, pp. 64-77.

References

Appendices

Appendix A Flow rate

A.1 Starflow instruments calibration

Table A-1 Starflows calibrations

Starflow Serial Number	Water depth calibration equation	Water velocity calibration equation
1410	d_{cal} = 1.0847 d - 42.018	V_{cal} = 0.8807 V - 14.487
1619	d_{cal} = 0.9499 d + 10.073	V_{cal} = 0.9824 V - 21.987
1627	d_{cal} = 0.938 d + 31.083	V_{cal} = 0.9321 V - 15.121
1642	d_{cal} = 0.9944 d + 8.2895	V_{cal} = 0.9442 V - 22.666
1643	d_{cal} = 0.9266 d - 4.9878	V_{cal} = 0.9602 V - 16.883
1645	d_{cal} = 0.9692 d + 6.3785	V_{cal} = 1.0278 V - 29.563
1652	d_{cal} = 0.935 d - 11.17	V_{cal} = 0.9401 V - 11.628
1900	d_{cal} = 0.9632 d + 3.527	V_{cal} = 0.9298 V - 18.724
1904	d_{cal} = 0.9016 d + 2.2538	V_{cal} = 0.9991 V - 29.823
1912	d_{cal} = 1.0211 d + 5.2173	V_{cal} = 0.9198 V - 9.376
1913	d_{cal} = 0.9256 d + 9.6524	V_{cal} = 0.9575 V - 16.645
3483	d_{cal} = 0.9642 d + 3.4127	V_{cal} = 0.8657 V + 6.9956
20088	d_{cal} = 1.1156 d + 5.6155	V_{cal} = 0.9357 V - 12.75
20320	d_{cal} = 0.8585 d + 8.2984	V_{cal} = 0.9099 V - 5.3355

A.2 Flow rate at field scale

Sample of flow rate data (or measurements) at the field scale for one irrigation event conducted on 10-02-2018.

Table A-2 Flow rate of supply pipe of Field 2 logged by Starflow with serial number 1619, for the irrigation event on 10-02-2018.

Time	Flow area	Water velocity	Calibrated velocity	Amended velocity	Flow rate	Flow rate
	cm²	mm/s	mm	mm/s	m^3/s	m^3/ (5 min.)
6:15 AM	6362	3157	3079	3079	1.959	587.7
6:20 AM	6362	3129	3052	3052	1.942	582.5
6:25 AM	6362	3242	3163	3163	2.012	603.7
6:30 AM	6362	3159	3081	3081	1.960	588.1
6:35 AM	6362	3256	3177	3177	2.021	606.3
6:40 AM	6362	3242	3163	3163	2.012	603.7
6:45 AM	6362	3079	3003	3003	1.910	573.1
6:50 AM	6362	3133	3056	3056	1.944	583.2
6:55 AM	6362	3182	3104	3104	1.975	592.4
7:00 AM	6362	3127	3050	3050	1.940	582.1

Time	Flow area	Water velocity	Calibrated velocity	Amended velocity	Flow rate	Flow rate
	cm²	mm/s	mm	mm/s	m^3/s	m^3/ (5 min.)
7:05 AM	6362	1689	1637	3053*	1.942	582.7
7:10 AM	6362	2569	2502	2502	1.592	477.5
7:15 AM	6362	3220	3141	3141	1.999	599.6
7:20 AM	6362	1898	1843	2937*	1.868	560.5
7:25 AM	6362	1862	1807	2908*	1.850	555.1
7:30 AM	6362	3171	3093	3093	1.968	590.4
7:35 AM	6362	2441	2376	2376	1.512	453.5
7:40 AM	6362	3099	3022	3022	1.923	576.9
7:45 AM	6362	2631	2563	2563	1.630	489.1
7:50 AM	6362	3053	2977	2977	1.894	568.2
7:55 AM	6362	1330	1285	2735*	1.740	521.9
8:00 AM	6362	2462	2397	2397	1.525	457.4
8:05 AM	6362	2972	2898	2898	1.844	553.1
8:10 AM	6362	2891	2818	2818	1.793	537.9
8:15 AM	6362	3014	2939	2939	1.870	560.9
8:20 AM	6362	2341	2278	2278	1.449	434.7
8:25 AM	6362	3076	3000	3000	1.909	572.6
8:30 AM	6362	3072	2996	2996	1.906	571.8
8:35 AM	6362	2410	2346	2346	1.492	447.7
8:40 AM	6362	2396	2332	2332	1.484	445.1
8:45 AM	6362	3067	2991	2991	1.903	570.9
8:50 AM	6362	3083	3007	3007	1.913	573.9
8:55 AM	6362	2462	2397	2397	1.525	457.4
9:00 AM	6362	3009	2934	2934	1.867	560.0
9:05 AM	6362	3025	2950	2950	1.877	563.0
9:10 AM	6362	2514	2448	2448	1.557	467.2
9:15 AM	6362	3119	3042	3042	1.935	580.6
9:20 AM	6362	2981	2907	2907	1.849	554.7
9:25 AM	6362	3137	3060	3060	1.947	584.0
9:30 AM	6362	2476	2410	2410	1.534	460.1
9:35 AM	6362	3115	3038	3038	1.933	579.9
9:40 AM	6362	2484	2418	2418	1.539	461.6
9:45 AM	6362	2937	2863	2863	1.822	546.5
9:50 AM	6362	2948	2874	2874	1.829	548.6
9:55 AM	6362	3020	2945	2945	1.874	562.1
10:00AM	6362	2405	2341	2341	1.489	446.7
10:05 AM	6362	3059	2983	2983	1.898	569.4
10:10 AM	6362	3045	2969	2969	1.889	566.7
10:15 AM	6362	2951	2877	2877	1.830	549.1
10:20 AM*	6362	3025	2950	2950	1.877	563.0
10:25 AM	6362	3056	2980	2980	1.896	568.8
10:30 AM	6362	1825	1771	2944*	1.873	561.9
10:35 AM	6362	1731	1679	2938*	1.869	560.7
10:40 AM	6362	2423	2358	2358	1.500	450.1
10:45 AM	6362	2890	2817	2817	1.792	537.7
10:50 AM	6362	2354	2291	2291	1.457	437.2
10:55 AM	6362	3069	2993	2993	1.904	571.2
11:00 AM	6362	3021	2946	2946	1.874	562.2
11:05 AM	6362	1401	1354	2762*	1.757	527.1
11:10 AM	6362	1233	1189	2748*	1.748	524.4
11:15 AM	6362	3001	2926	2926	1.862	558.5

Time	Flow area	Water velocity	Calibrated velocity	Amended velocity	Flow rate	Flow rate
	cm^2	mm/s	mm	mm/s	m^3/s	m^3/ (5 min.)
11:20 AM	6362	2392	2328	2328	1.481	444.3
11:25 AM	6362	1556	1507	2691*	1.712	513.6
11:30 AM	6362	2347	2284	2284	1.453	435.9
11:35 AM	6362	2404	2340	2340	1.489	446.6
11:40 AM	6362	3086	3010	3010	1.915	574.4
11:45 AM	6362	1747	1694	2581*	1.642	492.6
11:50 AM	6362	3094	3018	3018	1.920	575.9
11:55 AM	6362	2278	2216	2216	1.410	422.9
12:00 PM	6362	3000	2925	2925	1.861	558.3
12:05 PM	6362	2537	2470	2470	1.572	471.5
12:10 PM	6362	2434	2369	2369	1.507	452.2
12:15 PM	6362	3087	3011	3011	1.915	574.6
12:20 PM	6362	2441	2376	2376	1.512	453.5
12:25 PM	6362	2993	2918	2918	1.857	557.0
12:30 PM	6362	2922	2849	2849	1.812	543.7
12:35 PM	6362	3114	3037	3037	1.932	579.7
12:40 PM	6362	3050	2974	2974	1.892	567.7
12:45 PM	6362	2380	2316	2316	1.474	442.1
12:50 PM	6362	3008	2933	2933	1.866	559.8
12:55 PM	6362	1459	1411	2815*	1.791	537.3
1:00 PM	6362	3112	3035	3035	1.931	579.3
1:05 PM	6362	2429	2364	2364	1.504	451.2
1:10 PM	6362	2963	2889	2889	1.838	551.4
1:15 PM	6362	2991	2916	2916	1.855	556.6
1:20 PM	6362	2402	2338	2338	1.487	446.2
1:25 PM	6362	2408	2344	2344	1.491	447.3
1:30 PM	6362	3045	2969	2969	1.889	566.7
1:35 PM	6362	3006	2931	2931	1.865	559.4
1:40 PM	6362	1741	1688	2645*	1.683	504.9
1:45 PM	6362	3079	3003	3003	1.910	573.1
1:50 PM	6362	2976	2902	2902	1.846	553.8
1:55 PM	6362	3043	2967	2967	1.888	566.4
2:00 PM	6362	3035	2960	2960	1.883	564.9
2:05 PM	6362	3057	2981	2981	1.897	569.0
2:10 PM	6362	2987	2912	2912	1.853	555.9
2:15 PM	6362	3069	2993	2993	1.904	571.2
2:20 PM	6362	3010	2935	2935	1.867	560.2
2:25 PM	6362	2980	2906	2906	1.849	554.6
2:30 PM	6362	911	873	873	0.555	166.6

* Amended water velocity. ** Open the top check gate.

Table A-3 Flow rate of check gate top of Field 2 logged by Starflow with serial number 1652, for the irrigation event on 10-02-2018.

Time	Water depth	Water velocity	Calibrated depth + offset (66 mm)	Calibrated velocity	Calibrated flow rate	Corrected flow rate	Corrected flow rate
	mm	mm/s	mm	mm/s	m^3/s	m^3/s	m^3/ (5 min.)
10:25 AM	345	816	377	755	2.019	1.635	490.544
10:30 AM	370	949	401	881	2.499	2.024	607.139
10:35 AM	369	1058	400	983	2.783	2.254	676.213
10:40 AM	366	772	397	714	2.007	1.626	487.810
10:45 AM	367	748	398	692	1.949	1.578	473.510
10:50 AM	367	671	398	619	1.745	1.413	423.947
10:55 AM	369	661	400	610	1.726	1.398	419.472
11:00 AM	372	639	403	589	1.679	1.360	408.087
11:05 AM	373	607	404	559	1.597	1.294	388.147
11:10 AM	375	712	405	658	1.888	1.529	458.802
11:15 AM	377	684	407	631	1.821	1.475	442.472
11:20 AM	379	689	409	636	1.843	1.493	447.812
11:25 AM	381	623	411	574	1.671	1.353	405.978
11:30 AM	380	721	410	666	1.934	1.567	470.062
11:35 AM	379	712	409	658	1.905	1.543	463.034
11:40 AM	380	723	410	668	1.940	1.571	471.389
11:45 AM	381	726	411	671	1.953	1.582	474.458
11:50 AM	381	636	411	586	1.706	1.382	414.622
11:55 AM	381	717	411	662	1.928	1.562	468.474
12:00 PM	380	674	410	622	1.806	1.463	438.885
12:05 PM	383	677	413	625	1.827	1.480	443.891
12:10 PM	381	667	411	615	1.791	1.451	435.232
12:15 PM	383	662	413	611	1.785	1.446	433.872
12:20 PM	383	732	413	677	1.978	1.602	480.624
12:25 PM	383	732	413	677	1.978	1.602	480.624
12:30 PM	382	731	412	676	1.971	1.596	478.869
12:35 PM	382	642	412	592	1.727	1.399	419.563
12:40 PM	382	690	412	637	1.858	1.505	451.548
12:45 PM	383	612	413	564	1.648	1.335	400.479
12:50 PM	382	645	412	595	1.735	1.405	421.562
12:55 PM	382	721	412	666	1.943	1.574	472.205
1:00 PM	381	755	411	698	2.032	1.646	493.739
1:05 PM	383	762	413	705	2.060	1.669	500.660
1:10 PM	383	684	413	631	1.846	1.495	448.566
1:15 PM	385	690	415	637	1.871	1.515	454.622
1:20 PM	385	699	415	646	1.896	1.536	460.661
1:25 PM	386	696	416	643	1.892	1.532	459.682
1:30 PM	386	730	416	675	1.986	1.608	482.544
1:35 PM	388	678	418	626	1.850	1.499	449.591
1:40 PM	387	683	417	630	1.860	1.507	451.955
1:45 PM	386	551	416	506	1.490	1.207	362.182
1:50 PM	385	602	415	554	1.628	1.319	395.583
1:55 PM	384	713	414	659	1.930	1.563	468.994

Time	Water depth	Water velocity	Calibrated depth + offset (66 mm)	Calibrated velocity	Calibrated flow rate	Corrected flow rate	Corrected flow rate
	mm	mm/s	mm	mm/s	m^3/s	m^3/s	$m^3/$ (5 min.)
2:00 PM	388	652	418	601	1.778	1.440	432.030
2:05 PM	385	725	415	670	1.968	1.594	478.104
2:10 PM	385	739	415	683	2.006	1.625	487.497
2:15 PM	386	701	416	647	1.906	1.543	463.044
2:20 PM	388	735	418	679	2.009	1.627	488.091
2:25 PM	388	740	418	684	2.023	1.638	491.469
2:30 PM	388	737	418	681	2.014	1.631	489.442
2:35 PM	380	579	410	533	1.547	1.253	375.868
2:40 PM	366	388	397	353	0.993	0.804	241.218
2:45 PM	355	410	387	374	1.024	0.829	248.731
2:50 PM	346	309	378	279	0.747	0.605	181.515
2:55 PM	339	-76	372	-83	-0.219	-0.177	-53.139
3:00 PM	335	-80	368	-87	-0.226	-0.183	-54.986
3:05 PM	332	-32	365	-42	-0.108	-0.087	-26.211
3:10 PM	332	-153	365	-155	-0.402	-0.326	-97.692
3:15 PM	334	258	367	231	0.600	0.486	145.850
3:20 PM	329	141	362	121	0.310	0.251	75.405
3:25 PM	326	-101	360	-107	-0.271	-0.220	-65.944
3:30 PM	328	-106	362	-111	-0.285	-0.231	-69.210
3:35 PM	328	-117	362	-122	-0.311	-0.252	-75.642
3:40 PM	321	-89	355	-95	-0.239	-0.194	-58.197
3:45 PM	321	-75	355	-82	-0.206	-0.167	-50.160
3:50 PM	321	-163	355	-165	-0.414	-0.336	-100.682
3:55 PM	321	-191	355	-191	-0.480	-0.389	-116.757
4:00 PM	321	-158	355	-160	-0.403	-0.326	-97.811
4:05 PM	317	-117	351	-122	-0.302	-0.245	-73.490
4:10 PM	313	-108	347	-113	-0.278	-0.225	-67.649
4:15 PM	309	-84	344	-91	-0.220	-0.179	-53.578
4:20 PM	308	-96	343	-102	-0.247	-0.200	-60.086
4:25 PM	306	-66	341	-74	-0.178	-0.144	-43.215
4:30 PM	305	-39	340	-48	-0.116	-0.094	-28.249
4:35 PM	303	-119	338	-123	-0.296	-0.239	-71.845
4:40 PM	300	-388	335	-82	-0.194	-0.157	-47.204
4:45 PM	297	-65	333	-73	-0.171	-0.139	-41.611
4:50 PM	294	-120	330	-124	-0.290	-0.235	-70.590
4:55 PM	291	-62	327	-70	-0.162	-0.131	-39.322

When the flow stream (driving force for stream flow) in the bankless channel reaches to sort of equilibrium, the water could flow (slightly) in either directions. The Starflow was configured to read both positive and negative flow velocities based water flow direction. The positive values of flow velocities and flow rates indicate the normal (primary) flow direction while the negative values indicate the backwards flow direction.

Table A-4 Flow rate of check gate bottom of Field 2 logged by Starflow with serial number 1645, for the irrigation event on 10-02-2018.

Time	Water depth	Water velocity	Calibrated depth + offset (66 mm)	Calibrated velocity	Calibrated flow rate	Corrected flow rate	Corrected flow rate
	mm	mm/s	mm	mm/s	m^3/s	m^3/s	$m^3/$ (5 min.)
10:30 AM	86	2304	156	2339	1.936	1.568	470.468
10:35 AM	83	2305	153	2340	1.901	1.540	462.008
10:40 AM	65	2087	136	2116	1.525	1.236	370.680
10:45 AM	124	1828	192	1849	1.886	1.528	458.398
10:50 AM	178	1643	245	1659	2.155	1.746	523.711
10:55 AM	212	1576	278	1590	2.348	1.902	570.564
11:00 AM	243	1224	308	1229	2.012	1.630	488.851
11:05 AM	308	1149	371	1152	2.270	1.839	551.693
11:10 AM	296	925	359	921	1.759	1.425	427.357
11:15 AM	284	884	348	879	1.624	1.316	394.734
11:20 AM	281	1049	344	1049	1.918	1.554	466.099
11:25 AM	278	967	341	965	1.749	1.416	424.921
11:30 AM	285	1034	348	1033	1.911	1.548	464.308
11:35 AM	285	1056	348	1056	1.953	1.582	474.512
11:40 AM	289	1052	352	1052	1.966	1.593	477.838
11:45 AM	296	1169	359	1172	2.234	1.809	542.808
11:50 AM	297	1259	360	1265	2.417	1.958	587.369
11:55 AM	297	1247	360	1252	2.393	1.939	581.620
12:00 PM	299	1163	362	1166	2.240	1.814	544.250
12:05 PM	299	1070	363	1070	2.061	1.669	500.778
12:10 PM	299	981	362	979	1.884	1.526	457.801
12:15 PM	300	959	363	956	1.845	1.495	448.354
12:20 PM	303	835	366	829	1.611	1.305	391.376
12:25 PM	306	617	369	605	1.185	0.960	287.967
12:30 PM	306	653	369	642	1.258	1.019	305.717
12:35 PM	311	639	374	627	1.246	1.009	302.666
12:40 PM	313	636	376	624	1.246	1.009	302.701
12:45 PM	317	605	379	592	1.194	0.967	290.048
12:50 PM	323	563	385	549	1.123	0.909	272.795
12:55 PM	325	563	388	549	1.131	0.916	274.816
1:00 PM	328	501	390	485	1.006	0.815	244.455
1:05 PM	331	413	393	395	0.823	0.666	199.942
1:10 PM	336	430	398	412	0.870	0.705	211.410
1:15 PM	340	336	402	316	0.674	0.546	163.823
1:20 PM	343	324	405	303	0.652	0.528	158.471
1:25 PM	347	266	408	244	0.530	0.429	128.736
1:30 PM	352	291	413	269	0.591	0.478	143.527
1:35 PM	355	264	416	242	0.535	0.433	130.010
1:40 PM	358	243	419	220	0.490	0.397	119.103
1:45 PM	360	191	422	166	0.372	0.302	90.505
1:50 PM	363	211	425	187	0.422	0.342	102.502
1:55 PM	367	135	429	109	0.248	0.201	60.336
2:00 PM	371	134	432	108	0.248	0.201	60.291

Time	Water depth	Water velocity	Calibrated depth + offset (66 mm)	Calibrated velocity	Calibrated flow rate	Corrected flow rate	Corrected flow rate
	mm	mm/s	mm	mm/s	m^3/s	m^3/s	$m^3/$ (5 min.)
2:05 PM	374	79	435	52	0.120	0.097	29.125
2:10 PM	377	72	437	45	0.104	0.084	25.215
2:15 PM	380	105	440	78	0.182	0.147	44.249
2:20 PM	383	59	443	31	0.073	0.059	17.828
2:25 PM	387	51	447	23	0.054	0.044	13.193
2:30 PM	390	32	450	3	0.008	0.006	1.832
2:35 PM	393	41	453	12	0.030	0.024	7.299
2:40 PM	395	49	455	21	0.050	0.041	12.199
2:45 PM	393	190	453	166	0.399	0.323	96.925
2:50 PM	394	-40	454	-71	-0.170	-0.138	-41.424
2:55 PM	392	125	452	99	0.238	0.192	57.727
3:00 PM	390	258	450	236	0.563	0.456	136.918
3:05 PM	388	310	448	289	0.688	0.558	167.253
3:10 PM	386	226	446	203	0.481	0.389	116.791
3:15 PM	383	71	444	43	0.102	0.083	24.847
3:20 PM	381	-160	442	-194	-0.455	-0.369	-110.560
3:25 PM	379	-104	440	-136	-0.319	-0.258	-77.419
3:30 PM	377	-167	438	-201	-0.468	-0.379	-113.654
3:35 PM	375	257	436	235	0.543	0.440	131.920
3:40 PM	373	-111	434	-144	-0.331	-0.268	-80.423
3:45 PM	370	-48	431	-79	-0.181	-0.146	-43.876
3:50 PM	368	-241	429	-277	-0.632	-0.512	-153.495
3:55 PM	366	-43	427	-74	-0.167	-0.135	-40.649
4:00 PM	363	-7	424	-37	-0.083	-0.067	-20.119
4:05 PM	361	-78	422	-110	-0.246	-0.199	-59.788
4:10 PM	359	-59	420	-90	-0.201	-0.163	-48.922
4:15 PM	357	-164	418	-198	-0.440	-0.357	-106.957
4:20 PM	354	47	415	19	0.041	0.033	10.048
4:25 PM	351	-1	413	-31	-0.067	-0.054	-16.285
4:30 PM	347	-103	409	-135	-0.294	-0.238	-71.417
4:35 PM	345	-20	407	-50	-0.108	-0.088	-26.305
4:40 PM	343	-11	405	-41	-0.088	-0.071	-21.348
4:45 PM	340	-92	402	-124	-0.265	-0.215	-64.368
4:50 PM	338	-82	400	-114	-0.242	-0.196	-58.753
4:55 PM	336	-35	398	-66	-0.139	-0.112	-33.659
5:00 PM	333	-108	395	-141	-0.295	-0.239	-71.666
5:05 PM	331	-41	393	-72	-0.150	-0.121	-36.377
5:10 PM	328	-16	390	-46	-0.095	-0.077	-23.169
5:15 PM	326	32	388	3	0.007	0.006	1.667
5:20 PM	323	-47	385	-78	-0.159	-0.129	-38.727
5:25 PM	321	-25	383	-55	-0.113	-0.091	-27.343
5:30 PM	317	-17	380	-47	-0.095	-0.077	-23.039
5:35 PM	314	-26	377	-56	-0.113	-0.091	-27.359
5:40 PM	311	-64	374	-95	-0.189	-0.153	-45.986
5:45 PM	308	29	371	0	0.000	0.000	0.116
5:50 PM	305	45	368	17	0.033	0.026	7.924

Time	Water depth	Water velocity	Calibrated depth + offset (66 mm)	Calibrated velocity	Calibrated flow rate	Corrected flow rate	Corrected flow rate
	mm	mm/s	mm	mm/s	m^3/s	m^3/s	$m^3/$ (5 min.)
5:55 PM	302	45	365	17	0.032	0.026	7.861
6:00 PM	299	89	362	62	0.119	0.096	28.932
6:05 PM	296	65	359	37	0.071	0.058	17.265
6:10 PM	294	57	357	29	0.055	0.045	13.381
6:15 PM	290	50	353	22	0.041	0.033	9.954
6:20 PM	287	46	351	18	0.033	0.027	8.013
6:25 PM	283	68	347	40	0.074	0.060	18.039
6:30 PM	279	76	343	49	0.088	0.072	21.474
6:35 PM	275	80	339	53	0.095	0.077	23.029
6:40 PM	272	71	336	43	0.077	0.063	18.821
6:45 PM	268	40	332	12	0.020	0.016	4.949
6:50 PM	266	28	330	-1	-0.001	-0.001	-0.334
6:55 PM	262	65	326	37	0.065	0.052	15.681
7:00 PM	258	69	322	41	0.071	0.057	17.206
7:05 PM	255	64	320	36	0.061	0.050	14.932
7:10 PM	250	62	315	34	0.057	0.046	13.871
7:15 PM	247	62	312	34	0.057	0.046	13.742
7:20 PM	243	60	308	32	0.052	0.043	12.755
7:25 PM	239	62	304	34	0.055	0.045	13.401
7:30 PM	236	56	301	28	0.045	0.036	10.876
7:35 PM	231	54	296	26	0.041	0.033	9.916
7:40 PM	227	54	292	26	0.040	0.033	9.786
7:45 PM	222	56	288	28	0.043	0.035	10.386
7:50 PM	218	53	284	25	0.038	0.030	9.118
7:55 PM	213	57	279	29	0.043	0.035	10.441
8:00 PM	208	56	274	28	0.041	0.033	9.896
8:05 PM	203	50	269	22	0.031	0.025	7.580
8:10 PM	198	61	264	33	0.046	0.038	11.299
8:15 PM	193	55	259	27	0.037	0.030	9.027
8:20 PM	187	54	254	26	0.035	0.028	8.488
8:25 PM	181	55	248	27	0.035	0.029	8.622
8:30 PM	175	57	242	29	0.037	0.030	9.062
8:35 PM	169	57	236	29	0.036	0.029	8.844
8:40 PM	163	45	230	17	0.020	0.017	4.960
8:45 PM	156	47	224	19	0.022	0.018	5.407
8:50 PM	149	51	217	23	0.026	0.021	6.393
8:55 PM	142	43	210	15	0.016	0.013	3.965
9:00 PM	134	38	202	9	0.010	0.008	2.478
9:05 PM	126	44	194	16	0.016	0.013	3.930
9:10 PM	116	55	185	27	0.026	0.021	6.430
9:15 PM	108	44	177	16	0.015	0.012	3.578
9:20 PM	98	29	167	0	0.000	0.000	0.053
9:25 PM	87	29	157	0	0.000	0.000	0.049
9:30 PM	75	29	145	0	0.000	0.000	0.046
9:35 PM	64	29	134	0	0.000	0.000	0.042
9:40 PM	51	29	122	0	0.000	0.000	0.038
9:45 PM	40	29	111	0	0.000	0.000	0.035
9:50 PM	30	29	101	0	0.000	0.000	0.032
9:55 PM	21	29	93	0	0.000	0.000	0.029

When the flow stream (driving force for stream flow) in the bankless channel reaches to sort of equilibrium, the water could flow (slightly) in either directions. The Starflow was configured to read both positive and negative flow velocities based water flow direction. The positive values of flow velocities and flow rates indicate the normal (primary) flow direction while the negative values indicate the backwards flow direction.

Table A-5 Flow rate of check gate bottom of Field 2 logged by Starflow with serial number 1900, for the irrigation event on 10-02-2018.

Time	Water depth	Water velocity	Calibrated depth + offset (66 mm)	Calibrated velocity	Calibrated flow rate	Corrected flow rate	Corrected flow rate
	mm	mm/s	mm	mm/s	m^3/s	m^3/s	$m^3/$ (5 min.)
10:30 AM	27	2033	95	1872	0.949	0.768	230.497
10:35 AM	50	2615	118	2413	1.507	1.220	366.126
10:40 AM	62	2520	129	2325	1.594	1.291	387.346
10:45 AM	91	2387	157	2200	1.834	1.486	445.775
10:50 AM	103	2463	169	2271	2.033	1.646	493.939
10:55 AM	132	2101	196	1935	2.018	1.634	490.273
11:00 AM	173	1594	237	1464	1.839	1.490	446.862
11:05 AM	231	1347	292	1233	1.913	1.550	464.952
11:10 AM	241	1190	302	1088	1.742	1.411	423.230
11:15 AM	242	1149	302	1049	1.686	1.365	409.643
11:20 AM	256	1126	316	1028	1.725	1.397	419.088
11:25 AM	279	1019	339	929	1.671	1.353	405.968
11:30 AM	301	1225	359	1120	2.137	1.731	519.185
11:35 AM	304	1199	362	1096	2.107	1.707	512.014
11:40 AM	301	1028	360	937	1.791	1.451	435.156
11:45 AM	307	1090	366	995	1.932	1.565	469.427
11:50 AM	307	1056	366	963	1.870	1.515	454.450
11:55 AM	311	1091	369	996	1.954	1.583	474.798
12:00 PM	311	1186	369	1084	2.122	1.719	515.744
12:05 PM	316	1181	373	1080	2.141	1.734	520.207
12:10 PM	315	1120	373	1023	2.028	1.643	492.772
12:15 PM	321	847	378	769	1.544	1.251	375.233
12:20 PM	320	742	378	671	1.347	1.091	327.280
12:25 PM	322	826	379	749	1.509	1.222	366.568
12:30 PM	323	801	381	726	1.469	1.190	356.914
12:35 PM	324	686	382	619	1.254	1.016	304.759
12:40 PM	327	686	384	619	1.264	1.023	307.049
12:45 PM	330	660	387	595	1.223	0.991	297.165
12:50 PM	332	611	390	549	1.137	0.921	276.251
12:55 PM	335	568	392	509	1.061	0.859	257.848
1:00 PM	340	540	397	483	1.019	0.825	247.516
1:05 PM	342	470	399	418	0.886	0.718	215.390
1:10 PM	346	460	403	409	0.875	0.709	212.555
1:15 PM	349	387	406	341	0.735	0.595	178.525
1:20 PM	353	357	410	314	0.682	0.552	165.746
1:25 PM	357	303	414	263	0.578	0.468	140.448
1:30 PM	360	295	417	256	0.565	0.458	137.354
1:35 PM	363	272	419	234	0.521	0.422	126.539
1:40 PM	367	249	423	213	0.479	0.388	116.339
1:45 PM	369	213	425	179	0.405	0.328	98.434
1:50 PM	373	234	428	199	0.453	0.367	110.065
1:55 PM	376	168	432	138	0.316	0.256	76.772
2:00 PM	379	119	434	91	0.211	0.171	51.274
2:05 PM	382	86	437	61	0.142	0.115	34.518
2:10 PM	385	95	440	70	0.163	0.132	39.580
2:15 PM	388	95	443	70	0.164	0.133	39.835

Time	Water depth	Water velocity	Calibrated depth + offset (66	Calibrated velocity	Calibrated flow rate	Corrected flow rate	Corrected flow rate
	mm	mm/s	mm	mm/s	m^3/s	m^3/s	$m^3/$ (5 min.)
2:20 PM	391	65	446	41	0.098	0.079	23.755
2:25 PM	394	70	449	46	0.110	0.089	26.646
2:30 PM	396	24	451	3	0.008	0.007	1.995
2:35 PM	399	61	454	38	0.093	0.075	22.497
2:40 PM	401	71	456	47	0.114	0.092	27.595
2:45 PM	400	188	455	156	0.377	0.305	91.595
2:50 PM	399	136	454	108	0.260	0.210	63.087
2:55 PM	398	206	453	173	0.416	0.337	100.987
3:00 PM	396	239	451	203	0.487	0.395	118.411
3:05 PM	393	306	448	266	0.632	0.512	153.670
3:10 PM	392	223	447	189	0.448	0.363	108.817
3:15 PM	390	287	445	248	0.587	0.475	142.531
3:20 PM	388	-18	443	-35	-0.083	-0.068	-20.281
3:25 PM	385	140	440	111	0.261	0.211	63.326
3:30 PM	383	-67	438	-81	-0.189	-0.153	-45.835
3:35 PM	381	90	437	65	0.151	0.122	36.587
3:40 PM	379	-70	435	-84	-0.193	-0.157	-46.997
3:45 PM	377	-49	433	-64	-0.148	-0.120	-35.888
3:50 PM	375	9	431	-10	-0.024	-0.019	-5.756
3:55 PM	372	-139	428	-148	-0.336	-0.272	-81.685
4:00 PM	370	84	426	59	0.134	0.109	32.633
4:05 PM	367	78	423	54	0.121	0.098	29.366
4:10 PM	365	-80	421	-93	-0.208	-0.169	-50.590
4:15 PM	362	128	418	100	0.223	0.180	54.119
4:20 PM	360	133	416	105	0.232	0.188	56.367
4:25 PM	358	-154	414	-162	-0.356	-0.289	-86.567
4:30 PM	355	-50	411	-65	-0.142	-0.115	-34.624
4:35 PM	353	71	410	47	0.103	0.083	24.991
4:40 PM	351	3	408	-16	-0.034	-0.028	-8.381
4:45 PM	348	-59	405	-74	-0.158	-0.128	-38.426
4:50 PM	346	-70	403	-84	-0.179	-0.145	-43.559
4:55 PM	344	-27	401	-44	-0.093	-0.076	-22.670
5:00 PM	340	-96	397	-108	-0.228	-0.184	-55.318
5:05 PM	338	72	395	48	0.101	0.082	24.583
5:10 PM	336	-32	393	-48	-0.101	-0.082	-24.593
5:15 PM	334	-43	391	-59	-0.122	-0.099	-29.636
5:20 PM	331	-15	388	-33	-0.067	-0.055	-16.371
5:25 PM	329	-35	386	-51	-0.105	-0.085	-25.562
5:30 PM	326	36	384	15	0.030	0.024	7.299
5:35 PM	324	4	382	-15	-0.030	-0.025	-7.388
5:40 PM	320	34	378	13	0.026	0.021	6.282
5:45 PM	318	-24	376	-41	-0.082	-0.066	-19.901
5:50 PM	314	-33	372	-49	-0.098	-0.079	-23.714
5:55 PM	311	-37	369	-53	-0.104	-0.084	-25.301
6:00 PM	308	-37	366	-53	-0.103	-0.084	-25.103
6:05 PM	305	-18	363	-35	-0.068	-0.055	-16.623
6:10 PM	302	55	360	32	0.062	0.050	15.075
6:15 PM	299	58	358	35	0.067	0.054	16.241
6:20 PM	296	51	355	29	0.054	0.044	13.131
6:25 PM	293	73	352	49	0.092	0.074	22.308

Time	Water depth	Water velocity	Calibrated depth + offset (66	Calibrated velocity	Calibrated flow rate	Corrected flow rate	Corrected flow rate
	mm	mm/s	mm	mm/s	m^3/s	m^3/s	$m^3/$ (5 min.)
6:30 PM	290	77	349	53	0.098	0.079	23.799
6:35 PM	286	77	345	53	0.097	0.078	23.536
6:40 PM	283	74	342	50	0.091	0.074	22.108
6:45 PM	279	69	338	45	0.082	0.066	19.830
6:50 PM	276	40	335	18	0.033	0.027	7.992
6:55 PM	273	70	332	46	0.082	0.066	19.890
7:00 PM	269	71	329	47	0.083	0.067	20.054
7:05 PM	266	69	326	45	0.079	0.064	19.096
7:10 PM	262	66	322	43	0.073	0.059	17.711
7:15 PM	258	66	318	43	0.072	0.058	17.499
7:20 PM	254	38	314	17	0.028	0.022	6.733
7:25 PM	250	62	310	39	0.064	0.052	15.586
7:30 PM	246	58	306	35	0.057	0.046	13.922
7:35 PM	242	61	303	38	0.061	0.049	14.836
7:40 PM	238	34	299	13	0.020	0.017	4.969
7:45 PM	233	60	294	37	0.058	0.047	14.058
7:50 PM	229	62	290	39	0.060	0.049	14.570
7:55 PM	224	57	285	34	0.052	0.042	12.617
8:00 PM	220	58	281	35	0.053	0.043	12.784
8:05 PM	214	54	276	31	0.046	0.037	11.199
8:10 PM	210	58	272	35	0.051	0.041	12.347
8:15 PM	204	60	266	37	0.052	0.042	12.722
8:20 PM	199	54	261	31	0.044	0.035	10.612
8:25 PM	193	55	255	32	0.044	0.036	10.683
8:30 PM	187	62	250	39	0.052	0.042	12.538
8:35 PM	181	66	244	43	0.055	0.045	13.418
8:40 PM	175	62	238	39	0.049	0.040	11.958
8:45 PM	169	64	232	41	0.050	0.041	12.225
8:50 PM	162	60	226	37	0.044	0.036	10.788
8:55 PM	154	54	218	31	0.036	0.030	8.851
9:00 PM	147	63	211	40	0.045	0.036	10.857
9:05 PM	139	62	203	39	0.042	0.034	10.216
9:10 PM	130	59	195	36	0.037	0.030	9.080
9:15 PM	121	49	186	27	0.027	0.021	6.443
9:20 PM	111	47	176	25	0.023	0.019	5.686
9:25 PM	100	38	166	17	0.015	0.012	3.554
9:30 PM	89	38	155	17	0.014	0.011	3.327
9:35 PM	78	38	145	17	0.013	0.010	3.100
9:40 PM	66	38	133	17	0.012	0.010	2.852

When the flow stream (driving force for stream flow) in the bankless channel reaches to sort of equilibrium, the water could flow (slightly) in either directions. The Starflow was configured to read both positive and negative flow velocities based water flow direction. The positive values of flow velocities and flow rates indicate the normal (primary) flow direction while the negative values indicate the backwards flow direction.

Table A-6 Flow rate of head drain box of Field 2 logged by Starflow with serial number 20320, for the irrigation event on 10-02-2018., using pipe energy equations.

Time	Water depth	Calibrated depth	Calibrated depth + Elevation depth	Flow rate, assumed	Water velocity	Re	*f*	Water velocity	Flow rate	Flow rate
	mm	mm	mm	m^3/s	m/s			m/s	m^3/s	m^3/ (5 min.)
2:40 PM	537	469	751	0.1	1.4147	375586	0.0150	2.7147	0.194	58
2:45 PM	654	570	852					2.8905	0.206	62
2:50 PM	654	570	852					2.8905	0.206	62
2:55 PM	653	569	851					2.8890	0.206	62
3:00 PM	647	564	846					2.8802	0.205	62
3:05 PM	654	570	852					2.8905	0.206	62
3:10 PM	636	554	836					2.8641	0.204	61
3:15 PM	636	554	836					2.8641	0.204	61
3:20 PM	635	553	836					2.8627	0.204	61
3:25 PM	636	554	836					2.8641	0.204	61
3:30 PM	630	549	831					2.8553	0.204	61
3:35 PM	626	546	828					2.8494	0.203	61
3:40 PM	628	547	830					2.8523	0.203	61
3:45 PM	623	543	825					2.8450	0.203	61
3:50 PM	623	543	825					2.8450	0.203	61
3:55 PM	624	544	826					2.8464	0.203	61
4:00 PM	624	544	826					2.8464	0.203	61
4:05 PM	610	532	814					2.8256	0.202	60
4:10 PM	615	536	818					2.8331	0.202	61
4:15 PM	614	535	818					2.8316	0.202	61
4:20 PM	608	530	812					2.8227	0.201	60
4:25 PM	613	535	817					2.8301	0.202	61
4:30 PM	611	533	815					2.8271	0.202	60
4:35 PM	608	530	812					2.8227	0.201	60
4:40 PM	602	525	807					2.8137	0.201	60
4:45 PM	594	518	800					2.8017	0.200	60
4:50 PM	593	517	799					2.8002	0.200	60
4:55 PM	593	517	799					2.8002	0.200	60
5:00 PM	589	514	796					2.7942	0.199	60
5:05 PM	591	516	798					2.7972	0.200	60
5:10 PM	582	508	790					2.7836	0.199	60
5:15 PM	577	504	786					2.7760	0.198	59
5:20 PM	573	500	782					2.7700	0.198	59
5:25 PM	572	499	781					2.7685	0.197	59
5:30 PM	568	496	778					2.7624	0.197	59
5:35 PM	555	485	767					2.7425	0.196	59
5:40 PM	555	485	767					2.7425	0.196	59
5:45 PM	548	479	761					2.7317	0.195	58
5:50 PM	549	480	762					2.7333	0.195	58
5:55 PM	544	475	757					2.7255	0.194	58
6:00 PM	541	473	755					2.7209	0.194	58
6:05 PM	538	470	752					2.7163	0.194	58
6:10 PM	533	466	748					2.7085	0.193	58
6:15 PM	526	460	742					2.6976	0.192	58
6:20 PM	525	459	741					2.6960	0.192	58
6:25 PM	519	454	736					2.6866	0.192	57
6:30 PM	509	445	727					2.6709	0.191	57
6:35 PM	503	440	722					2.6615	0.190	57
6:40 PM	492	431	713					2.6440	0.189	57
6:45 PM	488	427	709					2.6376	0.188	56
6:50 PM	469	411	693					2.6071	0.186	56
6:55 PM	455	399	681					2.5844	0.184	55
7:00 PM	436	383	665					2.5533	0.182	55
7:05 PM	406	357	639					2.5033	0.179	54
7:10 PM	334	295	577					2.3792	0.170	51
7:15 PM	248	221	503					2.2218	0.158	48
7:20 PM	195	176	458					2.1190	0.151	45
7:25 PM	160	146	428					2.0482	0.146	44
7:30 PM	148	135	417					2.0234	0.144	43
7:35 PM	142	130	412					2.0109	0.143	43
7:40 PM	137	126	408					2.0004	0.143	43

Time	Water depth	Calibrated depth	Calibrated depth + Elevation depth	Flow rate, assumed	Water velocity	Re	*f*	Water velocity	Flow rate	Flow rate
	mm	mm	mm	m^3/s	m/s			m/s	m^3/s	m^3/ (5 min.)
7:45 PM	138	127	409					2.0025	0.143	43
7:50 PM	139	128	410					2.0046	0.143	43
7:55 PM	140	128	411					2.0067	0.143	43
8:00 PM	141	129	411					2.0088	0.143	43
8:05 PM	142	130	412					2.0109	0.143	43
8:10 PM	142	130	412					2.0109	0.143	43
8:15 PM	142	130	412					2.0109	0.143	43
8:20 PM	142	130	412					2.0109	0.143	43
8:25 PM	142	130	412					2.0109	0.143	43
8:30 PM	142	130	412					2.0109	0.143	43
8:35 PM	141	129	411					2.0088	0.143	43
8:40 PM	141	129	411					2.0088	0.143	43
8:45 PM	141	129	411					2.0088	0.143	43
8:50 PM	140	128	411					2.0067	0.143	43
8:55 PM	139	128	410					2.0046	0.143	43
9:00 PM	138	127	409					2.0025	0.143	43
9:05 PM	137	126	408					2.0004	0.143	43
9:10 PM	135	124	406					1.9962	0.142	43
9:15 PM	133	122	405					1.9920	0.142	43
9:20 PM	131	121	403					1.9877	0.142	43
9:25 PM	128	118	400					1.9814	0.141	42
9:30 PM	126	116	399					1.9771	0.141	42
9:35 PM	124	115	397					1.9729	0.141	42
9:40 PM	120	111	393					1.9643	0.140	42
9:45 PM	117	109	391					1.9579	0.140	42
9:50 PM	113	105	387					1.9493	0.139	42
9:55 PM	110	103	385					1.9428	0.139	42
10:00 PM	107	100	382					1.9363	0.138	41
10:05 PM	102	96	378					1.9253	0.137	41
10:10 PM	99	93	375					1.9188	0.137	41
10:15 PM	95	90	372					1.9100	0.136	41
10:20 PM	92	87	369					1.9034	0.136	41
10:25 PM	88	84	366					1.8945	0.135	41
10:30 PM	86	82	364					1.8900	0.135	40
10:35 PM	83	80	362					1.8833	0.134	40
10:40 PM	80	77	359					1.8766	0.134	40
10:45 PM	78	75	357					1.8721	0.134	40
10:50 PM	76	74	356					1.8676	0.133	40
10:55 PM	73	71	353					1.8609	0.133	40
11:00 PM	71	69	351					1.8563	0.132	40
11:05 PM	70	68	350					1.8541	0.132	40
11:10 PM	68	67	349					1.8495	0.132	40
11:15 PM	65	64	346					1.8427	0.131	39
11:20 PM	62	62	344					1.8358	0.131	39
11:25 PM	59	59	341					1.8289	0.130	39
11:30 PM	56	56	338					1.8220	0.130	39
11:35 PM	53	54	336					1.8150	0.129	39
11:40 PM	50	51	333					1.8081	0.129	39
11:45 PM	48	50	332					1.8034	0.129	39
11:50 PM	45	47	329					1.7964	0.128	38
11:55 PM	42	44	326					1.7894	0.128	38
12:00 AM	40	43	325					1.7846	0.127	38
12:05 AM	39	42	324					1.7823	0.127	38
12:10 AM	38	41	323					1.7799	0.127	38
12:15 AM	37	40	322					1.7775	0.127	38
12:20 AM	36	39	321					1.7752	0.127	38
12:25 AM	35	38	320					1.7728	0.126	38
12:30 AM	34	37	320					1.7704	0.126	38
12:35 AM	34	37	320					1.7704	0.126	38
12:40 AM	33	37	319					1.7680	0.126	38
12:45 AM	33	37	319					1.7680	0.126	38
12:50 AM	32	36	318					1.7657	0.126	38
12:55 AM	32	36	318					1.7657	0.126	38
1:00 AM	32	36	318					1.7657	0.126	38
1:05 AM	32	36	318					1.7657	0.126	38

Time	Water depth	Calibrated depth	Calibrated depth + Elevation depth	Flow rate, assumed	Water velocity	Re	*f*	Water velocity	Flow rate	Flow rate
	mm	mm	mm	m^3/s	m/s			m/s	m^3/s	m^3/ (5 min.)
1:10 AM	32	36	318					1.7657	0.126	38
1:15 AM	32	36	318					1.7657	0.126	38
1:20 AM	31	35	317					1.7633	0.126	38
1:25 AM	31	35	317					1.7633	0.126	38
1:30 AM	31	35	317					1.7633	0.126	38
1:35 AM	31	35	317					1.7633	0.126	38
1:40 AM	30	34	316					1.7609	0.126	38
1:45 AM	30	34	316					1.7609	0.126	38
1:50 AM	30	34	316					1.7609	0.126	38
1:55 AM	30	34	316					1.7609	0.126	38
2:00 AM	29	33	315					1.7585	0.125	38
2:05 AM	29	33	315					1.7585	0.125	38
2:10 AM	30	34	316					1.7609	0.126	38
2:15 AM	32	36	318					1.7657	0.126	38
2:20 AM	33	37	319					1.7680	0.126	38
2:25 AM	32	36	318					1.7657	0.126	38
2:30 AM	31	35	317					1.7633	0.126	38
2:35 AM	31	35	317					1.7633	0.126	38
2:40 AM	30	34	316					1.7609	0.126	38
2:45 AM	31	35	317					1.7633	0.126	38
2:50 AM	30	34	316					1.7609	0.126	38
2:55 AM	30	34	316					1.7609	0.126	38
3:00 AM	29	33	315					1.7585	0.125	38
3:05 AM	29	33	315					1.7585	0.125	38
3:10 AM	28	32	314					1.7561	0.125	38
3:15 AM	28	32	314					1.7561	0.125	38
3:20 AM	28	32	314					1.7561	0.125	38
3:25 AM	27	31	314					1.7537	0.125	38
3:30 AM	27	31	314					1.7537	0.125	38
3:35 AM	26	31	313					1.7513	0.125	37
3:40 AM	26	31	313					1.7513	0.125	37
3:45 AM	26	31	313					1.7513	0.125	37
3:50 AM	25	30	312					1.7489	0.125	37
3:55 AM	25	30	312					1.7489	0.125	37
4:00 AM	25	30	312					1.7489	0.125	37
4:05 AM	25	30	312					1.7489	0.125	37
4:10 AM	25	30	312					1.7489	0.125	37
4:15 AM	25	30	312					1.7489	0.125	37
4:20 AM	24	29	311					1.7465	0.125	37
4:25 AM	24	29	311					1.7465	0.125	37
4:30 AM	24	29	311					1.7465	0.125	37
4:35 AM	24	29	311					1.7465	0.125	37
4:40 AM	24	29	311					1.7465	0.125	37
4:45 AM	24	29	311					1.7465	0.125	37
4:50 AM	24	29	311					1.7465	0.125	37
4:55 AM	24	29	311					1.7465	0.125	37
5:00 AM	24	29	311					1.7465	0.125	37
5:05 AM	24	29	311					1.7465	0.125	37
5:10 AM	24	29	311					1.7465	0.125	37
5:15 AM	24	29	311					1.7465	0.125	37
5:20 AM	24	29	311					1.7465	0.125	37
5:25 AM	24	29	311					1.7465	0.125	37
5:30 AM	24	29	311					1.7465	0.125	37
5:35 AM	23	28	310					1.7441	0.124	37
5:40 AM	23	28	310					1.7441	0.124	37
5:45 AM	23	28	310					1.7441	0.124	37
5:50 AM	23	28	310					1.7441	0.124	37
5:55 AM	22	27	309					1.7417	0.124	37
6:00 AM	22	27	309					1.7417	0.124	37
6:05 AM	22	27	309					1.7417	0.124	37
6:10 AM	22	27	309					1.7417	0.124	37
6:15 AM	22	27	309					1.7417	0.124	37
6:20 AM	22	27	309					1.7417	0.124	37
6:25 AM	22	27	309					1.7417	0.124	37
6:30 AM	22	27	309					1.7417	0.124	37
6:35 AM	22	27	309					1.7417	0.124	37
6:40 AM	22	27	309					1.7417	0.124	37
6:45 AM	22	27	309					1.7417	0.124	37
6:50 AM	21	26	308					1.7392	0.124	37
6:55 AM	21	26	308					1.7392	0.124	37
7:00 AM	22	27	309					1.7417	0.124	37
7:05 AM	21	26	308					2.7147	0.000	0

Table A-7 Flow rate of tail drain box of Field 2 logged by Starflow with serial number 1410, for the irrigation event on 10-02-2018, using sharp crested weir equation.

Time	Water depth	Calibrated depth	Depth above weir crest	Flow rate	Flow rate
	mm	mm	mm	m^3/s	$m^3/$ (5 min.)
1:15 PM	379	370	301.570	1.253	376.027
1:20 PM	381	372	303.578	1.267	380.107
1:25 PM	383	373	304.916	1.276	382.838
1:30 PM	384	375	306.924	1.290	386.950
1:35 PM	383	374	305.586	1.281	384.207
1:40 PM	382	372	304.247	1.272	381.472
1:45 PM	381	371	302.909	1.262	378.745
1:50 PM	379	369	300.901	1.249	374.671
1:55 PM	378	368	299.562	1.240	371.965
2:00 PM	376	366	297.555	1.226	367.922
2:05 PM	375	364	296.216	1.217	365.237
2:10 PM	373	363	294.878	1.209	362.561
2:15 PM	372	362	293.539	1.200	359.892
2:20 PM	370	360	291.531	1.186	355.906
2:25 PM	370	359	290.862	1.182	354.581
2:30 PM	368	357	288.854	1.169	350.620
2:35 PM	366	356	287.516	1.160	347.989
2:40 PM	365	354	286.177	1.151	345.367
2:45 PM	363	352	283.500	1.134	340.149
2:50 PM	362	350	282.162	1.125	337.552
2:55 PM	360	349	280.823	1.117	334.964
3:00 PM	360	348	280.154	1.112	333.672
3:05 PM	358	346	278.146	1.099	329.812
3:10 PM	356	344	276.139	1.087	325.970
3:15 PM	355	343	274.800	1.078	323.420
3:20 PM	354	341	273.462	1.070	320.878
3:25 PM	351	339	270.785	1.053	315.819
3:30 PM	350	338	270.115	1.049	314.560
3:35 PM	350	338	270.115	1.049	314.560
3:40 PM	347	335	266.769	1.028	308.294
3:45 PM	346	333	265.431	1.019	305.803
3:50 PM	345	332	264.092	1.011	303.320
3:55 PM	344	331	263.423	1.007	302.082
4:00 PM	340	327	258.738	0.978	293.473
4:05 PM	336	323	254.723	0.954	286.177
4:10 PM	334	321	252.715	0.942	282.558
4:15 PM	331	317	249.369	0.922	276.568
4:20 PM	330	316	248.030	0.914	274.187
4:25 PM	328	314	246.022	0.902	270.632
4:30 PM	327	313	244.684	0.894	268.272
4:35 PM	325	311	242.676	0.882	264.749
4:40 PM	323	309	240.669	0.871	261.245
4:45 PM	321	307	238.661	0.859	257.760
4:50 PM	319	304	235.984	0.844	253.144
4:55 PM	315	300	231.968	0.821	246.284

Time	Water depth	Calibrated depth	Depth above weir crest	Flow rate	Flow rate
	mm	mm	mm	m^3/s	m^3/ (5 min.)
5:00 PM	313	298	229.961	0.810	242.883
5:05 PM	311	295	227.284	0.795	238.378
5:10 PM	309	293	225.276	0.783	235.022
5:15 PM	305	289	221.260	0.761	228.369
5:20 PM	303	287	218.583	0.747	223.977
5:25 PM	300	283	215.237	0.728	218.536
5:30 PM	298	281	213.229	0.718	215.298
5:35 PM	296	279	210.552	0.703	211.010
5:40 PM	292	275	207.206	0.686	205.700
5:45 PM	290	273	204.529	0.672	201.491
5:50 PM	284	266	197.837	0.637	191.123
5:55 PM	191	165	97.449	0.211	63.169
					17148

Appendix B Water advance and recession measurements using UAV

B.1 Water advance measurements using UAV

Sample of UAV advance data (or measurements) at the field scale for one irrigation event conducted on 19-1-2018.

Table B-1 UAV advance data extracted from the Flight Mission #1 conducted at Border 1 of Field 2 for the irrigation event conducted on 19-1-2018. The empty cells mean that the water advance did not reach this distance at that time of the flight mission

Furrow no.	UAV flight mission paths at specific distances, m				
	x_1 =150	x_2 = 250	x_3 = 350	x_4 = 450	x_5 = 570
1	150	250			
2	150	250			
3	150	250			
4	150	250	350		
5	150	250	350		
6*	150	250	350	450	
7	150	250	350		
8*	150	250	350	450	
9	150	250	350		
10	150	250	350		
11	150	250			
12	150	250			
13	150	250	350		
14	150	250	350		
15	150	250			
16	150	250	350		
17	150	250	350		
18*	150	250	350	450	570
19	150	250	350		
20*	150	250	350	450	570
21	150	250	350		
22	150	250	350		
23	150	250			
24	150	250			
25	150	250			
26	150	250			
27	150	250			
28	150	250	350		
29	150	250	350		
30*	150	250	350	450	
31	150	250	350	450	
32*	150	250	350	450	
33	150	250	350		
34	150	250	350		
35	150	250			

Furrow no.	UAV flight mission paths at specific distances, m				
	x_1 =150	x_2 = 250	x_3 = 350	x_4 = 450	x_5 = 570
36	150	250			
37	150	250	350		
38	150	250			
39	150	250			
40	150	250	350		
41	150	250	350		
42*	150	250	350	450	506
43	150	250	350		
44*	150	250	350	450	570
45	150	250	350		
46	150	250	350		
47	150	250			
48	150	250			
49	150	250			
50	150	250			
51	150	250			
52	150	250	350		
53	150	250	350	450	
54*	150	250	350	450	508
55	150	250	350		
56*	150	250	350	450	
57	150	250	350		
58	150	250	350		
59	150	250			
60	150	250	350		
61	150	250	350	450	
62	150	250	350		
63	150	250			
64	150	250	350		
65	150	250	350		
66*	150	250	350	450	570
67	150	250	350		
68*	150	250	350	450	570
69	150	250	350		
70	150	250	350		
71	150	250	350		
72	150	250			
73	150	250			
74	150	250			
75	150	250			
76	150	250	350	409	
77	150	250	350		
78*	150	250	350	450	570
79	150	250	350	450	
80*	150	250	350	450	
81	150	250	350		
82	150	250	350	450	
83	150	250			
84	150	250			
85	150	250	350		
86	150	250			
87	150	250			
88	150	250	350	410	
89	150	250	350		
90*	150	250	350	450	570
91	150	250	350		
92*	150	250	350	450	570
93	150	250	350		
94	150	250	350		
95	150	250	350		
96	150	250	350		

Furrow no.	UAV flight mission paths at specific distances, m				
	x_1 =150	x_2 = 250	x_3 = 350	x_4 = 450	x_5 = 570
97	150	250			
98	150	250			
99	150	250			
100	150	250	350	450	
101	150	250	350	409	
102*	150	250	350	450	570
103	150	250	350	450	
104*	150	250	350	450	570
105	150	250	350	450	
106	150	250	350	408	
107	150	250	350		
108	150	250	350		
109	150	250	350	450	
110	150	250	350		
111	150	250	350		
112	150	250	350	450	
113	150	250	350		
114*	150	250	350	450	570
115	150	250	350		
100*	150	250	350	450	570
117	150	250	350	405	
118	150	250	350	450	
119	150	250	350	450	
120	150	250	350	450	
121	150	250	350	450	
122	150	250	350	450	
123	150	250	350	450	
124	150	250	350	450	
125	150	250	350	450	
126*	150	250	350	450	570
127	150	250	350	450	
128*	150	250	350	450	570
129	150	250	350		
130	150	250	350	450	
131	150	250			
132	150	250			
133	150	250	350		
134	150	250			
135	150	250	350		
136	150	250	350		
137	150	250	350		
138*	150	250	350	450	570
139	150	250	350	450	
140*	150	250	350	450	570
141	150	250	350		
142	150	250	350	450	
143	150	250	350		
144	150	250	350		
145	150	250	350		
146	150	250			
147	150	250	350	450	
148	150	250	350		
149	150	250	350	450	
150*	150	250	350	450	570
151	150	250	350	450	
152*	150	250	350	450	570
153	150	250	350	450	
154	150	250	350		
155	150	250	350		
156	150	250	350		
157	150	250	350		

Furrow no.	**UAV flight mission paths at specific distances, m**				
	x_1 **=150**	x_2 **= 250**	x_3 **= 350**	x_4 **= 450**	x_5 **= 570**
158	150	250	350		
159	150	250	350		
160	150	250	350		
161	150	250	350	450	
162*	150	250	350	450	570
163	150	250	350	450	
164*	150	250	350	450	570
165	150	250	350	450	
166	150	250	350		
167	150	250	350		
168	150	250	350		
169	150	250			
170	150	250			
171	150	250	350	450	
172	150	250	350	407	
173	150	250	350	450	
174*	150	250	350	450	570
175	150	250	350	450	
176*	150	250	350	450	570
177	150	250	350	450	
178	150	250	350		
179	150	250	350		
180	150	250	350		
181	150	250	350		
182	150	250			
183	150	250			
184	150	250	350		
185	150	250	350	450	
186*	150	250	350	450	570
187	150	250	350	450	
188*	150	250	350	450	570
189	150	250	350	450	
190	150	250	350		
191	150	250	350		
192	150	250	350		
193	150	250	350		
194	150	250			
195	150	250	350	450	
196	150	250	350	450	
197	150	250	350	450	
198*	150	250	350	450	570
199	150	250	350	450	
200*	150	250	350	450	570
201	150	250	350	450	
202	150	250	350		
203	150	250	350		
204	150	250	350	450	
205	150	250	350		
206	150	250	350		
207	150	250			
208	150	250	350		
209	150	250	350		
210*	150	250	350	450	570
211	150	250	350		
212*	150	250	350	450	570
213	150	250	350	450	
214	150	250	350		
215	150	250	350		
200	150	250	350		
217	150	250			
218	150	250			

Furrow no.	UAV flight mission paths at specific distances, m				
	x_1 =150	x_2 = 250	x_3 = 350	x_4 = 450	x_5 = 570
219	150	250	350		
220	150	250	350	408	
221	150	250	350	450	
222*	150	250	350	450	570
223	150	250	350		
224*	150	250	350	450	570
225	150	250	350		
226	150	250	350		
227	150	250	350		
228	150	250	350		
229	150	250	350		
230	150	250	350		
231	150	250			
232	150	250	350		
233	150	250	350		
234*	150	250	350	450	570
235	150	250	350		
236*	150	250	350	450	570
237	150	250	350	407	
238	150	250	350		
239	150	250	350		
240	150	250			
241	150	250			
242	150	250	350	450	
243	150	250	350		
244	150	250	350	450	
245	150	250	350		
246*	150	250	350	450	570
247	150	250	350	450	
248*	150	250	350	450	570
249	150	250	350		
250	150	250	350		
251	150	250	350	407	
252	150	250	350		
253	150	250	350		
254	150	250	350	450	
255	150	250	350		
256	150	250	350	450	
257	150	250	350	450	
258*	150	250	350	450	570
259	150	250	350	409	
260*	150	250	350	450	570
261	150	250	350	450	
262	150	250	350		
263	150	250	350		
264	150	250	350		
265	150	250	350		
266	150	250	350		
267	150	250	350	450	
268	150	250	350	450	
269	150	250	350	450	
270*	150	250	350	450	570
271	150	250	350	450	
272*	150	250	350	450	570
273	150	250	350	450	
274	150	250	350		
275	150	250	350		
276	150	250	350	450	
277	150	250	350		
278	150	250	350		
279	150	250	350		

Furrow no.	UAV flight mission paths at specific distances, m				
	x_1 =150	x_2 = 250	x_3 = 350	x_4 = 450	x_5 = 570
280	150	250	350		
281	150	250	350		
282*	150	250	350	450	570
283	150	250	350	450	
284*	150	250	350	450	570
285	150	250	350	408	
286	150	250	350	450	
287	150	250	350		
288	150	250	350		
289	150	250			
290	150	250	350		
291	150	250	350	450	
292	150	250	350	450	570
293	150	250	350	450	570
294*	150	250	350	450	570
295	150	250	350	450	570
296*	150	250	350	450	570
297	150	250	350	450	
298	150	250	350		
299	150	250	350		
300	150	250	350	450	
301	150	250	350		
302	150	250	350		
303	150	250	350		
304	150	250	350		
305	150	250			
306*	150	250	350	450	570
307	150	250			
308*	150	250	350	450	570
309	150	250	350		
310	150	250	350		
311	150	250	350		
312	150	250	350		

* Wheeled furrows

B.2 Water recession measurements using UAV

Table B-2 Recession time data collected from three UAV flight missions in Border 1 of Field 2 of the irrigation event conducted on 19-1-2018. The empty cells refer to the parts of the furrows that have not receded.

Furrow no.	UAV flight mission recession time at specific distances, min.				
	x_1 =150	x_2 = 250	x_3 = 350	x_4 = 450	x_5 = 570
1	356	356	504	504	
2	356	356	504	504	
3	412	412	412	412	
4	412	412	412	412	
5	412	412	412	412	412
6*	504	504	504	504	

Furrow no.	UAV's flight mission recession time at specific distances, min.				
	x_1 =150	x_2 = 250	x_3 = 350	x_4 = 450	x_5 = 570
7	412	412	412	412	412
8*	356	356	504	504	
9	356	412	412	412	412
10	504	504	504	504	
11	356	412	412	412	412
12	356	412	412	412	412
13	412	504	504	504	
14	356	356	412	412	
15	356	356	412	412	412
16	356	356	412	412	
17	356	356	412	412	
18*	356	356	504	504	
19	356	356	412	504	
20*	412	412	504	504	
21	356	412	412	504	
22	356	356	504	504	
23	356	356	412	504	
24	356	412	412	504	
25	412	412	412	504	
26	356	356	412	504	
27	356	356	412	412	
28	356	356	412	412	412
29	356	356	412	412	412
30*	356	356	504	504	
31	356	412	412	504	
32*	356	356	412	504	
33	356	412	412	412	
34	356	356	412	412	412
35	356	412	412	412	412
36	356	412	412	412	412
37	356	356	412	412	412
38	356	356	504	504	
39	356	356	412	412	412
40	412	412	412	412	
41	412	412	412	412	
42*	356	356	504	504	
43	356	412	412	412	412
44*	412	412	504	504	
45	356	412	412	412	412
46	356	412	412	412	412
47	356	412	412	412	412
48	412	412	412	412	412
49	356	356	412	412	
50	356	356	412	412	
51	356	412	412	504	
52	356	412	412	504	
53	356	412	412	504	
54*	356	504	504	504	
55	356	412	412	504	
56*	412	504	504	504	
57	356	412	412	412	
58	356	412	412	412	
59	356	356	412	412	412
60	356	356	412	412	412
61	356	412	412	412	
62	356	356	412	412	
63	356	356	412	504	
64	412	412	412	412	
65	356	356	412	504	
66*	412	504	504	504	
67	356	412	412	504	

Furrow no.	UAV flight mission recession time at specific distances, min.				
	x_1 =150	x_2 = 250	x_3 = 350	x_4 = 450	x_5 = 570
68*	412	412	504	504	
69	356	504	504	504	
70	412	412	412	504	
71	356	412	412	412	
72	356	412	412	412	
73	356	412	412	412	
74	412	412	412	412	
75	412	412	412	412	
76	412	412	412	412	
77	356	356	412	412	
78*	412	412	504	504	
79	356	356	412	504	
80*	412	412	504	504	
81	356	356	412	504	
82	356	356	412	412	
83	356	356	412	412	
84	356	356	412	504	
85	356	412	412	412	
86	356	412	412	504	
87	356	356	412	504	
88	412	412	412	504	
89	412	412	504	504	
90*	412	412	504	504	
91	356	356	412	504	
92*	412	412	504	504	
93	356	356	412	412	
94	412	412	412	504	
95	356	356	412	504	
96	356	412	412	504	
97	356	356	412	412	412
98	356	356	412	412	412
99	356	356	412	412	
100	356	356	412	412	
101	412	412	412	504	
102*	356	356	504	504	
103	356	356	504	504	
104*	412	504	504	504	
105	356	356	356	504	
106	412	412	412	504	
107	356	356	412	412	412
108	356	356	412	412	412
109	356	356	412	412	
110	356	356	356	412	
111	356	356	412	504	
112	412	412	412	412	
113	412	412	504	504	
114*	412	412	504	504	
115	356	356	412	504	
100*	504	504	504	504	
117	412	412	412	412	
118	356	356	412	504	
119	356	356	356	412	412
120	412	412	412	412	412
121	412	412	412	412	412
122	356	356	412	412	412
123	356	356	412	504	
124	356	356	412	504	
125	356	356	412	504	
126*	504	504	504	504	
127	412	412	504	504	

Furrow no.	UAV flight mission recession time at specific distances, min.				
	x_1 =150	x_2 = 250	x_3 = 350	x_4 = 450	x_5 = 570
128*	504	504	504	504	
129	356	356	356	504	
130	412	412	412	504	
131	356	356	504	504	
132	356	356	412	504	
133	356	356	412	412	
134	356	356	504	412	
135	356	356	412	412	
136	356	356	504	504	
137	412	412	412	412	412
138*	412	412	504	504	
139	356	356	504	504	
140*	412	412	504	504	
141	356	356	504	504	
142	412	412	504	504	
143	412	412	412	504	
144	356	356	412	412	412
145	356	356	412	412	412
146	356	356	412	412	412
147	356	356	504	504	
148	412	412	504	504	
149	412	412	504	504	
150*	504	504	504	504	
151	504	504	504	504	
152*	504	504	504	504	
153	504	504	504	504	
154	504	504	504	504	
155	504	504	504	504	
156	504	504	504	504	
157	412	412	412	412	412
158	504	504	504	504	
159	356	412	412	412	412
160	504	504	504	504	
161	412	504	504	504	
162*	412	504	504	504	
163	504	504	504	504	
164*	504	504	504	504	
165	412	412	412	412	
166	356	356	356	504	
167	412	504	504	504	
168	412	412	412	504	
169	412	412	412	412	
170	412	412	412	412	
171	412	412	412	412	
172	412	412	504	504	
173	412	412	412	504	
174*	412	504	504	504	
175	412	412	412	504	
176*	412	504	504	504	
177	504	504	504	504	
178	504	504	504	504	
179	504	504	504	504	
180	504	504	504	504	
181	412	504	504	504	
182	412	412	412	412	412
183	412	412	412	412	412
184	412	504	504	504	
185	412	504	504	504	
186*	504	504	504	504	
187	504	504	504	504	

Furrow no.	UAV flight mission recession time at specific distances, min.				
	x_1 =150	x_2 = 250	x_3 = 350	x_4 = 450	x_5 = 570
188*	504	504	504	504	
189	412	504	504	504	
190	412	504	504	504	
191	412	504	504	504	
192	412	412	412	412	412
193	412	412	412	412	412
194	412	412	504	504	
195	412	504	504	504	
196	412	412	504	504	
197	504	504	504	504	
198*	504	504	504	504	
199	504	504	504	504	
200*	504	504	504	504	
201	412	504	504	504	
202	412	504	504	504	
203	412	412	412	412	
204	412	412	412	412	
205	412	504	504	504	
206	412	504	504	504	
207	412	412	412	504	
208	412	412	504	504	
209	504	504	504	504	
210*	504	504	504	504	
211	412	412	504	504	
212*	504	504	504	504	
213	504	504	504	504	
214	504	504	504	504	
215	504	504	504	504	
200	412	504	504	504	
217	412	412	504	504	
218	504	504	504	504	
219	504	504	504	504	
220	412	412	504	504	
221	504	504	504	504	
222*	504	504	504	504	
223	412	504	504	504	
224*	504	504	504	504	
225	412	412	412	504	
226	412	412	412	504	
227	412	504	504	504	
228	504	504	504	504	
229	504	504	504	504	
230	504	504	504	504	
231	504	504	504	504	
232	504	412	504	504	
233	412	412	412	504	
234*	504	504	504	504	
235	504	504	504	504	
236*	504	504	504	504	
237	504	504	504	504	
238	504	504	504	504	
239	504	504	504	504	504
240	504	504	504	504	504
241	412	412	504	504	504
242	412	412	504	504	504
243	504	504	504	504	504
244	504	504	504	504	504
245	504	504	504	504	504
246*	504	504	504	504	504
247	504	504	504	504	504
248*	504	504	504	504	504

Furrow no.	UAV flight mission recession time at specific distances, min.				
	x_1 =150	x_2 = 250	x_3 = 350	x_4 = 450	x_5 = 570
249	412	412	412	504	504
250	412	412	412	504	504
251	412	412	412	504	504
252	412	412	504	504	504
253	504	412	504	504	504
254	504	504	504	504	504
255	504	504	504	504	504
256	504	504	504	504	504
257	504	504	504	504	504
258*	504	504	504	504	504
259	504	504	504	504	
260*	504	504	504	504	504
261	504	504	504	504	
262	504	504	504	504	504
263	412	412	412	504	504
264	412	412	412	504	504
265	412	412	412	504	504
266	504	504	504	504	504
267	504	504	504	504	504
268	504	504	504	504	504
269	412	412	412	504	504
270*	504	504	504	504	504
271	412	412	412	504	504
272*	412	504	504	504	504
273	412	504	504	504	504
274	504	504	504	504	504
275	412	412	412	412	504
276	412	412	412	412	504
277	412	412	412	412	504
278	412	412	504	504	504
279	412	412	504	504	504
280	504	504	504	504	504
281	412	412	504	504	504
282*	504	504	504	504	504
283	412	412	504	504	
284*	412	504	504	504	504
285	412	504	504	504	
286	412	504	504	504	
287	412	412	504	504	504
288	412	412	412	504	
289	412	504	504	504	504
290	412	504	504	504	
291	504	504	504	504	
292	412	412	412	504	
293	504	504	504	504	
294*	504	504	504	504	
295	412	504	504	504	
296*	504	504	504	504	
297	412	504	504	504	504
298	412	504	504	504	
299	412	504	504	504	504
300	412	504	504	504	
301	412	504	504	504	504
302	412	504	504	504	504
303	412	412	412	504	504
304	412	504	504	504	
305	504	504	504	504	504
306*	504	504	504	504	
307	412	504	504	504	504
308*	412	504	504	504	504

Furrow no.	**UAV flight mission recession time at specific distances, min.**				
	x_1 **=150**	x_2 **= 250**	x_3 **= 350**	x_4 **= 450**	x_5 **= 570**
309	356	504	504	504	504
310	504	504	504	504	504
311	504	504	504	504	504
312	504	504	504	504	504

* Wheeled furrows

Appendix C Estimating the SWD using IrriSAT

Soil water deficit (SWD) prior to each irrigation event throughout the whole season was estimated using IrriSAT (https://irrisat-cloud.appspot.com/) based on simple water balance approach (Hornbuckle et al. 2016). IrriSAT "is a weather based irrigation scheduling technology that uses remote sensing to provide site specific crop water management information across large spatial scales" (Montgomery et al. 2015). The methodology adopted by IrriSAT to estimate the SWD uses a water balance based on crop evapotranspiration (ET_c). The term ET_c expresses the crop water use (mm/day) based on the climatic demand and crop conditions as shown in the Equation C-1.

$$ET_c = ET_o K_c \quad \text{(C-1)}$$

Where, ET_o is the reference evapotranspiration (mm/day) that shows the effect of climate on the crop water requirements. ET_o is calculated from meteorological data (temperature, solar radiation, humidity, wind) using the FAO56 Penman Monteith equation. Technically, ET_o represents the water transpiration of well-watered grass (reference crop). K_c is the crop coefficient that shows the effect of the crop status (crop type, growth stage, leaf area index) on the crop water requirements. Simply, IrriSAT uses satellite imagery to estimate K_c and weather station data to estimate ET_o. K_c is calculated from a relationship linked to satellite imagery called graphical indicator normalised difference vegetation index (NDVI). ET_o is calculated using ASCE Standard reference evapotranspiration equation as detailed in (Allen et al. 2005).

Figure C-1 shows the main screen of the IrriSAT with the boundaries of the borders of Field 2. IrriSAT generates a daily record of K_c and ET_c for the crop season. Figure C-2 shows the K_c and ET_c of Border 2 of Field 2 for the period 30-10-2017 to 17-2-2018. IrriSAT can present K_c and ET_c as a graph as shown in Figure C-2, or as a data table which can be exported as a CSV file.

In the setting icon located top of the Figure C-2, IrriSAT provides the ability to select the planting and harvesting dates and the weather station that will be adopted to estimate ET_o, and rainfall amount (Figure C-3). To conduct the water balance, IrriSAT provides the ability to enter the amount of irrigation as a water applied depth (mm), as shown in Figure C-4.

Figure C-1 Main screen of IrriSAT showing Border 1 and 2 of field 2.

IrriSAT allows the user to enter the depth applied for each irrigation event. In Figure C-4 an irrigation depth of 73.2 mm has been added to Border 1 of Field 2 for the irrigation conducted in 15-12-2018. The rest of the irrigation depths for the other irrigation events (shown in Table 9.10) were entered in similar manner. Although IrriSAT would use the rainfall depth according to the nearest weather station there is an ability to amend these data by adding a specific amount of rainfall recorded at that field. The lower part of Figure C-4 shows a graph of cumulative daily water balance components (soil water deficit, crop water use, total water applied, irrigation, and rainfall). Total water applied equals applied irrigation depth plus rainfall depth. IrriSAT also provides the ability to present these parameters as data in a spreadsheet file.

Table C-1 shows the data that gathered from the IrriSAT spreadsheet files which include Kc, E_o (daily), ET_c (daily), ET_c (cumulative), and cumulative water balance components (soil water deficit, crop water use, total water applied, irrigation, and rainfall), for Border 1 of Field 2 for the period extending from 30-10-2017 to 17-2-2018. Note that the season commenced in 30-10-2018 and ended on the 10-05-2018.

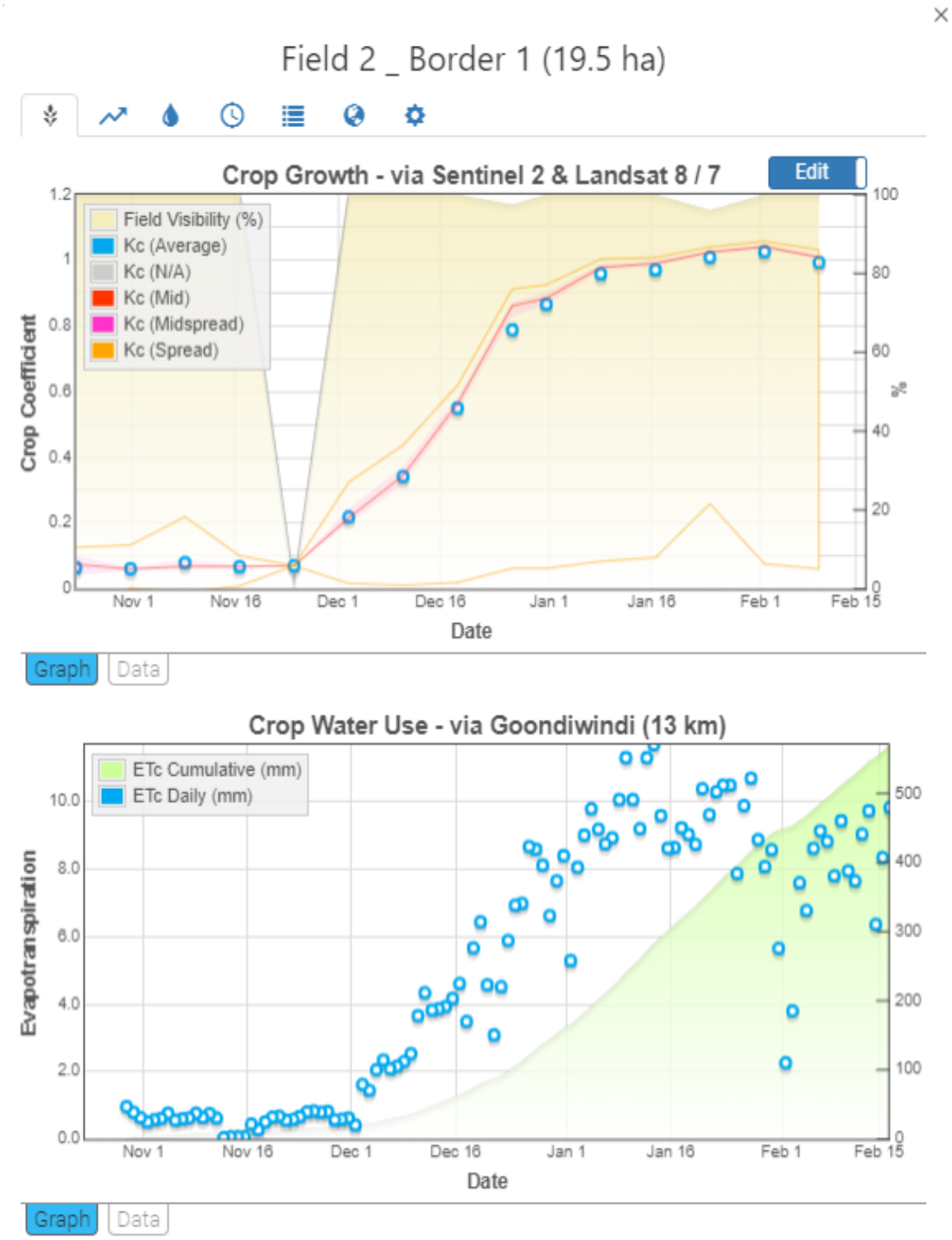

Figure C-2 K_c and ET_c of Border 2 of Field 2 for the period 30-10-2017 to 17-2-2018.

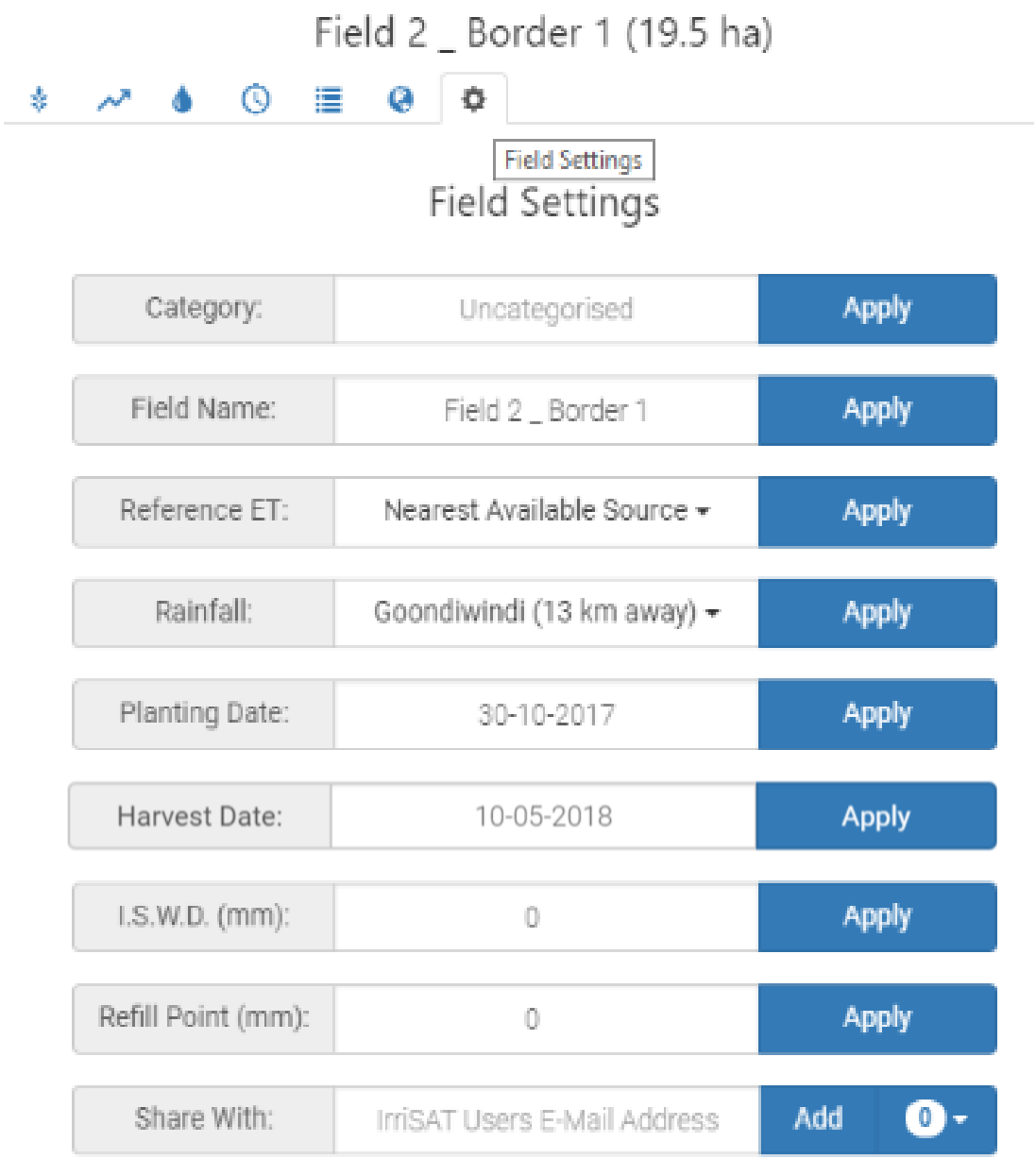

Figure C-3 Shows field setting of IrriSAT.

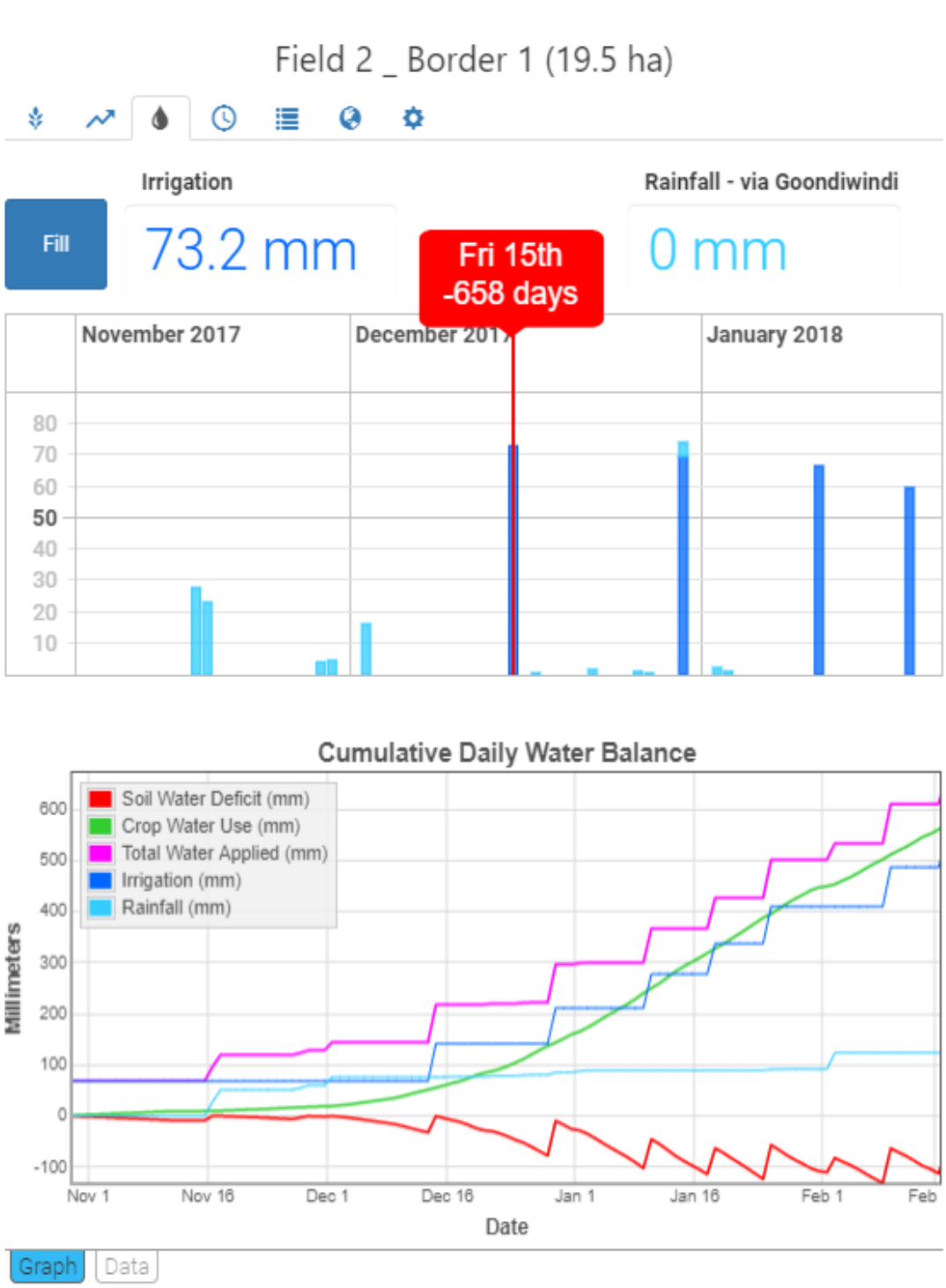

Figure C-4 Screen shot from IrriSAT showing the addition of irrigation and rainfall (Top) and a plot of the water balance for Border 1 of Field 2 (Bottom).

Table C-1 Shows the data gathered from the IrriSAT spreadsheet files including K_c, E_o (daily), ET_c (daily), ET_c (cumulative), and cumulative water balance components (soil water deficit, crop water use, total water applied, irrigation, and rainfall), for Border 1 of Field 2 for whole season.

Date	Kc (average)	ET_o daily, mm	ET_c daily, mm	Crop Water Use, or ETc cumulative, mm	Soil Water Deficit, mm	Rainfall (cumulative), mm	Irrigation (cumulative), mm	Total Water Applied (cumulative), mm
30/10/2017	0.0645	14.80	0.95	1.0	0.00	0	68.4	68.4
31/10/2017	0.0645	12.20	0.79	1.7	0.79	0	68.4	68.4
1/11/2017	0.0609	10.40	0.63	2.4	1.42	0	68.4	68.4
2/11/2017	0.0609	8.30	0.51	2.9	1.93	0	68.4	68.4
3/11/2017	0.0609	9.30	0.57	3.4	2.49	0	68.4	68.4
4/11/2017	0.0609	10.00	0.61	4.1	3.10	0	68.4	68.4
5/11/2017	0.0609	12.50	0.76	4.8	3.86	0	68.4	68.4
6/11/2017	0.0609	9.10	0.55	5.4	4.42	0	68.4	68.4
7/11/2017	0.0609	9.80	0.60	6.0	5.01	0	68.4	68.4
8/11/2017	0.0609	10.20	0.62	6.6	5.63	0	68.4	68.4
9/11/2017	0.0800	9.50	0.76	7.3	6.39	0	68.4	68.4
10/11/2017	0.0800	7.90	0.63	8.0	7.03	0	68.4	68.4
11/11/2017	0.0800	9.30	0.74	8.7	7.77	0	68.4	68.4
12/11/2017	0.0800	7.70	0.62	9.3	8.39	0	68.4	68.4
13/11/2017	0.0800	0.50	0.04	9.4	8.43	0	68.4	68.4
14/11/2017	0.0800	0.80	0.06	9.4	8.49	0	68.4	68.4
15/11/2017	0.0800	0.80	0.06	9.5	8.55	0	68.4	68.4
16/11/2017	0.0800	0.80	0.06	9.6	8.62	0	68.4	68.4
17/11/2017	0.0670	6.60	0.44	10.0	0.00	28	68.4	96.4
18/11/2017	0.0670	4.10	0.27	10.3	0.00	51.2	68.4	119.6
19/11/2017	0.0670	7.50	0.50	10.8	0.50	51.2	68.4	119.6
20/11/2017	0.0670	9.60	0.64	11.4	1.14	51.2	68.4	119.6
21/11/2017	0.0670	10.00	0.67	12.1	1.81	51.2	68.4	119.6
22/11/2017	0.0670	8.30	0.56	12.7	2.37	51.2	68.4	119.6

Date	Kc (average)	ET_o daily, mm	ET_c daily, mm	Crop Water Use, or ETc cumulative, mm	Soil Water Deficit, mm	Rainfall (cumulative), mm	Irrigation (cumulative), mm	Total Water Applied (cumulative), mm
23/11/2017	0.0670	8.60	0.58	13.2	2.95	51.2	68.4	119.6
24/11/2017	0.0670	9.90	0.66	13.9	3.61	51.2	68.4	119.6
25/11/2017	0.0702	11.40	0.80	14.7	4.41	51.2	68.4	119.6
26/11/2017	0.0702	11.80	0.83	15.5	5.24	51.2	68.4	119.6
27/11/2017	0.0702	11.20	0.79	16.3	6.02	51.2	68.4	119.6
28/11/2017	0.0702	11.60	0.81	17.1	3.04	55	68.4	123.4
29/11/2017	0.0702	8.00	0.56	17.7	0.00	59.8	68.4	128.2
30/11/2017	0.0702	8.30	0.58	18.3	0.58	59.8	68.4	128.2
1/12/2017	0.0702	8.80	0.62	18.9	1.20	59.8	68.4	128.2
2/12/2017	0.0702	5.80	0.41	19.3	0.00	76	68.4	144.4
3/12/2017	0.2183	7.40	1.62	20.9	1.62	76	68.4	144.4
4/12/2017	0.2183	6.60	1.44	22.4	3.06	76	68.4	144.4
5/12/2017	0.2183	9.40	2.05	24.4	5.11	76	68.4	144.4
6/12/2017	0.2183	10.70	2.34	26.7	7.44	76	68.4	144.4
7/12/2017	0.2183	9.50	2.07	28.8	9.52	76	68.4	144.4
8/12/2017	0.2183	9.90	2.16	31.0	11.68	76	68.4	144.4
9/12/2017	0.2183	10.50	2.29	33.3	13.97	76	68.4	144.4
10/12/2017	0.2183	11.60	2.53	35.8	16.50	76	68.4	144.4
11/12/2017	0.3413	10.70	3.65	39.4	20.15	76	68.4	144.4
12/12/2017	0.3413	12.70	4.33	43.8	24.49	76	68.4	144.4
13/12/2017	0.3413	11.20	3.82	47.6	28.31	76	68.4	144.4
14/12/2017	0.3413	11.30	3.86	51.5	**32.17****	76	68.4	144.4
15/12/2017*	0.3413	11.50	3.93	55.4	0.00	76	141.6	217.6
16/12/2017	0.3413	12.20	4.16	59.6	4.16	76	141.6	217.6
17/12/2017	0.3413	13.50	4.61	64.2	7.97	76.8	141.6	218.4
18/12/2017	0.3413	10.20	3.48	67.6	11.45	76.8	141.6	218.4
19/12/2017	0.5501	10.30	5.67	73.3	17.12	76.8	141.6	218.4

Date	Kc (average)	ET_o daily, mm	ET_c daily, mm	Crop Water Use, or ETc cumulative, mm	Soil Water Deficit, mm	Rainfall (cumulative), mm	Irrigation (cumulative), mm	Total Water Applied (cumulative), mm
20/12/2017	0.5501	11.70	6.44	79.7	23.56	76.8	141.6	218.4
21/12/2017	0.5501	8.30	4.57	84.3	28.12	76.8	141.6	218.4
22/12/2017	0.5501	5.60	3.08	87.4	29.60	78.4	141.6	220.0
23/12/2017	0.5501	8.20	4.51	91.9	34.11	78.4	141.6	220.0
24/12/2017	0.5501	10.70	5.89	97.8	40.00	78.4	141.6	220.0
25/12/2017	0.5501	12.60	6.93	104.7	46.93	78.4	141.6	220.0
26/12/2017	0.5501	12.70	6.99	111.7	52.52	79.8	141.6	221.4
27/12/2017	0.7886	11.00	8.67	120.4	60.39	80.6	141.6	222.2
28/12/2017	0.7886	10.90	8.60	129.0	68.99	80.6	141.6	222.2
29/12/2017	0.7886	10.30	8.12	137.1	**77.11****	80.6	141.6	222.2
30/12/2017*	0.7886	8.40	6.62	143.7	9.53	85.2	211.2	296.4
31/12/2017	0.7886	9.70	7.65	151.4	17.18	85.2	211.2	296.4
1/01/2018	0.8666	9.70	8.41	159.8	25.59	85.2	211.2	296.4
2/01/2018	0.8666	6.10	5.29	165.1	28.27	87.8	211.2	299.0
3/01/2018	0.8666	9.30	8.06	173.1	34.93	89.2	211.2	300.4
4/01/2018	0.8666	10.40	9.01	182.1	43.94	89.2	211.2	300.4
5/01/2018	0.8666	11.30	9.79	191.9	53.74	89.2	211.2	300.4
6/01/2018	0.8666	10.60	9.19	201.1	62.92	89.2	211.2	300.4
7/01/2018	0.8666	10.10	8.75	209.9	71.67	89.2	211.2	300.4
8/01/2018	0.8666	10.30	8.93	218.8	80.60	89.2	211.2	300.4
9/01/2018	0.9584	10.50	10.06	228.8	90.66	89.2	211.2	300.4
10/01/2018	0.9584	11.80	11.31	240.2	**101.97****	89.2	211.2	300.4
11/01/2018*	0.9584	10.50	10.06	250.2	45.44	89.2	277.8	367.0
12/01/2018	0.9584	9.60	9.20	259.4	54.64	89.2	277.8	367.0
13/01/2018	0.9584	11.80	11.31	270.7	65.95	89.2	277.8	367.0
14/01/2018	0.9584	12.20	11.69	282.4	77.64	89.2	277.8	367.0
15/01/2018	0.9584	10.00	9.58	292.0	87.22	89.2	277.8	367.0
16/01/2018	0.9584	9.00	8.63	300.6	95.85	89.2	277.8	367.0

Date	Kc (average)	ET_o daily, mm	ET_c daily, mm	Crop Water Use, or ETc cumulative, mm	Soil Water Deficit, mm	Rainfall (cumulative), mm	Irrigation (cumulative), mm	Total Water Applied (cumulative), mm
17/01/2018	0.9710	8.90	8.64	309.3	104.49	89.2	277.8	367.0
18/01/2018	0.9710	9.50	9.22	318.5	**113.72****	89.2	277.8	367.0
19/01/2018*	0.9710	9.30	9.03	327.5	63.05	89.2	337.5	426.7
20/01/2018	0.9710	9.00	8.74	336.3	71.79	89.2	337.5	426.7
21/01/2018	0.9710	10.70	10.39	346.7	82.18	89.2	337.5	426.7
22/01/2018	0.9710	9.90	9.61	356.3	91.79	89.2	337.5	426.7
23/01/2018	0.9710	10.60	10.29	366.6	102.08	89.2	337.5	426.7
24/01/2018	0.9710	10.80	10.49	377.1	112.57	89.2	337.5	426.7
25/01/2018	1.0091	10.40	10.50	387.5	**123.06****	89.2	337.5	426.7
26/01/2018*	1.0091	7.80	7.87	395.4	56.53	91.4	409.7	501.1
27/01/2018	1.0091	9.80	9.89	405.3	66.42	91.4	409.7	501.1
28/01/2018	1.0091	10.60	10.70	416.0	76.72	91.8	409.7	501.5
29/01/2018	1.0091	8.80	8.88	424.9	85.60	91.8	409.7	501.5
30/01/2018	1.0091	8.00	8.07	433.0	93.67	91.8	409.7	501.5
31/01/2018	1.0091	8.50	8.58	441.5	102.25	91.8	409.7	501.5
1/02/2018	1.0091	5.60	5.65	447.2	107.90	91.8	409.7	501.5
2/02/2018	1.0267	2.20	2.26	449.4	110.16	91.8	409.7	501.5
3/02/2018	1.0267	3.70	3.80	453.2	81.96	123.8	409.7	533.5
4/02/2018	1.0267	7.40	7.60	460.8	89.56	123.8	409.7	533.5
5/02/2018	1.0267	6.60	6.78	467.6	96.34	123.8	409.7	533.5
6/02/2018	1.0267	8.40	8.62	476.2	104.96	123.8	409.7	533.5
7/02/2018	1.0267	8.90	9.14	485.4	114.10	123.8	409.7	533.5
8/02/2018	1.0267	8.60	8.83	494.2	122.93	123.8	409.7	533.5
9/02/2018	1.0267	7.60	7.80	502.0	**130.73****	123.8	409.7	533.5
10/02/2018*	0.9935	9.50	9.44	511.5	63.17	123.8	486.7	610.5
11/02/2018	0.9935	8.00	7.95	519.4	71.12	123.8	486.7	610.5
12/02/2018	0.9935	7.70	7.65	527.1	78.77	123.8	486.7	610.5

Date	Kc (average)	ET_o daily, mm	ET_c daily, mm	Crop Water Use, or ETc cumulative, mm	Soil Water Deficit, mm	Rainfall (cumulative), mm	Irrigation (cumulative), mm	Total Water Applied (cumulative), mm
13/02/2018	0.9935	9.10	9.04	536.1	87.81	123.8	486.7	610.5
14/02/2018	0.9935	9.80	9.74	545.8	97.55	123.8	486.7	610.5
15/02/2018	0.9935	6.40	6.36	552.2	103.90	123.8	486.7	610.5
16/02/2018	0.9935	8.40	8.35	560.5	**112.25****	123.8	486.7	610.5
17/02/2018*	0.9935	9.90	9.84	570.4	61.39	123.8	547.4	671.2

***** Denotes to the irrigation event. ****** Denotes to the Soil water deficit (SWD) prior to the irrigation event.